INFORMATION TO USERS

This manuscript has been reproduced from the microfilm master. UMI films the text directly from the original or copy submitted. Thus, some thesis and dissertation copies are in typewriter face, while others may be from any type of computer printer.

The quality of this reproduction is dependent upon the quality of the copy submitted. Broken or indistinct print, colored or poor quality illustrations and photographs, print bleedthrough, substandard margins, and improper alignment can adversely affect reproduction.

In the unlikely event that the author did not send UMI a complete manuscript and there are missing pages, these will be noted. Also, if unauthorized copyright material had to be removed, a note will indicate the deletion.

Oversize materials (e.g., maps, drawings, charts) are reproduced by sectioning the original, beginning at the upper left-hand corner and continuing from left to right in equal sections with small overlaps.

Photographs included in the original manuscript have been reproduced xerographically in this copy. Higher quality 6" x 9" black and white photographic prints are available for any photographs or illustrations appearing in this copy for an additional charge. Contact UMI directly to order.

Bell & Howell Information and Learning
300 North Zeeb Road, Ann Arbor, MI 48106-1346 USA

UMI®
800-521-0600

DEVELOPMENT OF PARTIAL HYBRID FINITE ELEMENTS FOR 3-D GLOBAL/LOCAL ANALYSIS OF LAMINATED COMPOSITE STRUCTURES

Wei Feng

A Thesis

in

The Department

of

Mechanical Engineering

Presented on Partial Fulfilment of the Requirement

for the Degree of Doctor of Philosophy at

Concordia University

Montreal, Quebec, Canada

February 1998

ABSTRACT

Development of Partial Hybrid Finite Elements

for 3-D Global/Local Analysis of Laminated Composite Structures

Wei Feng, Ph. D.

Concordia University, 1998

The purpose of this work is to develop global/local finite element models using partial hybrid stress finite elements for stress analysis of laminated composite structures. Based on the composite variational principle, the general formulations of partial hybrid single-layer finite element and multilayer finite element are presented. These formulations can be used to develop a series of partial hybrid finite elements. A 4-node degenerated plate element, an 8-node degenerated plate element, a 3-D, 8-node solid element, a 3-D, 20-node solid element, a 6-node transition element, a 15-node transition element, a multilayer solid element, and a multilayer transition element are presented. The elements developed in this thesis are examined by the eigenvalue test to detect zero-energy deformation modes and the absence of rigid-body motion capability. The results show that the elements do

not have any kinematic deformation modes, and they have a desired capability for rigid-body displacement. In addition, the non-zero eigenvalues of the element stiffness matrices are real and positive.

In order to determine the optimal partial stress fields for the partial hybrid elements, a classification method of stress modes is presented. The method can be used to classify stress modes, select optimal stress modes, and set up an assumed stress matrix for a hybrid element. Also, the necessary and sufficient condition for avoiding spurious kinematic deformation mode is proposed and the optimal condition of an assumed stress field is presented.

A computer program COMSA is developed to implement the partial hybrid finite element method. The Global/Local finite element models are established using plate element, solid element, and transition element. In the thesis, a few numerical examples are presented to verify the accuracy and efficiency of the finite element models. It has been shown that the global/local models using partial hybrid element are efficient and accurate for stress analysis of laminated composites due to the fact that they take advantage of the capacity of both 3-D elements and 2-D elements.

ACKNOWLEDGEMENTS

I wish to thank Dr. S.V. Hoa for his patience, guidance, and financial support in my thesis research and academic work. I also wish to appreciate the services and equipment support of the Concordia Centre for Composites. Many people at the Concordia Centre for Composites helped in a variety of ways. In particular I would like to mention Mr. Jian-Yin Chen, Mr. Paul Ouellette, Ms. Lan Li, Ms. Sophie Merineau, Dr. Ming Xie, and Dr. Jianhua Han. I owe thanks to all of them.

The Concordia University Graduate Fellowship from Concordia University and International Student Fee Remission Award from Minister of Education, Quebec are gratefully acknowledged. The Duke University Certificate presented by the Department of Civil and Environmental Engineering of Duke University, USA and the Mechanical Engineering Recognition presented by the Department of Mechanical Engineering of Concordia University for being chosen as a finalist in the 1997 R.J. Melosh Medal Competition on Finite Element Analysis are also appreciated. The financial support and recognition of these organisations are highly valued.

I am vary grateful to Professor Wei-zang Chien and Professor Qian Huang of Shanghai University, China for introducing me to generalized variational principles and composite materials, and encouraging and helping me to study in Canada.

Also, I wish to thank my mother, Feng-zhen Sun; my father, Sui-gen Feng; my mother-in-law, Jin-ying Zhu; my father-in-law, Yun-long Zhang; my wife, Pei-jun Zhang; and my daughter, Fan Feng for their solid support.

Wei Feng 1998

CONTENTS

LIST OF FIGURES

LIST OF TABLES

LIST OF SYMBOLS

$A(\mathbf{u})$	the potential energy of an elastic body
$B(\mathbf{u})$	the complementary energy of an elastic body
$[B]$	the geometry matrix relating the strain vector with the nodal displacement vector
$[B_g]$	the partial geometry matrix relating the globally continuous strain vector with the nodal displacement vector
$[B_L]$	the partial derivative matrix
$[C]$	the stiffness matrix of materials
$\mathbf{d}$	the prescribed displacement
$\mathbf{d}^i$	the nodal displacement vector related to the lower surface of an sub-element
$\mathbf{d}^{i+1}$	the nodal displacement vector related to the upper surface of an sub-element
$\mathbf{D}$	the operator of the derivative of a displacement field
$\mathbf{D}_g$	the operator of the in-plane derivative of a displacement field
$\mathbf{D}_L$	the operator of the transverse derivative of a displacement field
$E(\mathbf{q})$	the composite energy of a laminated composite body
$\mathbf{f}$	the equivalent nodal force vector

$\mathbf{F}$	the body force
[G]	the leverage matrix
$[G^i]$	the leverage matrix of an sub-element
[H]	the flexibility matrix
$[H^i]$	the flexibility matrix of an sub-element
[J]	the Jacobian matrix
$[K_d]$	the semi-stiffness matrix which is a displacement-formulated stiffness matrix based on the globally continuous strains
$[K_d^i]$	the semi-stiffness matrix of an sub-element
$[K_h]$	the semi-stiffness matrix which is a hybrid-formulated stiffness matrix based on the globally continuous stresses
[K]	the element stiffness matrix
m	the total number of stress modes in an assumed stress field
$\mathbf{n}$	the outward unit normal
n	the total number of nodal displacement components in an element
[N]	the matrix of shape functions
$\mathbf{p}$	the locally continuous vector
[P]	the assumed stress matrix
$[P_g]$	the partial assumed stress matrix
$\mathbf{q}$	the globally continuous vector
r	the number of rigid body modes in an element
[R]	the combined constitutive matrix

S	the boundary of an elastic body
$[S]$	the compliance matrix of materials
$\mathbf{T}$	the prescribed surface force
$[T]$	the multiplying matrix to apply the traction conditions on the top and bottom surfaces of a plate
$[T_B]$	the transformation matrix for the derivatives of displacements
$\mathbf{u}$	the displacement vector
u, v, w	the three displacement components
u_i	the i-th displacement component of a displacement field
u_i^0	the i-th displacement component at the mid-surface of a plate
V	the volume of an elastic body
$\mathbf{V}_{1i}, \mathbf{V}_{2i}, \mathbf{V}_{3i}$	the unit vectors of the local co-ordinate system at node i
x, y, z	the global co-ordinates
ξ, η, ζ	the local co-ordinates
λ	the eigenvalue of the element stiffness matrix
ε	the strain vector
ε_g	the globally continuous strain vector containing three in-plane strain components
ε_L	the locally continuous strain vector containing three transverse strain components
$\varepsilon_x, \varepsilon_y, \gamma_{xy}$	the in-plane strain components
$\varepsilon_z, \gamma_{xz}, \gamma_{yz}$	the transverse strain components

σ	the stress vector
σ_i	the i-th stress modes in an assumed stress matrix
σ_g	the globally continuous stress vector containing three transverse stress components
σ_L	the locally continuous stress vector containing three in-plane stress components
σ_x, σ_y, τ_{xy}	the in-plane stress components
σ_z, τ_{xz}, τ_{yz}	the transverse stress components
Π	The variational functional
Π_{co}	The composite energy functional
α_T	the surface stress parameter vector relating to the upper surface of a sub-element
α_B	the surface stress parameter vector relating to the lower surface of a sub-element
$\boldsymbol{\beta}$	the internal stress parameter vector
$\boldsymbol{\varphi}$	the surface stress parameter vector
$\boldsymbol{\delta}$	the nodal displacement vector

Chapter 1

INTRODUCTION

The finite element method has become an important and practical numerical analysis tool. It has found application in almost all areas of engineering [1-7]. In the area of composite structure, it has been widely used due to the power of the technique to be able to model the laminated composite structures not only in the planar dimensions, but also in the thickness direction [8-10]. It is also due to the availability of many commercial finite element codes such as ABAQUS, ALGOR, ANSYS, COSMOS/M, MSC/NASTRAN, PATRAN3, and so on [11-14]. Application of the finite element method in the analysis of laminated composite structures involves the following three disciplines [15]:

1. Composite structure theory, for the correct formulation of mathematical models;
2. Numerical analysis, for the elaboration of algorithmic solutions of the discretized equations;
3. Computer programming, for the development of parametrized codes applicable to various problems.

Therefore, first of all, one must understand the behaviour of laminated composite

structures for developing the best finite element models. The laminated composites are made of a stack of bonded laminae which are manufactured in the form of thin sheets using long continuous fibres and isotropic matrix (see Figure 1-1). The analysis of laminated composite structures presents more complication than others made of isotropic materials due to the fact that the laminated composite structures contain inherent discontinuities. At the micromechanics level, there are discontinuities in material properties as one moves from fibre to matrix or vice versa. At the macroscopic level, although the individual laminae are treated as homogeneous orthotropic materials, there are discontinuities in stresses along the thickness of laminated composites due to the variation in fibre orientation from lamina to lamina. Laminated composite structures also contain discontinuities, such as open holes, ply drop-offs, free edges, or delamination, all of which are common in practice. The behaviour of laminated composite structures such as anisotropy and lamination result in large requirements in the computer storage space and CPU time if one wants to accurately analyze laminated composite structures.

In most applications, the thickness of a laminated composite structure is small compared to the planar dimensions and the 2-D theories, such as the classical lamination theory [16-22], are used to analyze a laminated composite structure for stresses. The 3-D stress analysis of a laminated composite structure is often required in the local regions near discontinuities. For example, the delamination in a laminated composite structure has been recognized as the most common failure mode. To predict the delamination failure of a composite structure, the stress state at the location of the delamination has to be carefully

investigated and the interlaminar stresses must be accurately determined using 3-D analysis method.

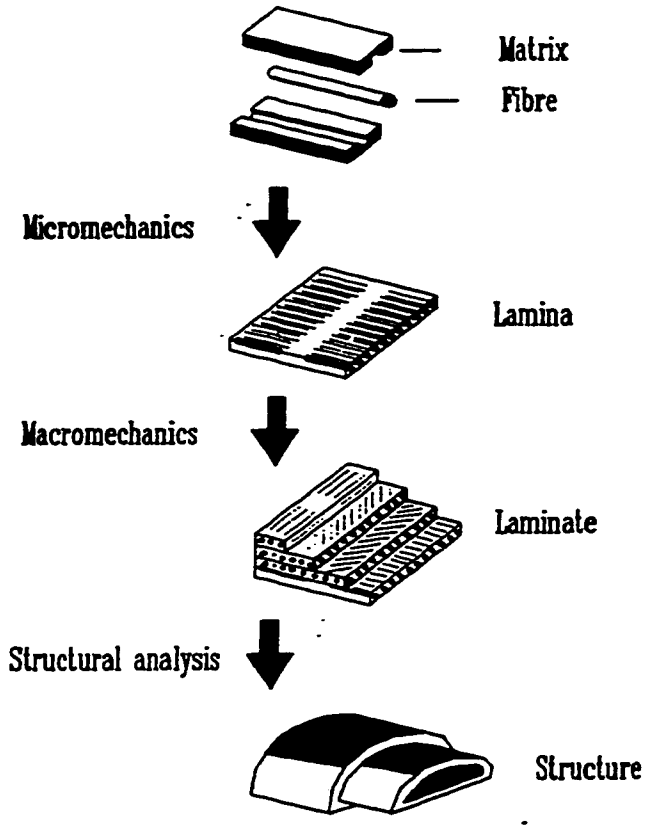

Figure 1-1 Characteristics of laminated composites

For 3-D stress analysis of laminated composite structures, there are many commercial finite element codes available. However, to provide accurate stress and strain, it is still

necessary to improve existing finite elements and to develop new finite elements that represent the true laminated composite material behaviour.

Taig evaluated the eight commercial finite element codes, I-DEAS, PATRAN, ANSYS, NISA, COSMOS/M, MSC/NASTRAN, PAFEC, and MICROFIELD, in 1991 [14]. In the report of the evaluation, Taig indicated that most FEA systems studied provide Kirchhoff and Mindlin-type plate and shell formulations with no attempt to improve the through-thickness modelling to represent the true laminated material behaviour. The only way to achieve such modelling is to use stackable solid elements, but this becomes impossibly cumbersome for large structures. Half of the systems studied do not recover interlaminar shear stresses although others do provide layer shear stresses. Through-thickness shear stresses in general are recovered in different ways. Most of the higher-functionality systems use an equilibrium based post-analysis calculation. It has been shown that the plate and shell models cannot recover meaningful stresses in the place where they are important: at the edges and near discontinuities. Composites analysis is limited to the solution of equivalent homogeneous plate and shell models and, on an occasional and local basis, to 3-D models either layer-by-layer or in stacked layer blocks or point-by-point through a 3-D material volume.

It is clear that the most important deficiencies are in through-thickness modelling for finite element analysis of laminated composite structures.

1.1 Three Finite Elements Classified by the Variational Principles

The common finite elements can be divided into three types: single-field finite elements (displacement elements and stress elements), hybrid finite elements (conventional hybrid element and partial hybrid stress elements), and mixed finite elements according to the character of the variational principle and the nature of the resulting discrete algebraic equations. For analysis of laminated composite structures, displacement elements [23-30], conventional hybrid stress elements [31-35], and partial hybrid stress elements [36-50] are often used. These three finite elements are formulated using three different variational principles.

1.1.1 Displacement Element

The majority of finite elements used for stress analysis of laminated composites is based on the displacement formulation. This is due to its simple approach to the element formulation.

Assumed Displacement Field

For the displacement finite elements, the principle of the stationary potential energy is often used to derive the element formulation and the displacement functions are assumed a priori. Although a number of mathematical functions such as trigonometric series and

exponential functions can be used as the displacement functions, orthogonal polynomials are more appropriate as the displacement functions because of the ease and simplification they provide in the finite element formulation.

In the regular finite element method in solid mechanics, the nodal displacement components of an element are often used as the dependent variables. In this case, for a compatible element, the number of terms in the displacement polynomial is determined by the element type and must be equal to the total number of degrees of freedom associated with the element. Otherwise, the polynomial may not be unique. In addition, the polynomial series must satisfy the continuity and completeness conditions to ensure convergence to the correct result.

Continuity means that these functions and their derivatives, where required, must be continuous within the element domain and across the interface between adjacent elements. For example, a linear function $(a_1 + a_2x)$ is indeed continuous within the elements. For compatibility and continuity condition across the interface between adjacent elements, it is necessary that the coordinates and displacements of the elements at the interface be the same. Because the coordinates and displacements of an element at the interface are determined only by nodes and nodal degrees of freedom at that interface, compatibility is satisfied if the adjacent elements have the same nodes at the interface and the coordinates and displacements at the interface are defined in each element by the same polynomial functions.

Completeness means that the polynomial functions must contain the constant and linear terms so that the element nodes can be given rigid body displacements without producing strain within the element and can always recover state of constant strain. For instance, the linear approximation contains the constant term a_1 which allows for the rigid body displacement mode. Also, the linear approximation contains linear term a_2x which guarantees that the element is able to recover the state of constant strain. This condition implies that, when the element becomes smaller and smaller, the strain in the element approaches a constant value. The necessary terms for a complete polynomial are presented by Pascal's triangle. It indicates that the displacement polynomials must use the least-order terms in the displacement functions.

A Major Deficiency of Displacement Elements

The displacement elements have a major deficiency: the transverse stresses are computed from displacements, and the continuity of these stresses can not be satisfied well.

In the displacement finite element method, the finite element process first calculates the displacements (primary variables) at the nodes of the elements. The displacement field is then determined by these nodal displacements. The strains and stresses (second quantities), which are more important for design purposes, are calculated by numerically differentiating the approximate solutions. For stress analysis of homogeneous materials, the displacement finite element method can provide accurate results efficiently. However,

for laminated composites, the "from the top" and "from the bottom" values of transverse stresses at interfaces will be discontinuous if the stress-strain relation is used to calculate these stresses. This is due to the change of fibre orientation in adjacent layers between the interfaces. From this point of view, any improvement in the displacement finite element models, namely, use of additional discretization or higher order polynomials, can only minimize the jumps of transverse stresses at the interfaces, but not ensure the continuity of these stresses. Any displacement approximation that possesses a continuous first derivative (with respect to the thickness coordinate) at the interfaces is in contradiction with the continuity of transverse stresses. Any attempt to develop as smooth displacement approximation as possible by enforcing continuity of the displacement derivatives (with respect to the thickness coordinate) at the interfaces, something very natural in the traditional analysis of homogeneous structures, leads to wrong results when applied to the laminated composite structures. The continuity of transverse stresses can be satisfied only if transverse strains are discontinuous at the interfaces between distinct layers, as follows from the stress-strain relation. This means, in turn, that the first derivatives of displacement must be discontinuous with respect to the thickness coordinate at interfaces. Although such a discontinuity is the necessary requirement for the correct solution, it is not a sufficient one [51].

In order to overcome this deficiency, a good alternate, the hybrid element, has drawn more and more attention from engineers and designers of laminated composite structures.

1.1.2 Conventional Hybrid Stress Element

Since 1964, a great number of multifield finite elements have been presented [31-50,52-61]. The hybrid stress finite element formulation assumes the stresses as the independent variables at the outset. Therefore, the degree of accuracy of the stress is the same as the degree of accuracy of the displacement. This is due to the fact that the stresses are obtained directly from the process of minimization and without having to go through the differentiation of the displacements. This is the inherent advantage of the hybrid finite element method.

Originally, the hybrid stress finite elements were formulated based on the principle of the minimum complementary energy and the introduction of Lagrange multipliers to enforce the constraint conditions along the inter-element boundary [52]. In this element formulation, the assumed stress field in the element must satisfy equilibrium equations a priori. This causes difficulty to assume an optimal stress field for the hybrid elements. Later on, it was realized that the equilibrium conditions can be relaxed if the hybrid element formulation is based on the generalized variational principles such as Hellinger-Reissner variational principle. The stress field may satisfy the equilibrium equations only in a variational sense. Thus, the stress field can be described in the isoparametric co-ordinate system of the element, which would make the element less sensitive to mesh distortion.

Assumed Stress Field

For the hybrid stress element, the physical fields that must be independently assumed within the element at the beginning are not only displacement field, but also stress field. An assumed stress field consists of a set of stress modes and a set of the corresponding stress parameters. Although a number of mathematical functions such as trigonometric series and exponential functions can be used as stress mode functions, orthogonal polynomials are more appropriate as stress mode functions due to their ease and simplification. It is similar to the displacement functions in the assumed displacement field. However, while the displacement polynomial is constrained by the number of displacement nodal degrees of freedom associated with an element, the stress polynomials have no such constraint. If an assumed stress field does not contain enough stress modes, the rank of the element stiffness matrix will be less than the total degrees of deformation freedom and the numerical solution of the finite element model will be unstable. In that case, there may be too many kinematic deformation modes. It is possible to suppress kinematic deformation modes by adding stress modes of higher order terms, but this can not guarantee that all kinematic deformation modes are suppressed. Moreover, each extra term will add more stiffness[62] and overuse of stress modes will cost more computational time because the calculation of element stiffness matrix requires inversion of the flexibility matrix. The lack of a rational way for deriving the optimal assumed stress modes has obstructed the development of the hybrid finite element method.

Some mathematical basis for the stability of the numerical solution of the hybrid finite element model has been established and a number of approaches for obtaining the optimal stress modes have been proposed. A *necessary condition* to avoid kinematic deformation modes [54, 63] is

> *The total number of stress modes in an assumed stress field must be equal to or larger than the total number of nodal displacements minus the number of rigid body modes in an element.*

or

$$m \geq n - r \tag{1-1}$$

in which, m is the total number of stress modes in an assumed stress field, n is the total number of nodal displacements, and r is the number of rigid body modes in an element.

Brezzi [64], Babuska, Oden and Lee [65] presented necessary and sufficient conditions for stability and convergence of a hybrid element by means of functional analysis. However, this can be used only as a posteriori check on a formulation. Fraeijs de Veubeke [66] presented a limitation principle for hybrid elements based on the Hellinger-Reissner variational principle. This work was extended to the hybrid stress/strain elements based on the Hu-Washizu variational principle [67]. The limitation principle [66] states that a hybrid element would be equivalent to its displacement counterpart if a stress space consisted of all the displacement-derived stress modes as a subspace of the assumed stress. This means that the eigenvalues of a hybrid element would be no different from

those of a displacement element when the assumed stress field contains all stress modes derived from the assumed displacement field.

There are a few approaches for determining an assumed stress field. Using group theory, Punch, Rubinstein, and Atluri [68-69] established a set of least-order stable invariant stress selections for three-dimensional brick elements and two-dimensional rectangular elements. Pian and Chen [70] used the product $\{\sigma\}^T \{\varepsilon\}$, the deformation energy due to the assumed stresses and displacements, to determine the necessary assumed stress modes. Pian and Tong [71] introduced the internal displacement parameters to relax the stress equilibrium condition and used isoparametric interpolation to construct hybrid element. Pian, Wu, and Cheung [72-73] introduced incompatible displacements to maintain completeness of the polynomials. The initial stress terms chosen are unconstrained and form complete polynomials. The additional displacements are used as Lagrange multipliers to enforce the stress equilibrium constraint. Chen et al [74-75] constrained the stress by setting the inner product of the non-constant stress modes with the deformation derived from the incompatible displacement to zero. Huang [41] introduced the concept of natural deformation mode and natural stress mode and developed a model analysis technique to find natural stress modes for hybrid elements. Sze [76-78] used orthogonal lower- and higher-order stress modes to construct hybrid element. It allows the partition of the element stiffness matrix into a lower- and a higher-order stiffness matrix. When the lower-order stiffness turns out to be identical to the sub-integrated element, the higher-order stiffness matrix plays the role of stabilization matrix. Han [43] presented an iso-function

method to derive stress modes directly from the assumed displacement field.

Difficulties with Conventional Hybrid Finite Elements

The conventional hybrid elements introduce an assumed stress field which includes all six stress components from the beginning. The elements satisfy the continuity condition of the interlaminar stresses exactly. This can greatly improve the accuracy of computing transverse stresses. However, the hybrid stress element has two important disadvantages: the presence of spurious kinematic deformation modes and the inversion of the flexibility matrix [H] whose expression will be given later.

Because the assumed stress field of the conventional hybrid elements contains six stress components, there always exist a large number of stress parameters in the stress field. So, the inversion of the flexibility matrix is the most costly operation. For instance, an assumed stress field may contain more than fifty stress parameters for the stress analysis of 3-D structures and hundreds of stress parameters for the analysis of composite structure [33]. This usually requires much computer CPU time for solving a practical problem. If the CPU time for calculating the element stiffness matrix [K] of 3-D, 20-node displacement element is assumed as 1, in general, it is 1.48 for corresponding conventional hybrid element by using minimum number (m=54) of stress parameters. This suggests poor performance in terms of computing time when compared with the single-field displacement models. However, this limitation can be overcome by reducing the

number of stress components in the assumed stress field of conventional hybrid elements for the analysis of composite structures. Therefore, the partial hybrid elements [36-50] are proposed.

In addition, the number of the stress parameters (or stress modes) in assumed stress field should be reduced to as small as possible. According to the necessary condition (1-1), the minimum number of stress parameters (or stress modes) may equal m (= n - r). However, in the practice, there are many examples indicating that there are spurious kinematic deformation modes in the hybrid elements when the requirement (1-1) is satisfied. In order to suppress these kinematic deformation modes, it is proposed to add stress modes of high order terms in the assumed stress field. This means to increase the number of stress parameters in the stress field. Therefore, the question arises as to how many and what kind of stress modes must be introduced into the assumed stress field. An ideal situation is that an assumed stress field contains m (=n-r) least-order stress modes and its resulting element is free from kinematic deformation modes. This kind of assumed stress fields is considered to be best and is optimal with respect to computer resources. The procedure to derive this optimal stress field is presented in Chapter 3 of this thesis.

1.1.3 Partial Hybrid Stress Element

For analysis of composite structures, in fact, it is not necessary to introduce all components of stresses into an assumed stress field. Although all components of

displacement, strain and stress must be continuous within each layer of a laminated composite, only the in-plane derivatives ε_x , ε_y , γ_{xy} and transverse stresses σ_z , τ_{xz} ,τ_{yz} must be continuous at the interfaces between distinct layers with prefect bonding. Therefore, the main requirement in developing finite elements is to satisfy all of the continuity conditions on displacements and transverse stresses at the interfaces and traction-free condition on the upper and lower surfaces. In order to enforce the transverse stress continuity, it is needed only to introduce three transverse stresses into the assumed stress field [40-41].

To formulate the partial hybrid stress element, a new variational principle is required. Reissner [79-80] suggested a mixed variational principle and it was derived independently by Moriya [81]. Huang [41] presented a combined energy variational principle by means of weighted residual method. Based on the modified variational principles, Hoa and his students proposed a series of partial hybrid stress elements [39-50, 82]. Pian and Li [36] developed two types of mixed form hybrid stress element for 2-D and 3-D problem. Wang and Ching [38] presented several modified partial stress finite elements which are 3-D elements or layer-wise elements.

A partial hybrid stress element only includes three transverse stresses in its assumed stress field and still satisfies the continuity condition of the interlaminar stresses. The element is computationally more efficient than the conventional hybrid element. For example, the CPU time to calculate the element stiffness matrix [K] is 1.29 for 3-D, 20-node partial

hybrid element by using minimum number (m=23) of stress parameters. It saves more 20% CPU time than conventional hybrid element on calculation of element stiffness matrix and still provide more accurate stresses than conventional displacement element.

1.2 Three Finite Elements Classified by Composite Structure Theories

The power of a finite element program not only depends on the variational principle formulating the element, but also on the composite structure theory used in the element formulation. In general, composite structures are modelled using one of the following three classes of theories[25, 83]:

1. Equivalent single-layer 2-D theories[17-23], in which deformable models are based on global through-the-thickness displacement, strain and stress approximations;

2. Layer-wise theories [24-25, 84-86], in which displacement models are based on piecewise approximations of the response quantities in the thickness direction.

3. 3-D continuum theories[87-89], in which each of the individual layers of a composite structure is treated as a three-dimensional continuum.

Corresponding to three classes of theories above, the finite elements can be classified into three classes: the laminated elements based on the equivalent single-layer 2-D theories; the multilayer elements based on the layer-wise theories, and the 3-D solid elements based on the 3-D continuum theories.

1.2.1 Laminated Element

In the laminated elements [17-23], the variation in orientations and properties across the thickness is integrated to obtain a single property across the thickness. The laminated elements can be used to model the overall behaviour of composite structures. In the finite element model using this element, the number of unknowns through the thickness of a structure is independent of the number of layers in the composite. For this type of element, the lower-order elements have 'locking' problems due to inconsistencies in the modelling of transverse shear energy and membrane energy. Although the higher-order elements are less sensitive to locking, the continuity condition of transverse stresses can not be satisfied. These elements can be used for problems such as vibration or buckling but these do not accurately predict interlaminar stresses.

1.2.2 Multilayer Element

The multilayer elements are capable of providing interlaminar stresses with the same level of accuracy as the 3-D solid elements. There are two types of multilayer elements: one is based on the layer-wise theories; another is based on the 3-D continuum theories. In the multilayer elements based on the layer-wise theories [24-25, 84-86], the individual laminae are taken as 2-D layers. These layers are then assembled through the thickness. Their aspect ratio is restricted to only 2-D (in-plane) consideration because they separate 3-D discretization into 2-D (in-plane) discretization and 1-D (thickness) discretization.

However the number of degrees of freedom is still dependent on the number of layers in composite structures. Therefore, it is still expensive to compute interlaminar stresses near the free edge of composite structures in order to satisfy the continuity of interlaminar stresses.

In the multilayer elements based on the 3-D continuum theories [42-43], the individual laminae are modeled using one or more 3-D sub-elements. These sub-elements are then assembled through the thickness according to the continuity conditions on displacements and stresses. In order to minimise the problem of large aspect ratios, the planar dimensions of the elements should be kept to be not too large compared to the thickness of the element. Because composite laminae are very thin and a typical laminated composite may contain many laminae, this usually results in an excessively large number of elements which means large requirements in computer space and time.

1.2.3 Solid Element

In 3-D solid elements [87-89], no specific kinematic assumptions are introduced regarding the behaviour of a laminate. It takes the behaviour of the individual laminae into consideration. However, since the composite laminae are very thin and the composite structures have discontinuities, a fine finite element mesh is usually needed. It will quickly exhaust the computer storage.

In general, the 3-D solid elements are used to accurately determine stresses in composite structures near discontinuities. However each layer in composites needs at least one element along the thickness of the structure. The number of unknowns in a finite element model will depend on the number of layers. Near the free edge of composite structures, three or more elements will be needed within a layer along the thickness. In addition, 3-D solid elements show numerical instability under bending deformation when the aspect ratio is large. The aspect ratio is the ratio between the in-plane dimension and thickness dimension of the elements. Usually, the thickness of a layer in composite structures is very small. So this type of modelling is computationally expensive because it needs to maintain the aspect ratio.

1.3 Global/Local Analysis

The accurate determination of layer level stresses in laminated composite structures containing large numbers of distinct material plies remains a formidable computational problem. For example, free edges and rivet holes always result in interlaminar stresses and initiate delamination. In general, it is not possible to account for this phenomenon adequately through laminated elements. The use of 3-D solid elements and multilayer elements becomes unavoidable. But the use of 3-D finite element scheme is not always practical because it traditionally requires that each distinct layer be discretized in order to assign the correct ply-dependent material response. It usually needs fine finite element mesh. This increases drastically the number of elements and result in the large requirement on the computer resource. So complete three dimensional analysis is prohibitive. In order to solve such problems, some more efficient means of conducting three-dimensional analysis of laminated composites structures are required, although there exist a great variety of finite elements (see Table 1-1).

Table 1-1 Various Finite Element Models in Composite Structures

Type	Through-the-thickness variable assumptions	Number of nodal variables
laminated element (1971)	$u_i = u_i^0 + \sum^{m_i} u_i^k z^k$	$3+m_1+m_2+m_3$
	The number of nodal unknowns is independent on the number of layers. The computing time is less than other elements. The higher-order elements do not satisfy continuity condition of interlaminar stresses	
multilayer element (1973)	$u_i = u_i^0 + \sum^{n_i} u_i^j \phi_j(z)$	$3+n_1+n_2+n_3$
	$\phi_j(z)$ is piecewise continuous functions. The number of nodal unknowns depends on the number of layers and the degree of interpolation used.	
3-D solid element (1971)	$u_i = \sum^{l_i} u_i^k z^k$	$3+l_1+l_2+l_3$
	Every layer needs at least one element along the thickness. It is computationally expensive.	
hybrid element (1972)	$u_i = u_i^0 + \sum^{m_i} u_i^k z^k$ $\{\sigma\} = [P]\{\beta\}$	$3+n_1+n_2+n_3$
	There are six stress components in assumed stress field. Transverse stresses satisfy continuity exactly.	
partial hybrid element (1989)	$u_i = u_i^0 + \sum^{m_i} u_i^k z^k$ $\{\sigma_g\} = [P_g]\{\beta\}$	$3+n_1+n_2+n_3$
	There are three stress components in assumed stress field. Transverse stresses satisfy continuity exactly.	
global/local models (1984)	Different combinations of different elements on requirement. It takes advantage of the properties of different elements.	

Note: l_i, m_i, n_i are the number of polynomial terms.

There is a growing body of literature on global/local finite element analysis[90-95]. The phrase global/local analysis has a lot of definitions among analysts. The concept of global and local may change with every analysis level, and also from one analyst to another. The advantage of applying the global/local approach is that accurate analyses are performed with considerably reduced computer resource requirements.

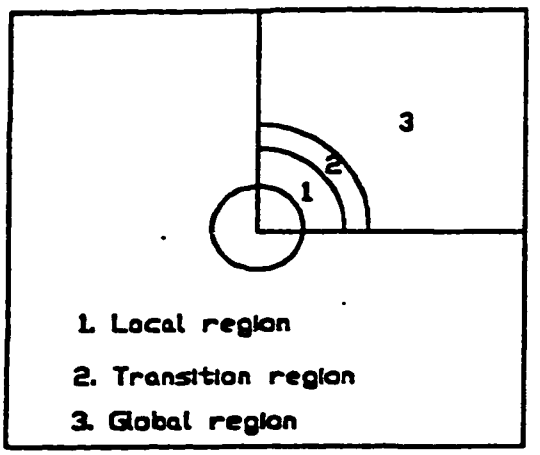

Figure 1-2 Global/Local Finite Element Model

The global/local finite element analysis includes such methods as substructuring [96], variable kinematic element [26,97], domain decomposition [98], s version [99], zooming [100], and Domain division [101-104]. In general, global/local models can be classified into sequential global/local model and simultaneous global/local model. The main difficulty with the sequential model is the maintenance of displacement continuity along

boundaries separating incompatible subregions. In this model, the iterative methods are used to establish equilibrium along the global/local boundaries. It requires much computing time. For the simultaneous model, the domain of the structure to be analyzed is divided into three areas: local region, global region, and transition region as shown in Fig. 1-2. This model saves computing time but a special transition element is required in the transition region.

1.4 Thesis Work

This thesis is to develop the global/local finite element models using partial hybrid stress finite elements for stress analysis of laminated composite structures. In order to determine optimal stress polynomials for hybrid stress elements, a classification method of stress modes is presented. A series of partial hybrid stress elements are developed for the global/local finite element models, a computer program COMSA is introduced, and a few numerical examples are presented.

Chapter 2 of this thesis will review a few basic concepts such as the basic variables, the combined constitutive relation, and composite energy for stress analysis of laminated composites; describe the elastic problem of laminated composite structures; derive the composite variational principle again to reveal the relationship between the Hellinger-Reissner principle and the composite variational principle; and present the general formulation of single-layer finite element and multilayer finite element.

Chapter 3 of this thesis will present a classification method to determine optimal stress polynomials for an assumed stress field. A few basic concepts are defined firstly, and then classification condition is presented. The procedure to classify stress modes, select optimal stress modes, and set up an assumed stress matrix is described in detail. In addition, the optimal condition of assumed stress field is presented. Thus, by means of iso-function method [43] and classification method, the stress polynomials are constrained by the number of degrees of freedom associated with a hybrid stress element. Following this process, both the displacement polynomials and the stress polynomials are constrained by the number of degrees of freedom of the hybrid elements .

Chapter 4 will formulate 3-D, 8-node partial hybrid solid element and 3-D, 20-node partial hybrid solid element using the general formulation of single-layer element in Chapter 2. The two elements are isoparametric compatible elements. Therefore, the displacement functions are the same as the shape functions of the elements. The stress polynomials are derived by the classification method. The eigenvalue test is used to detect zero-energy deformation modes and the absence of rigid-body motion capability.

Similarly, Chapter 5 will present 4-node partial hybrid degenerated plate element and 8-node partial hybrid degenerated plate element.

Chapter 6 will present 6-node partial hybrid transition element and 15-node partial hybrid transition element. The two elements are used to smoothly connect the 3-D solid elements

with the degenerated plate elements. In order to enforce the compatibility at the interfaces between different elements, the shape functions of 3-D solid element and degenerated plate element are carefully investigated. Then, new shape functions are derived for the transition elements.

Chapter 7 will formulate multilayer solid element and multilayer transition element using the general formulation of multilayer element in Chapter 2. They consist of a stack of 3-D, 8-node partial hybrid solid element and 6-node partial hybrid transition element, respectively.

Chapter 8 will apply the new elements to solve a few problems of laminated composite structures, and present two global/local finite element models using these new elements.

Chapter 9 will sum the contribution of the current research work and give a few suggestion for future work.

In the appendix, the general procedure of finite element analysis using the computer program COMSA, the basic variables and arrays in COMSA, and the input data files are introduced.

Chapter 2

PARTIAL HYBRID STRESS FINITE ELEMENT FORMULATION

In order to develop new hybrid finite elements for laminated composites, it is necessary to understand the behaviour of laminated composite structures. As mentioned in Chapter 1, the laminated composites are made of a stack of bonded laminae which are manufactured in the form of thin sheets using long continuous fibres and isotropic matrix (see Figure 1-1). In analysis of laminated composite structures, the laminae are assumed to be bonded perfectly and the individual laminae are treated as homogeneous orthotropic materials. Therefore, the lamination and anisotropy are the instinct behaviours of the laminated composite structures. They lead to the conjunction conditions at interfaces between different layers in laminated composite structures. The conjunction conditions refer to the continuity conditions of partial stresses and strains at interfaces.

In order to satisfy conjunction conditions, the first task is the identification of globally continuous variables and locally continuous variables. Usually, the lamina plane is denoted

by the Cartesian co-ordinates x, y, and the thickness direction by z (shown in figure 2-1).

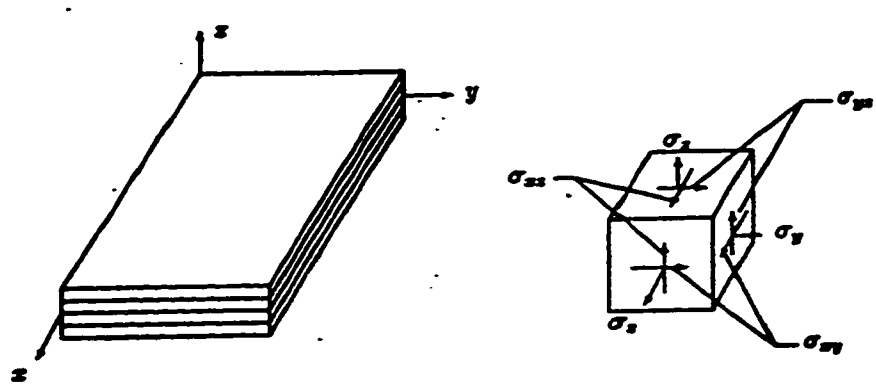

Figure 2-1 Composite structure and its co-ordinate system

In the laminated composites, all components of displacement, strain, and stress are continuous within each layer due to the fact that the individual laminae are treated as homogeneous orthotropic materials. At the layer interface with perfect bonding, the displacements are also continuous due to the compatibility condition. As a result, the in-plane derivatives (three inplane strains) ε_x, ε_y, ε_{xy} are continuous across the thickness. Meanwhile, the reaction forces give rise to transverse stresses (interlaminar stresses) σ_z, σ_{zx}, σ_{zy}, and they are also continuous across the thickness because of the equilibrium condition. This means, along the thickness of composites, the in-plane strains (ε_x, ε_y, ε_{xy}) and transverse stresses (σ_z, σ_{zx}, σ_{zy}) are globally continuous variables. On the other hand, the transverse strains ε_z, ε_{zx}, ε_{zy} and in-plane stresses σ_x, σ_y, σ_{xy} are not necessarily

continuous across the interfaces between different layers, although they must be continuous within each layer. So, they are locally continuous variables. Thus, the *globally continuous variables* are those that are continuous not only within the plane of the laminate but also across the interface from one layer to the next. This is the result of consideration for compatibility and equilibrium. The *locally continuous variables* are those that are continuous only within the plane of the lamina but are not necessarily continuous across the interface from one lamina to the next.

2.1 Basic Variables

By classifying the variables into globally continuous variables and locally continuous variables, the stress σ and strain ε can be divided into the following two parts,

$$\sigma_L = [\ \sigma_x\ \sigma_y\ \tau_{xy}\ ]^T \quad \text{and} \quad \sigma_g = [\ \sigma_z\ \tau_{zy}\ \tau_{zx}\ ]^T$$

$$\varepsilon_g = [\ \varepsilon_x\ \varepsilon_y\ \gamma_{xy}\ ]^T \quad \text{and} \quad \varepsilon_L = [\ \varepsilon_z\ \gamma_{zy}\ \gamma_{zx}\ ]^T \qquad (2\text{-}1)$$

Combining the globally continuous variables in composites, the globally continuous vector is defined as

$$q = \begin{Bmatrix} \varepsilon_g \\ \sigma_g \end{Bmatrix} \qquad (2\text{-}2)$$

Similarly, combining the locally continuous variables, the locally continuous vector is defined as

$$\boldsymbol{p}=\begin{Bmatrix}\boldsymbol{\sigma}_L\\ -\boldsymbol{\varepsilon}_L\end{Bmatrix} \qquad (2\text{-}3)$$

in which the negative sign is introduced to ensure the symmetry of the combined constitutive relation which is

$$\mathbf{p} = [\,\mathrm{R}\,]\,\mathbf{q} \qquad (2-4)$$

or

$$\begin{Bmatrix}\sigma_L\\ -\varepsilon_L\end{Bmatrix}=\begin{bmatrix}R_1 & R_2\\ R_2^T & R_3\end{bmatrix}\begin{Bmatrix}\varepsilon_g\\ \sigma_g\end{Bmatrix} \qquad (2\text{-}4)'$$

where [R] is called the combined constitutive matrix. Because the constitutive relation can be expressed in the form,

$$\boldsymbol{\sigma}=[C]\,\boldsymbol{\varepsilon} \quad or \quad \begin{Bmatrix}\sigma_L\\ \sigma_g\end{Bmatrix}=\begin{bmatrix}C_1 & C_2\\ C_2^T & C_3\end{bmatrix}\begin{Bmatrix}\varepsilon_g\\ \varepsilon_L\end{Bmatrix} \qquad (2\text{-}5)$$

where [C] is the stiffness matrix of materials, and

$$\boldsymbol{\varepsilon}=[S]\,\boldsymbol{\sigma} \quad or \quad \begin{Bmatrix}\varepsilon_g\\ \varepsilon_L\end{Bmatrix}=\begin{bmatrix}S_1 & S_2\\ S_2^T & S_3\end{bmatrix}\begin{Bmatrix}\sigma_L\\ \sigma_g\end{Bmatrix} \qquad (2\text{-}5)'$$

where [S] is the compliance matrix of materials, the matrix [R] can be expressed as

$$[R] = \begin{bmatrix} R_1 & R_2 \\ R_2^T & R_3 \end{bmatrix} = \begin{bmatrix} C_1 - C_2 C_3^{-1} C_2^T & C_2 C_3^{-1} \\ C_3^{-1} C_2^T & -C_3^{-1} \end{bmatrix} \tag{2-6}$$

and

$$[R] = \begin{bmatrix} R_1 & R_2 \\ R_2^T & R_3 \end{bmatrix} = \begin{bmatrix} S_1^{-1} & -S_1^{-1} S_2 \\ -S_2^T S_1^{-1} & S_2^T S_1^{-1} S_2 - S_3 \end{bmatrix} \tag{2-6}'$$

Due to the fact that the matrices [C] and [S] are symmetric matrices, the matrix [R] can be proven to be a symmetric matrix. It can be shown that

$$[R]^T = [R] \tag{2-7}$$

To satisfy continuity condition at layer interfaces (or interlaminar surfaces), the six globally continuous variables should be taken as basic variables in the problem of laminated composite structures. The basic variables, in the partial hybrid stress elements, are displacements u, v, and w and transverse stresses σ_z, τ_{zy}, and τ_{zx}. Thus, an elasticity problem for composite structures can be adequately described.

2.2 Elasticity Problem for Composite Structures

Consider a linear anisotropic elastic body under static loading. The body occupies the volume V and is bounded by the surface S, which is decomposed into S: $S_d \cup S_t$. Boundary

displacements are prescribed on S_d , whereas surface tractions are prescribed on S_t. The outward unit normal on S is denoted by **n**. The following relations between three fields: globally continuous vector **q**, locally continuous vector **p**, and displacement **u** in the volume have to be satisfied.

1. the in-plane strain-displacement equations:

$$\varepsilon_{ij}=\frac{1}{2}(u_{i,j}+u_{j,i}) \qquad i,j=1,2 \tag{2-8}$$

or

$$\boldsymbol{\varepsilon}_g=\boldsymbol{D}_g\boldsymbol{u} \tag{2-8}'$$

2. the transverse strain-displacement relations:

$$\varepsilon_{ij}=\frac{1}{2}(u_{i,j}+u_{j,i}) \qquad i=1,2,3 \quad j=3 \tag{2-9}$$

or

$$\boldsymbol{\varepsilon}_L=\boldsymbol{D}_L\boldsymbol{u} \tag{2-9}'$$

3. the stress-strain equations (constitutive equations):

$$\mathbf{p} = [\,R\,]\,\mathbf{q} \tag{2 - 10}$$

4. the equilibrium equations:

$$\sigma_{ij,j}+F_i=0 \tag{2-11}$$

in which, **F** is the body force in V.

Moreover, there are three sets of boundary conditions for the displacement field and stress field.

a. the traction boundary conditions:

$$\boldsymbol{\sigma} \cdot \boldsymbol{n} = \boldsymbol{T}_n \quad and \quad \boldsymbol{T}_n = \boldsymbol{T} \tag{2-12}$$

or

$$\sigma_{ij} n_j = T_{ni} \quad and \quad T_{ni} = T_i \quad on \ S_t \tag{2-12)'}$$

in which, **T** is the prescribed surface force on S_t.

b. the displacement boundary conditions:

$$\boldsymbol{u} = \boldsymbol{d} \tag{2-13}$$

or

$$u_i = d_i \quad on \ S_d \tag{2-13)'}$$

in which, **d** is the prescribed displacement on S_d.

c. the conjunction conditions at interlayer surfaces:

$$\begin{aligned} u_i^k &= u_i^{k+1} \qquad i=1,2,3 \\ \sigma_{i3}^k &= \sigma_{i3}^{k+1} \qquad k=1,2,\ldots,N \end{aligned} \tag{2-14}$$

where N is the number of layers along the thickness of composite structures.

2.3 Composite Variational Principle

To present the composite variational principle, the composite energy has to be defined and the composite variational functional has to be derived.

2.3.1 Composite Energy

For a linear elastic body, the potential energy can be expressed as a quadratic form of strains,

$$A(\boldsymbol{u}) = \frac{1}{2}\boldsymbol{\varepsilon}^{T}[C]\,\boldsymbol{\varepsilon} \tag{2-15}$$

and the complementary energy can be expressed as a quadratic form of stress,

$$B(\boldsymbol{u}) = \frac{1}{2}\boldsymbol{\sigma}^{T}[S]\,\boldsymbol{\sigma} \tag{2-16}$$

Similarly, one can define a new energy, named *composite energy*, as a quadratic form of the globally continuous variables due to the fact that the constitutive matrix [R] is symmetric matrix (2-7),

$$E(\boldsymbol{q}) = \frac{1}{2}\boldsymbol{q}^{T}[R]\,\boldsymbol{q} \tag{2-17}$$

or

$$E=\frac{1}{2}\sum_{i=1}^{6}\sum_{j=1}^{6}R_{ij}q_iq_j \qquad (2\text{-}18)$$

Thus, the constitutive equations (2-10) can be written in the form,

$$\frac{\partial E(\boldsymbol{q})}{\partial q_i}=p_i \qquad (2\text{-}10)'$$

2.3.2 Composite Energy Functional

The variational functional based on the composite energy can be derived through different ways. Huang [41] established the variational functional by weighted residual method, Reissner [79-80] developed it using Lagrange multiplier and 'partial' Legendre transformation method, and Moriya [81] developed it through the Hu-Washizu variational principle. Lately, Pian [36] used the Hellinger-Reissner variational principle to obtain the functional. In view of simplicity, the variational functional, termed *composite energy functional,* is derived again by means of the Hellinger-Reissner variational principle in order to reveal their difference.

The Hellinger-Reissner variational principle contains two fields: displacement field and stress field. The constraint conditions are constitutive equations (2-10) and displacement boundary conditions (2-13) only. The strain-displacement equations (2-8) and (2-9),

equilibrium equations (2-11), and traction boundary conditions (2-12) are only satisfied a posteriori. Satisfying the displacement boundary conditions (2-13) a priori, the Hellinger-Reissner variational functional can be expressed as follows,

$$\Pi=\int_v [-\frac{1}{2}\boldsymbol{\sigma}^T[S]\,\boldsymbol{\sigma}+\boldsymbol{\sigma}^T(\boldsymbol{D}\boldsymbol{u})-\boldsymbol{F}^T\boldsymbol{u}]\,dV-\int_{S_t}\boldsymbol{T}^T\boldsymbol{u}\,dS \qquad (2\text{-}19)$$

in which,

$$\boldsymbol{\sigma}=\begin{Bmatrix}\boldsymbol{\sigma}_L\\ \boldsymbol{\sigma}_g\end{Bmatrix} \quad and \quad \boldsymbol{D}\boldsymbol{u}=\begin{Bmatrix}\boldsymbol{D}_g\boldsymbol{u}\\ \boldsymbol{D}_L\boldsymbol{u}\end{Bmatrix} \qquad (2\text{-}20)$$

Substituting them into the (2-19), the functional is written in the form,

$$\Pi=\int_v [-\frac{1}{2}[\boldsymbol{\sigma}_L^T\ \boldsymbol{\sigma}_g^T]\,[S]\begin{Bmatrix}\boldsymbol{\sigma}_L\\ \boldsymbol{\sigma}_g\end{Bmatrix}+[\boldsymbol{\sigma}_L^T\ \boldsymbol{\sigma}_g^T]\begin{Bmatrix}\boldsymbol{D}_g\boldsymbol{u}\\ \boldsymbol{D}_L\boldsymbol{u}\end{Bmatrix} \qquad (2\text{-}21)$$
$$-\boldsymbol{F}^T\boldsymbol{u}]\,dV-\int_{S_t}\boldsymbol{T}^T\boldsymbol{u}\,dS$$

Using the constitutive equations (2-4) to eliminate the in-plane stress σ_L , the first term in the functional becomes

$$\int_v -\frac{1}{2}[\boldsymbol{\sigma}_L^T\ \boldsymbol{\sigma}_g^T]\,[S]\begin{Bmatrix}\boldsymbol{\sigma}_L\\ \boldsymbol{\sigma}_g\end{Bmatrix}dV=\int_v(-\frac{1}{2}\boldsymbol{e}_g^T[R_1]\,\boldsymbol{e}_g+\frac{1}{2}\boldsymbol{\sigma}_g^T[R_3]\,\boldsymbol{\sigma}_g)\,dV \qquad (2\text{-}22)$$

and the second term becomes after adding and subtracting $\sigma_L^T\,\varepsilon_g$

$$\int_v [\boldsymbol{\sigma}_L^T \ \boldsymbol{\sigma}_g^T] \begin{Bmatrix} \boldsymbol{D}_g \boldsymbol{u} \\ \boldsymbol{D}_L \boldsymbol{u} \end{Bmatrix} dV = \int_v (\boldsymbol{\varepsilon}_g^T [R_1]^T \boldsymbol{\varepsilon}_g + \boldsymbol{\sigma}_g^T [R_2]^T \boldsymbol{\varepsilon}_g + \boldsymbol{\sigma}_L^T (\boldsymbol{D}_g \boldsymbol{u} - \boldsymbol{\varepsilon}_g) + \boldsymbol{\sigma}_g^T \boldsymbol{D}_L \boldsymbol{u}) \, dV \tag{2-23}$$

Substituting them into the functional (2-21), it is modified to

$$\Pi = \int_v [\frac{1}{2} \boldsymbol{q}^T [R] \boldsymbol{q} + \boldsymbol{\sigma}_L^T (\boldsymbol{D}_g \boldsymbol{u} - \boldsymbol{\varepsilon}_g) + \boldsymbol{\sigma}_g^T \boldsymbol{D}_L \boldsymbol{u} - \boldsymbol{F}^T \boldsymbol{u}] \, dV - \int_{S_t} \boldsymbol{T}^T \boldsymbol{u} \, dS \tag{2-24}$$

If the in-plane strain-displacement equations (2-8) are satisfied a priori, a new functional is obtained as follows [41],

$$\Pi_{co} = \int_v [E(\boldsymbol{q}) + \boldsymbol{\sigma}_g^T \boldsymbol{D}_L \boldsymbol{u} - \boldsymbol{F}^T \boldsymbol{u}] \, dV - \int_{S_t} \boldsymbol{T}^T \boldsymbol{u} \, dS \tag{2-25}$$

In this new variational functional, there are two fields: displacement field and partial stress field. The constraint conditions are the constitutive equations (2-10), the in-plane strain-displacement equations (2-8), and displacement boundary conditions (2-13). This new variational functional is named by *composite energy functional.* It is different from the Hellinger-Reissner variational functional because the in-plane strain-displacement equations (2-8) become constraint conditions in the new functional [9].

2.3.3 Composite Variational Principle

In order to present variational principle, it is assumed that the composite energy function E is a positive definite function of the components of globally continuous vector, and the body forces and surface forces are derivable from potential functions $\Omega(\mathbf{u})$ and $\Psi(\mathbf{u})$ such that

$$\begin{aligned} -\delta\Omega(\boldsymbol{u}) &= \boldsymbol{F}^T\delta\boldsymbol{u} \\ -\delta\Psi(\boldsymbol{u}) &= \boldsymbol{T}^T\delta\boldsymbol{u} \end{aligned} \tag{2-26}$$

Thus, the composite variational principle states

Among all the admissible displacement fields and partial stress (transverse stress) fields, which satisfy the in-plane strain-displacement equations (2-8), constitutive equations (2-10), and prescribed displacement boundary conditions (2-13), the actual displacement field and partial stress field make the total composite energy

$$\Pi_{co}=\int_v [E(\boldsymbol{q}) + \boldsymbol{\sigma}_g^T\boldsymbol{D}_L\boldsymbol{u} - \boldsymbol{F}^T\boldsymbol{u}]\,dV - \int_{S_t} \boldsymbol{T}^T\boldsymbol{u}\,dS \tag{2-25}$$

an absolute minimum $\delta\Pi_{CO}=0$.

In this principle, the transverse strain-displacement equations (2-9) and equilibrium equations (2-11) are Euler equations; prescribed traction boundary conditions (2-12) are the natural boundary conditions. For composites, the conjunction conditions at interlayer

surface (2-14) must be satisfied a priori.

2.4 General Formulation of Partial Hybrid Stress Finite Element

In chapter 1, finite elements are classified in view of the composite structure theories (laminated element, multilayer element, and solid element) and the variational principles (displacement element, hybrid element, and mixed element). Furthermore, finite elements for laminated composites can also be classified in view of the assumption of the displacement and stress fields along the thickness direction. From this point, finite elements can be divided into two categories: single-layer elements and multi-layer elements [49-50].

The single-layer element assumes a displacement field and/or a stress field over the element along the thickness direction. The number of degrees of freedom associated with the element is independent of the number of material layers within the element. If the element contains only one material layer, it is a 3-D solid element; if the element contains more than one material layer along the thickness direction, the equivalent single-layer two-dimensional model must be used to obtain single properties across the thickness of the element, and it becomes a laminated element.

On the other hand, the multi-layer element assumes many displacement fields and/or stress fields within the element. Each displacement/stress field is related to a layer along the

thickness of a laminated composite structure. The element matrices are assembled through the thickness by means of continuity conditions at the interfaces between different layers. The number of degrees of freedom in the element depends on the number of material layers in the laminated composite structure.

In this chapter, the general formulation of the partial hybrid element is presented. They will be used to formulate a few special elements in the next chapters.

2.4.1 Formulation of Partial Hybrid Single-Layer Element

The composite variational functional has been obtained in the form,

$$\Pi_{co}=\int_v [E(\boldsymbol{q}) + \boldsymbol{\sigma}_g^T \boldsymbol{D}_L \boldsymbol{u} - \boldsymbol{F}^T \boldsymbol{u}]\, dV - \int_{S_t} \boldsymbol{T}^T \boldsymbol{u}\, dS \tag{2-25}$$

in which, the composite energy is

$$E(\boldsymbol{q}) = \frac{1}{2} \boldsymbol{q}^T [R]\, \boldsymbol{q} \tag{2-17}$$

and the vector of global variables includes in-plane strains and transverse stresses,

$$\boldsymbol{q}=\begin{Bmatrix} \boldsymbol{\varepsilon}_g \\ \boldsymbol{\sigma}_g \end{Bmatrix} \tag{2-2}$$

and the layer material matrix [R] is

$$[R]=\begin{bmatrix} R_1 & R_2 \\ R_2^T & R_3 \end{bmatrix}=\begin{bmatrix} S_1^{-1} & -S_1^{-1}S_2 \\ -S_2^T S_1^{-1} & S_2^T S_1^{-1} S_2 - S_3 \end{bmatrix} \tag{2-6}$$

where [S] is the compliance matrix of layer materials. Substituting equations (2-17), (2-2) and (2-6) into equation (2-25), the functional becomes

$$\begin{aligned} \Pi_{co}=\int_v [\frac{1}{2}\boldsymbol{\varepsilon}_g^T[R_1]\boldsymbol{\varepsilon}_g+\frac{1}{2}\boldsymbol{\sigma}_g^T[R_3]\boldsymbol{\sigma}_g+\boldsymbol{\sigma}_g^T[R_2]^T\boldsymbol{\varepsilon}_g \\ +\boldsymbol{\sigma}_g^T\boldsymbol{D}_L\boldsymbol{u}-\boldsymbol{F}^T\boldsymbol{u}]\,dV-\int_{S_t}\boldsymbol{T}^T\boldsymbol{u}\,dS \end{aligned} \tag{2-27}$$

Within a single-layer finite element (see figure 2-2), a displacement field is assumed along the thickness of the element. Using isoparametric shape functions, the displacement field is described by the nodal displacement δ as follows,

$$\boldsymbol{u}=\begin{Bmatrix} u \\ v \\ w \end{Bmatrix}=[N]\,\boldsymbol{\delta} \tag{2-28}$$

where [N] is the matrix of shape functions. Thus, the partial strains are

$$\boldsymbol{\varepsilon}_g=\begin{Bmatrix} \varepsilon_x \\ \varepsilon_y \\ \varepsilon_{xy} \end{Bmatrix}=\boldsymbol{D}_g\boldsymbol{u}=\left[\frac{\partial u}{\partial x},\frac{\partial v}{\partial y},\frac{\partial u}{\partial y}+\frac{\partial v}{\partial x}\right]^T=[B_g]\,\boldsymbol{\delta} \tag{2-29}$$

and the partial derivatives are

$$\boldsymbol{D}_L\boldsymbol{u}=\left[\frac{\partial w}{\partial z},\frac{\partial w}{\partial y}+\frac{\partial v}{\partial z},\frac{\partial w}{\partial x}+\frac{\partial u}{\partial z}\right]^T=[B_L]\,\boldsymbol{\delta} \tag{2-30}$$

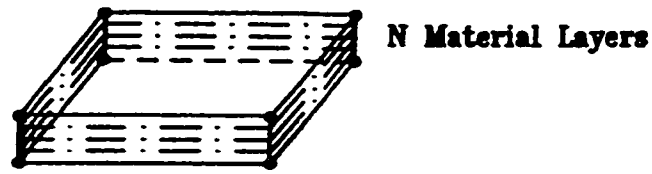

Figure 2-2 A Single-layer element

in which, $[B_g]$ is a partial geometry matrix and $[B_L]$ is a partial derivative matrix. Along the thickness of the laminates, a partial stress field is also assumed independently as

$$\sigma_g = \begin{Bmatrix} \sigma_z \\ \sigma_{yz} \\ \sigma_{zx} \end{Bmatrix} = [P_g]\,\beta = [\sigma_{g1}\sigma_{g2}\ldots\sigma_{gI}] \begin{Bmatrix} \beta_1 \\ \beta_2 \\ \cdot \\ \cdot \\ \beta_I \end{Bmatrix} \qquad (2\text{-}31)$$

where $[P_g]$ is an assumed stress matrix, σ_{gj} are the partial stress modes, and β_j are the corresponding stress parameters. If the composite structure consists of N material layers, substituting equations (2-28)-(2-31) into the composite variational functional (2-27), the functional becomes

$$\begin{aligned}\Pi_{co}=\sum_{i=1}^{N}\{&\frac{1}{2}\boldsymbol{\delta}^T\int_V [B_g]^T[R_1^i]\,[B_g]\,dV\,\boldsymbol{\delta}\\&+\frac{1}{2}\boldsymbol{\beta}^T\int_V [P_g]^T[R_3^i]\,[P_g]\,dV\,\boldsymbol{\beta}\\&+\boldsymbol{\beta}^T\int_V [P_g]^T([B_L]+[R_2^i]^T[B_g])\,dV\,\boldsymbol{\delta}\}\\&-\boldsymbol{\delta}^T\int_V [N]^T\boldsymbol{F}^i dV\;\;-\boldsymbol{\delta}^T\int_S [N]^T\boldsymbol{T}^i dS\end{aligned} \tag{2-32}$$

Denote

$$\begin{aligned}[H]&=-\sum_{i=1}^{N}\int_V[P_g]^T[R_3^i]\,[P_g]\,dV\\[G]&=\sum_{i=1}^{N}\int_V[P_g]^T([B_L]+[R_2^i]^T[B_g])\,dV\\[K_d]&=\sum_{i=1}^{N}\int_V[B_g]^T[R_1^i]\,[B_g]\,dV\\\boldsymbol{f}&=\sum_{i=1}^{N}\int_V [N]^T\boldsymbol{F}^i dV+\int_S [N]^T\boldsymbol{T}^i dS\end{aligned} \tag{2-33}$$

Note that, when the number of material layers is more than one, the variation in fibre orientations and material properties across the thickness of the element is integrated to obtain a single property across the thickness. Therefore, the size of the element matrices does not depend on the number of material layers in the element. Then, the functional can be expressed as

$$\Pi_{co}=\frac{1}{2}\boldsymbol{\delta}^T[K_d]\,\boldsymbol{\delta}-\frac{1}{2}\boldsymbol{\beta}^T[H]\,\boldsymbol{\beta}+\boldsymbol{\beta}^T[G]\,\boldsymbol{\delta}-\boldsymbol{\delta}^T\boldsymbol{f} \tag{2-34}$$

In this variational functional, there are two independent variables subject to variation. From the two partial stationary conditions with respect to β and δ as follows,

$$\frac{\partial \Pi_{co}}{\partial \boldsymbol{\beta}} = 0 \qquad and \qquad \frac{\partial \Pi_{co}}{\partial \boldsymbol{\delta}} = 0 \tag{2-35}$$

the relation between stress parameters β and nodal displacements δ is obtained,

$$[H]\,\boldsymbol{\beta} = [G]\,\boldsymbol{\delta} \tag{2-36}$$

and

$$[K_d]\,\boldsymbol{\delta} + [G]^T\boldsymbol{\beta} = \boldsymbol{f} \tag{2-37}$$

The equation (2-36) can be expressed in the form,

$$\boldsymbol{\beta} = [H]^{-1}[G]\,\boldsymbol{\delta} \tag{2-38}$$

At this point, one can say that, as nodal displacements are prescribed, the partial stress field within the element has been obtained by finding the value of β that define the best stress field (2-31). Eliminating β in equation (2-37) using (2-38), one obtains

$$\left([K_d] + [G]^T [H]^{-1} [G] \right) \boldsymbol{\delta} = \boldsymbol{f} \tag{2-39}$$

Denote

$$[K_h] = [G]^T [H]^{-1} [G]$$
$$[K] = [K_d] + [K_h] \qquad (2\text{-}40)$$

in which, the semi-stiffness matrix $[K_d]$ is a displacement-formulated stiffness matrix based on the globally continuous strains, and the semi-stiffness matrix $[K_h]$ is a hybrid-formulated stiffness matrix based on the globally continuous stresses. Then, the governing equation of the element is obtained,

$$[K]\,\boldsymbol{\delta} = \boldsymbol{f} \qquad (2\text{-}41)$$

where [K] is the element stiffness matrix. For the partial hybrid element, the element stiffness matrix consists of a displacement-formulated stiffness matrix $[K_d]$ and a hybrid-formulated stiffness matrix $[K_h]$. In the single-layer element, the size of the element matrix [K] is not related to the number of material layers within the element. If there are more than one material layer, the single-layer element is a laminated element; if there is only one layer in the element, the element becomes a 3-D solid element.

After obtaining the nodal displacement δ in a finite element model, the displacement field, stress field, and strain field can be obtained using the following equations:

1. Displacement field

$$\boldsymbol{u}=\begin{Bmatrix} U \\ V \\ W \end{Bmatrix} = [N]\,\boldsymbol{\delta} \tag{2-28}$$

2. Partial globally continuous strains

$$\boldsymbol{\varepsilon_g}=\begin{Bmatrix} \varepsilon_x \\ \varepsilon_y \\ \varepsilon_{xy} \end{Bmatrix} = \boldsymbol{D_g u} = [B_g]\,\boldsymbol{\delta} \tag{2-29}$$

3. Partial globally continuous stresses

$$\boldsymbol{\beta} = [H]^{-1}[G]\,\boldsymbol{\delta} \tag{2-38}$$

and

$$\boldsymbol{\sigma_g}=\begin{Bmatrix} \sigma_z \\ \sigma_{yz} \\ \sigma_{zx} \end{Bmatrix} = [P_g]\,\boldsymbol{\beta} = [P_g]\,[H]^{-1}[G]\,\boldsymbol{\delta} \tag{2-31}$$

4. Partial locally continuous stresses within i-th layer

$$\begin{aligned} \boldsymbol{\sigma_L^i}=\begin{Bmatrix} \sigma_x \\ \sigma_y \\ \sigma_{xy} \end{Bmatrix} &= [R_1^i]\,\boldsymbol{\varepsilon_g} + [R_2^i]\,\boldsymbol{\sigma_g} \\ &= \{[R_1^i]\,[B_g] + [R_2^i]\,[P_g]\,[H]^{-1}[G]\}\boldsymbol{\delta} \\ &= \{[S_1^i]^{-1}[B_g] + [C_2^i]\,[C_3^i]^{-1}[P_g]\,[H]^{-1}[G]\}\boldsymbol{\delta} \end{aligned} \tag{2-42}$$

5. Partial locally continuous strains within i-th layer

$$\begin{aligned}
\boldsymbol{\varepsilon}_L^i &= \begin{Bmatrix} \varepsilon_z \\ \varepsilon_{yz} \\ \varepsilon_{zx} \end{Bmatrix} = -[R_2^i]^T \boldsymbol{\varepsilon}_g - [R_3^i]\,\boldsymbol{\sigma}_g \\
&= \{-[R_2^i]^T[B_g] - [R_3^i]\,[P_g]\,[H]^{-1}[G]\}\boldsymbol{\delta} \\
&= \{[S_2^i]^T[S_1^i]^{-1}[B_g] + [C_3^i]^{-1}[P_g]\,[H]^{-1}[G]\}\boldsymbol{\delta}
\end{aligned} \tag{2-43}$$

For convenience, all element matrices are given here again,

$$\begin{aligned}
[K] &= [K_d] + [K_h] \\
[K_d] &= \sum_{i=1}^{N} \int_V [B_g]^T [R_1^i]\,[B_g]\,dV \\
[K_h] &= [G]^T [H]^{-1} [G] \\
[H] &= -\sum_{i=1}^{N} \int_V [P_g]^T [R_3^i]\,[P_g]\,dV \\
[G] &= \sum_{i=1}^{N} \int_V [P_g]^T ([B_L] + [R_2^i]^T [B_g])\,dV \\
\boldsymbol{f} &= \sum_{i=1}^{N} \int_V [N]^T \boldsymbol{F}^i dV + \int_S [N]^T \boldsymbol{T}^i dS
\end{aligned} \tag{2-44}$$

These general equations of the single-layer elements will be used to develop two degenerated plate elements in Chapter 4, two 3-D solid elements in Chapter 5, and two transition elements in Chapter 6.

2.4.2 Formulation of Partial Hybrid Multilayer Element

Usually, a multilayer element consists of a stack of sub-elements. According to the distribution of the material layers, a composite structure is divided into many sub-layers along the thickness and each sub-layer is modeled by a sub-element. The matrices of sub-elements are firstly formulated, and they are assembled through the thickness using continuity conditions at the interfaces between different sub-elements to form the multilayer element matrices. Therefore, there are two steps to obtain a multilayer element matrix: the first is to formulate the sub-element matrices and the second is to assemble them to form a multilayer element matrix.

In the above section, the composite variational functional has been expressed in the form,

$$\Pi_{co}=\int_v [\frac{1}{2}\boldsymbol{e}_g^T[R_1]\,\boldsymbol{e}_g+\frac{1}{2}\boldsymbol{\sigma}_g^T[R_3]\,\boldsymbol{\sigma}_g+\boldsymbol{\sigma}_g^T[R_2]^T\boldsymbol{e}_g +\boldsymbol{\sigma}_g D_L\boldsymbol{u}-\boldsymbol{F}^T\boldsymbol{u}]\,dV-\int_{S_\sigma}\boldsymbol{T}^T\boldsymbol{u}\,dS \tag{2-27}$$

If a composite structure contains N different material layers, the multilayer element will consist of N sub-elements (see figure 2-3). Therefore, the variational functional becomes

$$\Pi_{co}=\sum_{i=1}^{N}\int_v [\frac{1}{2}\boldsymbol{e}_g^{iT}[R_1^i]\,\boldsymbol{e}_g^i+\frac{1}{2}\boldsymbol{\sigma}_g^{iT}[R_3^i]\,\boldsymbol{\sigma}_g^i+\boldsymbol{\sigma}_g^{iT}[R_2^i]^T\boldsymbol{e}_g^i +\boldsymbol{\sigma}_g^{iT}D_L\boldsymbol{u}^i-\boldsymbol{F}^T\boldsymbol{u}^i]\,dV-\int_S\boldsymbol{T}^T\boldsymbol{u}^i\,dS \tag{2-45}$$

Sub-Element Matrices

In multilayer element, the displacement field and the partial stress field must be assumed within each sub-element. Suppose the displacement fields in different sub-elements have the same expression form, and the partial stress field in different sub-elements have the same expression form. Thus, for the i-th sub-element, the displacement field can be assumed as

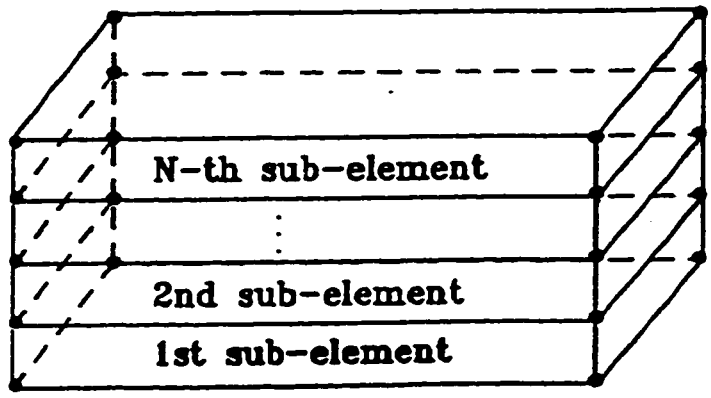

Figure 2-3 A multilayer element

$$u^i = \begin{Bmatrix} U^i \\ V^i \\ W^i \end{Bmatrix} = [N]\,\delta^i \qquad (2\text{-}46)$$

where [N] is the matrix of shape functions. Then, the partial strains are

$$\boldsymbol{\varepsilon}_g^i=\begin{Bmatrix}\varepsilon_x^i\\ \varepsilon_y^i\\ \varepsilon_{xy}^i\end{Bmatrix}=\boldsymbol{D}_g\boldsymbol{u}^i=\left[\frac{\partial u^i}{\partial x},\frac{\partial v^i}{\partial y},\frac{\partial u^i}{\partial y}+\frac{\partial v^i}{\partial x}\right]^T=[B_g]\,\boldsymbol{\delta}^i \qquad (2\text{-}47)$$

and the partial derivatives are

$$\boldsymbol{D}_L\boldsymbol{u}^i=\left[\frac{\partial w^i}{\partial z},\frac{\partial w^i}{\partial y}+\frac{\partial v^i}{\partial z},\frac{\partial w^i}{\partial x}+\frac{\partial u^i}{\partial z}\right]^T=[B_L]\,\boldsymbol{\delta}^i \qquad (2\text{-}48)$$

in which, $[B_g]$ is a partial geometry matrix and $[B_L]$ is a partial derivative matrix. Along the thickness of the sub-element, a partial stress field is also assumed independently as

$$\boldsymbol{\sigma}_g^i=\begin{Bmatrix}\sigma_z^i\\ \sigma_{yz}^i\\ \sigma_{zx}^i\end{Bmatrix}=[P_g]\,\boldsymbol{\beta}^i=[\sigma_{g1}\ \sigma_{g2}\ldots\sigma_{gI}]\begin{Bmatrix}\beta_1^i\\ \beta_2^i\\ .\\ .\\ \beta_I^i\end{Bmatrix} \qquad (2\text{-}49)$$

where $[P_g]$ is an assumed stress matrix, $\{\sigma_{gj}\}$ are partial stress modes, and β_j^i are stress parameters. Substituting equations (2-46)-(2-49) into the composite energy functional (2-45), the functional becomes

$$\begin{aligned}\Pi_{co}=\sum_{i=1}^{N}\{&\frac{1}{2}\boldsymbol{\delta}^{iT}\int_V[B_g]^T[R_1^i]\,[B_g]\,dV\,\boldsymbol{\delta}^i\\ &+\frac{1}{2}\boldsymbol{\beta}^{iT}\int_V[P_g]^T[R_3^i]\,[P_g]\,dV\,\boldsymbol{\beta}^i\\ &+\boldsymbol{\beta}^{iT}\int_V[P_g]^T([B_L]+[R_2^i]^T[B_g])\,dV\,\boldsymbol{\delta}^i\\ &-\boldsymbol{\delta}^{iT}\int_V[N]^T\boldsymbol{F}dV\ -\boldsymbol{\delta}^{iT}\int_{S_c}[N]^T\boldsymbol{T}dS\ \}\end{aligned} \qquad (2\text{-}50)$$

Denote

$$
\begin{aligned}
[H^i] &= -\int_V [P_g]^T [R_3^i]\ [P_g]\, dV \\
[G^i] &= \int_V [P_g]^T ([B_L] + [R_2^i]^T [B_g])\, dV \\
[K_d^i] &= \int_V [B_g]^T [R_1^i]\ [B_g]\, dV \\
\mathbf{f}^i &= \int_V [N]^T \mathbf{F} dV + \int_{S_t} [N]^T \mathbf{T} dS
\end{aligned}
\tag{2-51}
$$

The matrices in the equation (2-51) are the sub-element matrices. They will be assembled using continuity conditions at the interfaces between different sub-elements.

Multilayer Element Matrices

Using the expression (2-51), the variational functional (2-50) can be expressed as

$$
\begin{aligned}
\Pi_{co} = \sum_{i=1}^{N} \Big(& \frac{1}{2} \boldsymbol{\delta}^{iT} [K_d^i]\, \boldsymbol{\delta}^i - \frac{1}{2} \boldsymbol{\beta}^{iT} [H^i]\, \boldsymbol{\beta}^i \\
& + \boldsymbol{\beta}^{iT} [G^i]\, \boldsymbol{\delta}^i - \boldsymbol{\delta}^{iT} \mathbf{f}^i \Big)
\end{aligned}
\tag{2-52}
$$

In this variation functional, the stress parameters β_j^i in equation (2-49) are internal parameters, called layer stress parameters. They are not independent and the sub-element matrices can not be assembled based on these layer stress parameters. Therefore, they must be replaced by independent parameters. There are two ways to formulate multilayer matrices: one is to introduce a group of laminated stress parameters [33,105], and another is to introduce a group of surface stress parameters[42-43]. Laminated stress parameters or surface stress parameters are a group of independent parameters. By means of the

continuity conditions at interfaces between different sub-elements, the layer stress parameters β^i can be replaced by the laminate stress parameter β or the surface stress parameters α. Then, the sub-element matrices can be assembled to form multilayer matrices. The operations to assemble the sub-element matrices are analogous to element 'assembly' operations; a set of layer-to-laminate stress parameter 'pointers' and nodal displacement 'pointers' are used to locate (and add in) sub-element matrix contributions in the multilayer element matrices.

In the two approaches above, it is necessary to transfer internal stress parameters (or layer stress parameters) to surface stress parameters (or laminate stress parameters). However, if surface stress parameters are used directly in the assumed partial stress field (2-49), the transformation will be not necessary. One can assume a partial stress field in the following form,

$$\sigma_g^i = [P_g]\,\phi^i = [P]\,\frac{1}{2}\left\{(1+\zeta)\,\alpha_T^i + (1-\zeta)\,\alpha_B^i\right\} \qquad (2\text{-}53)$$

where α_T^i and α_B^i are the surface stress parameters corresponding to upper and lower surfaces of the i-th sub-element, respectively. In this expression, a stress mode σ_j in the matrix [P] is related to both of upper and lower surfaces α_T^i and α_B^i and corresponds to two stress modes $0.5*(1+\zeta)*\sigma_j$ and $0.5*(1-\zeta)*\sigma_j$ in the assumed stress matrix $[P_g]$. The matrix [P] is determined by displacement polynomials, iso-function method, and classification method. At the interface between the sub-element i and i+1, the surface stress parameters α_T^i is the same as α_B^{i+1} . This means:

$$\alpha_T^i = \alpha_B^{i+1} \tag{2-54}$$

Furthermore, the continuity condition at interface of the laminated structure can be expressed as:

$$\sigma_g^i|_{\zeta^i=1} = \sigma_g^{i+1}|_{\zeta^{i+1}=-1} \tag{2-55}$$

Thus, one can obtain the condition

$$[P]\,|_{\zeta^i=+1} = [P]\,|_{\zeta^{i+1}=-1} \tag{2-56}$$

Therefore, the matrix [P] must be a function consisted of even order terms of the coordinate ζ. In order to assemble all the sub-elements in the multilayer element, define the assembling rule as

$$\boldsymbol{\delta} = \sum_{i=1}^{N} \boldsymbol{\delta}^i = [\boldsymbol{d}^1 \;\; \boldsymbol{d}^2 \;\; \ldots \;\; \boldsymbol{d}^{N+1}]^T \tag{2-57}$$

where $\mathbf{d}^k$ is the nodal displacement vector at the k-th surface, and

$$\boldsymbol{\varphi} = \sum_{i=1}^{N} \boldsymbol{\alpha}^i = [\boldsymbol{\alpha}^1 \;\; \boldsymbol{\alpha}^2 \;\; \ldots \;\; \boldsymbol{\alpha}^{N+1}]^T \tag{2-58}$$

Applying these assembling rules, the multilayer element matrices are obtained by

$$[K_d] = \sum_{i=1}^{N} [K_d^i] \qquad [H] = \sum_{i=1}^{N} [H^i]$$
$$[G] = \sum_{i=1}^{N} [G^i] \qquad \boldsymbol{f} = \sum_{i=1}^{N} \boldsymbol{f}^i \tag{2-59}$$

Summations indicate assembly of sub-element matrices by addition of overlapping terms. Thus, the variational functional (2-52) becomes

$$\Pi_{co} = \frac{1}{2}\boldsymbol{\delta}^T [K_d] \boldsymbol{\delta} - \frac{1}{2}\boldsymbol{\varphi}^T [H] \boldsymbol{\varphi} + \boldsymbol{\varphi}^T [G] \boldsymbol{\delta} - \boldsymbol{\delta}^T \boldsymbol{f} \tag{2-60}$$

Similar to single-layer element, the stiffness matrix of the multilayer element can be derived using the variational principle of composite energy,

$$[K] = [K_d] + [K_h]$$
$$[K_h] = [G]^T [H]^{-1} [G] \tag{2-61}$$

in which, [K] is the element stiffness matrix, the semi-stiffness matrix $[K_d]$ is a displacement-formulated stiffness matrix based on the globally continuous strains, and the semi-stiffness matrix $[K_h]$ is a hybrid-formulated stiffness matrix based on the globally continuous stresses. Then, the governing equation of the multilayer element is

$$[K] \boldsymbol{\delta} = \boldsymbol{f} \tag{2-62}$$

After obtaining the nodal displacement δ by means of system equations, the displacement field, stress field, and strain field can be obtained using the following equations:

1. Displacement field

$$\boldsymbol{u}^{i}=\begin{Bmatrix} u^{i} \\ v^{i} \\ w^{i} \end{Bmatrix}=[N]\,\boldsymbol{\delta}^{i} \tag{2-46}$$

2. Partial globally continuous strains

$$\boldsymbol{\varepsilon}_{g}^{i}=\begin{Bmatrix} \varepsilon_{x}^{i} \\ \varepsilon_{y}^{i} \\ \varepsilon_{xy}^{i} \end{Bmatrix}=\boldsymbol{D}_{g}\boldsymbol{u}^{i}=[B_{g}]\,\boldsymbol{\delta}^{i} \tag{2-47}$$

3. Partial globally continuous stresses

$$\boldsymbol{\varphi}=[H]^{-1}[G]\,\boldsymbol{\delta} \tag{2-63}$$

$$\boldsymbol{\sigma}_{g}^{i}=\begin{Bmatrix} \sigma_{z}^{i} \\ \sigma_{yz}^{i} \\ \sigma_{zx}^{i} \end{Bmatrix}=[P_{g}]\,\boldsymbol{\phi}^{i} \tag{2-53}$$

4. Partial locally continuous stresses within i-th layer

$$\boldsymbol{\sigma}_{L}^{i}=\begin{Bmatrix} \sigma_{x}^{i} \\ \sigma_{y}^{i} \\ \sigma_{xy}^{i} \end{Bmatrix}=[R_{1}^{i}]\,\boldsymbol{\varepsilon}_{g}^{i}+[R_{2}^{i}]\,\boldsymbol{\sigma}_{g}^{i} \tag{2-64}$$

5. Partial locally continuous strains within i-th layer

$$\boldsymbol{\varepsilon}_L^i=\begin{Bmatrix}\varepsilon_z^i\\ \varepsilon_{yz}^i\\ \varepsilon_{zx}^i\end{Bmatrix}=-[R_2^i]^T\boldsymbol{\varepsilon}_g^i-[R_3^i]\boldsymbol{\sigma}_g^i \tag{2-65}$$

For convenience, all element matrices are given here again,

$$\begin{aligned}
&[K]=[K_d]+[K_h]\\
&[K_h]=[G]^T[H]^{-1}[G]\\
&[K]_d=\sum_{i=1}^{N}[K_d^i] \qquad [H]=\sum_{i=1}^{N}[H^i]\\
&[G]=\sum_{i=1}^{N}[G^i] \qquad \boldsymbol{f}=\sum_{i=1}^{N}\boldsymbol{f}^i\\
&[H^i]=-\int_V[P_g]^T[R_3^i]\,[P_g]\,dV\\
&[G^i]=\int_V[P_g]^T([B_L]+[R_2^i]^T[B_g])\,dV\\
&[K_d^i]=\int_V[B_g]^T[R_1^i]\,[B_g]\,dV\\
&\boldsymbol{f}^i=\int_V[N]^T\boldsymbol{F}dV+\int_{S_c}[N]^T\boldsymbol{T}dS
\end{aligned} \tag{2-66}$$

These general equations of the multilayer elements will be used to develop two multilayer elements in Chapter 7.

Chapter 3

CLASSIFICATION METHOD

For hybrid stress elements, the displacement interpolation functions are determined by the number of degrees of freedom associated with the elements. However, the stress interpolation functions are not constrained by it. It is possible to present many stress interpolation functions for a type of hybrid stress element. In order to find optimal stress polynomials, this chapter presents a classification method to determine stress polynomials. For the purpose of a clear presentation, it is useful to give the definitions of the stress field, stress mode, stress matrix, natural deformation mode, rigid body mode, zero-energy stress mode, kinematic deformation mode, and stress mode group at the beginning of the chapter.

Stress field:

In the hybrid formulation, a stress field is assumed independently from the beginning,

$$\sigma = [\, P \,]\, \beta \tag{3-1}$$

It can be expressed in the form

$$\sigma = [\, \sigma_1 \; \sigma_2 \; \ldots \; \sigma_m \,] \begin{Bmatrix} \beta_1 \\ \beta_2 \\ . \\ . \\ \beta_m \end{Bmatrix} \tag{3-2}$$

In which, the parameters β_i are the stress parameters.

Stress modes:

Stress modes are vectors which are functions of the coordinates. For example, vectors $\{\sigma_i\}$ in equation (3-2) are stress modes.

Stress matrix:

An assumed stress matrix consists of several stress modes. In equation (3-1), the matrix [P] is a stress matrix.

Natural deformation modes:

Deformation modes in an element that are independent from each other. In this thesis, the eigenvectors of an element stiffness matrix are regarded as the natural deformation modes of the element.

Rigid body modes:

Rigid body modes are displacement modes in an element that do not produce deformation energy.

Zero-energy stress modes:

Stress modes in the stress matrix of a hybrid element that do not produce deformation energy. The eigenvalues of the element stiffness matrix corresponding to these stress modes equal zero. These zero-energy stress modes correspond to rigid body modes.

Kinematic deformation modes:

Deformation modes in an element corresponding to spurious zero stiffness may be caused by unsuitable numerical integration technique or unsuitable assumed stress fields. In this work, it is assumed that suitable numerical integration technique is used. Even though zero-energy stress modes may not appear in the stress matrix, spurious zero stiffness mode can occur. This happens when more than one stress mode is picked from one eligible stress mode group. This zero stiffness mode is called kinematic deformation mode in this work. The exception for this case is when the stress modes are interchangeable between different stress mode groups. This exception is discussed in section 3.5 of this chapter.

Stress mode group:

A stress mode group contains many stress modes that are interchangeable in the stress matrix [P] and does not cause kinematic deformation modes. The m stress mode groups

correspond to m natural deformation modes and the zero-energy stress mode group corresponds to rigid body modes.

If an element has n degrees of freedom, its nodal displacement vector must consist of n components. The displacement distribution in the element can be represented by m (=n-r) natural deformation modes and r rigid body modes. In this work, it will be shown that the m natural deformation modes can be used to classify stress modes in various assumed stress fields for a hybrid element. All existing stress modes are classified into m (=n-r) stress mode groups corresponding to m natural deformation modes and a zero-energy stress mode group corresponding to rigid body modes in the element.

3.1 Hybrid Stress Element

The Hellinger-Reissner variational principle contains two fields: displacement field and stress field. Satisfying the displacement boundary conditions (2-13) a priori, the variational functional (2-19) is,

$$\Pi=\int_v[-\frac{1}{2}\boldsymbol{\sigma}^T[S]\boldsymbol{\sigma}+\boldsymbol{\sigma}^T(D\boldsymbol{u})-\boldsymbol{F}^T\boldsymbol{u}]dV-\int_{S_t}\boldsymbol{T}^T\boldsymbol{u}\ dS \qquad (2\text{-}19)$$

in which, [S] is the material properties matrix relating stresses to strains. Within the element, an assumed displacement field is assumed,

$$u = [N_1\ N_2\ \ldots\ N_n]\begin{Bmatrix}\delta_1\\ \delta_2\\ \ldots\\ \delta_n\end{Bmatrix} \qquad (3\text{-}3)$$

$$=[N]\boldsymbol{\delta}$$

where [N] is the shape functions and δ is a nodal displacement vector. At the same time, a stress field is also assumed independently in the form of equation (3-2). Thus, the derivatives of the displacements are

$$\boldsymbol{Du}=[B]\boldsymbol{\delta} \qquad (3\text{-}4)$$

where [B] is the geometry matrix relating strains to displacements. Substituting equations (3-2)-(3-4) into the functional (2-19), it is transformed to

$$\Pi=-\frac{1}{2}\boldsymbol{\beta}^T\left(\int_v [P]^T[S][P]dV\right)\boldsymbol{\beta}+\boldsymbol{\beta}^T\left(\int_v [P]^T[B]dV\right)\boldsymbol{\delta}$$

$$-\boldsymbol{\delta}^T\left(\int_v [N]^T\boldsymbol{F}\ dV+\int_{S_t} [N]^T\boldsymbol{T}\ dS\right) \qquad (3\text{-}5)$$

Denote

$$[H]=\int_v [P]^T[S][P]dV$$

$$[G]=\int_v [P]^T[B]dV \qquad (3\text{-}6)$$

$$f=\int_v [N]^T F\ dV+\int_{S_t} [N]^T T\ dS$$

where [H] is the flexibility matrix, [G] is the leverage matrix, and **f** is the equivalent nodal force vector. Thus, the functional (3-5) can be rewritten in the form,

$$\Pi=-\frac{1}{2}\boldsymbol{\beta}^T[H]\boldsymbol{\beta}+\boldsymbol{\beta}^T[G]\boldsymbol{\delta}-\boldsymbol{\delta}^T f \qquad (3\text{-}7)$$

In this variational functional, there are two independent variables β and δ subject to variation. From the partial stationary condition with respect to β,

$$\frac{\partial \Pi}{\partial \boldsymbol{\beta}}=0 \qquad (3\text{-}8)$$

the relation between stress parameters β and nodal displacements δ is obtained,

$$[H]\boldsymbol{\beta}=[G]\boldsymbol{\delta} \qquad (3\text{-}9)$$

By means of this relation, then, the functional (3-7) becomes

$$\Pi=\frac{1}{2}\boldsymbol{\delta}^T([G]^T[H]^{-1}[G])\boldsymbol{\delta}-\boldsymbol{\delta}^T f \qquad (3\text{-}10)$$

It can be rewritten as

$$\Pi=\frac{1}{2}\boldsymbol{\delta}^T[K]\boldsymbol{\delta}-\boldsymbol{\delta}^T f \tag{3-11}$$

in which, [K] is the element stiffness matrix. It can be expressed in the form,

$$[K]=[G]^T[H]^{-1}[G] \tag{3-12}$$

From the partial stationary condition with respect to δ, the governing equation of the element is obtained,

$$[K]\ \boldsymbol{\delta}=f \tag{3-13}$$

When the element equations are obtained, the system equations of the finite element model for analysis of structures can be established. After solving the system equation, the displacement field is obtained by finding the value of δ that define the best displacement field (3-3). And then, the stress field is also obtained by finding the value of β that define the best stress field (3-2) within the elements.

3.2 Classification Method

The hybrid formulation based on the Hellinger-Reissner principle relaxes the stress equilibrium condition. The stress field would satisfy the equilibrium equations only in a variational sense. Since 1964, many assumed stress fields have been proposed for 2-D, 4-node hybrid stress plane element and 3-D, 8-node hybrid stress solid element. For

example, Pian [70] proposed an assumed stress field for 2-D, 4-node plane element and another for 3-D, 8-node solid element. Punch and Atluri [68-69] gave two assumed stress fields for 2-D, 4-node plane element, and eight assumed stress fields for 3-D, 8-node solid element. Huang [41] presented an assumed stress field for 3-D, 8-node solid element. Although each of these assumed stress fields may contain the same number of stress modes, the stress modes in these fields are different. In order to study the relationship between different stress modes, the concept of natural deformation modes is used.

A finite element has a finite number of degrees of freedom. For instance, a 2-D, 4-node displacement element has (n=) 8 degrees of freedom, and a 3-D, 8-node displacement element has (n=) 24 degrees of freedom. In an element, there exist (n-r) natural deformation modes and r rigid body modes. The displacement distribution in the element can be represented by them. The equilibrium equation of a displacement element is

$$[K]\boldsymbol{\delta} = \boldsymbol{f} \tag{3-14}$$

If the nodal force vector is proportional to the nodal displacement vector, the equilibrium equation becomes a eigenvalue equation. It can be expressed as follows

$$([K]-\lambda[I])\boldsymbol{\delta} = 0 \tag{3-15}$$

[K] is an n×n element stiffness matrix. This equation will give (n-r) non-zero eigenvalues and r zero eigenvalues, and (n-r) eigenvectors corresponding to the (n-r) non-zero

eigenvalues. The (n-r) eigenvectors δ_i (i=1,2,3, ... m) depend only on the geometry and material properties of the element, and they are unique. If vectors δ_i (i=1,2,...m) are the eigenvectors of the stiffness matrix [K], they must satisfy the condition:

$$\begin{aligned} \boldsymbol{\delta}_i^T \boldsymbol{\delta}_j &= 0 \qquad i \neq j \\ \boldsymbol{\delta}_i^T \boldsymbol{\delta}_j &= 1 \qquad i = j \end{aligned} \tag{3-16}$$

In this work, these eigenvectors are considered to be the natural deformation modes of the element. They can represent the deformation in the element.

In the hybrid element, the eigenvectors and eigenvalues of the stiffness matrix will be sensitive to the assumed stress modes. The eigenvalue examination will give r zero eigenvalues corresponding to rigid body mode and m (= n-r) non-zero eigenvalues corresponding to natural deformation modes if the assumed stress field is suitable. For a hybrid element, if stress modes can be classified, there exist at least m stress mode groups because the stiffness matrix of hybrid element must have m non-zero eigenvalues, except zero-energy stress mode group. Otherwise, the hybrid element will contain kinematic deformation modes. On the other hand, no matter how many stress modes there are in a stress matrix [P], the maximum number of non-zero eigenvalues of an element stiffness matrix is always equal to or less than m. Therefore, the number of stress mode groups is equal to or less than m. Thus, it can be considered that there exist and only exist m stress mode groups except zero-energy modes. All stress modes in various assumed stress matrices can be classified into the m stress mode groups corresponding to m natural

deformation modes and the zero-energy stress mode group corresponding to rigid body modes [106].

Postulate:

There exist and only exist m (=n-r) natural deformation modes in a hybrid element. All stress modes in assumed stress matrices can be classified into m stress mode groups corresponding to m natural deformation modes and a zero energy mode group corresponding to rigid body modes of the element which has n degrees of freedom and r rigid body modes.

Based on this postulate, it can be considered that an assumed stress field can be represented by stress modes in the m stress mode groups related to m natural deformation modes, except zero-energy stress modes. This can be expressed as follows,

$$\boldsymbol{\sigma} = [P]\boldsymbol{\beta} = [\,\sigma_1, \sigma_2, \ldots, \sigma_m\,] \begin{Bmatrix} \beta_1 \\ \beta_2 \\ \vdots \\ \beta_m \end{Bmatrix} = \sum_{i=1}^{m} [P_i]\boldsymbol{\beta}_i \tag{3-17}$$

where σ_i is the representative stress mode of the i-th stress mode group, and $[P_i]$ and β_i (i=1,2,...m) are the stress matrices and stress-coefficient vectors related to the i-th stress mode group which corresponds to the i-th natural deformation mode. They are

$$[P_i] = [\,0 \ldots 0, \sigma_i, 0 \ldots 0] \tag{3-18}$$

and

$$\boldsymbol{\beta}_i=[\ 0\ \ldots\ 0\ \beta_i\ 0\ \ldots\ 0]^T \tag{3-19}$$

The stress mode which belongs to the i-th stress mode group can be expressed in the form,

$$\boldsymbol{\sigma}_i = [P]\boldsymbol{\beta}_i \tag{3-20}$$

Therefore, the vector β_i can be used to identify the i-th stress mode group which corresponds to the natural deformation mode δ_i (i=1,2,..m). Using equation (3-9), one has

$$[H]\ \boldsymbol{\beta}_i=[G]\ \boldsymbol{\delta}_i \tag{3-21}$$

If the stress matrix [P] does not contain any stress mode which belongs to the i-th stress mode group, the value of β_i in the vector β_i should be equal to zero. Then, one can add a new stress mode into the stress matrix [P]. The new stress mode will be classified by m natural deformation modes. Corresponding to the i-th natural deformation mode δ_i, the condition to check whether the new stress mode belongs to the i-th stress mode group can be expressed in the form,

$\beta_i = 0$ if new stress mode does not belong to i-th stress mode group

$\beta_i \neq 0$ if new stress mode belongs to i-th stress mode group

Using equations (3-15), (3-16), and (3-21), the eigenvalues are obtained as follows,

$$\lambda_i=\boldsymbol{\delta}_i^T[K]\boldsymbol{\delta}_i=\boldsymbol{\beta}_i^T[H]\boldsymbol{\beta}_i \tag{3-22}$$

Because the flexibility matrix [H] is symmetric and positive, all of the diagonal elements in the matrix [H] may not be equal to zero. Thus, the classification condition above becomes

$\lambda_i = 0$ if new stress mode does not belong to i-th stress mode group

$\lambda_i \neq 0$ if new stress mode belongs to i-th stress mode group

Before classifying stress modes, one can find a number of initial stress modes since there are many ways to derive assumed stress matrices for a hybrid element. For example, Pian and Chen [70] used the product $\{\sigma\}^T\{\varepsilon\}$ to determine the necessary assumed stress modes, and gave an assumed stress matrix for 2-D, 4-node plane element and another for 3-D, 8-node solid element. Punch and Atluri [68-69] used group theory to obtain two assumed stress matrices for 2-D, 4-node hybrid element, eight assumed stress matrices for 3-D, 8-node hybrid element, and three hundred eighty four assumed stress matrices for 3-D, 20-node hybrid element. One can also derive an assumed stress matrix using iso-function method[43]. However, the number of the stress modes is large in the iso-function stress matrix which is derived directly from displacement field using iso-function method. According to the limitation principle [66] in Chapter 1, a hybrid stress element constructed by the iso-function stress matrix is equivalent to its displacement counterpart due to the fact that the iso-function stress field is a displacement-derived stress field.

In order to present a systematic procedure for classifying stress modes and constructing assumed stress fields, the iso-function method[43] is used to derive initial stress modes to be classified in this work. This is because the hybrid element constructed by the iso-

function stress matrix has the same eigenvalues and eigenvectors as its displacement counterpart. Also, the method using iso-function is straightforward and can be followed easily. After obtaining initial stress modes, one can use eigenvalue examination to find m representative stress modes that represent m stress mode groups corresponding to m natural deformation modes. The stress matrix consisted of the m representative stress modes is an optimal stress matrix. Then, all existing stress modes can be classified into m+1 stress mode groups. This procedure is presented in the following text [106].

3.2.1 Determination of optimal stress matrix from the iso-function stress matrix

Step 1:

Derive an initial stress matrix $[P]_{iso}$ by iso-function method. The number of initial stress modes in the matrix is always larger than m (=n-r). In order to select m necessary stress modes, these initial stress modes have to be classified into (n-r) stress mode groups.

Step 2:

Select stress modes in the order from low order term to high order term. Now select a stress mode from the existing stress matrix $[P]_{iso}$ and form an assumed stress matrix $[P_1]$. The element stiffness matrix [K] corresponding to stress matrix $[P_1]$ can be obtained by using equations (3-12) and (3-6). If the eigenvalue examination gives a non-zero eigenvalue, the stress mode is a non-zero-energy stress mode; otherwise, it is a zero-energy stress mode. Repeating the eigenvalue examination to check whether a stress mode

is a zero-energy stress mode for all stress modes in the existing stress matrix $[P]_{iso}$.

Take all zero-energy stress modes out and keep non-zero-energy stress modes in the matrix $[P]_{iso}$. All zero-energy stress modes form a zero-energy stress mode group.

Step 3:

Take a non-zero-energy stress mode from the existing stress matrix $[P]_{iso}$ and form an assumed stress matrix $[P_1]$. The stress mode $\{\sigma_1\}$ is the representative stress mode which represents group 1 of stress modes.

Step 4:

Add another stress mode selected in the existing stress matrix $[P]_{iso}$ into the assumed stress matrix $[P_1]$ and form a new stress matrix $[P_2]$,

$$[P_2] = [\{\sigma_1\}\ \{\sigma_2\}] \tag{3-23}$$

Step 5:

The eigenvalue examination gives the eigenvalues of the stiffness matrix. If there is only one non-zero eigenvalue, continue to step 6. If there are two non-zero eigenvalues, go to step 7.

Step 6:

In this case, the added stress mode belongs to group 1 of stress modes. Take the second

stress mode out and put it in group 1 of stress modes. Then, go back to step 4.

Step 7:

The two stress modes belong to two different groups of stress modes. The second stress mode $\{\sigma_2\}$ is the representative stress mode which represents group 2 of stress modes.

Step 8:

Add another stress mode selected from the matrix $[P]_{iso}$ into the assumed stress matrix $[P_2]$ and form a new stress matrix $[P_3]$,

$$[P_3] = [\{\sigma_1\}\ \{\sigma_2\}\ \{\sigma_3\}] \tag{3-24}$$

Step 9:

The element stiffness matrix [K] and its eigenvalues are calculated. If there are only two non-zero eigenvalues, continue to step 10. If there are three non-zero eigenvalues, go to step 11.

Step 10:

In this case, the new stress mode $\{\sigma_3\}$ belongs to one of the two stress mode groups. Construct the matrices $[P'_2]$ and $[P''_2]$ as follows,

$$[P_2'] = [\{\sigma_1\}\ \{\sigma_3\}] \quad or \quad [P_2''] = [\{\sigma_2\}\ \{\sigma_3\}] \tag{3-25}$$

If the stiffness matrix corresponding to the stress matrix $[P_2']$ has two non-zero eigenvalues, the stress mode $\{\sigma_3\}$ belongs to the group 2 of stress modes. Otherwise, the stress mode $\{\sigma_3\}$ belongs to the group 1 of stress modes. Put the stress mode $\{\sigma_3\}$ into the corresponding stress mode group, and go back to step 8.

Step 11:

In this case, the three stress modes belong to three different stress mode groups. The added stress mode $\{\sigma_3\}$ is the representative stress mode which represents group 3 of stress modes.

Step 12:

Add one more stress mode selected from the matrix $[P]_{iso}$ into the matrix $[P_3]$ and form a new stress matrix $[P_4]$,

$$[P_4] = [\{\sigma_1\}\ \{\sigma_2\}\ \{\sigma_3\}\ \{\sigma_4\}] \tag{3-26}$$

and so on. Repeating the same process until m representative stress modes that represent m stress mode groups are obtained. The m(=n-r) representative stress modes correspond to m natural deformation modes and form a optimal stress matrix $[P]_{opt}$ from the existing stress matrix $[P]_{iso}$.

3.2.2 Classification of other stress modes

Step 13:

After m representative stress modes are obtained, other initial stress modes that remain in the existing stress matrix $[P]_{iso}$ can be classified into the m stress mode groups. Many other stress modes derived by different methods also can be classified into the m stress mode groups corresponding to m natural deformation modes and the zero-energy stress mode group corresponding to rigid body modes.

Based on the optimal stress matrix $[P]_{opt}$, any remaining stress mode in $[P]_{iso}$ can be classified by using it to replace each and every stress mode in the matrix $[P]_{opt}$ in order. Once the eigenvalue examination results in m non-zero eigenvalues, the representative stress mode which is replaced and the remaining stress mode which replaces the stress mode in $[P]_{opt}$ belong to the same stress mode group. Put the remaining stress mode into the corresponding stress mode group and recover the optimal stress matrix $[P]_{opt}$. Then, classify another remaining stress mode.

Step 14:

Repeating the same process until all remaining stress modes are classified. Thus, all existing stress modes are classified into m+1 different mode groups. Every stress mode group contains many interchangeable stress modes. For a stress mode derived by other method, if eigenvalue examination always give m-1 non-zero eigenvalues when this stress

mode replaces each and every stress mode in the matrix $[P]_{opt}$, this stress mode is a zero-energy stress mode.

3.3 Illustration for the Classification of Stress Modes

As an illustration for the above procedure, the stress modes presented in ref. [41, 68-70] and those derived by iso-function method are classified.

3.3.1 2-D, 4-node plane hybrid element

Determination of optimal stress matrix from the existing stress matrix derived by iso-function method

The 2-D, 4-node plane element has (n=) 8 degrees of freedom and (r=) 3 rigid body modes. So it has (m=n-r=) 5 natural deformation modes. Firstly, an assumed stress matrix can be derived from the assumed displacement field of the element by the iso-function method [43],

$$[P_I] = \begin{bmatrix} 1 & 0 & 0 & x & y & 0 & 0 & 0 & 0 \\ 0 & 1 & 0 & 0 & 0 & x & y & 0 & 0 \\ 0 & 0 & 1 & 0 & 0 & 0 & 0 & x & y \end{bmatrix} \tag{3-27}$$

The number of stress modes in the stress matrix is larger than m (=5). The eigenvalue examination indicates that the eigenvalues and eigenvectors of the hybrid element stiffness

matrix constructed by the assumed stress matrix $[P_I]$ are the same as that of displacement element stiffness matrix. Here, one takes the stress modes in the stress matrix as initial stress modes to be classified. There are nine stress modes in the matrix $[P_I]$,

$$\{\sigma_1\}=\begin{Bmatrix}1\\0\\0\end{Bmatrix} \quad \{\sigma_2\}=\begin{Bmatrix}0\\1\\0\end{Bmatrix} \quad \{\sigma_3\}=\begin{Bmatrix}0\\0\\1\end{Bmatrix}$$

$$\{\sigma_4\}=\begin{Bmatrix}x\\0\\0\end{Bmatrix} \quad \{\sigma_5\}=\begin{Bmatrix}y\\0\\0\end{Bmatrix} \quad \{\sigma_6\}=\begin{Bmatrix}0\\x\\0\end{Bmatrix} \qquad (3\text{-}28)$$

$$\{\sigma_7\}=\begin{Bmatrix}0\\y\\0\end{Bmatrix} \quad \{\sigma_8\}=\begin{Bmatrix}0\\0\\x\end{Bmatrix} \quad \{\sigma_9\}=\begin{Bmatrix}0\\0\\y\end{Bmatrix}$$

The stress matrix derived by iso-function method contains a few unnecessary stress modes. It will save computation time for calculating element stiffness matrix if the number of the stress modes can be reduced to m (=n-r). In order to do it, the initial stress modes in the existing stress matrix have to be classified into m stress mode groups. First of all, one must find m representative stress modes corresponding to m natural deformation modes. Following step 2 - step 12 in the procedure of the classification method given in the above section, one can obtain 5 representative stress modes $\{\sigma_1\ \sigma_2\ \sigma_3\ \sigma_5\ \sigma_6\}$ corresponding to (m=)of 5 natural deformation modes and the zero-energy stress modes $\{\sigma_4\}$ and $\{\sigma_7\}$ corresponding to rigid body modes. The eigenvalues of the stiffness

matrix related to $\{\sigma_1\ \sigma_2\ \sigma_3\ \sigma_5\ \sigma_6\}$ are not equal to zero, and the eigenvalue of stiffness matrix related to $\{\sigma_4\}$ or $\{\sigma_7\}$ is equal to zero. The 5 representative stress modes form an optimal stress matrix $[P_{II}]$ from the existing stress matrix $[P_I]$,

$$[P_{II}] = [\sigma_1\ \sigma_2\ \sigma_3\ \sigma_5\ \sigma_6] = \begin{bmatrix} 1 & 0 & 0 & y & 0 \\ 0 & 1 & 0 & 0 & x \\ 0 & 0 & 1 & 0 & 0 \end{bmatrix} \tag{3-29}$$

The stress matrix is the same as that given by Pian [70].

Classification of other stress modes

After obtaining the optimal stress matrix, one can classify stress modes in the existing stress matrix $[P_I]$ into (m+1=) 6 stress mode groups by following step 13 - step 14 in the procedure,

Tension mode (Group 1):	$\{\ \sigma_1\ \}$
Tension mode (Group 2):	$\{\ \sigma_2\ \}$
Shear mode (Group 3):	$\{\ \sigma_3\ \}$
Bending mode (Group 4):	$\{\ \sigma_5\ \}, \{\ \sigma_8\ \}$
Bending mode (Group 5):	$\{\ \sigma_6\ \}, \{\ \sigma_9\ \}$
Zero-energy stress mode (Group 6):	$\{\ \sigma_4\ \}, \{\ \sigma_7\ \}$

The first 5 stress mode groups correspond to 5 natural deformation modes and the zero-

energy stress mode group corresponds to rigid body modes.

There are many methods to derive initial stress modes. For example, in the two assumed stress matrices derived by means of group theory[68-69] for the same finite element, there are 4 stress modes that are different from stress modes $\{\sigma_1\}$-$\{\sigma_9\}$:

$$\{\sigma_{10}\}=\begin{Bmatrix}1\\1\\0\end{Bmatrix} \quad \{\sigma_{11}\}=\begin{Bmatrix}1\\-1\\0\end{Bmatrix} \quad \{\sigma_{12}\}=\begin{Bmatrix}0\\-y\\x\end{Bmatrix} \quad \{\sigma_{13}\}=\begin{Bmatrix}-x\\0\\y\end{Bmatrix} \tag{3-30}$$

Moreover, one may want to introduce some stress modes of high order term into the assumed stress matrix [P] in order to describe special stress distribution in a local region of a structure to be solved. For example,

$$\{\sigma_{14}\}=\begin{Bmatrix}x^2\\0\\0\end{Bmatrix} \quad \{\sigma_{15}\}=\begin{Bmatrix}0\\x^2\\0\end{Bmatrix} \quad \{\sigma_{16}\}=\begin{Bmatrix}0\\0\\x^2\end{Bmatrix}$$

$$\{\sigma_{17}\}=\begin{Bmatrix}y^2\\0\\0\end{Bmatrix} \quad \{\sigma_{18}\}=\begin{Bmatrix}0\\y^2\\0\end{Bmatrix} \quad \{\sigma_{19}\}=\begin{Bmatrix}0\\0\\y^2\end{Bmatrix} \tag{3-31}$$

$$\{\sigma_{20}\}=\begin{Bmatrix}xy\\0\\0\end{Bmatrix} \quad \{\sigma_{21}\}=\begin{Bmatrix}0\\xy\\0\end{Bmatrix} \quad \{\sigma_{22}\}=\begin{Bmatrix}0\\0\\xy\end{Bmatrix}$$

According to the steps 13-14 in the procedure of classification method, these new stress modes $\{\sigma_{10}\}$-$\{\sigma_{22}\}$ can also be classified into the 6 stress mode groups above,

Tension mode (Group 1): $\{ \sigma_1 \}, \{ \sigma_{10} \}, \{ \sigma_{14} \}, \{ \sigma_{17} \}$

Tension mode (Group 2): $\{ \sigma_2 \}, \{ \sigma_{11} \}, \{ \sigma_{15} \}, \{ \sigma_{18} \}$

Shear mode (Group 3): $\{ \sigma_3 \}, \{ \sigma_{16} \}, \{ \sigma_{19} \}$

Bending mode (Group 4): $\{ \sigma_5 \}, \{ \sigma_8 \}, \{ \sigma_{12} \}$

Bending mode (Group 5): $\{ \sigma_6 \}, \{ \sigma_9 \}, \{ \sigma_{13} \}$

Zero-energy stress mode (Group 6): $\{ \sigma_4 \}, \{ \sigma_7 \}, \{ \sigma_{20} \}, \{\sigma_{21} \}, \{\sigma_{22} \}$

More high-order stress modes can be classified into the 6 stress mode groups above by using the classification method. If the flexibility matrix [H] is a diagonal matrix, the classification of the stress modes is unique (see section 3.5).

3.3.2 3-D, 8-node solid hybrid element

Determination of optimal stress matrix from the existing stress matrix derived by iso-function method

The 3-D, 8-node solid element has (n=) 24 degrees of freedom and (r=) 6 rigid body modes. So it has (m=n-r=) 18 natural deformation modes. By means of iso-function method [43], an initial stress matrix [P] can be derived from the assumed displacement field of the element as follows

$$[P]_{ISO} = \begin{vmatrix} 1 & 0 & 0 & 0 & 0 & 0 & x & 0 & 0 & 0 & 0 & 0 & y & 0 & 0 & 0 & 0 & 0 & z & 0 & 0 & 0 & 0 & 0 \\ 0 & 1 & 0 & 0 & 0 & 0 & 0 & x & 0 & 0 & 0 & 0 & 0 & y & 0 & 0 & 0 & 0 & 0 & z & 0 & 0 & 0 & 0 \\ 0 & 0 & 1 & 0 & 0 & 0 & 0 & 0 & x & 0 & 0 & 0 & 0 & 0 & y & 0 & 0 & 0 & 0 & 0 & z & 0 & 0 & 0 \\ 0 & 0 & 0 & 1 & 0 & 0 & 0 & 0 & 0 & x & 0 & 0 & 0 & 0 & 0 & y & 0 & 0 & 0 & 0 & 0 & z & 0 & 0 \\ 0 & 0 & 0 & 0 & 1 & 0 & 0 & 0 & 0 & 0 & x & 0 & 0 & 0 & 0 & 0 & y & 0 & 0 & 0 & 0 & 0 & z & 0 \\ 0 & 0 & 0 & 0 & 0 & 1 & 0 & 0 & 0 & 0 & 0 & x & 0 & 0 & 0 & 0 & 0 & y & 0 & 0 & 0 & 0 & 0 & z \end{vmatrix}$$

$$\begin{vmatrix} xy & 0 & 0 & 0 & 0 & yz & 0 & 0 & 0 & 0 & zx & 0 & 0 & 0 & 0 \\ 0 & xy & 0 & 0 & 0 & 0 & yz & 0 & 0 & 0 & 0 & zx & 0 & 0 & 0 \\ 0 & 0 & xy & 0 & 0 & 0 & 0 & yz & 0 & 0 & 0 & 0 & zx & 0 & 0 \\ 0 & 0 & 0 & 0 & 0 & 0 & 0 & 0 & yz & 0 & 0 & 0 & 0 & zx & 0 \\ 0 & 0 & 0 & xy & 0 & 0 & 0 & 0 & 0 & 0 & 0 & 0 & 0 & 0 & zx \\ 0 & 0 & 0 & 0 & xy & 0 & 0 & 0 & 0 & yz & 0 & 0 & 0 & 0 & 0 \end{vmatrix} \qquad (3\text{-}32)$$

There are 39 stress modes to be classified in the stress matrix. The number of stress modes is larger than m (=18). The eigenvalue examination shows that the eigenvalues and eigenvectors of the hybrid element stiffness matrix constructed by the assumed stress matrix $[P]_{ISO}$ are the same as its displacement counterpart. One takes the stress modes in the matrix $[P]_{ISO}$ as initial stress modes to be classified. The 39 stress modes in the matrix $[P]_{ISO}$ are numbered as follows:

$$\{\sigma_1 \ \sigma_2 \ \sigma_3 \ \sigma_4 \ \sigma_5 \ \sigma_6\} = \begin{Bmatrix} 1 & 0 & 0 & 0 & 0 & 0 \\ 0 & 1 & 0 & 0 & 0 & 0 \\ 0 & 0 & 1 & 0 & 0 & 0 \\ 0 & 0 & 0 & 1 & 0 & 0 \\ 0 & 0 & 0 & 0 & 1 & 0 \\ 0 & 0 & 0 & 0 & 0 & 1 \end{Bmatrix} \qquad (3\text{-}33)$$

$$\{\sigma_7\ \sigma_8\ \sigma_9\ \sigma_{10}\ \sigma_{11}\ \sigma_{12}\} = \begin{Bmatrix} x & 0 & 0 & 0 & 0 & 0 \\ 0 & x & 0 & 0 & 0 & 0 \\ 0 & 0 & x & 0 & 0 & 0 \\ 0 & 0 & 0 & x & 0 & 0 \\ 0 & 0 & 0 & 0 & x & 0 \\ 0 & 0 & 0 & 0 & 0 & x \end{Bmatrix} \tag{3-34}$$

$$\{\sigma_{13}\ \sigma_{14}\ \sigma_{15}\ \sigma_{16}\ \sigma_{17}\ \sigma_{18}\} = \begin{Bmatrix} y & 0 & 0 & 0 & 0 & 0 \\ 0 & y & 0 & 0 & 0 & 0 \\ 0 & 0 & y & 0 & 0 & 0 \\ 0 & 0 & 0 & y & 0 & 0 \\ 0 & 0 & 0 & 0 & y & 0 \\ 0 & 0 & 0 & 0 & 0 & y \end{Bmatrix} \tag{3-35}$$

$$\{\sigma_{19}\ \sigma_{20}\ \sigma_{21}\ \sigma_{22}\ \sigma_{23}\ \sigma_{24}\} = \begin{Bmatrix} z & 0 & 0 & 0 & 0 & 0 \\ 0 & z & 0 & 0 & 0 & 0 \\ 0 & 0 & z & 0 & 0 & 0 \\ 0 & 0 & 0 & z & 0 & 0 \\ 0 & 0 & 0 & 0 & z & 0 \\ 0 & 0 & 0 & 0 & 0 & z \end{Bmatrix} \tag{3-36}$$

$$\{\sigma_{25}\ \sigma_{26}\ \sigma_{27}\ \sigma_{28}\ \sigma_{29}\} = \begin{Bmatrix} xy & 0 & 0 & 0 & 0 \\ 0 & xy & 0 & 0 & 0 \\ 0 & 0 & xy & 0 & 0 \\ 0 & 0 & 0 & 0 & 0 \\ 0 & 0 & 0 & xy & 0 \\ 0 & 0 & 0 & 0 & xy \end{Bmatrix} \tag{3-37}$$

$$\{\sigma_{30}\ \sigma_{31}\ \sigma_{32}\ \sigma_{33}\ \sigma_{34}\} = \begin{Bmatrix} yz & 0 & 0 & 0 & 0 \\ 0 & yz & 0 & 0 & 0 \\ 0 & 0 & yz & 0 & 0 \\ 0 & 0 & 0 & yz & 0 \\ 0 & 0 & 0 & 0 & 0 \\ 0 & 0 & 0 & 0 & yz \end{Bmatrix} \tag{3-38}$$

$$\{\sigma_{35}\ \sigma_{36}\ \sigma_{37}\ \sigma_{38}\ \sigma_{39}\} = \begin{Bmatrix} zx & 0 & 0 & 0 & 0 \\ 0 & zx & 0 & 0 & 0 \\ 0 & 0 & zx & 0 & 0 \\ 0 & 0 & 0 & zx & 0 \\ 0 & 0 & 0 & 0 & zx \\ 0 & 0 & 0 & 0 & 0 \end{Bmatrix} \tag{3-39}$$

In order to reduce the number of stress modes in the assumed stress matrix $[P]_{ISO}$, these

stress modes have to be classified one by one in the order from low order term to high order term. Following the steps 2 - step 12 in the procedure of the classification, one can obtain (m=) 18 representative stress modes { σ_1 σ_2 σ_3 σ_4 σ_5 σ_6 σ_8 σ_9 σ_{11} σ_{13} σ_{15} σ_{18} σ_{19} σ_{20} σ_{22} σ_{27} σ_{30} σ_{36} } corresponding to 18 natural deformation modes. These representative stress modes form an optimal stress matrix $[P_1]$ from the existing stress matrix $[P]_{iso}$ as follows:

$$[P_1]=[\sigma_1\ \sigma_2\ \sigma_3\ \sigma_4\ \sigma_5\ \sigma_6\ \sigma_{13}\ \sigma_{20}\ \sigma_9\ \sigma_{19}\ \sigma_8\ \sigma_{15}\ \sigma_{22}\ \sigma_{11}\ \sigma_{18}\ \sigma_{30}\ \sigma_{36}\ \sigma_{27}]$$

$$= \begin{bmatrix} 1 & 0 & 0 & 0 & 0 & 0 & y & 0 & 0 & z & 0 & 0 & 0 & 0 & 0 & yz & 0 & 0 \\ 0 & 1 & 0 & 0 & 0 & 0 & 0 & z & 0 & 0 & x & 0 & 0 & 0 & 0 & 0 & zx & 0 \\ 0 & 0 & 1 & 0 & 0 & 0 & 0 & 0 & x & 0 & 0 & y & 0 & 0 & 0 & 0 & 0 & xy \\ 0 & 0 & 0 & 1 & 0 & 0 & 0 & 0 & 0 & 0 & 0 & 0 & z & 0 & 0 & 0 & 0 & 0 \\ 0 & 0 & 0 & 0 & 1 & 0 & 0 & 0 & 0 & 0 & 0 & 0 & 0 & x & 0 & 0 & 0 & 0 \\ 0 & 0 & 0 & 0 & 0 & 1 & 0 & 0 & 0 & 0 & 0 & 0 & 0 & 0 & y & 0 & 0 & 0 \end{bmatrix} \quad (3\text{-}40)$$

This stress matrix is the same as that proposed by Pian [70].

Classification of other stress modes

Following the steps 13-14 in the procedure, other stress modes that remain in the existing stress matrix $[P]_{iso}$ can be classified into m+1 (=19) stress mode groups as follows:

Tension and compressive modes (3 groups): $[\{\sigma_1\}_{G1}, \{\sigma_2\}_{G2}, \{\sigma_3\}_{G3}]$

Pure shear modes (3 groups): $[\{\sigma_4\}_{G4}, \{\sigma_5\}_{G5}, \{\sigma_6\}_{G6}]$

Bending modes (6 groups): $[\{\sigma_8\ \sigma_{16}\}_{G7}, \{\sigma_9\ \sigma_{24}\}_{G8}, \{\sigma_{13}\ \sigma_{10}\}_{G9},$

$\{\sigma_{15}\ \sigma_{23}\}_{G10}, \{\sigma_{19}\ \sigma_{12}\}_{G11}, \{\sigma_{20}\ \sigma_{17}\}_{G12}]$

Torsion modes (3 groups): $[\{\sigma_{11}\}_{G13}, \{\sigma_{18}\}_{G14}, \{\sigma_{22}\}_{G15}]$

Saddle modes (3 groups): $[\{\sigma_{29}\ \sigma_{30}\ \sigma_{38}\}_{G16}, \{\sigma_{28}\ \sigma_{33}\ \sigma_{36}\}_{G17}, \{\sigma_{27}\ \sigma_{34}\ \sigma_{39}\ \}_{G18}]$

Zero-energy stress modes (1 group): $[\{\sigma_7, \sigma_{14}, \sigma_{21}, \sigma_{25}, \sigma_{26}, \sigma_{31}, \sigma_{32}, \sigma_{35}, \sigma_{37}\}_{G19}]$

The first 18 stress mode groups correspond to (m=n-r=) 18 natural deformation modes and the last group corresponds to rigid body modes. There are many other ways to derive initial stress modes. For example, in the assumed stress matrix presented in ref. [41], there are 12 stress modes that are different from stress modes $\{\sigma_1\}$-$\{\sigma_{39}\}$. These stress modes can be expressed as follows,

Tension and compressive modes,

$$\{\sigma_{40}\}=\begin{Bmatrix}1\\1\\1\\0\\0\\0\end{Bmatrix} \qquad \{\sigma_{41}\}=\begin{Bmatrix}1\\-1\\0\\0\\0\\0\end{Bmatrix} \qquad \{\sigma_{42}\}=\begin{Bmatrix}-1\\-1\\2\\0\\0\\0\end{Bmatrix} \tag{3-41}$$

Symmetric bending modes,

$$\{\sigma_{43}\}=\begin{Bmatrix}z\\z\\0\\0\\0\\0\end{Bmatrix} \qquad \{\sigma_{44}\}=\begin{Bmatrix}0\\x\\x\\0\\0\\0\end{Bmatrix} \qquad \{\sigma_{45}\}=\begin{Bmatrix}y\\0\\y\\0\\0\\0\end{Bmatrix} \tag{3-42}$$

Anti-symmetric bending modes,

$$\{\sigma_{46}\}=\begin{Bmatrix} z \\ -z \\ 0 \\ 0 \\ 0 \\ 0 \end{Bmatrix} \qquad \{\sigma_{47}\}=\begin{Bmatrix} 0 \\ x \\ -x \\ 0 \\ 0 \\ 0 \end{Bmatrix} \qquad \{\sigma_{48}\}=\begin{Bmatrix} y \\ 0 \\ -y \\ 0 \\ 0 \\ 0 \end{Bmatrix} \tag{3-43}$$

Torsion modes,

$$\{\sigma_{49}\}=\begin{Bmatrix} 0 \\ 0 \\ 0 \\ z \\ x \\ y \end{Bmatrix} \qquad \{\sigma_{50}\}=\begin{Bmatrix} 0 \\ 0 \\ 0 \\ z \\ -x \\ 0 \end{Bmatrix} \qquad \{\sigma_{51}\}=\begin{Bmatrix} 0 \\ 0 \\ 0 \\ z \\ x \\ -2y \end{Bmatrix} \tag{3-44}$$

In the stress matrices derived by means of the symmetric group theory[68-69], there are eleven stress modes that are different from stress modes $\{\sigma_1\}$-$\{\sigma_{51}\}$. They can be expressed in the form,

Tension and compressive mode,

$$\{\sigma_{52}\}=\begin{Bmatrix} 0 \\ 1 \\ -1 \\ 0 \\ 0 \\ 0 \end{Bmatrix} \tag{3-45}$$

Torsion modes,

$$\{\sigma_{53}\}=\begin{Bmatrix} 0 \\ 0 \\ 0 \\ 0 \\ -x \\ y \end{Bmatrix} \tag{3-46}$$

Bending modes,

$$\{\sigma_{54}\ \sigma_{55}\ \sigma_{56}\}=\begin{bmatrix} 2x & 0 & 0 \\ 0 & 2y & 0 \\ 0 & 0 & 2z \\ -y & -x & 0 \\ 0 & -z & -y \\ -z & 0 & -x \end{bmatrix} \quad \textit{and} \quad \{\sigma_{57}\ \sigma_{58}\ \sigma_{59}\}=\begin{bmatrix} 0 & 0 & 0 \\ 0 & 0 & 0 \\ 0 & 0 & 0 \\ y & x & 0 \\ 0 & -z & -y \\ -z & 0 & x \end{bmatrix} \tag{3-47}$$

Saddle modes,

$$\{\sigma_{60}\ \sigma_{61}\ \sigma_{62}\}=\begin{bmatrix} 0 & 0 & 0 \\ 0 & 0 & 0 \\ 0 & 0 & 0 \\ -2xz & -2yz & x^2+y^2 \\ y^2+z^2 & -2xy & -2xz \\ -2xy & x^2+z^2 & -2yz \end{bmatrix} \tag{3-48}$$

Other stress modes may be also needed in an assumed stress matrix in order to describe special stress distribution in a local region of a structure to be analyzed. For instance,

Bending modes,

$$\{\sigma_{63}\}=\begin{Bmatrix} z \\ z \\ z \\ 0 \\ 0 \\ 0 \end{Bmatrix} \qquad \{\sigma_{64}\}=\begin{Bmatrix} x \\ x \\ x \\ 0 \\ 0 \\ 0 \end{Bmatrix} \qquad \{\sigma_{65}\}=\begin{Bmatrix} y \\ y \\ y \\ 0 \\ 0 \\ 0 \end{Bmatrix} \tag{3-49}$$

Saddle modes,

$$\{\sigma_{66}\}=\begin{Bmatrix} yz \\ yz \\ yz \\ 0 \\ 0 \\ 0 \end{Bmatrix} \qquad \{\sigma_{67}\}=\begin{Bmatrix} zx \\ zx \\ zx \\ 0 \\ 0 \\ 0 \end{Bmatrix} \qquad \{\sigma_{68}\}=\begin{Bmatrix} xy \\ xy \\ xy \\ 0 \\ 0 \\ 0 \end{Bmatrix} \tag{3-50}$$

Tension and compressive mode,

$$\{\sigma_{69}\}=\begin{Bmatrix} z^2 \\ z^2 \\ 0 \\ 0 \\ 0 \\ 0 \end{Bmatrix} \tag{3-51}$$

According to the steps 13 -14 in the proposed procedure of classification, the 30 new stress modes $\{\sigma_{40}\}$-$\{\sigma_{69}\}$ can be classified into different stress mode groups above as follows,

Tension and compressive modes (3 groups): $[\{\sigma_1, \sigma_{40}, \sigma_{69}\}_{G1}, \{\sigma_2, \sigma_{41}\}_{G2}, \{\sigma_3, \sigma_{42}, \sigma_{52}\}_{G3}]$

Pure shear modes (3 groups): $[\{\sigma_4\}_{G4}, \{\sigma_5\}_{G5}, \{\sigma_6\}_{G6}]$

Bending modes (6 groups): $[\{\sigma_8, \sigma_{16}, \sigma_{44}, \sigma_{54}, \sigma_{64}\}_{G7}, \{\sigma_9, \sigma_{24}, \sigma_{47}, \sigma_{57}\}_{G8}, \{\sigma_{13}, \sigma_{10}, \sigma_{45}, \sigma_{55}, \sigma_{65}\}_{G9}, \{\sigma_{15}, \sigma_{23}, \sigma_{48}, \sigma_{58}\}_{G10}, \{\sigma_{19}, \sigma_{12}, \sigma_{43}, \sigma_{56}, \sigma_{63}\}_{G11}, \{\sigma_{20}, \sigma_{17}, \sigma_{46}, \sigma_{59}\}_{G12}]$

Torsion modes (3 groups): $[\{\sigma_{11}, \sigma_{49}\}_{G13}, \{\sigma_{18}, \sigma_{50}\}_{G14}, \{\sigma_{22}, \sigma_{51}, \sigma_{53}\}_{G15}]$

Saddle modes (3 groups): $[\{\sigma_{29}, \sigma_{30}, \sigma_{38}, \sigma_{66}, \sigma_{60}\}_{G16}, \{\sigma_{28}, \sigma_{33}, \sigma_{36}, \sigma_{67}, \sigma_{61}\}_{G17}, \{\sigma_{27}, \sigma_{34}, \sigma_{39}, \sigma_{68}, \sigma_{62}\}_{G18}]$

Zero-energy stress modes (1 group): $[\{\sigma_7, \sigma_{14}, \sigma_{21}, \sigma_{25}, \sigma_{26}, \sigma_{31}, \sigma_{32}, \sigma_{35}, \sigma_{37}\}_{G19}]$

More stress modes can be classified into the stress mode groups above. If the flexibility matrix [H] is a diagonal matrix, the stress modes are uncoupled and the classification of the stress modes is unique (see section 6). Otherwise, some stress modes may appear in more than one group.

3.4 Construction of Assumed Stress Matrices

As shown above, by means of the proposed procedure for the classification of stress mode, stress modes can be classified into m (=n-r) stress mode groups corresponding to m natural deformation modes and a zero energy mode group corresponding to rigid body modes. Each natural deformation mode is related to a stress mode group except zero

energy mode group, and each stress mode group may contain many different stress modes that are interchangeable in the stress matrix [P].

The classification of stress modes reveals the relationship among the different stress modes that are used in the different stress matrices for any type of a hybrid element proposed by different researchers. In order to avoid kinematic deformation mode, the stress matrix [P] must contain m stress modes at least. No matter how many stress modes there are in the stress matrix [P], the order of the stiffness matrix is equal to or less than m. Therefore, m stress modes is necessary and sufficient to form a stress matrix for avoiding kinematic deformation modes in the hybrid element. Moreover, in view of the classification of stress modes, the m stress modes in the stress matrix [P] must come from m different stress mode groups except zero energy mode group. Thus, for a hybrid element to be free from kinematic deformation mode, we have

The necessary and sufficient condition:

> *The number of stress modes in an assumed stress matrix must be equal to or more than m (= n-r) and at least m stress modes in the stress matrix [P] must be chosen from m different stress mode groups corresponding to m natural deformation modes of an element which has n degrees of freedom and r rigid body modes.*

In this statement, the necessary condition is that the number of stress modes for a hybrid

element must be equal to or more than m (=n-r). It was presented by F. Veubeke [63] and Pian [54]. The sufficient condition is that the stress matrix [P] must contain m stress modes chosen from m different stress mode groups corresponding to m natural deformation modes. This condition explains why in some examples there exist kinematic deformation modes even when the necessary condition (m' > n-r) is satisfied. In these examples, the stress modes in the stress matrix [P] do not come from m different stress mode groups except the zero energy mode group.

For a hybrid element, overuse of stress modes will result in over-rigid element [62], and will cost more computational time because the calculation of element stiffness matrix requires an inversion of the flexibility matrix [H]. Therefore, an assumed stress field, its stress matrix contains m (=n-r) least-order stress modes and its resulting finite element is free from kinematic deformation modes, is considered to be best and is optimal with respect to computer resources [62,68]. By means of the m classified stress mode groups and the necessary and sufficient condition, this kind of stress matrices can be constructed. Furthermore, it is convenient to construct an assumed stress matrix according to the problem to be solved because there are many stress modes in every stress mode group for choice. The procedure of constructing stress matrix is presented as follows,

Step 1: Using the iso-function method[43], one can derive a number of initial stress modes to be classified.

Step 2: One may put the initial stress modes one by one into stress matrix [P] in the order from low order term to high order term. By means of the classification method, one can obtain m representative stress modes corresponding to m natural deformation modes. These representative stress modes form an optimal stress matrix $[P]_{opt}$ from the existing stress matrix $[P]_{iso}$.

Step 3: One may obtain other initial stress modes derived by different methods. Following the step 13 - 14 in the procedure of the classification, one can classify all initial stress modes into m+1 different stress mode groups.

Step 4: By means of the m+1 classified stress mode groups and the necessary and sufficient condition above, many stress matrices [P] can be constructed according to the problem to be solved. It is necessary to choose one stress mode at least from each group except the zero energy mode group in order to avoid kinematic deformation modes.

The necessary steps have been illustrated in the section above. The following gives some examples to illustrate the procedure for constructing a stress matrix [P] which has minimum number of stress modes.

3.4.1 2-D, 4-node Plane Hybrid Element

By means of the m+1 stress mode groups classified above and the necessary and sufficient

condition for avoiding kinematic deformation modes, one can choose one stress mode from each/every stress mode group except zero energy mode group to form a stress matrix. For example,

$$[P_{III}] = [\sigma_{10}\ \sigma_{11}\ \sigma_3\ \sigma_{12}\ \sigma_{13}] = \begin{bmatrix} 1 & 1 & 0 & 0 & -x \\ 1 & -1 & 0 & -y & 0 \\ 0 & 0 & 1 & x & y \end{bmatrix} \tag{3-52}$$

and

$$[P_{IV}] = [\sigma_{10}\ \sigma_{11}\ \sigma_3\ \sigma_7\ \sigma_5] = \begin{bmatrix} 1 & 1 & 0 & y & 0 \\ 1 & -1 & 0 & 0 & x \\ 0 & 0 & 1 & 0 & 0 \end{bmatrix} \tag{3-53}$$

Five stress modes in each stress matrix come from five different stress mode groups corresponding to five natural deformation modes. The two stress matrices are the same as that proposed by Atluri [68-69]. More stress matrices can be constructed on purpose. For example,

$$[P_V] = [\sigma_{10}\ \sigma_{11}\ \sigma_3\ \sigma_7\ \sigma_{13}] = \begin{bmatrix} 1 & 1 & 0 & y & -x \\ 1 & -1 & 0 & 0 & 0 \\ 0 & 0 & 1 & 0 & y \end{bmatrix} \tag{3-54}$$

and

$$[P_{VI}] = [\sigma_{14}\ \sigma_{11}\ \sigma_3\ \sigma_{12}\ \sigma_{13}] = \begin{bmatrix} x^2 & 1 & 0 & 0 & -x \\ 0 & -1 & 0 & -y & 0 \\ 0 & 0 & 1 & x & y \end{bmatrix} \tag{3-55}$$

The eigenvalue examination shows that the hybrid element constructed by $[P_I]$ - $[P_{VI}]$ are

free from kinematic deformation modes as shown in Table 3-1. In the last column of the table, the eigenvalues of its displacement counterpart are given. If stress modes in a stress matrix [P] come from m_1 (<m) stress mode groups, the hybrid element will have kinematic deformation modes even if the number of stress modes is larger than m. This is why a hybrid element contains kinematic deformation modes when the necessary condition (m' > n-r) is satisfied. A stress matrix [P] must have m stress modes corresponding to m natural deformation modes of an element.

Table 3-1 Eigenvalues of stiffness matrices (4-node plane element, ν=0.3)

$[P_I]$	$[P_{II}]$	$[P_{III}]$	$[P_{IV}]$	$[P_V]$	$[P_{VI}]$	Disp.
0.4945	0.3333	0.09259	0.3333	0.09259	0.09259	0.4945
0.4945	0.3333	0.09259	0.3333	0.3333	0.09259	0.4945
0.7692	0.7692	0.7692	0.7692	0.7692	0.7692	0.7692
0.7692	0.7692	0.7692	0.7692	0.7692	0.7692	0.7692
1.4290	1.4290	1.4290	1.4290	1.4290	1.4290	1.4290

3.4.2 3-D, 8-node Solid Hybrid Element

Using the same way as 2-D case, one can choose m stress modes from m classified stress

mode groups except zero energy mode group above to form the eight stress matrices $[P_2]$ - $[P_9]$ proposed by Atluri et al [68-69] as follows,

$$[P_2] = [\sigma_{40}\ \sigma_{41}\ \sigma_{42}\ \sigma_4\ \sigma_5\ \sigma_6\ \sigma_{49}\ \sigma_{50}\ \sigma_{53}\ \sigma_{54}\ \sigma_{55}\ \sigma_{56}\ \sigma_{57}\ \sigma_{58}\ \sigma_{59}\ \sigma_{60}\ \sigma_{61}\ \sigma_{62}]$$

$$= \begin{bmatrix} 1 & 1 & 0 & 0 & 0 & 0 & 0 & 0 & 0 & 2x & 0 & 0 & 0 & 0 & 0 & 0 & 0 & 0 \\ 1 & -1 & 1 & 0 & 0 & 0 & 0 & 0 & 0 & 0 & 2y & 0 & 0 & 0 & 0 & 0 & 0 & 0 \\ 1 & 0 & -1 & 0 & 0 & 0 & 0 & 0 & 0 & 0 & 0 & 2z & 0 & 0 & 0 & 0 & 0 & 0 \\ 0 & 0 & 0 & 1 & 0 & 0 & z & z & 0 & -y & -x & 0 & y & x & 0 & -2xz & -2yz & x^2+y^2 \\ 0 & 0 & 0 & 0 & 1 & 0 & x & -x & -x & 0 & -z & -y & 0 & -z & -y & y^2+z^2 & -2xy & -2xz \\ 0 & 0 & 0 & 0 & 0 & 1 & y & 0 & y & -z & 0 & -x & -z & 0 & x & -2xy & x^2+z^2 & -2yz \end{bmatrix} \quad (3\text{-}56)$$

$$[P_3] = [\sigma_{40}\ \sigma_{41}\ \sigma_{42}\ \sigma_4\ \sigma_5\ \sigma_6\ \sigma_{49}\ \sigma_{50}\ \sigma_{53}\ \sigma_{54}\ \sigma_{55}\ \sigma_{56}\ \sigma_{57}\ \sigma_{58}\ \sigma_{59}\ \sigma_{27}\ \sigma_{36}\ \sigma_{30}]$$

$$= \begin{bmatrix} 1 & 1 & 0 & 0 & 0 & 0 & 0 & 0 & 0 & 2x & 0 & 0 & 0 & 0 & 0 & 0 & 0 & yz \\ 1 & -1 & 1 & 0 & 0 & 0 & 0 & 0 & 0 & 0 & 2y & 0 & 0 & 0 & 0 & 0 & xz & 0 \\ 1 & 0 & -1 & 0 & 0 & 0 & 0 & 0 & 0 & 0 & 0 & 2z & 0 & 0 & 0 & xy & 0 & 0 \\ 0 & 0 & 0 & 1 & 0 & 0 & z & z & 0 & -y & -x & 0 & y & x & 0 & 0 & 0 & 0 \\ 0 & 0 & 0 & 0 & 1 & 0 & x & -x & -x & 0 & -z & -y & 0 & -z & -y & 0 & 0 & 0 \\ 0 & 0 & 0 & 0 & 0 & 1 & y & 0 & y & -z & 0 & -x & -z & 0 & x & 0 & 0 & 0 \end{bmatrix} \quad (3\text{-}57)$$

and

$$
\begin{aligned}
[P_4] &= [\sigma_{40}\ \sigma_{41}\ \sigma_{42}\ \sigma_4\ \sigma_5\ \sigma_6\ \sigma_{49}\ \sigma_{50}\ \sigma_{53}\ \sigma_{54}\ \sigma_{55}\ \sigma_{56}\ \sigma_{48}\ \sigma_{47}\ \sigma_{46}\ \sigma_{60}\ \sigma_{61}\ \sigma_{62}] \\
[P_5] &= [\sigma_{40}\ \sigma_{41}\ \sigma_{42}\ \sigma_4\ \sigma_5\ \sigma_6\ \sigma_{49}\ \sigma_{50}\ \sigma_{53}\ \sigma_{54}\ \sigma_{55}\ \sigma_{56}\ \sigma_{48}\ \sigma_{47}\ \sigma_{46}\ \sigma_{27}\ \sigma_{36}\ \sigma_{30}] \\
[P_6] &= [\sigma_{40}\ \sigma_{41}\ \sigma_{42}\ \sigma_4\ \sigma_5\ \sigma_6\ \sigma_{49}\ \sigma_{50}\ \sigma_{53}\ \sigma_{45}\ \sigma_{44}\ \sigma_{43}\ \sigma_{57}\ \sigma_{58}\ \sigma_{59}\ \sigma_{60}\ \sigma_{61}\ \sigma_{62}] \\
[P_7] &= [\sigma_{40}\ \sigma_{41}\ \sigma_{42}\ \sigma_4\ \sigma_5\ \sigma_6\ \sigma_{49}\ \sigma_{50}\ \sigma_{53}\ \sigma_{45}\ \sigma_{44}\ \sigma_{43}\ \sigma_{57}\ \sigma_{58}\ \sigma_{59}\ \sigma_{27}\ \sigma_{36}\ \sigma_{30}] \\
[P_8] &= [\sigma_{40}\ \sigma_{41}\ \sigma_{42}\ \sigma_4\ \sigma_5\ \sigma_6\ \sigma_{49}\ \sigma_{50}\ \sigma_{53}\ \sigma_{45}\ \sigma_{44}\ \sigma_{43}\ \sigma_{48}\ \sigma_{47}\ \sigma_{46}\ \sigma_{60}\ \sigma_{61}\ \sigma_{62}] \\
[P_9] &= [\sigma_{40}\ \sigma_{41}\ \sigma_{42}\ \sigma_4\ \sigma_5\ \sigma_6\ \sigma_{49}\ \sigma_{50}\ \sigma_{53}\ \sigma_{45}\ \sigma_{44}\ \sigma_{43}\ \sigma_{48}\ \sigma_{47}\ \sigma_{46}\ \sigma_{27}\ \sigma_{36}\ \sigma_{30}]
\end{aligned}
\tag{3-58}
$$

The assumed stress matrix given by Huang [41] also can be formed by means of the same way,

$$
[P_{10}] = [\sigma_{40}\ \sigma_{41}\ \sigma_{42}\ \sigma_4\ \sigma_5\ \sigma_6\ \sigma_{43}\ \sigma_{44}\ \sigma_{45}\ \sigma_{46}\ \sigma_{47}\ \sigma_{48}\ \sigma_{49}\ \sigma_{50}\ \sigma_{51}\ \sigma_{27}\ \sigma_{36}\ \sigma_{30}]
$$

$$
= \begin{bmatrix}
1 & 1 & -1 & 0 & 0 & 0 & z & 0 & y & z & 0 & y & 0 & 0 & 0 & yz & 0 & 0 \\
1 & -1 & -1 & 0 & 0 & 0 & z & x & 0 & -z & x & 0 & 0 & 0 & 0 & 0 & zx & 0 \\
1 & 0 & 2 & 0 & 0 & 0 & 0 & x & y & 0 & -x & -y & 0 & 0 & 0 & 0 & 0 & xy \\
0 & 0 & 0 & 1 & 0 & 0 & 0 & 0 & 0 & 0 & 0 & 0 & z & z & z & 0 & 0 & 0 \\
0 & 0 & 0 & 0 & 1 & 0 & 0 & 0 & 0 & 0 & 0 & 0 & x & -x & -x & 0 & 0 & 0 \\
0 & 0 & 0 & 0 & 0 & 1 & 0 & 0 & 0 & 0 & 0 & 0 & y & 0 & -2y & 0 & 0 & 0
\end{bmatrix}
\tag{3-59}
$$

Moreover, many stress matrices [P] can be constructed on purpose. Three new stress matrices are given as follows,

$$[P_1^*] = [\sigma_{40}\ \sigma_{41}\ \sigma_{42}\ \sigma_4\ \sigma_5\ \sigma_6\ \sigma_{63}\ \sigma_{64}\ \sigma_{65}\ \sigma_{46}\ \sigma_{47}\ \sigma_{48}\ \sigma_{49}\ \sigma_{50}\ \sigma_{51}\ \sigma_{66}\ \sigma_{67}\ \sigma_{68}]$$

$$= \begin{bmatrix} 1 & 1 & -1 & 0 & 0 & 0 & z & x & y & z & 0 & y & 0 & 0 & 0 & yz & xz & xy \\ 1 & -1 & -1 & 0 & 0 & 0 & z & x & y & -z & x & 0 & 0 & 0 & 0 & yz & xz & xy \\ 1 & 0 & 2 & 0 & 0 & 0 & z & x & y & 0 & -x & -y & 0 & 0 & 0 & yz & xz & xy \\ 0 & 0 & 0 & 1 & 0 & 0 & 0 & 0 & 0 & 0 & 0 & 0 & z & z & z & 0 & 0 & 0 \\ 0 & 0 & 0 & 0 & 1 & 0 & 0 & 0 & 0 & 0 & 0 & 0 & x & -x & -x & 0 & 0 & 0 \\ 0 & 0 & 0 & 0 & 0 & 1 & 0 & 0 & 0 & 0 & 0 & 0 & y & 0 & -2y & 0 & 0 & 0 \end{bmatrix} \quad (3\text{-}60)$$

$$[P_2^*] = [\sigma_{40}\ \sigma_{41}\ \sigma_{42}\ \sigma_4\ \sigma_5\ \sigma_6\ \sigma_{43}\ \sigma_{44}\ \sigma_{45}\ \sigma_{57}\ \sigma_{58}\ \sigma_{59}\ \sigma_{22}\ \sigma_{11}\ \sigma_{18}\ \sigma_{30}\ \sigma_{36}\ \sigma_{27}]$$

$$= \begin{bmatrix} 1 & 0 & 0 & 0 & 0 & 0 & z & 0 & y & 0 & 0 & 0 & 0 & 0 & 0 & yz & 0 & 0 \\ 0 & 1 & 0 & 0 & 0 & 0 & z & x & 0 & 0 & 0 & 0 & 0 & 0 & 0 & 0 & xz & 0 \\ 0 & 0 & 1 & 0 & 0 & 0 & 0 & x & y & 0 & 0 & 0 & 0 & 0 & 0 & 0 & 0 & xy \\ 0 & 0 & 0 & 1 & 0 & 0 & 0 & 0 & 0 & y & x & 0 & z & 0 & 0 & 0 & 0 & 0 \\ 0 & 0 & 0 & 0 & 1 & 0 & 0 & 0 & 0 & 0 & -z & -y & 0 & x & 0 & 0 & 0 & 0 \\ 0 & 0 & 0 & 0 & 0 & 1 & 0 & 0 & 0 & -z & 0 & x & 0 & 0 & y & 0 & 0 & 0 \end{bmatrix} \quad (3\text{-}61)$$

$$[P_3^*] = [\sigma_{69}\ \sigma_{41}\ \sigma_{42}\ \sigma_4\ \sigma_5\ \sigma_6\ \sigma_{63}\ \sigma_{64}\ \sigma_{65}\ \sigma_{46}\ \sigma_{47}\ \sigma_{48}\ \sigma_{49}\ \sigma_{50}\ \sigma_{51}\ \sigma_{66}\ \sigma_{67}\ \sigma_{68}]$$

$$= \begin{bmatrix} z^2 & 1 & -1 & 0 & 0 & 0 & z & x & y & z & 0 & y & 0 & 0 & 0 & yz & xz & xy \\ z^2 & -1 & -1 & 0 & 0 & 0 & z & x & y & -z & x & 0 & 0 & 0 & 0 & yz & xz & xy \\ 0 & 0 & 2 & 0 & 0 & 0 & z & x & y & 0 & -x & -y & 0 & 0 & 0 & yz & xz & xy \\ 0 & 0 & 0 & 1 & 0 & 0 & 0 & 0 & 0 & 0 & 0 & 0 & z & z & z & 0 & 0 & 0 \\ 0 & 0 & 0 & 0 & 1 & 0 & 0 & 0 & 0 & 0 & 0 & 0 & x & -x & -x & 0 & 0 & 0 \\ 0 & 0 & 0 & 0 & 0 & 1 & 0 & 0 & 0 & 0 & 0 & 0 & y & 0 & -2y & 0 & 0 & 0 \end{bmatrix} \quad (3\text{-}62)$$

The results of eigenvalue examination are given in Table 3-2. It shows that each of the stiffness matrices constructed by the assumed stress matrices $[P_1]$ - $[P_{10}]$, $[P_1^*]$, $[P_2^*]$, and $[P_3^*]$ has m non-zero eigenvalues. The resulting hybrid elements do not have any kinematic deformation modes.

More assumed stress matrices can also be constructed by means of this method. If one stress mode group is missed except the zero energy mode group in the process of choosing stress modes, the hybrid element will contain kinematic deformation modes. In the previous work, it is proposed to suppress kinematic deformation modes by adding stress modes of high order term. Actually, it can not guarantee that all kinematic deformation modes are suppressed. If the high order stress modes do not belong to the stress mode groups which are missed in the construction of the assumed stress matrix except the zero energy mode group, adding stress modes of high order term can not

Table 3-2 Eigenvalues of stiffness matrices (8-node solid element, v=0.3)

$[P_2]$	$[P_4]$	$[P_1],[P_9],[P_{10}]$	$[P_7]$, $[P_2^*]$	$[P_1^*]$	$[P_3^*]$
0.07123	0.07123	0.1111	0.1111	0.09259	0.09259
0.07123	0.07123	0.1111	0.1111	0.09259	0.09259
0.07123	0.07123	0.1111	0.1111	0.09259	0.09259
0.1282	0.2564	0.2564	0.1282	0.2564	0.2564
0.1282	0.2564	0.2564	0.1282	0.2564	0.2564
0.1282	0.2564	0.2564	0.1282	0.2564	0.2564
0.1282	0.1282	0.1282	0.1282	0.1282	0.1282
0.1282	0.1282	0.1282	0.1282	0.1282	0.1282
0.07246	0.07264	0.4762	0.4762	0.5556	0.5556
0.07246	0.07264	0.4762	0.4762	0.5556	0.5556
0.07246	0.07264	0.4762	0.4762	0.5556	0.5556
0.5128	0.5128	0.5128	0.5128	0.5128	0.5128
0.7692	0.7692	0.7692	0.7692	0.7692	0.7692
0.7692	0.7692	0.7692	0.7692	0.7692	0.7692
0.7692	0.7692	0.7692	0.7692	0.7692	0.7692
0.7692	0.7692	0.7692	0.7692	0.7692	0.7692
0.7692	0.7692	0.7692	0.7692	0.7692	0.7692
2.5000	2.5000	2.5000	2.5000	2.5000	0.8065

improve the hybrid element any more. Moreover, overuse of stress modes will result in

over-rigid elements. Therefore, an ideal situation is to choose m (=n-r) least-order stress modes, but with the suppression of all kinematic deformation modes. Thus, an assumed stress matrix [P] can be constructed by choosing m stress modes from m stress mode groups that correspond to m natural deformation modes.

3.5 Uniqueness of Stress Mode Groups

When stress modes are classified, it is observed that if the flexibility matrix [H] is a diagonal matrix, the classification of stress modes is unique; otherwise, some stress modes may be interchangeable between two stress mode groups. For example, the stress modes $\{\sigma_1\}$ and $\{\sigma_2\}$ for 2-D, 4-node plane hybrid element may be interchanged between group 1 and group 2. This makes the flexibility matrix [H] not diagonal when the stress matrix [P] consists of $(\{\sigma_1\}, \{\sigma_2\}, \{\sigma_3\}, \{\sigma_5\}, \{\sigma_6\})$. Therefore, the first two stress mode groups for 4-node plane element may become

Tension mode (Group 1): $\{ \sigma_1 \}$ (or $\{\sigma_2\}$), $\{ \sigma_{10} \}$, $\{ \sigma_{14} \}$, $\{ \sigma_{17} \}$

Tension mode (Group 2): $\{ \sigma_2 \}$ (or $\{\sigma_1\}$), $\{ \sigma_{11} \}$, $\{ \sigma_{15} \}$, $\{ \sigma_{18} \}$

However, the stress modes $\{\sigma_{10}\}$ and $\{\sigma_{11}\}$ for the plane element can not be interchanged between the two groups because the matrix [H] is diagonal when the stress matrix [P] consists of $(\{\sigma_{10}\}, \{\sigma_{11}\}, \{\sigma_3\}, \{\sigma_5\}, \{\sigma_6\})$. In fact, if the flexibility matrix [H] is a diagonal matrix, the stress modes that form the stress matrix [P] are a set of uncoupled

stress modes. It has been proved by Huang [14] that if the matrix [H] is a diagonal matrix, the stiffness matrix satisfies the superposition principle:

$$[K]=\sum_{i=1}^{m}[K_i] \tag{3-63}$$

where

$$\begin{aligned}[K_i]&=[G_i]^T[H_i]^{-1}[G_i]\\ [H_i]&=\int_v[P_i]^T[S][P_i]dV\\ [G_i]&=\int_v[P_i]^T[B]dV\end{aligned} \tag{3-64}$$

and

$$\begin{aligned}[K]&=[G]^T[H]^{-1}[G]\\ [H]&=\int_v[P]^T[S][P]dV\\ [G]&=\int_v[P]^T[B]dV\end{aligned} \tag{3-65}$$

in which

$$[P]=[\{\sigma_1\}\ \{\sigma_2\}\ \{\sigma_3\}\ .....\ \{\sigma_m\}\ ]$$

$$[P_i]=[\{0\}\ \{0\}\ ...\ \{\sigma_i\}\ ...\ \{0\}\ ]$$

$$[G]=\begin{Bmatrix}G_1\\G_2\\...\\G_m\end{Bmatrix} \tag{3-66}$$

Therefore, the elastic energy of the element is decomposable if the flexibility matrix [H] is a diagonal matrix.

3.5.1 Classification condition of stress modes

A hybrid element stiffness matrix [K] can be formulated using equations (3-65) and (3-66). Its eigenvalues and eigenvectors are calculated from equation (3-15). The eigenvectors $\{\delta_i\}$ (i=1,2,...m) satisfy the condition (3-16). Using equations (3-15) and (3-16), the eigenvalue equation is changed to

$$\lambda_i=\{\delta_i\}^T[K]\{\delta_i\} \tag{3-67}$$

For any stress mode $\{\sigma_j\}$ among m stress modes $\{\sigma_1, \sigma_2, ..., \sigma_m\}$, the stiffness matrix $[K_j]$ can be derived using equations (3-64) and (3-66). Corresponding to the i-th natural deformation mode, one has

$$\lambda_i=\{\delta_i\}^T[K_j]\{\delta_i\} \tag{3-68}$$

According to the classification condition of stress modes, if the stress mode $\{\sigma_j\}$ belongs to the i-th stress mode group corresponding to the natural deformation mode $\{\delta_i\}$, the eigenvalue λ_i is a non-zero value; otherwise, the eigenvalue λ_i equals zero. This condition can be expressed in the form,

$$\{\delta_i\}^T[K_j]\{\delta_i\}=0 \qquad i\neq j$$
$$\{\delta_i\}^T[K_j]\{\delta_i\}=\lambda_i \qquad i=j \tag{3-69}$$

If the stress mode $\{\sigma_j\}$ is a zero-energy stress mode, all eigenvalue λ_i (i=1,2,....,m) equal zero.

3.5.2 Theorem

Theorem 1

If and only if the flexibility matrix [H] is a diagonal matrix, the eigenvalues obtained from separate mode equations

$$([K_i]-\lambda[I])\{\delta\}=0, \qquad i=1,2,3....,m \tag{3-70}$$

are equal to the eigenvalues obtained from the total equation

$$([K]-\lambda[I])\{\delta\}=0 \tag{3-71}$$

In which, the matrices $[K_i]$ and [K] are defined in equations (3-64) and (3-65). This was stated as a postulate in ref [14].

Proof:

From the equations (3-67), (3-65) and (3-21), one has

$$\lambda = \{\delta_i\}^T [K] \{\delta_i\} = \{\beta_i\}^T [H] \{\beta_i\} \tag{3-72}$$

Because the matrix [H] is a diagonal matrix, one has

$$[H] = \sum_{j=1}^{m} [H_j] \tag{3-73}$$

Thus, using equations (3-18), (3-19) and (3-64), the eigenvalue of the matrix [K] is

$$\lambda = \sum_{j=1}^{m} \{\beta_i\}^T [H_j] \{\beta_i\} = \{\beta_i\}^T [H_i] \{\beta_i\} \tag{3-74}$$

Furthermore, using equations (3-21) and (3-69), one obtains

$$\lambda = \{\beta_i\}^T [H_i] \{\beta_i\} = \{\delta_i\}^T [K_i] \{\delta_i\} = \lambda_i \tag{3-75}$$

End of proof.

Theorem 2

If the flexibility matrix [H] is a diagonal matrix, the classification of m stress modes is unique.

Proof:

If a stress mode among m stress modes that form the stress matrix [P] appears in more than one stress mode group, one of the m stress mode groups must contain two stress modes. Assume that the stress modes $\{\sigma_i\}$ and $\{\sigma_j\}$ belong to the i-th stress mode group $\{\beta_i\}$ corresponding to the natural deformation modes $\{\delta_i\}$. Thus, one has

$$\lambda_{ii}=\{\delta_i\}^T [K_i]\{\delta_i\} \quad \textit{and} \quad \lambda_{ij}=\{\delta_i\}^T [K_j]\{\delta_i\} \tag{3-76}$$

Corresponding to the natural deformation mode $\{\delta_i\}$, one can obtain the eigenvalue of the stiffness matrix [K] formulated by m stress modes as follows,

$$\lambda=\{\delta_i\}^T [K]\{\delta_i\} \tag{3-77}$$

Because the flexibility matrix [H] is diagonal, the stiffness matrix satisfies the superposition principle. From equations (3-63) and (3-76), one obtains

$$\lambda=\{\delta_i\}^T [K]\{\delta_i\}=\sum_{k=1}^{m} \{\delta_i\}^T [K_k]\{\delta_i\}=\lambda_{ii}+\lambda_{ij} \tag{3-78}$$

using theorem 1, one has

$$\lambda = \lambda_{ii} \tag{3-79}$$

From the equation (3-78) and (3-79), one obtains

$$\lambda_{ij} = 0 \tag{3-80}$$

According to the condition of classification, the stress modes $\{\sigma_j\}$ does not belong to the i-th stress mode group. The stress mode group $\{\beta_i\}$ only contains $\{\sigma_i\}$. Therefore, the

stress modes $\{\sigma_j\}$ can not appear in two stress mode groups $\{\beta_i\}$ and $\{\beta_j\}$. Thus, if the matrix [H] is diagonal, the classification of m stress modes is unique.

End of proof

3.6 Optimal Stress Matrix for Partial Hybrid Element

The classification method can be used to determine an optimal stress matrix for a hybrid element. It is also available to determine an optimal partial stress matrix for a partial hybrid element. The difference is the number of stress mode groups. For partial hybrid element, the number of stress modes groups is equal to

$$m=n-r-n_d \tag{3-81}$$

Where n and r is the same as that in conventional hybrid elements. In section 2.4 of Chapter 2, it has been shown that the stiffness matrix of a partial hybrid element (2-44) or (2-66) consists of two parts: the displacement-formulated stiffness matrix and the hybrid-formulated stiffness matrix. In equation (3-81), n_d is the rank of the displacement-formulated stiffness matrix. Therefore, it is necessary to calculate the rank of the displacement-formulated stiffness matrix to determine an optimal stress matrix for a partial hybrid element. The necessary and sufficient condition for partial hybrid elements becomes

The necessary and sufficient condition.

The number of stress modes in an assumed partial stress matrix must be equal to or more than m (= n-r-n_d) and at least m stress modes in the partial stress matrix [P] must be chosen from m different stress mode groups corresponding to m natural deformation modes of an element which has n degrees of freedom, r rigid body modes, and n_d order displacement-formulated stiffness matrix .

The procedure to construct an optimal partial stress matrix for a partial hybrid element becomes

Step 1:

Examine the rank of the displacement-formulated stiffness matrix of a partial hybrid element.

Step 2:

Using the iso-function method, one can derive a number of initial stress modes to be classified.

Step 3:

One may put the initial stress modes one by one into partial stress matrix [P] in the order from low order term to high order term. By means of the classification method, one can

obtain m representative stress modes corresponding to m natural deformation modes. These representative stress modes form an optimal partial stress matrix $[P_g]_{opt}$ from the existing partial stress matrix $[P_g]_{iso}$.

Following this procedure, an optimal assumed partial stress field can be determined. Some examples will be given in the next chapters.

3.7 Conclusion

A new method for classifying stress modes in assumed stress matrices is presented. It is assumed that there are m (=n-r) natural deformation modes of an element which has n degrees of freedom and r rigid body modes. For any type of hybrid element, all stress modes in various stress matrices derived by different methods can be classified into m stress mode groups corresponding to m natural deformation modes and a zero energy mode group corresponding to rigid body modes. If the flexibility matrix [H] is diagonal, the deformation energy of the element is decomposable and the classification of stress modes is unique. The necessary and sufficient condition for avoiding kinematic deformation modes is that an assumed stress matrix [P] must contain m stress modes chosen from m different stress mode groups, except zero energy mode group. The reason of the existence of kinematic deformation modes when the criterion (m' > n-r) is satisfied is that the stress modes in the assumed stress matrix [P] are not chosen from m different stress mode groups corresponding to m natural deformation modes.

The classification method can be applied to any type of hybrid elements and be used for two purposes:

1. to determine the optimal stress matrix from the existing stress matrix $[P]_{iso}$ or any other stress matrix [P] derived using other method, and classify stress modes into m different stress mode groups;

2. to construct many new assumed stress matrices by using minimum number of stress modes according to the problems to be analyzed. These stress matrices are without zero-energy stress modes, and the resulting element stiffness matrices are free from kinematic deformation modes.

The classification of stress modes reveals the relationship among the different assumed stress fields for any type of hybrid element proposed by different researchers. An assumed stress matrix [P], which consists of m (=n-r) least-order stress modes and results in the element stiffness matrix without kinematic deformation modes, is considered to be best and is optimal with respect to computer resources because overuse of stress modes will result in over-rigid element and cost more computational time.

Chapter 4

3-D PARTIAL HYBRID SOLID ELEMENTS

In Chapter 2, a general formation of the single-layer element is presented. In the element formulation, when N=1, the single-layer element becomes a 3-D solid element because the element only contains a material layer. Many 3-D solid elements can be derived using the general formulation. In this chapter, 3-D, 8-node and 20-node solid elements are presented.

4.1 3-D, 8-node Partial Hybrid Solid Element

The 3-D, 8-node element (shown in figure 4-1) is the simplest finite element for 3-D analysis of structures. Therefore, it is presented first to show the formulation procedure of partial hybrid finite elements [9].

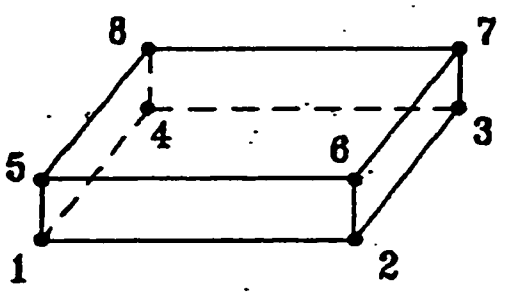

Figure 4-1 3-D, 8-node partial hybrid element

4.1.1 Geometry of Element

To formulate a finite element, the first task is to approximate the element geometry. For an isoparametric element, the element geometric shape is required to be mapped from the global coordinate system to the parametric coordinate system. To map the element geometric shape of a 3-D, 8-node solid element, the global co-ordinates (x,y,z) of any point within the element can be written to interpolate the local co-ordinates (ξ, η, ζ) as follows:

$$x=\sum_{i=1}^{8} N_i x_i \quad y=\sum_{i=1}^{8} N_i y_i \quad z=\sum_{i=1}^{8} N_i z_i \qquad (4\text{-}1)$$

where (x_i y_i z_i) are the global co-ordinates of the i-th node (i=1,2,...,8), and N_i are the

shape functions which can be expressed as follows:

$$N_i=\frac{1}{8}(1+\xi_0)(1+\eta_0)(1+\zeta_0) \tag{4-2}$$

in which,

$$\xi_0=\xi_i\xi \quad \eta_0=\eta_i\eta \quad \zeta_0=\zeta_i\zeta \tag{4-3}$$

where ξ_i, η_i and ζ_i are the local co-ordinates of node i in the element parametric space.

4.1.2 Displacement Field

For an isoparametric element, both the geometry and the displacement field are defined by the same interpolation polynomial. Therefore, within the element, a displacement field is assumed independently as follows:

$$u=\sum_{i=1}^{8} N_i u_i \quad v=\sum_{i=1}^{8} N_i v_i \quad w=\sum_{i=1}^{8} N_i w_i \tag{4-4}$$

where (u_i v_i w_i) are the i-th nodal displacements in the global co-ordinate system (i=1,2,...,8), and N_i are still the shape functions which are the same as that in the geometry formulation of the element (4-2)-(4-3). In the matrix form, the displacement field can be expressed as

$$\boldsymbol{u} = [N]\,\boldsymbol{\delta} = [N_1\boldsymbol{I}\ N_2\boldsymbol{I}\ \ldots\ N_8\boldsymbol{I}]\begin{Bmatrix}\boldsymbol{\delta}_1\\ \boldsymbol{\delta}_2\\ \ldots\\ \boldsymbol{\delta}_8\end{Bmatrix} \tag{4-5}$$

in which, [I] is a 3×3 unit matrix and the nodal displacement vector is

$$\boldsymbol{\delta}_i = \begin{Bmatrix}u_i\\ v_i\\ w_i\end{Bmatrix} \qquad i=1,2,\ldots,8 \tag{4-6}$$

4.1.3 Partial Strain Field and Partial Derivatives of the Displacement Field

After assuming the displacement field, one can derive a partial strain field directly from the displacement field as follows,

$$\boldsymbol{\varepsilon}_g = \begin{Bmatrix}\varepsilon_x\\ \varepsilon_y\\ \varepsilon_{xy}\end{Bmatrix} = \boldsymbol{D}_g\boldsymbol{u} = \begin{Bmatrix}\dfrac{\partial u}{\partial x}\\ \dfrac{\partial v}{\partial y}\\ \dfrac{\partial u}{\partial y}+\dfrac{\partial v}{\partial x}\end{Bmatrix} = [B_g]\boldsymbol{\delta} \tag{4-7}$$

in which,

$$[B_g] = [B_{g1}\ B_{g2}\ \ldots\ B_{g8}] \tag{4-8}$$

and

$$[B_{gi}]=\begin{bmatrix} N_{i,x} & 0 & 0 \\ 0 & N_{i,y} & 0 \\ N_{i,y} & N_{i,x} & 0 \end{bmatrix} \tag{4-9}$$

Due to the fact that the transverse strain-displacement relation (2-9) is satisfied a posteriori, the locally continuous strains can not be derived directly and will be calculated using equation (2-43) after the nodal displacements having been obtained. Also the partial derivatives of displacement field can be obtained as follows,

$$\boldsymbol{D_L u}=\begin{Bmatrix} \dfrac{\partial w}{\partial z} \\ \dfrac{\partial v}{\partial z}+\dfrac{\partial w}{\partial y} \\ \dfrac{\partial w}{\partial x}+\dfrac{\partial u}{\partial z} \end{Bmatrix}=[B_L]\boldsymbol{\delta} \tag{4-10}$$

in which,

$$[B_L]=[B_{L1}\ B_{L2}\ \cdots\ B_{L8}] \tag{4-11}$$

and

$$[B_{Li}]=\begin{bmatrix} 0 & 0 & N_{i,z} \\ 0 & N_{i,z} & N_{i,y} \\ N_{i,z} & 0 & N_{i,x} \end{bmatrix} \tag{4-12}$$

where i=1,2,....,8. In order to perform the evaluation of isoparametric element matrices, a coordinate transformation of derivatives is required because the displacements are described in terms of parametric coordinates. To map the derivatives from global co-

ordinate system to local co-ordinate system, one can write

$$\begin{Bmatrix} N_{i,\xi} \\ N_{i,\eta} \\ N_{i,\zeta} \end{Bmatrix} = \begin{bmatrix} x_{,\xi} & y_{,\xi} & z_{,\xi} \\ x_{,\eta} & y_{,\eta} & z_{,\eta} \\ x_{,\zeta} & y_{,\zeta} & z_{,\zeta} \end{bmatrix} \begin{Bmatrix} N_{i,x} \\ N_{i,y} \\ N_{i,z} \end{Bmatrix} = [J] \begin{Bmatrix} N_{i,x} \\ N_{i,y} \\ N_{i,z} \end{Bmatrix} \tag{4-13}$$

where

$$x_{,\xi} = \sum_{i=1}^{8} N_{i,\xi} x_i, \quad \cdots \quad z_{,\zeta} = \sum_{i=1}^{8} N_{i,\zeta} z_i \tag{4-14}$$

The equation (4-13) can be rewritten

$$\begin{Bmatrix} N_{i,x} \\ N_{i,y} \\ N_{i,z} \end{Bmatrix} = [J]^{-1} \begin{Bmatrix} N_{i,\xi} \\ N_{i,\eta} \\ N_{i,\zeta} \end{Bmatrix} \tag{4-15}$$

in which

$$\begin{aligned} N_{i,\xi} &= \frac{1}{8} \xi_i (1+\eta_0)(1+\zeta_0) \\ N_{i,\eta} &= \frac{1}{8} \eta_i (1+\xi_0)(1+\zeta_0) \\ N_{i,\zeta} &= \frac{1}{8} \zeta_i (1+\xi_0)(1+\eta_0) \end{aligned} \tag{4-16}$$

For mapping the derivatives, it is convenient to introduce a radius vector and its derivatives:

$$\boldsymbol{r}=\begin{pmatrix}x\\y\\z\end{pmatrix} \qquad \boldsymbol{S}=\boldsymbol{r}_{,\xi}=\begin{pmatrix}x_{,\xi}\\y_{,\xi}\\z_{,\xi}\end{pmatrix} \tag{4-17}$$

$$\boldsymbol{T}=\boldsymbol{r}_{,\eta}=\begin{pmatrix}x_{,\eta}\\y_{,\eta}\\z_{,\eta}\end{pmatrix} \qquad \boldsymbol{V}=\boldsymbol{r}_{,\zeta}=\begin{pmatrix}x_{,\zeta}\\y_{,\zeta}\\z_{,\zeta}\end{pmatrix} \tag{4-18}$$

Then, the Jacobian matrix is

$$[J]=[\boldsymbol{S}\ \boldsymbol{T}\ \boldsymbol{V}]^T \tag{4-19}$$

Furthermore, one has

$$|J|=\boldsymbol{S}\cdot\boldsymbol{T}\times\boldsymbol{V} \tag{4-20}$$

and

$$[J]^{-1}=[\boldsymbol{T}\times\boldsymbol{V}\ \boldsymbol{V}\times\boldsymbol{S}\ \boldsymbol{S}\times\boldsymbol{T}]/|J| \tag{4-21}$$

4.1.4 Partial Stress Field

Within the element, a partial stress field is also assumed independently as follows,

$$\boldsymbol{\sigma}_g = \begin{Bmatrix} \sigma_z \\ \sigma_{yz} \\ \sigma_{zx} \end{Bmatrix} = [P_g]\,\boldsymbol{\beta} = [\boldsymbol{\sigma}_{g1}\boldsymbol{\sigma}_{g2}\ldots\boldsymbol{\sigma}_{gI}] \begin{Bmatrix} \beta_1 \\ \beta_2 \\ . \\ . \\ \beta_I \end{Bmatrix} \tag{4-22}$$

Using iso-function method [43], an iso-function partial stress matrix can be derived directly from the displacement field as follows,

$$[P_g] = \begin{bmatrix} 1 & 0 & 0 & \xi & 0 & 0 & \eta & 0 & 0 & \zeta & 0 & 0 & \xi\eta & 0 & 0 & \eta\zeta & 0 & \xi\zeta & 0 \\ 0 & 1 & 0 & 0 & \xi & 0 & 0 & \eta & 0 & 0 & \zeta & 0 & 0 & \xi\eta & 0 & 0 & 0 & 0 & \xi\zeta \\ 0 & 0 & 1 & 0 & 0 & \xi & 0 & 0 & \eta & 0 & 0 & \zeta & 0 & 0 & \xi\eta & 0 & \eta\zeta & 0 & 0 \end{bmatrix} \tag{4-23}$$

In this partial stress matrix, there are 19 stress modes and some of them are not necessary. According to the necessary and sufficient condition presented in section 3.6 of Chapter 3, the number of stress modes in the stress matrix is

$$n_h \geq n - r - n_d \tag{4-24}$$

For the 3-D, 8-node solid element, there are (n=) 24 degrees of freedom and (r=) 6 degrees of the rigid body motion because each node has three components of displacements. Thus, the element has (n-r=) 18 natural deformation modes. By means of eigenvalue examination of the element, the rank of the partial stiffness matrix $[K_d]$ can be determined and it is (n_d=) 10. In order to avoid any kinematic deformation modes, the number of necessary stress modes is equal to 8. Using the classification method, the optimal partial stress matrix is

$$[P_g] = \begin{bmatrix} 1 & 0 & 0 & \xi & \eta & 0 & 0 & \xi\eta \\ 0 & 1 & 0 & 0 & 0 & \xi & -\xi & 0 \\ 0 & 0 & 1 & 0 & 0 & \eta & \eta & 0 \end{bmatrix} \tag{4-25}$$

This partial stress matrix only contains minimum number of stress modes.

4.1.5 Examination of Partial Hybrid Element

After one determines the interpolation functions of the geometry, displacements and partial stress field, the element matrices can be calculated using equations (2-44) in Chapter 2. Then, the new hybrid element has to be examined.

The element quality can be examined by the eigenvalue test which is one of several common tests. The test can detect spurious zero stiffness and absence of rigid-body displacement capability. In testing an element, it must be examined if the element stiffness matrix [K] has as many zero eigenvalues ($\lambda_i = 0$) as expected. Too few suggests that the element lacks a desired capability for rigid-body displacement. Too many suggests the presence of spurious zero stiffness mode. Moreover, nonzero eigenvalues must be real and positive due to that fact that the element stiffness matrix [K] is symmetric and positive semidefinite [6].

The stiffness matrix of a partial hybrid element is in the form,

$$[K] = [K_d] + [K_h] \tag{4-26}$$

There are two parts: a displacement-formulated stiffness matrix and a hybrid-formulated stiffness matrix. The examination of element shows that there is not any kinematic deformation modes, and it has a desired capability for rigid-body displacement.

4.2 3-D, 20-node Partial Hybrid Solid Element

A 3-D, 20-node element [46] is shown in figure 4-2. It also can be obtained using the general formulation of single-layer partial hybrid element in Chapter 2.

4.2.1 Geometry of Element

Firstly, the geometry of the element must be approximated. The global co-ordinates (x,y,z) of any point within the element can be expressed in the form as follows:

$$x=\sum_{I=1}^{20} N_I x_I \quad y=\sum_{I=1}^{20} N_I y_I \quad z=\sum_{I=1}^{20} N_I z_I \tag{4-26}$$

where (x_i y_i z_i) are the global co-ordinates of the i-th node (i=1,2,...,20), and N_i are the shape functions which are the functions of the local co-ordinates (ξ, η, ζ) as follows:

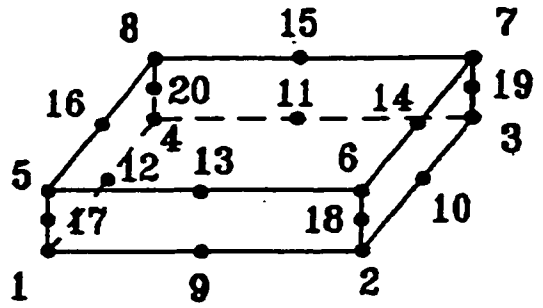

Figure 4-2 3-D, 20-node partial hybrid element

$$
\begin{aligned}
N_I=&\frac{1}{8}(1+\xi_0)(1+\eta_0)(1+\zeta_0)(\xi_0+\eta_0+\zeta_0-2)\xi_I^2\eta_I^2\zeta_I^2\\
&+\frac{1}{4}(1-\xi^2)(1+\eta_0)(1+\zeta_0)(1-\xi_I^2)\eta_I^2\zeta_I^2\\
&+\frac{1}{4}(1-\eta^2)(1+\zeta_0)(1+\xi_0)(1-\eta_I^2)\zeta_I^2\xi_I^2\\
&+\frac{1}{4}(1-\zeta^2)(1+\xi_0)(1+\eta_0)(1-\zeta_I^2)\xi_I^2\eta_I^2
\end{aligned}
\qquad (4\text{-}28)
$$

in which,

$$\xi_0=\xi_i\xi \quad \eta_0=\eta_i\eta \quad \zeta_0=\zeta_i\zeta \qquad (4\text{-}29)$$

where ξ_i, η_i and ζ_i are the local co-ordinates of node i in the element parametric space.

4.2.2 Displacement Field

The element is also an isoparametric element and the interpolation functions of the displacement field are the same as that of the element geometry. Within the element, a displacement field is assumed independently as follows:

$$u=\sum_{i=1}^{20} N_i u_i \qquad v=\sum_{i=1}^{20} N_i v_i \qquad w=\sum_{i=1}^{20} N_i w_i \tag{4-30}$$

where (u_i v_i w_i) are the i-th nodal displacements in the global co-ordinates system (i=1,2,...,20), and N_i are the shape functions. In the matrix form, the displacement field can be expressed as

$$\boldsymbol{u}=[N]\,\boldsymbol{\delta}=[N_1\boldsymbol{I}\ N_2\boldsymbol{I}\ \ldots\ N_{20}\boldsymbol{I}]\begin{Bmatrix}\boldsymbol{\delta}_1\\ \boldsymbol{\delta}_2\\ \ldots\\ \boldsymbol{\delta}_{20}\end{Bmatrix} \tag{4-31}$$

in which, [I] is a 3×3 unit matrix and the nodal displacement vector is

$$\boldsymbol{\delta}_i=\begin{Bmatrix}u_i\\ v_i\\ w_i\end{Bmatrix} \qquad i=1,2,\ldots,20 \tag{4-32}$$

4.2.3 Partial Strain Field and Partial Derivatives of the Displacement Field

Within the partial hybrid element, similar to the 8-node element above, a partial strain

field can be derived directly from the displacement field. It is

$$\boldsymbol{\varepsilon}_g=\begin{Bmatrix}\varepsilon_x\\ \varepsilon_y\\ \varepsilon_{xy}\end{Bmatrix}=\boldsymbol{D}_g\boldsymbol{u}=\begin{Bmatrix}\dfrac{\partial u}{\partial x}\\ \dfrac{\partial v}{\partial y}\\ \dfrac{\partial u}{\partial y}+\dfrac{\partial v}{\partial x}\end{Bmatrix}=[B_g]\boldsymbol{\delta} \tag{4-33}$$

in which,

$$[B_g]=[B_{g1}\ B_{g2}\ \cdots\ B_{g20}] \tag{4-34}$$

and

$$[B_{gi}]=\begin{bmatrix}N_{i,x} & 0 & 0\\ 0 & N_{i,y} & 0\\ N_{i,y} & N_{i,x} & 0\end{bmatrix} \tag{4-35}$$

Because the transverse strain-displacement relation is satisfied a posteriori, only the partial derivatives of displacement field can be derived from the displacement field as follows,

$$\boldsymbol{D}_L\boldsymbol{u}=\begin{Bmatrix}\dfrac{\partial w}{\partial z}\\ \dfrac{\partial v}{\partial z}+\dfrac{\partial w}{\partial y}\\ \dfrac{\partial w}{\partial x}+\dfrac{\partial u}{\partial z}\end{Bmatrix}=[B_L]\boldsymbol{\delta} \tag{4-36}$$

in which,

$$[B_L]=[B_{L1}\ B_{L2}\ \cdots\ B_{L20}] \tag{4-37}$$

and

$$[B_{Li}]=\begin{bmatrix} 0 & 0 & N_{i,z} \\ 0 & N_{i,z} & N_{i,y} \\ N_{i,z} & 0 & N_{i,x} \end{bmatrix} \tag{4-38}$$

where i=1,2,....,20. To map the derivatives from global co-ordinate system to local co-ordinate system, the following equations are used,

$$\begin{Bmatrix} N_{i,\xi} \\ N_{i,\eta} \\ N_{i,\zeta} \end{Bmatrix}=\begin{bmatrix} x_{,\xi} & y_{,\xi} & z_{,\xi} \\ x_{,\eta} & y_{,\eta} & z_{,\eta} \\ x_{,\zeta} & y_{,\zeta} & z_{,\zeta} \end{bmatrix}\begin{Bmatrix} N_{i,x} \\ N_{i,y} \\ N_{i,z} \end{Bmatrix}=[J]\begin{Bmatrix} N_{i,x} \\ N_{i,y} \\ N_{i,z} \end{Bmatrix} \tag{4-39}$$

where

$$x_{,\xi}=\sum_{i=1}^{20} N_{i,\xi}x_i, \quad \cdots \quad z_{,\zeta}=\sum_{i=1}^{20} N_{i,\zeta}z_i \tag{4-40}$$

The equation (4-39) can be rewritten as

$$\begin{Bmatrix} N_{i,x} \\ N_{i,y} \\ N_{i,z} \end{Bmatrix}=[J]^{-1}\begin{Bmatrix} N_{i,\xi} \\ N_{i,\eta} \\ N_{i,\zeta} \end{Bmatrix} \tag{4-41}$$

where

$$
\begin{aligned}
N_{i,\xi} = & \frac{1}{8}\xi_i(1+\eta_0)\,(1+\zeta_0)\,(2\xi_0+\eta_0+\zeta_0-1)\,\xi_i^2\eta_i^2\zeta_i^2 \\
& -\frac{1}{2}\xi\,(1+\eta_0)\,(1+\zeta_0)\,(1-\xi_i^2)\,\eta_i^2\zeta_i^2 \\
& +\frac{1}{4}\xi_i(1-\eta^2)\,(1+\zeta_0)\,(1-\eta_i^2)\,\zeta_i^2\xi_i^2 \\
& +\frac{1}{4}\xi_i(1-\zeta^2)\,(1+\eta_0)\,(1-\zeta_i^2)\,\xi_i^2\eta_i^2
\end{aligned}
\tag{4-42}
$$

$$
\begin{aligned}
N_{i,\eta} = & \frac{1}{8}\eta_i(1+\xi_0)\,(1+\zeta_0)\,(\xi_0+2\eta_0+\zeta_0-1)\,\xi_i^2\eta_i^2\zeta_i^2 \\
& +\frac{1}{4}\eta_i(1-\xi^2)\,(1+\zeta_0)\,(1-\xi_i^2)\,\eta_i^2\zeta_i^2 \\
& -\frac{1}{2}\eta\,(1+\zeta_0)\,(1+\xi_0)\,(1-\eta_i^2)\,\zeta_i^2\xi_i^2 \\
& +\frac{1}{4}\eta_i(1-\zeta^2)\,(1+\xi_0)\,(1-\zeta_i^2)\,\xi_i^2\eta_i^2
\end{aligned}
\tag{4-43}
$$

$$
\begin{aligned}
N_{i,\zeta} = & \frac{1}{8}\zeta_i(1+\xi_0)\,(1+\eta_0)\,(\xi_0+\eta_0+2\zeta_0-1)\,\xi_i^2\eta_i^2\zeta_i^2 \\
& +\frac{1}{4}\zeta_i(1-\xi^2)\,(1+\eta_0)\,(1-\xi_i^2)\,\eta_i^2\zeta_i^2 \\
& +\frac{1}{4}\zeta_i(1-\eta^2)\,(1+\xi_0)\,(1-\eta_i^2)\,\zeta_i^2\xi_i^2 \\
& -\frac{1}{2}\zeta\,(1+\xi_0)\,(1+\eta_0)\,(1-\zeta_i^2)\,\xi_i^2\eta_i^2
\end{aligned}
\tag{4-44}
$$

For mapping the derivatives, a radius vector and its derivatives defined by equations (4-17)-(4-21) are also used.

4.2.4 Partial Stress Field

Within the element, a partial stress field is assumed independently as follows,

$$\boldsymbol{\sigma}_g = \begin{Bmatrix} \sigma_x \\ \sigma_{yz} \\ \sigma_{zx} \end{Bmatrix} = [P_g]\,\boldsymbol{\beta} = [\boldsymbol{\sigma}_{g1}\boldsymbol{\sigma}_{g2}\ldots\boldsymbol{\sigma}_{gl}] \begin{Bmatrix} \beta_1 \\ \beta_2 \\ . \\ . \\ \beta_l \end{Bmatrix} \tag{4-45}$$

Using iso-function method, an iso-function partial stress matrix can be derived from the displacement field as follows,

$$[P_g] = \left|\begin{array}{cccccccccccccccccccc}
1 & 0 & 0 & \xi & 0 & 0 & \eta & 0 & 0 & \zeta & 0 & 0 & \xi\eta & 0 & 0 & \xi\zeta & 0 & 0 & & \\
0 & 1 & 0 & 0 & \xi & 0 & 0 & \eta & 0 & 0 & \zeta & 0 & 0 & \xi\eta & 0 & 0 & \xi\zeta & 0 & & \\
0 & 0 & 1 & 0 & 0 & \xi & 0 & 0 & \eta & 0 & 0 & \zeta & 0 & 0 & \xi\eta & 0 & 0 & \xi\zeta & &
\end{array}\right.$$

$$\left|\begin{array}{cccccccccccccccccccc}
\eta\zeta & 0 & 0 & \xi\eta\zeta & 0 & 0 & \xi^2 & 0 & 0 & \eta^2 & 0 & 0 & \zeta^2 & 0 & 0 & \xi^2\eta & & & & \\
0 & \eta\zeta & 0 & 0 & \xi\eta\zeta & 0 & 0 & \xi^2 & 0 & 0 & \eta^2 & 0 & 0 & \zeta^2 & 0 & 0 & & & & \\
0 & 0 & \eta\zeta & 0 & 0 & \xi\eta\zeta & 0 & 0 & \xi^2 & 0 & 0 & \eta^2 & 0 & 0 & \zeta^2 & 0 & & & &
\end{array}\right. \tag{4-46}$$

$$\left|\begin{array}{cccccccccccccccccccc}
0 & 0 & \xi^2\zeta & 0 & \xi\eta^2 & 0 & 0 & \eta^2\zeta & 0 & \xi\zeta^2 & 0 & \eta\zeta^2 & 0 & & & & & & & \\
\xi^2\eta & 0 & 0 & \xi^2\zeta & 0 & \xi\eta^2 & 0 & 0 & 0 & 0 & \xi\zeta^2 & 0 & 0 & & & & & & & \\
0 & \xi^2\eta & 0 & 0 & 0 & 0 & \xi\eta^2 & 0 & \eta^2\zeta & 0 & 0 & 0 & \eta\zeta^2 & & & & & & &
\end{array}\right|$$

In this partial stress matrix, there are 47 stress modes. In this element, there are 20 nodes and each node has three components of displacements. Therefore, the element has (n=) 60 degrees of freedom. The degrees of the rigid displacement are equal to (r=) 6. Thus, the element has (n-r=) 54 natural deformation modes. The examination of the partial stiffness matrix $[K_d]$ gives 31 non-zero eigenvalues. So the rank of the partial stiffness

matrix $[K_d]$ is (n_d=) 31. The minimum number of necessary stress modes in the stress matrix [P] is (m=) 23 in order to avoid any kinematic deformation modes mode.

In the iso-function stress matrix (4-46), there are 47 stress modes. It is more than double the number of necessary stress modes. The stress matrix (4-46) can be expressed in the form

$$[P_g] = [\sigma_1 \ \sigma_2 \ \sigma_3 \ \ldots \ \sigma_i \ \ldots \ \sigma_{47} \ ] \tag{4-47}$$

Based on this iso-function stress matrix, the classification method gives an optimal stress matrix as follows,

$$[P_g] = \left| \begin{array}{cccccccccccccccccccccccc} 1 & 0 & 0 & \xi & 0 & 0 & \eta & 0 & 0 & \zeta & 0 & 0 & \xi\eta & 0 & 0 & \xi\zeta & 0 & 0 & \eta\zeta & 0 & \xi\eta\zeta & 0 & 0 \\ 0 & 1 & 0 & 0 & \xi & 0 & 0 & \eta & 0 & 0 & \zeta & 0 & 0 & \xi\eta & 0 & 0 & \xi\zeta & 0 & 0 & \eta\zeta & 0 & \xi\eta\zeta & 0 \\ 0 & 0 & 1 & 0 & 0 & \xi & 0 & 0 & \eta & 0 & 0 & \zeta & 0 & 0 & \xi\eta & 0 & 0 & \xi\zeta & 0 & 0 & \eta\zeta & 0 & \xi\eta\zeta \end{array} \right| \tag{4-48}$$

or

$$[P_g] = [\sigma_1 \ \sigma_2 \ \sigma_3 \ \ldots \ \sigma_{20} \ \sigma_{22} \ \ldots \ \sigma_{24} \ ] \tag{4-49}$$

4.2.5 Examination of Partial Hybrid Element

After determining the interpolation functions of the geometry, displacements and partial stress field, the element matrices can be calculated using equations (2-44) in Chapter 2. The element quality is also examined by the eigenvalue test. The two stiffness matrices of the 3-D, 20-node partial hybrid elements are examined. One is for isotropic material (see table 4-1); another is for anisotropic material (see table 4-2). In the tables,

$$\underline{\lambda_i} = \frac{\lambda_{hi}}{\lambda_{ui}} \qquad (4\text{-}50)$$

where λ_{hi} is the eigenvalue of the partial hybrid element; and λ_{ui} is the eigenvalue of its displacement counterpart. In tables 4-1 and 4-2, there are not any spurious zero eigenvalues. So the elements do not have any spurious kinematic deformation modes. From the results in tables 4-1 and 4-2, it can be concluded that if an assumed partial stress field can be used to construct a partial hybrid element without kinematic deformation modes for the isotropic materials, it also can be used to construct the elements for anisotropic materials.

Table 4-1 Eigenvalues of stiffness matrix for the 20-node solid element with 23 stress modes and isotropic materials: E=1100 GPa, ν=0.1

No.	$\underline{\lambda}_i$	No.	$\underline{\lambda}_i$	No.	$\underline{\lambda}_i$
1	0.3822	19	0.9066	37	0.9594
2	0.3822	20	0.9106	38	0.9654
3	0.4759	21	0.9235	39	0.9694
4	0.5549	22	0.9272	40	0.9694
5	0.6403	23	0.9277	41	0.9694
6	0.6445	24	0.9296	42	0.9730
7	0.6846	25	0.9296	43	0.9782
8	0.7257	26	0.9366	44	0.9782
9	0.7257	27	0.9366	45	0.9782
10	0.7293	28	0.9376	46	0.9797
11	0.7679	29	0.9376	47	0.9881
12	0.7858	30	0.9389	48	0.9983
13	0.8467	31	0.9559	49	0.9983
14	0.8550	32	0.9559	50	0.9988
15	0.8657	33	0.9568	51	0.9989
16	0.8801	34	0.9573	52	1.0000
17	0.9001	35	0.9575	53	1.0000
18	0.9011	36	0.9575	54	1.0000

Table 4-2 Eigenvalues of stiffness matrix for the 20-node solid element with 23 stress modes and anisotropic materials: E_L=174.6 GPa, E_T=7.0 GPa, G_{LT}=3.5 GPa, G_{TT}=1.4 GPa, $\nu_{12}=\nu_{13}=\nu_{23}$=0.25

No.	$\underline{\lambda}_i$	No.	$\underline{\lambda}_i$	No.	$\underline{\lambda}_i$
1	0.5357	19	0.9641	37	0.9314
2	0.5888	20	0.9675	38	0.9994
3	0.5497	21	0.9206	39	0.9729
4	0.5013	22	0.9511	40	0.9593
5	0.6031	23	0.9316	41	0.9631
6	0.8726	24	0.8770	42	0.9807
7	0.7696	25	0.9044	43	0.9931
8	0.8002	26	0.9672	44	0.9442
9	0.9358	27	0.9759	45	1.0000
10	0.8494	28	0.9371	46	1.0000
11	0.5934	29	0.8017	47	0.9971
12	0.8294	30	0.8755	48	0.9975
13	0.8994	31	0.9618	49	0.9996
14	0.8053	32	0.9837	50	0.9961
15	0.8532	33	0.9952	51	0.9958
16	0.7674	34	0.9972	52	0.9975
17	0.7128	35	0.9974	53	0.9992
18	0.8763	36	0.9991	54	1.0000

In order to study the effect of extra stress modes on the stiffness of elements, the assumed partial stress field consisted of the first 33 stress modes in iso-function stress matrix is examined. The results of the eigenvalue analysis are presented in table 4-3. Comparing

the $\underline{\lambda}_i$ in the table 4-1 and the table 4-3, it is shown that the eigenvalue $\underline{\lambda}_i$ of the element using 33 stress modes is larger than that using 23 stress modes. Therefore, the added stress modes stiffen the elements. One can examine a series of partial hybrid elements using different number of stress modes in the assumed stress matrix. The examination will show that the more stress modes there are, the more stiffening the element is. If there are sufficient added stress modes in the assumed stress matrix, the stiffness of the partial hybrid element will be equal to its displacement counterpart. Such partial hybrid element has been presented by Han [43].

The examination of element shows that there is not any kinematic deformation modes, and it has a desired capability for rigid-body displacement.

Table 4-3 Eigenvalues of stiffness matrix for the 20-node solid element with 33 stress modes and isotropic materials: E=1100 GPa, ν=0.1

No.	λ_i	No.	λ_i	No.	λ_i
1	0.4685	19	0.9971	37	1.0000
2	0.4685	20	0.9971	38	1.0000
3	0.7293	21	0.9981	39	1.0000
4	0.8803	22	0.9983	40	1.0000
5	0.9014	23	0.9983	41	1.0000
6	0.9014	24	0.9988	42	1.0000
7	0.9277	25	1.0000	43	1.0000
8	0.9296	26	1.0000	44	1.0000
9	0.9296	27	1.0000	45	1.0000
10	0.9389	28	1.0000	46	1.0000
11	0.9497	29	1.0000	47	1.0000
12	0.9556	30	1.0000	48	1.0000
13	0.9573	31	1.0000	49	1.0000
14	0.9575	32	1.0000	50	1.0000
15	0.9575	33	1.0000	51	1.0000
16	0.9730	34	1.0000	52	1.0000
17	0.9782	35	1.0000	53	1.0000
18	0.9878	36	1.0000	54	1.0000

Chapter 5

PARTIAL HYBRID LAMINATED ELEMENTS

The degenerated plate element was originally introduced by Ahmed, Irons and Zienkiewicz [107] for the linear analysis of moderately thick and thin shells. Chao and Reddy [23] presented a degenerated element based on the total Lagrangian description of the motion of a layered anisotropic composite medium. But similar to the plate/shell elements based on the 2-D plate/shell theories, for analysis of composites, the degenerated plate/shell elements using displacement element formulation suffer from a common deficiency: constitutive equations lead to discontinuous interlaminar stresses. Equilibrium equations have been often used in recovering the interlaminar stresses. Regardless of the controversy and complexity, the use of equilibrium equations will reduce the accuracy of the stresses owing to the numerical differentiation. However, partial hybrid elements formulation can overcome the stress continuity limitations of single-layer models due to the fact that a partial stress field is assumed independently. Here, the 4-node and 8-node

degenerated plate elements [44,45] are presented using partial hybrid element formulation. Their number of degrees of freedom per node is independent from the number of layers in a composite structure.

5.1 4-node Partial Hybrid Degenerated Plate Element

5.1.1 Geometry of Element

Firstly, consider a typical thick plate element in figure 5-1. The co-ordinates of a typical point in the element can be written as

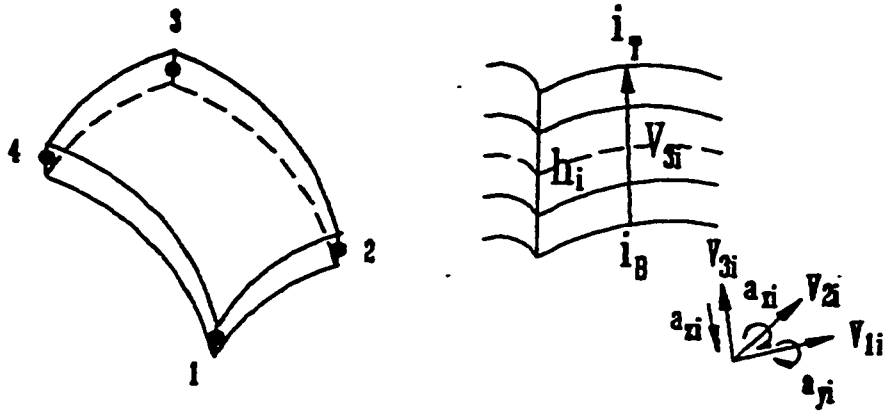

(a) (b)

Figure 5-1 A 4-node degenerated plate element

$$\begin{Bmatrix} x \\ y \\ z \end{Bmatrix} = \sum_{i=1}^{4} N_i(\xi,\eta)\,\frac{1+\zeta}{2}\begin{Bmatrix} x_i \\ y_i \\ z_i \end{Bmatrix}_{top} + \sum_{i=1}^{4} N_i(\xi,\eta)\,\frac{1-\zeta}{2}\begin{Bmatrix} x_i \\ y_i \\ z_i \end{Bmatrix}_{bottom} \qquad (5\text{-}1)$$

where $N_i(\xi,\eta)$ are shape functions, ξ and η are the normalized curvilinear co-ordinates in the middle plane of the plate, ζ is a linear co-ordinate in the thickness direction and only approximately normal to the middle surface, and (x_i, y_i, z_i) are the global co-ordinates at node i. The shape functions are

$$N_i = \frac{1}{4}(1+\xi_0)(1+\eta_0) \qquad (5\text{-}2)$$

in which,

$$\xi_0 = \xi_i\xi \quad \eta_0 = \eta_i\eta \quad (i=1,2,3,4) \qquad (5\text{-}3)$$

This equation can be rewritten in the form specified by the 'vector' connecting the upper and lower points (shown in figure 5-1) and the mid-surface co-ordinates as

$$\begin{Bmatrix} x \\ y \\ z \end{Bmatrix} = \sum_{i=1}^{4} N_i(\xi,\eta)\begin{Bmatrix} x_i \\ y_i \\ z_i \end{Bmatrix} + \sum_{i=1}^{4} N_i(\xi,\eta)\,h_i\,\frac{\zeta}{2}\mathbf{v}_{3i} \qquad (5\text{-}4)$$

where

$$\mathbf{v}_{3i} = \begin{Bmatrix} l_{3i} \\ m_{3i} \\ n_{3i} \end{Bmatrix} = \frac{1}{h_i}\left(\begin{Bmatrix} x_i \\ y_i \\ z_i \end{Bmatrix}_T - \begin{Bmatrix} x_i \\ y_i \\ z_i \end{Bmatrix}_B\right) \qquad (5\text{-}5)$$

and

$$h_i=\sqrt{(x_{iT}-x_{iB})^2+(y_{iT}-y_{iB})^2+(z_{iT}-z_{iB})^2} \qquad (5\text{-}6)$$

5.1.2 Displacement Field

In the element, the displacement field is assumed as a continuous field through the entire thickness of a composite structure. Although there are numerous plate theories which include transverse shear deformations in the literature, the transverse normal stress is always not taken into account. Actually, the hypothesis $\varepsilon_z = 0$ (or an equivalent hypothesis) should not be used [108] in order to construct the consistent high-order theory. For analysis of composite structures, the first-order shear deformation theory has to be improved. For this element, the following displacement field is assumed [44-45],

$$\begin{aligned} u &= u_0 + z\, a_x \\ v &= v_0 + z\, a_y \\ w &= w_0 + z\, a_z \end{aligned} \qquad (5\text{ - }7)$$

In this displacement field, it is assumed that a line that is straight and normal to the middle surface before deformation is still straight, but not necessarily 'normal' to the middle surface after deformation. Thus, the displacement throughout the element will be uniquely defined by three Cartesian components (u_i, v_i and w_i) of the displacement at

the mid-surface node i, two rotations (a_{xi} and a_{yi}) of the nodal vector $\mathbf{V}_{3i}$ about orthogonal directions normal to it, and one transverse normal deformation (a_{zi}) in the thickness direction. Based on this assumption, the i-th nodal displacement can be expressed as

$$\mathbf{u}_i=\begin{Bmatrix}u_i\\v_i\\w_i\end{Bmatrix}+\frac{h_i}{2}\zeta\,[\mathbf{V}_{1i}\ -\mathbf{V}_{2i}\ \mathbf{0}]\begin{Bmatrix}a_{xi}\\a_{yi}\\0\end{Bmatrix}+\frac{h_i}{2}\zeta\,[\mathbf{0}\ \mathbf{0}\ \mathbf{V}_{3i}]\begin{Bmatrix}0\\0\\a_{zi}\end{Bmatrix} \qquad (5\text{-}8)$$

in which, $\mathbf{V}_{1i}$, $\mathbf{V}_{2i}$ and $\mathbf{V}_{3i}$ are the unit vectors of the local co-ordinate (ξ, η, ζ) at node i. They can be calculated as follows:

$$\mathbf{V}_{1i}=\begin{Bmatrix}l_{1i}\\m_{1i}\\n_{1i}\end{Bmatrix}=\frac{\mathbf{i}\times\mathbf{V}_{3i}}{|\mathbf{i}\times\mathbf{V}_{3i}|} \qquad \mathbf{V}_{2i}=\begin{Bmatrix}l_{2i}\\m_{2i}\\n_{2i}\end{Bmatrix}=\mathbf{V}_{3i}\times\mathbf{V}_{1i} \qquad (5\text{-}9)$$

If $\mathbf{i}\times\mathbf{V}_{3i}=0$, $\mathbf{i}$ can be replaced by $\mathbf{j}$. Thus, the displacement field is

$$\begin{Bmatrix}u\\v\\w\end{Bmatrix}=\sum_{i=1}^{4}N_i\left[\begin{Bmatrix}u_i\\v_i\\w_i\end{Bmatrix}+\frac{\zeta}{2}h_i\begin{bmatrix}l_{1i}&-l_{2i}&l_{3i}\\m_{1i}&-m_{2i}&m_{3i}\\n_{1i}&-n_{2i}&n_{3i}\end{bmatrix}\begin{Bmatrix}a_{xi}\\a_{yi}\\a_{zi}\end{Bmatrix}\right] \qquad (5\text{-}10)$$

They can be rewritten in the form

$$\begin{Bmatrix}u\\v\\w\end{Bmatrix}=\sum_{i=1}^{4}N_i\left[\begin{Bmatrix}u_i\\v_i\\w_i\end{Bmatrix}+\zeta\,[b_i]\begin{Bmatrix}a_{xi}\\a_{yi}\\a_{zi}\end{Bmatrix}\right]=\sum_{i=1}^{4}[N]_i\boldsymbol{\delta}_i \qquad (5\text{-}11)$$

where

$$[b_i]=\begin{bmatrix} b_{11i} & b_{12i} & b_{13i} \\ b_{21i} & b_{22i} & b_{23i} \\ b_{31i} & b_{32i} & b_{33i} \end{bmatrix}=\frac{h_i}{2}[\boldsymbol{V}_{1i} \ -\boldsymbol{V}_{2i} \ \boldsymbol{V}_{3i}] \tag{5-12}$$

$$\boldsymbol{\delta}_i=[u_i \ v_i \ w_i \ a_{xi} \ a_{yi} \ a_{zi}]^T \tag{5-13}$$

$$[N]_i=\begin{bmatrix} N_i & 0 & 0 & N_i\zeta b_{11i} & N_i\zeta b_{12i} & N_i\zeta b_{13i} \\ 0 & N_i & 0 & N_i\zeta b_{21i} & N_i\zeta b_{22i} & N_i\zeta b_{23i} \\ 0 & 0 & N_i & N_i\zeta b_{31i} & N_i\zeta b_{32i} & N_i\zeta b_{33i} \end{bmatrix} \tag{5-14}$$

5.1.3 Partial Strain Field and Partial Derivatives of the Displacement Field

The partial globally continuous strains can be derived from the displacement field as follows,

$$\boldsymbol{\varepsilon}_g=\begin{Bmatrix} \varepsilon_x \\ \varepsilon_y \\ \varepsilon_{xy} \end{Bmatrix}=\boldsymbol{D}_g\boldsymbol{u}=\begin{Bmatrix} \dfrac{\partial u}{\partial x} \\ \dfrac{\partial v}{\partial y} \\ \dfrac{\partial u}{\partial y}+\dfrac{\partial v}{\partial x} \end{Bmatrix}=[B_g]\boldsymbol{\delta} \tag{5-15}$$

in which,

$$[B_g]=[B_{g1} \ B_{g2} \ \cdots \ B_{g4}] \tag{5-16}$$

and

$$\boldsymbol{\delta}=[\boldsymbol{\delta}_1 \ \boldsymbol{\delta}_2 \ \boldsymbol{\delta}_3 \ \boldsymbol{\delta}_4]^T \tag{5-17}$$

The partial geometric matrix at the i-th node is,

$$[B_{gi}] = \begin{vmatrix} N_{i,x} & 0 & 0 & b_{11i}c_{ix} & b_{12i}c_{ix} & b_{13i}c_{ix} \\ 0 & N_{i,y} & 0 & b_{21i}c_{iy} & b_{22i}c_{iy} & b_{23i}c_{iy} \\ N_{i,y} & N_{i,x} & 0 & b_{11i}c_{iy}+b_{21i}c_{ix} & b_{12i}c_{iy}+b_{22i}c_{ix} & b_{13i}c_{iy}+b_{23i}c_{ix} \end{vmatrix} \tag{5-18}$$

where

$$\begin{aligned} c_{ix} &= N_{i,x}\zeta + N_i\zeta_{,x} \\ c_{iy} &= N_{i,y}\zeta + N_i\zeta_{,y} \\ c_{iz} &= N_{i,z}\zeta + N_i\zeta_{,z} \end{aligned} \tag{5-19}$$

Because the transverse strain-displacement relation is satisfied a posteriori, the locally continuous strains can not be derived directly from the displacement field. Only the partial derivatives of displacement field can be derived as follows,

$$\boldsymbol{D}_L\boldsymbol{u} = \begin{Bmatrix} \dfrac{\partial w}{\partial z} \\ \dfrac{\partial v}{\partial z} + \dfrac{\partial w}{\partial y} \\ \dfrac{\partial w}{\partial x} + \dfrac{\partial u}{\partial z} \end{Bmatrix} = [B_L]\boldsymbol{\delta} \tag{5-20}$$

in which,

$$[B_L] = [B_{L1}\ B_{L2}\ \cdots\ B_{L4}] \tag{5-21}$$

and

$$[B_{Li}] = \begin{vmatrix} 0 & 0 & N_{i,z} & b_{31i}c_{iz} & b_{32i}c_{iz} & b_{33i}c_{iz} \\ 0 & N_{i,z} & N_{i,y} & b_{21i}c_{iz}+b_{31i}c_{iy} & b_{22i}c_{iz}+b_{32i}c_{iy} & b_{23i}c_{iz}+b_{33i}c_{iy} \\ N_{i,z} & 0 & N_{i,x} & b_{31i}c_{ix}+b_{11i}c_{iz} & b_{32i}c_{ix}+b_{12i}c_{iz} & b_{33i}c_{ix}+b_{13i}c_{iz} \end{vmatrix} \quad (5\text{-}22)$$

In order to perform the evaluation of isoparametric element matrices, a coordinate transformation of derivatives is required. For calculating $N_{i,x}$, $N_{i,y}$, $N_{i,z}$ and $\zeta_{,x}$, $\zeta_{,y}$, $\zeta_{,z}$, the following vectors are introduced:

$$\boldsymbol{S} = \begin{Bmatrix} x,_\xi \\ y,_\xi \\ z,_\xi \end{Bmatrix} = \sum_{i=1}^{4} N_{i,\xi} \left(\begin{Bmatrix} x_i \\ y_i \\ z_i \end{Bmatrix} + \frac{h_i}{2} \zeta \boldsymbol{V}_{3i} \right) \quad (5\text{-}23)$$

$$\boldsymbol{T} = \begin{Bmatrix} x,_\eta \\ y,_\eta \\ z,_\eta \end{Bmatrix} = \sum_{i=1}^{4} N_{i,\eta} \left(\begin{Bmatrix} x_i \\ y_i \\ z_i \end{Bmatrix} + \frac{h_i}{2} \zeta \boldsymbol{V}_{3i} \right) \quad (5\text{-}24)$$

$$\boldsymbol{V} = \begin{Bmatrix} x,_\zeta \\ y,_\zeta \\ z,_\zeta \end{Bmatrix} = \sum_{i=1}^{4} N_i \frac{h_i}{2} \boldsymbol{V}_{3i} \quad (5\text{-}25)$$

then, the Jacobian matrix is

$$[\,J\,] = [\,\mathbf{S}\ \ \mathbf{T}\ \ \mathbf{V}\,]^T \quad (5\text{-}26)$$

and then,

$$[\,J\,]^{-1} = [\,\mathbf{T}\times\mathbf{V}\quad \mathbf{V}\times\mathbf{S}\quad \mathbf{S}\times\mathbf{T}\,] \,/\, |\,J\,| \qquad (5-27)$$

and

$$|\,J\,| = \mathbf{S}\times\mathbf{T}\cdot\mathbf{V} \qquad (5-28)$$

Because

$$\begin{Bmatrix} N_{i,\xi} \\ N_{i,\eta} \\ N_{i,\zeta} \end{Bmatrix} = \begin{bmatrix} x_{,\xi} & y_{,\xi} & z_{,\xi} \\ x_{,\eta} & y_{,\eta} & z_{,\eta} \\ x_{,\zeta} & y_{,\zeta} & z_{,\zeta} \end{bmatrix} \begin{Bmatrix} N_{i,x} \\ N_{i,y} \\ N_{i,z} \end{Bmatrix} = [J] \begin{Bmatrix} N_{i,x} \\ N_{i,y} \\ N_{i,z} \end{Bmatrix} \qquad (5\text{-}29)$$

the derivatives of shape function with respect to global co-ordinates are

$$\begin{Bmatrix} N_{i,x} \\ N_{i,y} \\ N_{i,z} \end{Bmatrix} = \begin{bmatrix} \xi_{,x} & \eta_{,x} & \zeta_{,x} \\ \xi_{,y} & \eta_{,y} & \zeta_{,y} \\ \xi_{,z} & \eta_{,z} & \zeta_{,z} \end{bmatrix} \begin{Bmatrix} N_{i,\xi} \\ N_{i,\eta} \\ N_{i,\zeta} \end{Bmatrix} = [J]^{-1} \begin{Bmatrix} N_{i,\xi} \\ N_{i,\eta} \\ N_{i,\zeta} \end{Bmatrix} \qquad (5\text{-}30)$$

Due to $N_{i,\zeta} = 0$, the expression (5-30) can be rewritten as

$$\begin{Bmatrix} N_{i,x} \\ N_{i,y} \\ N_{i,z} \end{Bmatrix} = [\,\boldsymbol{T}\times\boldsymbol{V}\quad \boldsymbol{V}\times\boldsymbol{S}\,] \,/\, |J| \begin{Bmatrix} N_{i,\xi} \\ N_{i,\eta} \end{Bmatrix} \qquad (5\text{-}31)$$

and

$$\begin{Bmatrix} \zeta_{,x} \\ \zeta_{,y} \\ \zeta_{,z} \end{Bmatrix} = \frac{\boldsymbol{S}\times\boldsymbol{T}}{|J|} \qquad (5\text{-}32)$$

The geometric matrix [B'] in the local co-ordinate system can be obtained by means of transformation matrix [T],

$$[B'] = \begin{Bmatrix} B'_g \\ B'_L \end{Bmatrix} = [T_B] \begin{Bmatrix} B_g \\ B_L \end{Bmatrix} \tag{5-33}$$

and

$$[T_B] = \begin{bmatrix} l_1^2 & m_1^2 & l_1 m_1 & n_1^2 & m_1 n_1 & n_1 l_1 \\ l_2^2 & m_2^2 & l_2 m_2 & n_2^2 & m_2 n_2 & n_2 l_2 \\ 2l_1 l_2 & 2m_1 m_2 & l_1 m_2 + l_2 m_1 & 2n_1 n_2 & m_1 n_2 + m_2 n_1 & n_1 l_2 + n_2 l_1 \\ l_3^2 & m_3^2 & l_3 m_3 & n_3^2 & m_3 n_3 & n_3 l_3 \\ 2l_2 l_3 & 2m_2 m_3 & l_2 m_3 + l_3 m_2 & 2n_2 n_3 & m_2 n_3 + m_3 n_2 & n_2 l_3 + n_3 l_2 \\ 2l_3 l_1 & 2m_3 m_1 & l_3 m_1 + l_1 m_3 & 2n_3 n_1 & m_3 n_1 + m_1 n_3 & n_3 l_1 + n_1 l_3 \end{bmatrix} \tag{5-34}$$

$[T_B]$ is the transformation matrix for the derivatives of displacements from global co-ordinate (x, y, z) to local co-ordinate. The direction cosines of the local co-ordinates are

$$\boldsymbol{V}_3 = \begin{Bmatrix} l_3 \\ m_3 \\ n_3 \end{Bmatrix} = \frac{\sum_{i=1}^{4} N_i \boldsymbol{V}_{3i}}{\left| \sum_{i=1}^{4} N_i \boldsymbol{V}_{3i} \right|} \tag{5-35}$$

and

$$\boldsymbol{V}_1 = \begin{Bmatrix} l_1 \\ m_1 \\ n_1 \end{Bmatrix} = \frac{\boldsymbol{i} \times \boldsymbol{V}_3}{|\boldsymbol{i} \times \boldsymbol{V}_3|} \quad \boldsymbol{V}_2 = \begin{Bmatrix} l_2 \\ m_2 \\ n_2 \end{Bmatrix} = \boldsymbol{V}_3 \times \boldsymbol{V}_1 \tag{5-36}$$

5.1.4 Partial Stress Field

In the element, the partial stress field is assumed independently as continuous functions along the thickness of a composite structure.

$$\boldsymbol{\sigma}_g=\begin{Bmatrix}\sigma_z\\ \tau_{yz}\\ \tau_{zx}\end{Bmatrix}=[P_g]\,\boldsymbol{\beta}=[T]\,[P]\,\boldsymbol{\beta}=[T]\,[\boldsymbol{\sigma}_1\ \boldsymbol{\sigma}_2\ldots\boldsymbol{\sigma}_m]\begin{Bmatrix}\beta_1\\ \beta_2\\ \cdots\\ \beta_m\end{Bmatrix} \qquad (5\text{-}37)$$

where, β is the stress parameter vector. The matrix [T] is a multiplying matrix and is determined by the traction conditions on the top and bottom surfaces of the structure. For example, if there is a distributed normal load on the upper surface, the transverse shear stresses must be equal to zero on both surfaces of top and bottom, and the transverse normal stress must be equal to zero on the bottom surface and be equal to the distributed load on the top surface. Therefore, the multiplying matrix has to be assumed as

$$[T]=\begin{bmatrix}1+\zeta & 0 & 0\\ 0 & 1-\zeta^2 & 0\\ 0 & 0 & 1-\zeta^2\end{bmatrix} \qquad (5\text{-}38)$$

The matrix [P] consists of a group of stress modes which can be derived directly from the assumed displacement field using the iso-function method. The iso-function partial stress matrix of the element is

$$[P]=\begin{bmatrix}1&0&0&\xi&0&0&\eta&0&0&\zeta&0&0&\xi\eta&0&0&\eta\zeta&0&\xi\zeta&0\\ 0&1&0&0&\xi&0&0&\eta&0&0&\zeta&0&0&\xi\eta&0&0&0&0&\xi\zeta\\ 0&0&1&0&0&\xi&0&0&\eta&0&0&\zeta&0&0&\xi\eta&0&\eta\zeta&0&0\end{bmatrix} \qquad (5\text{-}39)$$

In the element, there are (n=) 24 degrees of freedom and (r=) 6 degrees of the rigid displacement. The element has (n-r=) 18 natural deformation modes. The eigenvalue examination of the semi-stiffness matrix $[K_d]$ gives 10 non-zero eigenvalues. So the rank of the partial stiffness matrix $[K_d]$ is (n_d=) 10. Thus, the minimum number of necessary stress modes in the stress matrix [P] equals (n-r-n_d=) 8 according to the condition (3-81)in section 3.6 of Chapter 3.

Based on the iso-function partial stress matrix (5-38), when the multiplying matrix [T] is an unit matrix [I], the classification method gives an optimal stress matrix as follows,

$$[P]=\begin{bmatrix} 1 & 0 & 0 & \xi & 0 & \eta & 0 & \xi\eta \\ 0 & 1 & 0 & 0 & 0 & 0 & \eta & 0 \\ 0 & 0 & 1 & 0 & \xi & 0 & 0 & 0 \end{bmatrix} \qquad (5\text{-}40)$$

5.1.5 Examination of Partial Hybrid Element

After determining the interpolation functions of the geometry, displacements and partial stress field, the element matrices can be calculated using equations (2-44) in Chapter 2. The element quality is examined by the eigenvalue test. Using the assumed partial stress matrix (5-40), the partial hybrid degenerated plate element is examined. The results of eigenvalue examination are given in Table 5-1. In the table, λ_i is the eigenvalue of the elements.

Table 5-1 Eigenvalues of stiffness matrix for 4-node degenerated plate element with 8 stress modes and E=1100 GPa, ν=0.3

No.	$\lambda_i(*10^3)$	No.	$\lambda_i(*10^3)$	No.	$\lambda_i(*10^3)$
1	0.2821	7	0.6822	13	1.6920
2	0.2821	8	0.6822	14	1.6920
3	0.3291	9	1.0480	15	1.6920
4	0.3626	10	1.1280	16	1.6920
5	0.3626	11	1.5740	17	1.6920
6	0.5641	12	1.5740	18	5.5000

On the free-traction surface, the transverse stresses must be zero in order to satisfy the boundary condition. In this case, the multiplying matrix is not a unit matrix. For example, if free traction condition is applied on both top and bottom surfaces, the multiplying matrix is

$$[T_1] = \begin{bmatrix} 1-\zeta^2 & 0 & 0 \\ 0 & 1-\zeta^2 & 0 \\ 0 & 0 & 1-\zeta^2 \end{bmatrix} \qquad (5\text{-}41)$$

The eigenvalues of the element are given in table 5-2. If the free traction condition is only applied on bottom surface, then the multiplying matrix becomes

$$[T_2] = \frac{1}{2}\begin{bmatrix} 1+\zeta & 0 & 0 \\ 0 & 1+\zeta & 0 \\ 0 & 0 & 1+\zeta \end{bmatrix} \qquad (5\text{-}42)$$

The results of eigenvalue examination are given in Table 5-3.

Table 5-2 Eigenvalues of stiffness matrix for 4-node degenerated plate element with multiplying matrix $[T_1]$ and E=1100 GPa, ν=0.3

No.	$\lambda_i(*10^3)$	No.	$\lambda_i(*10^3)$	No.	$\lambda_i(*10^3)$
1	0.2350	7	0.6214	13	1.4100
2	0.2637	8	0.6214	14	1.4100
3	0.2742	9	1.0060	15	1.5670
4	0.3626	10	1.0480	16	1.6920
5	0.3626	11	1.4100	17	1.6920
6	0.5641	12	1.4100	18	4.9510

Table 5-3 Eigenvalues of stiffness matrix for 4-node degenerated plate element with multiplying matrix $[T_2]$ and E=1100 GPa, ν=0.3

No.	$\lambda_i(*10^3)$	No.	λ_i $(*10^3)$	No.	$\lambda_i(*10^3)$
1	0.1838	7	0.5668	13	1.5220
2	0.2115	8	0.5668	14	1.5220
3	0.3262	9	0.9530	15	1.6160
4	0.3441	10	0.9826	16	1.6920
5	0.3441	11	1.2480	17	1.6920
6	0.5641	12	1.2480	18	4.7500

The examination of the element shows that there is not any kinematic deformation modes, and it has a desired capability for rigid-body displacement. Moreover, the non-zero eigenvalues in the tables are real and positive.

5.2 8-node Partial Hybrid Degenerated Plate Element

An 8-node degenerated plate element [44-45] is also presented here using partial hybrid element formulation.

5.2.1 Geometry of Element

Firstly, the element geometry is approximated using the parametric coordinate system. The global co-ordinates (x,y,z) of any point within the element are expressed in the form specified by the 'vector' connecting the upper and lower points (see figure 5-2) and the mid-surface co-ordinates as

$$\begin{Bmatrix} x \\ y \\ z \end{Bmatrix} = \sum_{i=1}^{8} N_i(\xi,\eta) \begin{Bmatrix} x_i \\ y_i \\ z_i \end{Bmatrix} + \sum_{i=1}^{8} N_i(\xi,\eta) h_i \frac{\zeta}{2} V_{3i} \qquad (5\text{-}43)$$

where (x_i, y_i, z_i) are the global co-ordinates of the i-th node. The shape functions $N_i(\xi,\eta)$ are

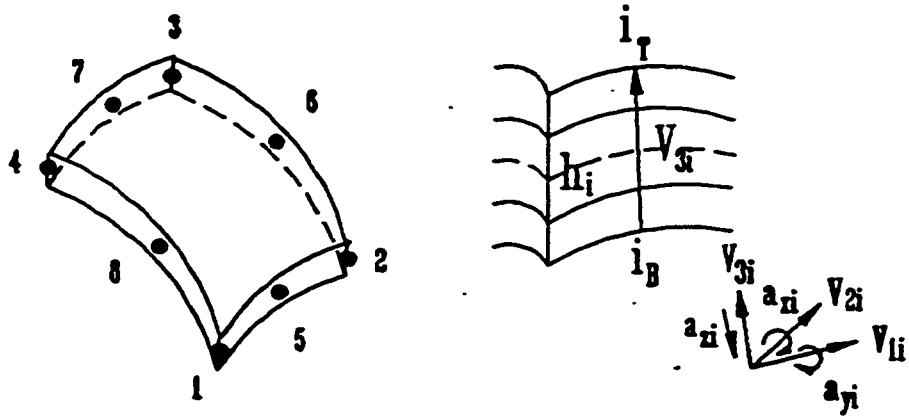

(a) (b)

Figure 5-2 An 8-node degenerated plate element

$$N_i=\frac{1}{4}(1+\xi_0)(1+\eta_0)(\xi_0+\eta_0-1)\xi_i^2\eta_i^2 + \frac{1}{2}(1-\xi^2)(1+\eta_0)(1-\xi_i^2)\eta_i^2 + \frac{1}{2}(1-\eta^2)(1+\xi_0)(1-\eta_i^2)\xi_i^2 \tag{5-44}$$

in which,

$$\xi_0=\xi_i\xi \quad \eta_0=\eta_i\eta \quad (i=1,2,\ldots,8) \tag{5-45}$$

The vector connecting the upper and lower points is

$$\mathbf{v}_{3i}=\begin{Bmatrix} l_{3i} \\ m_{3i} \\ n_{3i} \end{Bmatrix}=\frac{1}{h_i}\left(\begin{Bmatrix} x_i \\ y_i \\ z_i \end{Bmatrix}_T-\begin{Bmatrix} x_i \\ y_i \\ z_i \end{Bmatrix}_B\right) \tag{5-46}$$

and the parameter h_i is

$$h_i=\sqrt{(x_{iT}-x_{iB})^2+(y_{iT}-y_{iB})^2+(z_{iT}-z_{iB})^2} \tag{5-47}$$

5.2.2 Displacement Field

Similar to the 4-node degenerated element, it is assumed that a line that is straight and normal to the middle surface of the element before deformation is still straight, but not necessarily 'normal' to the middle surface after deformation. Therefore, a displacement

field is assumed as

$$\begin{Bmatrix} u \\ v \\ w \end{Bmatrix} = \sum_{i=1}^{8} N_i \left[\begin{Bmatrix} u_i \\ v_i \\ w_i \end{Bmatrix} + \frac{\zeta}{2} h_i \left[\mathbf{V}_{1i} \ \mathbf{V}_{2i} \ \mathbf{V}_{3i} \right] \begin{Bmatrix} a_{xi} \\ a_{yi} \\ a_{zi} \end{Bmatrix} \right] \tag{5-48}$$

in which, $\mathbf{V}_{1i}$, $\mathbf{V}_{2i}$ and $\mathbf{V}_{3i}$ are the unit vectors of the local co-ordinate (ξ, η, ζ) at node i. They can be calculated as follows:

$$\mathbf{V}_{1i} = \begin{Bmatrix} l_{1i} \\ m_{1i} \\ n_{1i} \end{Bmatrix} = \frac{\mathbf{i} \times \mathbf{V}_{3i}}{|\mathbf{i} \times \mathbf{V}_{3i}|} \qquad \mathbf{V}_{2i} = \begin{Bmatrix} l_{2i} \\ m_{2i} \\ n_{2i} \end{Bmatrix} = \mathbf{V}_{3i} \times \mathbf{V}_{1i} \tag{5-49}$$

The displacement field can be rewritten in the same form as that for the 4-node degenerated plate element,

$$\begin{Bmatrix} u \\ v \\ w \end{Bmatrix} = \sum_{i=1}^{8} N_i \left[\begin{Bmatrix} u_i \\ v_i \\ w_i \end{Bmatrix} + \zeta \left[b_i \right] \begin{Bmatrix} a_{xi} \\ a_{yi} \\ a_{zi} \end{Bmatrix} \right] = \sum_{i=1}^{8} \left[N \right]_i \boldsymbol{\delta}_i \tag{5-50}$$

where

$$\left[b_i \right] = \begin{bmatrix} b_{11i} & b_{12i} & b_{13i} \\ b_{21i} & b_{22i} & b_{23i} \\ b_{31i} & b_{32i} & b_{33i} \end{bmatrix} = \frac{h_i}{2} \left[\mathbf{V}_{1i} \ -\mathbf{V}_{2i} \ \mathbf{V}_{3i} \right] \tag{5-51}$$

and

$$\boldsymbol{\delta}_i = \left[u_i \ v_i \ w_i \ a_{xi} \ a_{yi} \ a_{zi} \right]^T \tag{5-52}$$

$$[N]_i=\begin{bmatrix} N_i & 0 & 0 & N_i\zeta b_{11i} & N_i\zeta b_{12i} & N_i\zeta b_{13i} \\ 0 & N_i & 0 & N_i\zeta b_{21i} & N_i\zeta b_{22i} & N_i\zeta b_{23i} \\ 0 & 0 & N_i & N_i\zeta b_{31i} & N_i\zeta b_{32i} & N_i\zeta b_{33i} \end{bmatrix} \tag{5-53}$$

5.2.3 Partial Strain Field and Partial Derivatives of the Displacement Field

The partial globally continuous strains can be derived from the displacement field by means of partial strain-displacement relation as follows,

$$\boldsymbol{e}_g=\begin{Bmatrix} \varepsilon_x \\ \varepsilon_y \\ \varepsilon_{xy} \end{Bmatrix}=\boldsymbol{D}_g\boldsymbol{u}=\begin{Bmatrix} \dfrac{\partial u}{\partial x} \\ \dfrac{\partial v}{\partial y} \\ \dfrac{\partial u}{\partial y}+\dfrac{\partial v}{\partial x} \end{Bmatrix}=[B_g]\boldsymbol{\delta} \tag{5-54}$$

in which,

$$[B_g]=[B_{g1}\ B_{g2}\ \cdots\ B_{g8}] \tag{5-55}$$

and

$$\boldsymbol{\delta}=[\boldsymbol{\delta}_1\ \boldsymbol{\delta}_2\ \cdots\ \boldsymbol{\delta}_8]^T \tag{5-56}$$

The expression of the partial geometric matrix at the i-th node $[B_{gi}]$ is the same as that of the 4-node degenerated plate element (5-18)-(5-19). The partial derivatives of displacement field can be also derived from the displacement field as follows,

$$\boldsymbol{D}_L\boldsymbol{u}=\begin{Bmatrix} \dfrac{\partial w}{\partial z} \\ \dfrac{\partial v}{\partial z}+\dfrac{\partial w}{\partial y} \\ \dfrac{\partial w}{\partial x}+\dfrac{\partial u}{\partial z} \end{Bmatrix}=[B_L]\boldsymbol{\delta} \tag{5-57}$$

in which,

$$[B_L]=[B_{L1}\ B_{L2}\ \cdots\ B_{L8}] \tag{5-58}$$

The expression of the partial geometric matrix at the i-th node $[B_{Li}]$ is the same as that of the 4-node degenerated plate element (5-22). In order to calculate $N_{i,x}$, $N_{i,y}$, $N_{i,z}$ and $\zeta_{,x}$, $\zeta_{,y}$, $\zeta_{,z}$, the following vectors are introduced:

$$\boldsymbol{g}=\begin{Bmatrix} x_{,\xi} \\ y_{,\xi} \\ z_{,\xi} \end{Bmatrix}=\sum_{i=1}^{8} N_{i,\xi}\left(\begin{Bmatrix} x_i \\ y_i \\ z_i \end{Bmatrix}+\frac{h_i}{2}\zeta \boldsymbol{V}_{3i}\right) \tag{5-59}$$

$$\boldsymbol{T}=\begin{Bmatrix} x_{,\eta} \\ y_{,\eta} \\ z_{,\eta} \end{Bmatrix}=\sum_{i=1}^{8} N_{i,\eta}\left(\begin{Bmatrix} x_i \\ y_i \\ z_i \end{Bmatrix}+\frac{h_i}{2}\zeta \boldsymbol{V}_{3i}\right) \tag{5-60}$$

$$\boldsymbol{V}=\begin{Bmatrix} x_{,\zeta} \\ y_{,\zeta} \\ z_{,\zeta} \end{Bmatrix}=\sum_{i=1}^{8} N_i\frac{h_i}{2}\boldsymbol{V}_{3i} \tag{5-61}$$

Thus, the Jacobian matrix, the derivatives of the shape functions, and the geometric matrix [B'] in the local co-ordinate system can be obtained using equations (5-26)-(5-36).

5.2.4 Partial Stress Field

In the element, the partial stress field is assumed independently as continuous functions across the thickness of a composite structure.

$$\boldsymbol{\sigma}_g = \begin{Bmatrix} \sigma_z \\ \tau_{yz} \\ \tau_{zx} \end{Bmatrix} = [P_g]\,\boldsymbol{\beta} = [T]\,[P]\,\boldsymbol{\beta} \qquad (5\text{-}62)$$

where the multiplying matrix [T] is assigned by the traction conditions on the top and bottom surfaces of the structure. The matrix [P] is derived directly from the assumed displacement field using the iso-function method. The iso-function partial stress matrix of the element is

$$[P] = \begin{vmatrix} 1 & 0 & 0 & \xi & 0 & 0 & \eta & 0 & 0 & \zeta & 0 & 0 & \xi\eta & 0 & 0 & \xi\zeta & 0 & 0 \\ 0 & 1 & 0 & 0 & \xi & 0 & 0 & \eta & 0 & 0 & \zeta & 0 & 0 & \xi\eta & 0 & 0 & \xi\zeta & 0 \\ 0 & 0 & 1 & 0 & 0 & \xi & 0 & 0 & \eta & 0 & 0 & \zeta & 0 & 0 & \xi\eta & 0 & 0 & \xi\zeta \end{vmatrix}$$

$$\begin{matrix} \eta\zeta & 0 & 0 & \xi\eta\zeta & 0 & 0 & \xi^2 & 0 & 0 & \eta^2 & 0 & 0 & \xi^2\eta \\ 0 & \eta\zeta & 0 & 0 & \xi\eta\zeta & 0 & 0 & \xi^2 & 0 & 0 & \eta^2 & 0 & 0 \\ 0 & 0 & \eta\zeta & 0 & 0 & \xi\eta\zeta & 0 & 0 & \xi^2 & 0 & 0 & \eta^2 & 0 \end{matrix} \qquad (5\text{-}63)$$

$$\begin{vmatrix} 0 & 0 & \xi^2\zeta & 0 & \xi\eta^2 & 0 & 0 & \eta^2\zeta & 0 \\ \xi^2\eta & 0 & 0 & \xi^2\zeta & 0 & \xi\eta^2 & 0 & 0 & 0 \\ 0 & \xi^2\eta & 0 & 0 & 0 & 0 & \xi\eta^2 & 0 & \eta^2\zeta \end{vmatrix}$$

There are 40 stress modes in the iso-function partial stress matrix.

In the element, there are 8 nodes and each node has six components of displacements. Therefore, the element has (n=) 48 degrees of freedom. For a 3-D elastic body, the

degrees of the rigid displacement are equal to (r=) 6. Thus, the element has (n-r=) 42 natural deformation modes. The eigenvalue examination indicates that the partial stiffness matrix $[K_d]$ has 26 non-zero eigenvalues. So the rank of the partial stiffness matrix $[K_d]$ is (n_d=) 26. Thus, the minimum number of necessary stress modes equals 16.

Based on the iso-function partial stress matrix (5-63), when the multiplying matrix [T] is a unit matrix [I], the classification method gives an optimal stress matrix as follows,

$$[P]=\begin{bmatrix} 1 & 0 & 0 & \xi & 0 & 0 & \eta & 0 & 0 & \xi\eta & 0 & 0 & 0 & 0 & 0 & 0 \\ 0 & 1 & 0 & 0 & \xi & 0 & 0 & \eta & 0 & 0 & \xi\eta & 0 & \xi\zeta & 0 & \xi\eta\zeta & 0 \\ 0 & 0 & 1 & 0 & 0 & \xi & 0 & 0 & \eta & 0 & 0 & \xi\eta & 0 & \eta\zeta & 0 & \xi\eta\zeta \end{bmatrix} \qquad (5\text{-}64)$$

5.2.5 Examination of Partial Hybrid Element

The degenerated plate elements with three types of materials are examined. The first is for isotropic material (see Table 5-4); the second is for anisotropic material (see Table 5-5); The third is for the composite structure with fibre orientation [90, 0, 90] (see Table 5-6). In the tables,

$$\lambda_i = \frac{\lambda_{hi}}{\lambda_{ui}} \qquad (5\text{-}65)$$

where λ_{hi} is the eigenvalue of the hybrid element; λ_{ui} is the eigenvalue of its displacement counterpart.

Table 5-4 Eigenvalues of stiffness matrix for the degenerated plate element with 16 stress modes and isotropic materials: E=1100 GPa, ν=0.3

No.	λ_i	No.	λ_i	No.	λ_i
1	0.7355	15	0.9253	29	0.9276
2	0.9392	16	0.9253	30	0.8042
3	0.7040	17	0.9241	31	1.0000
4	0.6753	18	0.7388	32	0.9966
5	0.8229	19	0.9190	33	0.9994
6	0.5870	20	0.9762	34	0.9994
7	0.6636	21	0.9790	35	0.9817
8	0.6092	22	0.8131	36	0.9841
9	0.7219	23	0.7528	37	0.8384
10	0.8699	24	0.7375	38	0.8432
11	0.8197	25	0.8694	39	0.9995
12	0.8974	26	0.8120	40	0.9114
13	0.8793	27	0.8195	41	1.0000
14	0.8793	28	0.8195	42	1.0000

Table 5-5 Eigenvalues of stiffness matrix for the degenerated plate element with 16 stress modes and anisotropic materials: E_L=174.6 GPa, E_T=7.0 GPa, G_{LT}=3.5 GPa, G_{TT}=1.4 GPa, $\nu_{12}=\nu_{13}=\nu_{23}$=0.25

No.	λ_i	No.	λ_i	No.	λ_i
1	0.9474	15	0.9094	29	0.9766
2	0.4623	16	0.8548	30	1.0000
3	0.5917	17	0.7773	31	0.9993
4	0.7961	18	0.7797	32	0.8925
5	0.8069	19	0.9696	33	0.9897
6	0.7233	20	0.8894	34	0.9968
7	0.7416	21	0.9453	35	0.9998
8	0.7526	22	0.9086	36	1.0000
9	0.8614	23	0.9842	37	0.9940
10	0.8387	24	0.8846	38	0.9918
11	0.8810	25	0.9896	39	0.9995
12	0.8917	26	0.9820	40	1.0000
13	0.9025	27	0.9996	41	0.9916
14	0.9138	28	0.9496	42	1.0000

Table 5-6 Eigenvalues of stiffness matrix for the degenerated plate element with fibre orientation [90, 0,90], 16 stress modes and materials: E_L=174.6 GPa, E_T=7.0 GPa, G_{LT}=3.5 GPa, G_{TT}=1.4 GPa, $\nu_{12}=\nu_{13}=\nu_{23}$=0.25

No.	λ_i	No.	λ_i	No.	λ_i
1	0.6746	15	0.8201	29	0.9094
2	0.5697	16	0.7790	30	0.9506
3	0.5951	17	0.7862	31	0.9982
4	0.7661	18	0.9046	32	1.0000
5	0.8326	19	0.9080	33	0.9999
6	0.7248	20	0.8470	34	0.9899
7	0.6863	21	0.8440	35	0.9915
8	0.6293	22	0.7805	36	0.9986
9	0.7808	23	0.9788	37	1.0000
10	0.8043	24	1.0000	38	0.9993
11	0.8668	25	0.9470	39	1.0000
12	0.7016	26	0.9717	40	0.9896
13	0.8314	27	0.8866	41	0.9998
14	0.8170	28	0.8840	42	0.9999

The examination of the element shows that the element does not have any kinematic deformation mode, and it has a desired capability for rigid-body displacement. Moreover, the non-zero eigenvalues in the tables are real and positive

Chapter 6

PARTIAL HYBRID TRANSITION ELEMENTS

In the global-local analysis, the treatment of interfaces between global and local regions is one of the key elements [91]. One of the commonly-used approaches for maintaining displacement compatibility and traction equilibrium at the interfaces is a special transition element. The major advantage of the transition element is to eliminate the constraint equations at these transition regions[7, 109-110]. Two partial hybrid transition elements are presented here [47-48, 101-104]. They will be used to connect the 3-D partial hybrid solid elements in local region with the partial hybrid degenerated plate elements in global region for the global/local analysis of composite structures in Chapter 8.

6.1 6-node Partial Hybrid Transition Element

The transition elements will be used to connect the partial hybrid degenerated plate

elements and the 3-D partial hybrid solid elements in a global/local finite element model. In order to ensure that the finite element model converges to the correct result, as mentioned in Chapter 1, the continuity condition of displacements across the interface between adjacent elements must be satisfied. Therefore, the interpolation functions of the displacement field have to be first investigated. For an isoparametric element, the displacement interpolation functions are the same as the shape functions which are used to approximate element geometry. So the shape functions are first discussed here.

The transition element has two line-of-nodes [111] where it meets the degenerated plate element and four point nodes on the remaining boundaries where it meets the 3-D solid element (see Figure 6-1). The line-of-nodes can accommodate any function across the

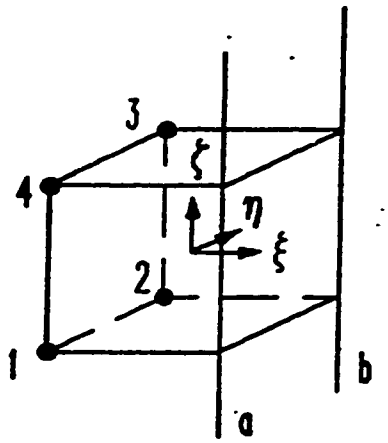

Figure 6-1 6-node partial hybrid transition element

thickness, allowing it to admit the any-order polynomials over the entire thickness from degenerated plate element, while the point nodes have the same polynomial shape functions as those used for the 3-D solid element. Once the shape functions of the transition element are established, the definitions of geometry and displacements for the element follow a similar path to those of the hybrid elements.

6.1.1 The Shape Functions of Different Elements

In the formulation of a typical 3-D element as shown in figure 6-2(a), shape functions dictate the form of a displacement field. It is clear that if two adjacent elements have identical shape functions and nodal locations on the interface, the continuity of the displacement field between the elements is achieved and the elements are compatible. Otherwise, the compatibility of elements will not be satisfied.

Suppose that a transition element in Figure 6-2(b) is used to connect a solid element (Fig. 6-2a) to a plate element (Fig. 6-2c) in the transition region of a global/local finite element model. On the left side, it meets with a solid element; on the right side, it meets a plate element. Thus, the transition element must have the same shape functions and nodal locations on its left side as that of solid element, and on its right side as that of plate/shell element.

Take a solid element as an "original" element for developing the transition element.

Obviously, the shape functions on the left side do not need to be modified. But, on the right side, new shape functions for satisfying continuity are required. For a general case, this amounts to developing a set of shape functions which can accommodate any arbitrary curve specified by the adjacent right-side element along the ζ axis (thickness) on the interface between elements. Before attempting to generate such shape functions, it is instructive to examine shape functions for a solid element.

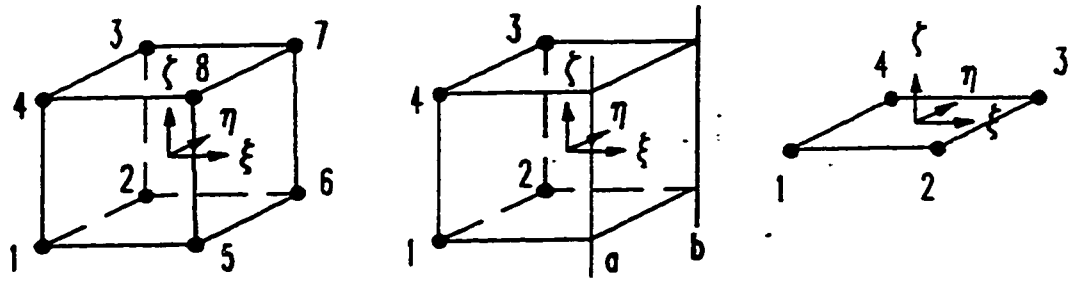

(a) solid element (b) transition element (c) plate element

Figure 6-2 Three types of element

In figure 6-2(a), a typical linear solid element is shown with the local curvilinear co-ordinates ξ, η and ζ. Its shape functions can be found elsewhere[112]. For developing a transition element, of particular interest are the shape functions for the nodes on the right side of this element, node 5-8:

$$N_i=\frac{1}{8}(1+\xi_i\xi)(1+\eta_i\eta)(1+\zeta_i\zeta) \tag{6-1}$$

The transition element in Fig. 6-2(b) is similar to the solid element in Fig 6-2(a) except for the nodes on its right face (5,6,7,8). Special treatment has to be done to these nodes so that their displacements can be compatible to those of the plate element in figure 6-2(c). Consider a function,

$$\Omega(\xi,\eta,\zeta)=\Omega_a(\xi,\eta,\zeta)+\Omega_b(\xi,\eta,\zeta) \tag{6-2}$$

in which,

$$\begin{aligned}\Omega_a(\xi,\eta,\zeta)&=\alpha_5 N_5+\alpha_8 N_8\\ \Omega_b(\xi,\eta,\zeta)&=\alpha_6 N_6+\alpha_7 N_7\end{aligned} \tag{6-3}$$

where α_i is the value of Ω at the node i of the solid element. Note that the function Ω can have the meaning of displacement function for the right face of the transition element in Fig. 6-2(b). Functions Ω_a and Ω_b can be of any degree (linear, quadratic etc.) between the two nodes 5-8 or 6-7 respectively. For a regular brick element, α_5 and α_8 would represent the displacements at the node 5 and 8 respectively. Normally, the displacements at node 5 and 8 are independent of each other. However, if the displacements at nodes 5 and 8 are constrained such that each of them is equal to a specific value of a function $\beta(\zeta)$, then one can write:

$$\alpha_5 = \beta(\zeta'_5)$$
$$\alpha_8 = \beta(\zeta'_8) \qquad (6-4)$$

where ζ'_5 and ζ'_8 are the global coordinates in the thickness direction of nodes 5 and 8 respectively.

Now consider the shape functions of the degenerated plate element. A middle surface of a degenerated plate element is shown with the local curvilinear co-ordinates ξ and η (in Figure 6-2(c)). The shape functions for the nodes on the left boundary of this element, nodes 1 and 4 are:

$$N'_1 = (1-\xi)(1-\eta)/4$$
$$N'_4 = (1-\xi)(1+\eta)/4 \qquad (6-5)$$

Consider another function meantime,

$$\Pi(\xi, \eta, \zeta') = \Pi_1(\xi, \eta, \zeta') + \Pi_4(\xi, \eta, \zeta') \qquad (6-6)$$

in which

$$\Pi_1(\xi, \eta, \zeta') = A_1\beta_1(\zeta')N'_1$$
$$\Pi_4(\xi, \eta, \zeta') = A_4\beta_4(\zeta')N'_4 \qquad (6-7)$$

and Π represents the displacements at the left face of the plate element. Note that the function Π can be considered to be the displacements of points lying on a plane normal

to the middle surface of the plate element at edge 1-4. Π_1 can be considered to be the displacements at all points on a line normal to the initial middle surface of the undeformed plate element at node 1 and Π_4 can be considered likewise to be the displacements at all points on a line normal to the initial middle surface of the undeformed plate element at node 4. Now consider the composition of Π_1 in detail. The composition of Π_4 follows.

In Π_1 , N'_1 represents the shape function in the plane ξ-η. A_1 represents the nodal displacement at the node 1 on the middle surface of the plate element. $\beta_1(\zeta')$ represents the variation of the displacement in the undeformed state of any point initially lying on the line normal to the middle surface of the plate element. If only one plate element is used for the whole laminate thickness, $\beta(\zeta')$ is a linear function of ζ'.

6.1.2 Matching the Two Shape Functions

From figure 6-2(b), Ω represents the displacement of the transition element at the interface. From figure 6-2(c), Π represents the displacement of the plate element at the interface. In order to satisfy the compatibility of displacement fields at the interface between the transition element and plate element, Ω and Π must be the same.

Function Ω consists of two functions Ω_a and Ω_b, and function Π consists of another two functions Π_1 and Π_4 . At the interface, Ω_a and Ω_b will need to match Π_1 and Π_4 ,

respectively. If Ω_i and Π_i can be matched exactly, compatibility of displacement fields at the interface will be satisfied. At the interface, ζ' is a function of ζ. In the interval $\zeta \in [-1,1]$ which corresponds to $\zeta' \in [\zeta'_1, \zeta'_{1+1}]$, one has

$$\zeta' = \frac{1-\zeta}{2}\zeta'_1 + \frac{1+\zeta}{2}\zeta'_{1+1} \tag{6-8}$$

Note that ζ' is the global thickness coordinate for the plate element while ζ is the smaller thickness coordinate for the solid or transition element. Using equation (6-1), the function Ω_a in equation (6-3) can be rewritten as follows:

$$\Omega_a = \frac{1}{8}(1+\xi)(1-\eta)[(1-\zeta)\alpha_5 + (1+\zeta)\alpha_8] \tag{6-9}$$

In this expression, the function Ω_a is split into two parts $N_a(\xi,\eta)$ and $\alpha_a(\zeta)$ that are

$$N_a(\xi,\eta) = \frac{1}{4}(1+\xi)(1-\eta)$$
$$\alpha_a(\zeta) = \frac{1}{2}[(1-\zeta)\alpha_5 + (1+\zeta)\alpha_8] \tag{6-10}$$

Thus,

$$\Omega_a = \alpha_a N_a \tag{6-11}$$

In order to accommodate any arbitrary curve $\beta_1(\zeta')$ specified by the adjoining plate element, a line of nodes connecting nodes 5-8 and a moving node which moves along this line are defined. At every point ζ' occupied by the moving node, the nodal value α_a is made to be equal to the value of the specified curve at the point, $A_1\beta_1(\zeta')$. Thus,

$$\alpha_a = A_1 \beta_1 (\zeta')$$

$$\Omega_a = A_1 \beta_1 (\zeta') N_a (\xi, \eta) \qquad (6\text{-}12)$$

Because the contribution of line 5-8 to the displacement field of the transition element is represented by the function Ω_a, this line is called as line of nodes "a" in order to use the standard word "node" in finite element method. Now, comparing functions Ω_a and Π_1 (6-7) and (6-12) at the interface, one can see that the functions Ω_a and Π_1 are the same (note that $N_a = N'_1$ at the interface). The Ω_a and Π_1 are matched exactly. In the same way as the functions Ω_a and Π_1 , The Ω_b and Π_4 can also be matched. The new shape functions and nodal values are defined by

$$\alpha_b = A_4 \beta_4 (\zeta')$$

$$N_b = (1+\xi)(1+\eta)/4 \qquad (6\text{-}13)$$

Thus

$$\Omega_b = \alpha_b N_b = A_4 \beta_4 (\zeta') N_b (\xi, \eta) \qquad (6\text{-}14)$$

The functions Ω_a and Ω_b of two lines of nodes "a" and "b" determine the displacements of the transition element at interface. Similarly, the functions Π_1 and Π_4 of two nodes 1 and 4 determine the displacements of the plate element at the interface. Because the functions Ω_a and Ω_b are the same as the functions Π_1 and Π_4 at the interface respectively, the function Ω is subsequently same as the function Π. Therefore, the displacements are

compatible at the interface between the transition element and plate element.

These two new shape functions N_a and N_b along with the other four shape functions as given in Reference [112] form a complete set of shape functions for the transition element. Thus, the approximation of the geometry and the displacement field of the element are determined

6.1.3 Geometry of the Element

A transition element is shown in Figure 6-3. The global co-ordinate (x, y, z) of any point in the element may be related to the non-dimensional co-ordinates by

$$\begin{Bmatrix} x \\ y \\ z \end{Bmatrix} = \sum_{1}^{4} N_i \begin{Bmatrix} x_i \\ y_i \\ z_i \end{Bmatrix} + \sum_{5}^{8} N_i \begin{Bmatrix} x_i \\ y_i \\ z_i \end{Bmatrix} \qquad (6\text{-}15)$$

In which, x_i , y_i and z_i are the co-ordinates of node i. Because the point nodes 5-8 are replaced by two lines of node a and b as follows,

$$\sum_{5}^{8} N_i \begin{Bmatrix} x_i \\ y_i \\ z_i \end{Bmatrix} = \sum_{a}^{b} N_i \left(\begin{Bmatrix} x_i^0 \\ y_i^0 \\ z_i^0 \end{Bmatrix} + \frac{\zeta'}{2} \begin{Bmatrix} \Delta x_i \\ \Delta y_i \\ \Delta z_i \end{Bmatrix} \right) \qquad (6\text{-}16)$$

where, x_i^0, y_i^0 and z_i^0 (i=a,b) are the co-ordinates of the line "a" and "b" at the middle surface of the composite structure, one has

$$\begin{Bmatrix} x \\ y \\ z \end{Bmatrix} = \sum_{1}^{4} N_i \begin{Bmatrix} x_i \\ y_i \\ z_i \end{Bmatrix} + \sum_{a}^{b} N_i \left(\begin{Bmatrix} x_i^0 \\ y_i^0 \\ z_i^0 \end{Bmatrix} + \frac{\zeta'}{2} \begin{Bmatrix} \Delta x_i \\ \Delta y_i \\ \Delta z_i \end{Bmatrix} \right) \tag{6-17}$$

Moreover, it can be rewritten in the form,

$$\begin{Bmatrix} x \\ y \\ z \end{Bmatrix} = \sum_{1}^{4} N_i \begin{Bmatrix} x_i \\ y_i \\ z_i \end{Bmatrix} + \sum_{a}^{b} N_i \left(\begin{Bmatrix} x_i^0 \\ y_i^0 \\ z_i^0 \end{Bmatrix} + \frac{\zeta'}{2} h_i \boldsymbol{V}_{3i} \right) \tag{6-18}$$

where

$$\boldsymbol{V}_{3i} = \begin{Bmatrix} l_{3i} \\ m_{3i} \\ n_{3i} \end{Bmatrix} = \frac{1}{h_i} \left(\begin{Bmatrix} x_i \\ y_i \\ z_i \end{Bmatrix}_T - \begin{Bmatrix} x_i \\ y_i \\ z_i \end{Bmatrix}_B \right) \tag{6-19}$$

and

$$h_i = \sqrt{(x_{iT} - x_{iB})^2 + (y_{iT} - y_{iB})^2 + (z_{iT} - z_{iB})^2} \tag{6-20}$$

The shape function N_i can be expressed as follows:

$$N_i = \frac{1}{8} (1 + \xi_0)(1 + \eta_0)(1 + \zeta_0) \tag{6-21}$$

in which

$$\xi_0 = \xi_i \xi \quad \eta_0 = \eta_i \eta \quad \zeta_0 = \zeta_i \zeta \qquad i = 1 - 4 \tag{6-22}$$

and

$$N_a=(1+\xi)(1-\eta)/4$$
$$N_b=(1+\xi)(1+\eta)/4 \qquad (6\text{-}23)$$

Note that coordinate ζ' is the global thickness coordinate for the plate element and coordinate ζ is the smaller thickness coordinate for the transition element. The relationship between coordinate ζ' and coordinate ζ is expressed in equation (6-8). The values ζ'_1 and ζ'_{l+1} represent the values of co-ordinate ζ' at the lower and upper surfaces of a layer while ζ=-1 and ζ=+1, respectively.

6.1.4 Displacement Field

In the element, the displacements (see figure 6-3) are expressed as follows:

$$\begin{Bmatrix} u \\ v \\ w \end{Bmatrix} = \sum_{1}^{4} N_i \begin{Bmatrix} u_i \\ v_i \\ w_i \end{Bmatrix} + \sum_{a}^{b} N_i \left[\begin{Bmatrix} u_i^0 \\ v_i^0 \\ w_i^0 \end{Bmatrix} + \zeta' [b_i] \begin{Bmatrix} \psi_{xi} \\ \psi_{yi} \\ \psi_{zi} \end{Bmatrix} \right] \qquad (6\text{-}24)$$

where

$$[b_i] = \begin{bmatrix} b_{11i} & b_{12i} & b_{13i} \\ b_{21i} & b_{22i} & b_{23i} \\ b_{31i} & b_{32i} & b_{33i} \end{bmatrix} = \frac{h_i}{2} [\boldsymbol{V}_{1i} \; -\boldsymbol{V}_{2i} \; \boldsymbol{V}_{3i}] \qquad (6\text{-}25)$$

and

$$V_{1i}=\begin{Bmatrix} l_{1i} \\ m_{1i} \\ n_{1i} \end{Bmatrix}=\frac{k\times V_{3i}}{|k\times V_{3i}|} \qquad V_{2i}=\begin{Bmatrix} l_{2i} \\ m_{2i} \\ n_{2i} \end{Bmatrix}=V_{3i}\times V_{1i} \tag{6-26}$$

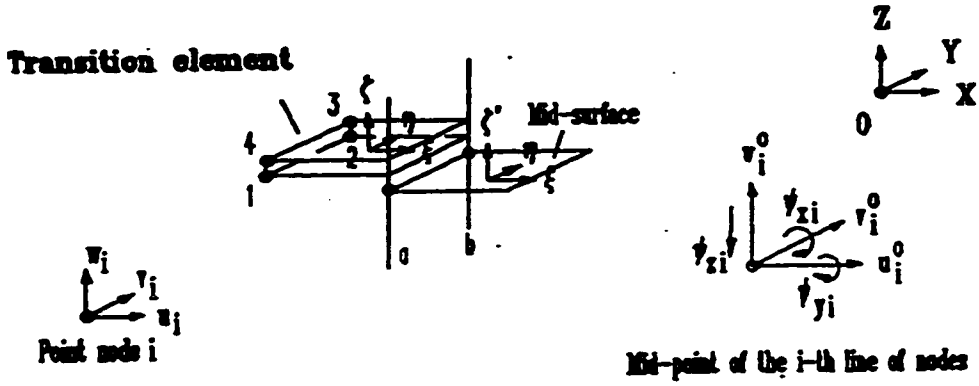

Figure 6-3 Nodal displacements in a transition element

in which, the displacement components u_i , v_i and w_i are the nodal displacements at point nodes 1,2,3 and 4. The displacement components u_i^0, v_i^0 and w_i^0 are the displacements of the line "a" and "b" at the middle surface of the composite structure, ψ_{xi} and ψ_{yi} are two rotations of the nodal vector $\mathbf{V}_{3i}$ about orthogonal directions normal to it, and ψ_{zi} is a transverse normal deformation in the thickness direction.

6.1.5 Partial Strain Field and Partial Derivatives of the Displacement Field

Due to the fact that the in-plane strain-displacement relation is satisfied a priori, the globally continuous strains can be derived directly from the displacement field. Therefore, the partial strain field is

$$\{\varepsilon_g\}=\begin{Bmatrix} \frac{\partial u}{\partial x} \\ \frac{\partial v}{\partial y} \\ \frac{\partial u}{\partial y}+\frac{\partial v}{\partial x} \end{Bmatrix}=[B_g]\boldsymbol{\delta}=[B_{g1}B_{g2}\cdots\cdots B_{g6}]\begin{Bmatrix} \delta_1 \\ \delta_2 \\ \cdot \\ \cdot \\ \delta_6 \end{Bmatrix} \qquad (6\text{-}27)$$

where $\delta_5 = \delta_a$ and $\delta_6 = \delta_b$. However, the locally continuous strains can not be derived directly from the displacement field. Only the partial derivatives of the displacement can be obtained as follows,

$$\boldsymbol{D_L u}=\begin{Bmatrix} \frac{\partial w}{\partial z} \\ \frac{\partial v}{\partial z}+\frac{\partial w}{\partial y} \\ \frac{\partial w}{\partial x}+\frac{\partial u}{\partial z} \end{Bmatrix}=[B_L]\boldsymbol{\delta}=\{B_{L1}B_{L2}\cdots\cdots B_{L6}]\begin{Bmatrix} \delta_1 \\ \delta_2 \\ \cdot \\ \cdot \\ \delta_6 \end{Bmatrix} \qquad (6\text{-}28)$$

For nodes i = 1 - 4, the geometric matrices are

$$[B_{gi}]=\begin{bmatrix} N_{i,x} & 0 & 0 \\ 0 & N_{i,y} & 0 \\ N_{i,y} & N_{i,x} & 0 \end{bmatrix} \qquad (6\text{-}29)$$

and

$$[B_{Li}]=\begin{bmatrix} 0 & 0 & N_{i,z} \\ 0 & N_{i,z} & N_{i,y} \\ N_{i,z} & 0 & N_{i,x} \end{bmatrix} \tag{6-30}$$

and the nodal displacements are

$$\boldsymbol{\delta}_i=\begin{Bmatrix} U_i \\ V_i \\ W_i \end{Bmatrix} \tag{6-31}$$

For nodes i = a and b, the geometric matrices are

$$[B_{gi}]=\begin{bmatrix} N_{i,x} & 0 & 0 & b_{11i}a_{ix} & b_{12i}a_{ix} & b_{13i}a_{ix} \\ 0 & N_{i,y} & 0 & b_{21i}a_{iy} & b_{22i}a_{iy} & b_{23i}a_{iy} \\ N_{i,y} & N_{i,x} & 0 & b_{11i}a_{iy}+b_{21i}a_{ix} & b_{12i}a_{iy}+b_{22i}a_{ix} & b_{13i}a_{iy}+b_{23i}a_{ix} \end{bmatrix} \tag{6-32}$$

and

$$[B_{Li}]=\begin{bmatrix} 0 & 0 & N_{i,z} & b_{31i}a_{iz} & b_{32i}a_{iz} & b_{33i}a_{iz} \\ 0 & N_{i,z} & N_{i,y} & b_{21i}a_{iz}+b_{31i}a_{iy} & b_{22i}a_{iz}+b_{32i}a_{iy} & b_{23i}a_{iz}+b_{33i}a_{iy} \\ N_{i,z} & 0 & N_{i,x} & b_{31i}a_{ix}+b_{11i}a_{iz} & b_{32i}a_{ix}+b_{12i}a_{iz} & b_{33i}a_{ix}+b_{13i}a_{iz} \end{bmatrix} \tag{6-33}$$

and the nodal displacements are

$$\boldsymbol{\delta}_i=[u_i^0 \;\; v_i^0 \;\; w_i^0 \;\; \psi_{xi} \;\; \psi_{yi} \;\; \psi_{zi}]^T \tag{6-34}$$

and

$$\begin{aligned} a_{ix} &= N_{i,x}\zeta' + N_i\zeta'_{,x} \\ a_{iy} &= N_{i,y}\zeta' + N_i\zeta'_{,y} \\ a_{iz} &= N_{i,z}\zeta' + N_i\zeta'_{,z} \end{aligned} \tag{6-35}$$

In order to calculate $N_{i,x}$, $N_{i,y}$, $N_{i,z}$ and $\zeta'_{,x}$, $\zeta'_{,y}$, $\zeta'_{,z}$, the following vectors are introduced:

$$\boldsymbol{r}=\begin{Bmatrix} x \\ y \\ z \end{Bmatrix} \qquad \boldsymbol{S}=\boldsymbol{r}_{,\xi}=\begin{Bmatrix} x_{,\xi} \\ y_{,\xi} \\ z_{,\xi} \end{Bmatrix} \tag{6-36}$$

$$\boldsymbol{T}=\boldsymbol{r}_{,\eta}=\begin{Bmatrix} x_{,\eta} \\ y_{,\eta} \\ z_{,\eta} \end{Bmatrix} \qquad \boldsymbol{V}=\boldsymbol{r}_{,\zeta}=\begin{Bmatrix} x_{,\zeta} \\ y_{,\zeta} \\ z_{,\zeta} \end{Bmatrix}$$

Then,

$$[J]=[\boldsymbol{S}\ \boldsymbol{T}\ \boldsymbol{V}]^T \quad and \quad |J|=\boldsymbol{S}\cdot\boldsymbol{T}\times\boldsymbol{V} \tag{6-37}$$

and

$$[J]^{-1}=[\boldsymbol{T}\times\boldsymbol{V}\ \ \boldsymbol{V}\times\boldsymbol{S}\ \ \boldsymbol{S}\times\boldsymbol{T}]/|J| \tag{6-38}$$

One can obtain

$$\begin{Bmatrix} N_{i,x} \\ N_{i,y} \\ N_{i,z} \end{Bmatrix} = [\boldsymbol{T}\times\boldsymbol{V}\ \ \boldsymbol{V}\times\boldsymbol{S}\ \ \boldsymbol{S}\times\boldsymbol{T}]\ /|J| \begin{Bmatrix} N_{i,\xi} \\ N_{i,\eta} \\ N_{i,\zeta} \end{Bmatrix} \tag{6-39}$$

and

$$\begin{Bmatrix} \zeta_{,x} \\ \zeta_{,y} \\ \zeta_{,z} \end{Bmatrix} = \frac{\boldsymbol{S} \times \boldsymbol{T}}{|J|} \tag{6-40}$$

6.1.6 Partial Stress Field

In the element, the partial stress field is assumed independently,

$$\boldsymbol{\sigma}_g = \begin{Bmatrix} \sigma_z \\ \tau_{yz} \\ \tau_{zx} \end{Bmatrix} = [P_g]\,\boldsymbol{\beta} \tag{6-41}$$

where the stress parameters β_i are the internal parameters. In some cases, it is convenient to use surface stress parameters α. For example, an assumed stress field can be assumed in the form,

$$\boldsymbol{\sigma}_g = [P_g]\,\boldsymbol{\beta} = [P]\,\frac{1}{2}\{(1+\zeta)\,\boldsymbol{\alpha}_T + (1-\zeta)\,\boldsymbol{\alpha}_B\} \tag{6-42}$$

where α_T and α_B are the surface stress parameters corresponding to upper and lower surfaces of the element, respectively. In this expression, a stress mode σ_i in the matrix [P] is related to both surface parameters (upper and lower surface parameters α_T and α_B) and corresponds two stress modes $0.5*(1+\zeta)*\sigma_i$ and $0.5*(1-\zeta)*\sigma_i$ in the assumed stress matrix $[P_g]$. The stress matrix [P] can be derived directly from the assumed displacement field using the iso-function method. The iso-function partial stress matrix of the element is

$$[P]=\begin{bmatrix} 1 & 0 & 0 & \xi & 0 & 0 & \eta & 0 & 0 & \zeta & 0 & 0 & \xi\eta & 0 & 0 & \eta\zeta & 0 & \xi\zeta & 0 \\ 0 & 1 & 0 & 0 & \xi & 0 & 0 & \eta & 0 & 0 & \zeta & 0 & 0 & \xi\eta & 0 & 0 & 0 & 0 & \xi\zeta \\ 0 & 0 & 1 & 0 & 0 & \xi & 0 & 0 & \eta & 0 & 0 & \zeta & 0 & 0 & \xi\eta & 0 & \eta\zeta & 0 & 0 \end{bmatrix} \qquad (6\text{-}43)$$

There are 19 stress modes in the stress matrix.

In this element, there are four point nodes and two lines of node. Each point node has three components of displacements and each line of nodes has six components. Therefore, the element has (n=) 24 degrees of freedom. Because the degrees of the rigid body motion are equal to (r=) 6, the element has (n-r=) 18 natural deformation modes. The eigenvalue examination indicates that the rank of the partial stiffness matrix $[K_d]$ is (n_d=) 10. Therefore, the minimum number of necessary stress modes in the stress matrix $[P_g]$ is equal to 8. Because a stress mode in the matrix [P] corresponds two stress modes in the assumed stress matrix $[P_g]$, the stress matrix [P] must have at least 4 stress modes.

Based on the iso-function partial stress matrix (6-43), the classification method gives an optimal stress matrix as follows,

$$[P]=\begin{bmatrix} 1 & 0 & 0 & 0 & 0 \\ 0 & 1 & 0 & \xi & 0 \\ 0 & 0 & 1 & 0 & \eta \end{bmatrix} \qquad (6\text{-}44)$$

6.1.7 Examination of Partial Hybrid Transition Element

The element is examined by using the eigenvalue test. The results of eigenvalue examination are given in Table 6-1. In the table, λ_i are the eigenvalues of the element. The results show that the element does not have any kinematic deformation modes, and it has a desired capability for rigid-body displacement. In addition, the non-zero eigenvalues in the table are real and positive

Table 6-1 Eigenvalues of stiffness matrix for hybrid transition element with 10 stress modes and isotropic materials: E=1100 GPa, ν=0.3

No.	λ_i (*10^3)	No.	λ_i (*10^3)	No.	λ_i(*10^3)
1	0.1088	7	0.2923	13	1.282
2	0.1621	8	0.4328	14	1.373
3	0.1850	9	0.6554	15	1.398
4	0.2115	10	0.7126	16	1.398
5	0.2209	11	0.7264	17	1.418
6	0.2438	12	0.9706	18	4.171

6.2 15-node Partial Hybrid Transition Element

In order to connect 8-node partial hybrid degenerated plate elements and 3-D, 20-node partial hybrid solid elements, a 15-node transition element is presented [47]. It has three lines of nodes [111] where they meet the degenerated plate/shell element and four point nodes on the remaining boundaries (see Figure 6-4). The line of nodes can accommodate

any function along the thickness, allowing it to admit the any-order polynomials over the entire thickness from degenerated plate element, while the point nodes have the same polynomial shape functions as those used for the 3-D solid element.

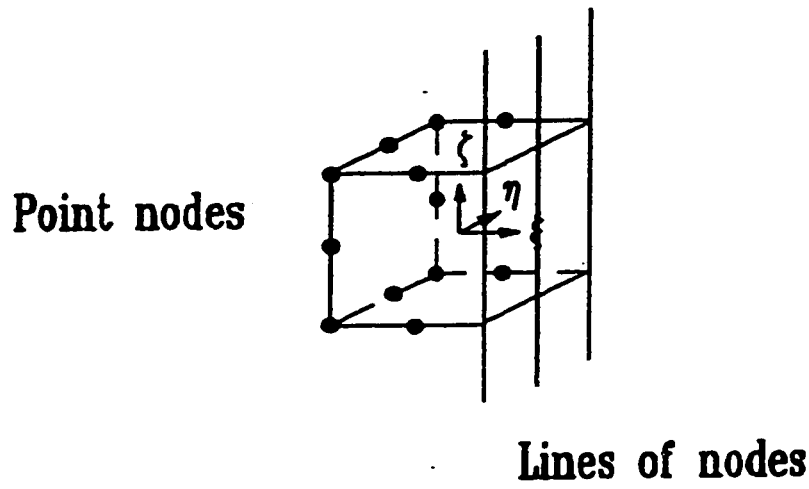

Figure 6-4 15-node partial hybrid transition element

6.2.1 The Shape Functions of Different Elements

Suppose that the 15-node transition element in Figure 6-5(b) is used to connect a 20-node solid sub-element (Fig. 6-5a) to an 8-node plate element (Fig. 6-5c) in the transition region of a global/local finite element model. On the left side, it meets with a solid element; on the right side, it meets a plate element.

Similar to the case in developing 6-node transition element, take a solid element as an "original" element for developing the transition element. Obviously, the shape functions on the left side do not need to be modified. But, on the right side, new shape functions for satisfying continuity are required.

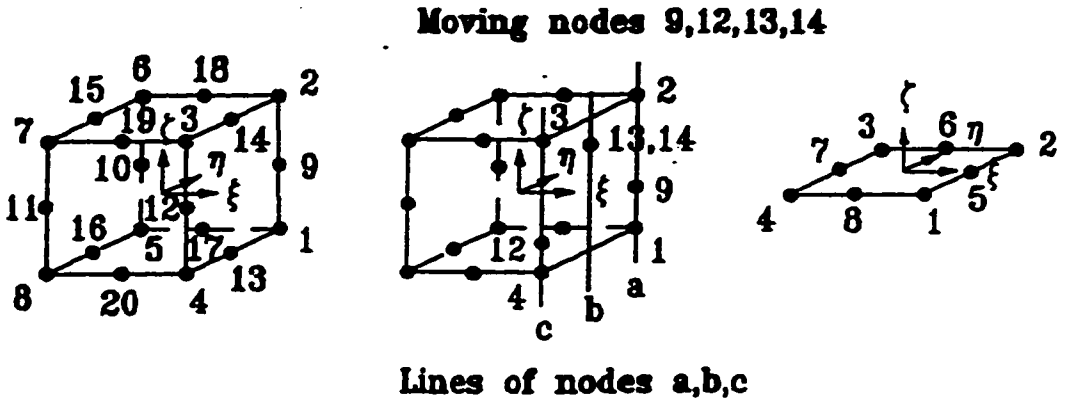

(a) solid element (b) transition element (c) plate element

Figure 6-5 Three types of element

In Figure 6-5(a), a typical quadratic solid element is shown with the local curvilinear co-ordinates ξ, η and ζ. Its shape functions can be found elsewhere[112]. For developing a transition element, of particular interest are the shape functions for the nodes on the right side of this element, node 1-4, 9, 12-14:

$$
\begin{aligned}
N_i = & \frac{1}{8}(1+\xi_0)(1+\eta_0)(1+\zeta_0)(\xi_0+\eta_0+\zeta_0-2)\xi_i^2\eta_i^2\zeta_i^2 \\
& +\frac{1}{4}(1-\xi^2)(1+\eta_0)(1+\zeta_0)(1-\xi_i^2)\eta_i^2\zeta_i^2 \\
& +\frac{1}{4}(1-\eta^2)(1+\zeta_0)(1+\xi_0)(1-\eta_i^2)\zeta_i^2\xi_i^2 \\
& +\frac{1}{4}(1-\zeta^2)(1+\xi_0)(1+\eta_0)(1-\zeta_i^2)\xi_i^2\eta_i^2
\end{aligned}
\tag{6.45}
$$

in which,

$$
\xi_0=\xi_i\xi \quad \eta_0=\eta_i\eta \quad \zeta_0=\zeta_i\zeta \tag{6-46}
$$

where ξ_i, η_i and ζ_i are the local co-ordinates of node i in the element parametric space.

The transition element in Fig. 6-5(b) is similar to the solid element in Fig 6-5(a) except for the nodes on its right face (1,2,3,4,9,12,13,14). Special treatment has to be done to these nodes so that their displacements can be compatible to those of the plate element in figure 6-5(c). Consider a function,

$$
\Omega(\xi,\eta,\zeta)=\Omega_a(\xi,\eta,\zeta)+\Omega_b(\xi,\eta,\zeta)+\Omega_c(\xi,\eta,\zeta) \tag{6-47}
$$

in which,

$$
\begin{aligned}
\Omega_a(\xi,\eta,\zeta) &= \alpha_1 N_1+\alpha_2 N_2+\alpha_9 N_9 \\
\Omega_b(\xi,\eta,\zeta) &= \alpha_{13} N_{13}+\alpha_{14} N_{14} \\
\Omega_c(\xi,\eta,\zeta) &= \alpha_3 N_3+\alpha_4 N_4+\alpha_{12} N_{12}
\end{aligned}
\tag{6-48}
$$

where α_i is the value of Ω at the node i of the solid element. Note that the function Ω can have the meaning of displacement function for the right face of the transition element in Fig. 6-5(b). Functions Ω_a, Ω_b and Ω_c can be of any degree (linear, quadratic etc.) between the two nodes 1-2, 13-14, or 3-4 respectively. For a regular solid element, α_1, α_9 and α_2 would represent the displacements at the node 1, 9 and 2 respectively. Normally, the displacements at node 1, 9 and 2 are independent of each other. However, if the displacements at nodes 1, 9 and 2 are constrained such that each of them is equal to a specific value of a function $\beta(\zeta')$, then one can write:

$$\begin{aligned} \alpha_1 &= \beta(\zeta'_1) \\ \alpha_9 &= \beta(\zeta'_9) \\ \alpha_2 &= \beta(\zeta'_2) \end{aligned} \qquad (6 - 49)$$

where ζ'_1, ζ'_9 and ζ'_2 are the global coordinates in the thickness direction of nodes 1, 9 and 2 respectively.

Now consider the shape functions of the degenerated plate element. A middle surface of a degenerated plate element is shown with the local curvilinear co-ordinates ξ and η (in Figure 6-5(c)). The shape functions for the nodes on the left boundary of this element, nodes 3, 7 and 4 are:

$$\begin{aligned} N'_i = & \frac{1}{4}(1+\xi_0)(1+\eta_0)(\xi_0+\eta_0-1)\xi_i^2\eta_i^2 \\ & + \frac{1}{2}(1-\xi^2)(1+\eta_0)(1-\xi_i^2)\eta_i^2 \\ & + \frac{1}{2}(1-\eta^2)(1+\xi_0)(1-\eta_i^2)\xi_i^2 \end{aligned} \qquad (6\text{-}50)$$

in which,

$$\xi_0=\xi_i\xi \quad \eta_0=\eta_i\eta \tag{6-51}$$

Consider another function meantime,

$$\Pi(\xi,\eta,\zeta')=\Pi_3(\xi,\eta,\zeta')+\Pi_7(\xi,\eta,\zeta')+\Pi_4(\xi,\eta,\zeta') \tag{6-52}$$

in which

$$\begin{aligned}\Pi_3(\xi,\eta,\zeta')&=A_3\beta_3(\zeta')N'_3\\ \Pi_7(\xi,\eta,\zeta')&=A_7\beta_7(\zeta')N'_7\\ \Pi_4(\xi,\eta,\zeta')&=A_4\beta_4(\zeta')N'_4\end{aligned} \tag{6-53}$$

Note that the function Π can be considered to be the displacements of points lying on a plane normal to the middle plane of the plate/shell element at edge 3-4. Π_3 can be considered to be the displacements at all points on a line normal to the initial mid surface of the undeformed plate element at node 3. Π_7 and Π_4 also can be considered likewise to be the displacements at all points on the lines normal to the initial middle surface of the undeformed plate element at node 7 and 4 respectively. Now consider the composition of Π_3 in detail. The compositions of Π_7 and Π_4 follow.

In Π_3 , N'_3 represents the shape function in the plane ξ-η. A_3 represents the nodal displacement at the node 3 on the middle surface of the plate element. $\beta_3(\zeta')$ represents the variation of the displacement in the undeformed state of any point initially lying on

the line normal to the middle surface of the plate element. If only one plate element is used for the whole laminate thickness, $\beta(\zeta')$ is a linear function of ζ'.

6.2.2 Matching the Two Shape Functions

From figure 6-5(b), Ω represents the displacement of the transition element at the interface. From figure 6-5(c), Π represents the displacement of the plate element at the interface. In order to satisfy the compatibility of displacement fields at the interface between the transition element and plate element, Ω and Π must be the same.

Function Ω consists of three functions Ω_a, Ω_b and Ω_c, and function Π consists of another three functions Π_3, Π_7 and Π_4. At the interface, Ω_a, Ω_b and Ω_c will need to match Π_3, Π_7 and Π_4, respectively. If Ω_i and Π_i can be matched exactly, compatibility of displacement fields at the interface will be satisfied. At the interface, ζ' is a function of ζ. In the interval $\zeta \in [-1,1]$ which corresponds to $\zeta' \in [\zeta'_I, \zeta'_{I+1}]$, one has

$$\zeta' = \frac{1-\zeta}{2}\zeta'_I + \frac{1+\zeta}{2}\zeta'_{I+1} \qquad (6\text{-}54)$$

Note that ζ' is the global thickness coordinate for the plate element while ζ is the smaller thickness coordinate for the solid or transition element.

Without losing generality, the function Ω_a is examined as an example along the line 'a' of nodes 1, 2 and 9. It can be rewritten as follows:

$$\begin{aligned}\Omega_a=&\alpha_1(1+\xi)(1+\eta)(1-\zeta)(\xi+\eta-1)/8\\&+\alpha_2(1+\xi)(1+\eta)(1+\zeta)(\xi+\eta-1)/8\\&+(\alpha_9-\frac{\alpha_1+\alpha_2}{2})(1+\xi)(1+\eta)(1-\zeta^2)/4\end{aligned} \tag{6-55}$$

It shows that the function Ω_a may be separated into two parts: (1) the contribution of the corner nodes which varies linearly along the ζ direction and quadratically along the ξ and η directions; and (2) the contribution of the mid-side node which is quadratic in the ζ direction and linear along ξ and η shown in figure 6-6(a). If the quadratic function

$$(\alpha_9-\frac{\alpha_1+\alpha_2}{2})(1-\zeta^2) \tag{6-56}$$

can be replaced by a arbitrary function

$$A_3\beta_3(\zeta')-\frac{(1-\zeta)\alpha_1+(1+\zeta)\alpha_2}{2} \tag{6-57}$$

shown in figure 6-6(b), then Ω_a will be exactly equal to the Π_3.

In order to accommodate any arbitrary curve $\beta_3(\zeta')$ specified by the adjoining plate element, a line of nodes connecting nodes 1-2 and a moving node 9 which moves along this line are defined (see figure 6-5). At every point ζ' occupied by the moving node, the nodal value α_9 is made to be equal to the value of the specified curve at the point, $A_3\beta_3(\zeta')$ (see equation (6-53). Taking α_1 and α_2 as $A_3\beta_3(\zeta'(-1))$ and $A_3\beta_3(\zeta'(+1))$, respectively, the new shape functions and the nodal value are defined by

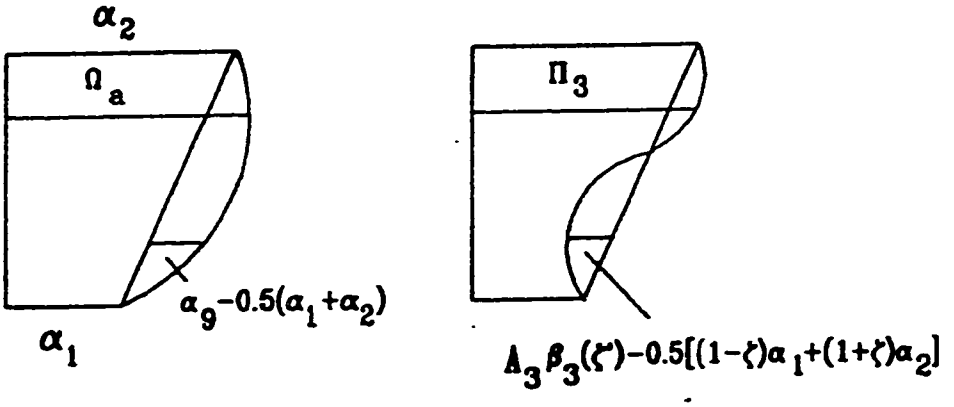

Figure 6-6 Variation of physical field on the line 'a' of nodes

$$N'_1=(1+\xi)\,(1+\eta)\,(1-\zeta)\,(\xi+\eta-1)/8$$
$$N''_2=(1+\xi)\,(1+\eta)\,(1+\zeta)\,(\xi+\eta-1)/8 \qquad (6\text{-}58)$$
$$N''_9=(1+\xi)\,(1+\eta)/4$$

$$\alpha''_9=A_3\beta_3(\zeta')-\frac{(1-\zeta)\,\alpha_1+(1+\zeta)\,\alpha_2}{2}$$

Thus

$$\Omega_a=\alpha_1 N''_1+\alpha_2 N''_2+\alpha''_9 N''_9 \qquad (6\text{-}59)$$

The equations (6-58) and (6-59) above can be transformed into the most convenient form as follows:

$$
\begin{aligned}
N'''_1 &= (1+\xi)(1+\eta)(1-\zeta)(\xi+\eta-2)/8 \\
N'''_2 &= (1+\xi)(1+\eta)(1+\zeta)(\xi+\eta-2)/8 \\
N'''_9 &= (1+\xi)(1+\eta)/4 \\
\alpha'''_9 &= A_3\beta_3(\zeta') \\
\Omega_a &= \alpha_1 N'''_1 + \alpha_2 N'''_2 + \alpha'''_9 N'''_9
\end{aligned}
\tag{6-60}
$$

and

$$
\Omega_a = A_3\left[\beta_3(\zeta'_1)N'''_1(\xi,\eta,\zeta) + \beta_3(\zeta'_{1+1})N'''_2(\xi,\eta,\zeta) + \beta_3(\zeta')N'''_9(\xi,\eta)\right] \tag{6-61}
$$

Thus, the Ω_a and Π_3 are matched exactly at the interface. Notes that the nodes 1, 2 and 9 are not independent nodes. They become sub-nodes on the line of node 'a'. Because the contribution of line 1-9-2 to the displacement field of the transition element is represented by the function Ω_a, this line is called as line of nodes "a".

In the same way as the functions Ω_a and Π_3, the Ω_b and Ω_c can also be converted to match Π_7 and Π_4. The new shape functions and nodal values are defined by

$$
\begin{aligned}
N'''_{13} &= N'''_{14} = (1+\xi)(1-\eta^2)/4 \\
\alpha_{13} &= \alpha_{14} = A_7\beta_7(\zeta') \\
\Omega_b &= \alpha_{13}N'''_{13} + \alpha_{14}N'''_{14}
\end{aligned}
\tag{6-62}
$$

and

$$
\Omega_b = A_7\left[\beta_7(\zeta')N'''_{13}(\xi,\eta) + \beta_7(\zeta')N'''_{14}(\xi,\eta)\right] \tag{6-63}
$$

and

$$
\begin{aligned}
N'''_3 &= (1+\xi)(1-\eta)(1+\zeta)(\xi-\eta-2)/8 \\
N'''_4 &= (1+\xi)(1-\eta)(1-\zeta)(\xi-\eta-2)/8 \\
N'''_{12} &= (1+\xi)(1-\eta)/4 \\
\alpha'''_{12} &= A_4 \beta_4(\zeta') \\
\Omega_c &= \alpha_3 N'''_3 + \alpha_4 N'''_4 + \alpha'''_{12} N'''_{12}
\end{aligned}
\tag{6-64}
$$

and

$$
\Omega_c = A_4 [\beta_4(\zeta'_I) N'''_4(\xi,\eta,\zeta) + \beta_4(\zeta'_{I+1}) N'''_3(\xi,\eta,\zeta) + \beta_4(\zeta') N'''_{12}(\xi,\eta)] \tag{6-65}
$$

The functions Ω_a , Ω_b and Ω_c of three lines of nodes "a", "b"and "c" determine the displacements of the transition element at interface. Similarly, the functions Π_3, Π_7 and Π_4 of three nodes 3, 7 and 4 determine the displacements of the plate element at the interface. Because the functions Ω_a, Ω_b and Ω_c are the same as the functions Π_3, Π_7 and Π_4 at the interface respectively, the function Ω is subsequently same as the function Π. Therefore, the displacements are compatible at the interface between the transition element and plate element.

These eight new shape functions (6-60), (6-62) and (6-64) along with the other twelve shape functions as given in Reference [112] form a complete set of shape functions for the transition element.

6.2.3 Geometry of the Element

Renumbering the nodes, a transition element is shown in Figure 6-7. The global co-ordinate (x, y, z) of any point in the element may be related to the non-dimensional co-ordinates by

$$\begin{Bmatrix} x \\ y \\ z \end{Bmatrix} = \sum_{1}^{12} N_i \begin{Bmatrix} x_i \\ y_i \\ z_i \end{Bmatrix} + \sum_{13,15}^{18,20} N''_i \begin{Bmatrix} x'_i \\ y'_i \\ z'_i \end{Bmatrix} + \sum_{14,16}^{17,19} N''_i \begin{Bmatrix} x'_i \\ y'_i \\ z'_i \end{Bmatrix}_{moving} \qquad (6\text{-}66)$$

in which, the expression of (x', y', z') is dependent on the assumptions used in the adjoining plate element.

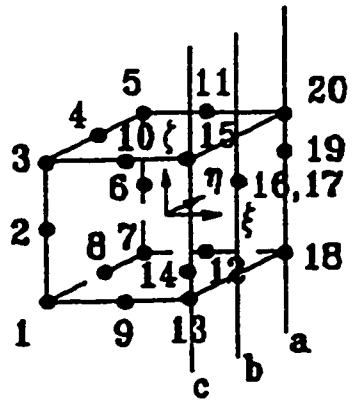

Moving nodes 14,16,17,19

Figure 6-7 Transition element

When the adjoining element is a degenerated plate element, the equation is written as

$$\begin{Bmatrix} x \\ y \\ z \end{Bmatrix} = \sum_{1}^{12} N_i \begin{Bmatrix} x_i \\ y_i \\ z_i \end{Bmatrix} + \sum_{13,15}^{18,20} N_i \left[\begin{Bmatrix} x_i^0 \\ y_i^0 \\ z_i^0 \end{Bmatrix} + \frac{\zeta'_i}{2} \begin{Bmatrix} \Delta x_i^0 \\ \Delta y_i^0 \\ \Delta z_i^0 \end{Bmatrix} \right] + \sum_{14,16}^{17,19} N_i \left[\begin{Bmatrix} x_i^0 \\ y_i^0 \\ z_i^0 \end{Bmatrix} + \frac{\zeta'}{2} \begin{Bmatrix} \Delta x_i^0 \\ \Delta y_i^0 \\ \Delta z_i^0 \end{Bmatrix} \right] \qquad (6\text{-}67)$$

in which, x_i , y_i and z_i (i=1,2,..12) are the co-ordinates of node i. x_i^0, y_i^0 and z_i^0 (i=13,14,..20) are the co-ordinates of the lines of node "a", "b", and "c" at the middle surface of the composite structure. The expression (6-67) can be rewritten as follows,

$$\begin{Bmatrix} x \\ y \\ z \end{Bmatrix} = \sum_{1}^{12} N_i \begin{Bmatrix} x_i \\ y_i \\ z_i \end{Bmatrix} + (N''_{18} + N''_{19} + N''_{20}) \begin{Bmatrix} x_a^0 \\ y_a^0 \\ z_a^0 \end{Bmatrix} + \frac{\zeta'_{18} N''_{18} + \zeta' N''_{19} + \zeta'_{20} N''_{20}}{2} \begin{Bmatrix} \Delta x_a^0 \\ \Delta y_a^0 \\ \Delta z_a^0 \end{Bmatrix}$$

$$+ (N''_{16} + N''_{17}) \left(\begin{Bmatrix} x_b^0 \\ y_b^0 \\ z_b^0 \end{Bmatrix} + \frac{\zeta'}{2} \begin{Bmatrix} \Delta x_b^0 \\ \Delta y_b^0 \\ \Delta z_b^0 \end{Bmatrix} \right) \qquad (6\text{-}68)$$

$$+ (N''_{13} + N''_{14} + N''_{15}) \begin{Bmatrix} x_c^0 \\ y_c^0 \\ z_c^0 \end{Bmatrix} + \frac{\zeta'_{13} N''_{13} + \zeta' N''_{14} + \zeta'_{15} N''_{15}}{2} \begin{Bmatrix} \Delta x_c^0 \\ \Delta y_c^0 \\ \Delta z_c^0 \end{Bmatrix}$$

In the simplified form,

$$\begin{Bmatrix} x \\ y \\ z \end{Bmatrix} = \sum_{1}^{12} N_i \begin{Bmatrix} x_i \\ y_i \\ z_i \end{Bmatrix} + \sum_{a,b}^{c} \left(N_j \begin{Bmatrix} x_j^0 \\ y_j^0 \\ z_j^0 \end{Bmatrix} + \frac{\overline{N_j}}{2} \begin{Bmatrix} \Delta x_j^0 \\ \Delta y_j^0 \\ \Delta z_j^0 \end{Bmatrix} \right) \qquad (6\text{-}69)$$

Note that coordinate ζ' is the global thickness coordinate for the plate/shell element and coordinate ζ is the smaller thickness coordinate for the transition element. Note that the

co-ordinate ζ' of the moving node varies along the line as follow

$$\zeta' = \frac{1-\zeta}{2}\zeta'_I + \frac{1+\zeta}{2}\zeta'_{I+1} \tag{6-70}$$

where the values ζ'_1 and ζ'_{l+1} represent the values of global co-ordinate ζ' at the lower and upper surfaces of a layer while ζ=-1 and ζ=+1, respectively. One can obtain

$$\begin{aligned}
N_a &= N'''_{18} + N'''_{19} + N'''_{20} \\
\overline{N_a} &= \zeta'_{18} N'''_{18} + \zeta' N'''_{19} + \zeta'_{20} N'''_{20} = N_a \zeta' \\
N_b &= N'''_{16} + N'''_{17} \\
\overline{N_b} &= \zeta' (N'''_{16} + N'''_{17}) = N_b \zeta' \\
N_c &= N'''_{13} + N'''_{14} + N'''_{15} \\
\overline{N_c} &= \zeta'_{13} N'''_{13} + \zeta' N'''_{14} + \zeta'_{15} N'''_{15} = N_c \zeta'
\end{aligned} \tag{6-71}$$

Thus, the co-ordinates can be expressed as in simple form,

$$\begin{Bmatrix} x \\ y \\ z \end{Bmatrix} = \sum_{1}^{12} N_i \begin{Bmatrix} x_i \\ y_i \\ z_i \end{Bmatrix} + \sum_{a,b}^{c} N_j \left(\begin{Bmatrix} x_j^0 \\ y_j^0 \\ z_j^0 \end{Bmatrix} + \frac{\zeta'}{2} \begin{Bmatrix} \Delta x_j^0 \\ \Delta y_j^0 \\ \Delta z_j^0 \end{Bmatrix} \right) \tag{6-72}$$

where N_i is the shape function which can be expressed as follows:

$$\begin{aligned}
N_i = {} & \frac{1}{8}(1+\xi_0)(1+\eta_0)(1+\zeta_0)(\xi_0+\eta_0+\zeta_0-2)\xi_i^2\eta_i^2\zeta_i^2 \\
& + \frac{1}{4}(1-\xi^2)(1+\eta_0)(1+\zeta_0)(1-\xi_i^2)\eta_i^2\zeta_i^2 \\
& + \frac{1}{4}(1-\eta^2)(1+\zeta_0)(1+\xi_0)(1-\eta_i^2)\zeta_i^2\xi_i^2 \\
& + \frac{1}{4}(1-\zeta^2)(1+\xi_0)(1+\eta_0)(1-\zeta_i^2)\xi_i^2\eta_i^2
\end{aligned} \tag{6-73}$$

in which

$$\xi_0=\xi_i\xi \quad \eta_0=\eta_i\eta \quad \zeta_0=\zeta_i\zeta \qquad i=1-12 \tag{6-74}$$

and

$$\begin{aligned} N_a&=(1+\xi)\,(1+\eta)\,(\xi+\eta-1)/4\\ N_b&=(1+\xi)\,(1-\eta^2)/2\\ N_c&=(1+\xi)\,(1-\eta)\,(\xi-\eta-1)/4 \end{aligned} \tag{6-75}$$

It can be seen that N_a, N_b and N_c are same as the shape functions used in the degenerated plate element. Furthermore, The expression (6-72) can be rewritten in the form,

$$\begin{Bmatrix} x\\ y\\ z \end{Bmatrix}=\sum_{1}^{12} N_i \begin{Bmatrix} x_i\\ y_i\\ z_i \end{Bmatrix}+\sum_{a,b}^{c} N_j \left(\begin{Bmatrix} x_j^0\\ y_j^0\\ z_j^0 \end{Bmatrix}+\frac{\zeta'}{2} h_j \boldsymbol{V}_{3j}\right) \tag{6-76}$$

and

$$\boldsymbol{V}_{3j}=\begin{Bmatrix} l_{3j}\\ m_{3j}\\ n_{3j} \end{Bmatrix}=\frac{1}{h_j}\left(\begin{Bmatrix} x_j\\ y_j\\ z_j \end{Bmatrix}_T-\begin{Bmatrix} x_j\\ y_j\\ z_j \end{Bmatrix}_B\right) \tag{6-77}$$

and

$$h_j=\sqrt{(x_{jT}-x_{jB})^2+(y_{jT}-y_{jB})^2+(z_{jT}-z_{jB})^2} \tag{6-78}$$

6.2.4 Displacement Field

In the element, the displacements (see figure 6-8) are expressed as follows:

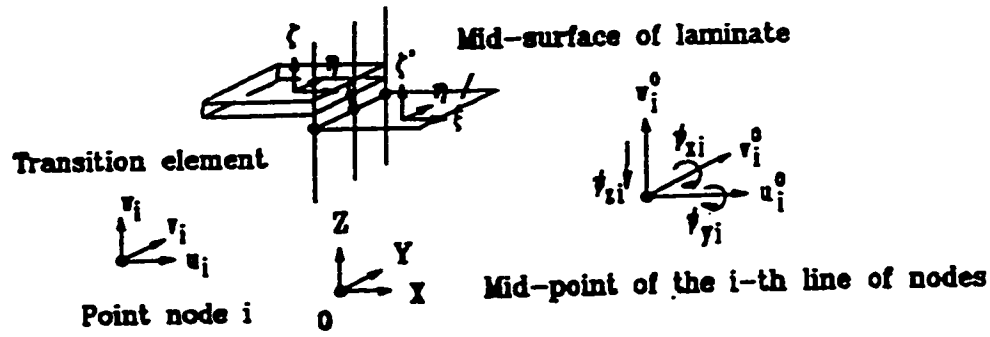

Figure 6-8 Nodal displacements in a transition element

$$\begin{Bmatrix} U \\ V \\ W \end{Bmatrix} = \sum_{1}^{12} N_i \begin{Bmatrix} u_i \\ v_i \\ w_i \end{Bmatrix} + \sum_{a,b}^{c} N_i \left[\begin{Bmatrix} u_i^0 \\ v_i^0 \\ w_i^0 \end{Bmatrix} + \zeta' [b_i] \begin{Bmatrix} \psi_{xi} \\ \psi_{yi} \\ \psi_{zi} \end{Bmatrix} \right] \qquad (6\text{-}79)$$

where

$$[b_i] = \begin{bmatrix} b_{11i} & b_{12i} & b_{13i} \\ b_{21i} & b_{22i} & b_{23i} \\ b_{31i} & b_{32i} & b_{33i} \end{bmatrix} = \frac{h_i}{2} [V_{1i} \; -V_{2i} \; V_{3i}] \qquad (6\text{-}80)$$

and

$$\boldsymbol{V}_{1i}=\begin{Bmatrix} l_{1i} \\ m_{1i} \\ n_{1i} \end{Bmatrix}=\frac{\boldsymbol{1}\times\boldsymbol{V}_{3i}}{|\boldsymbol{1}\times\boldsymbol{V}_{3i}|} \qquad \boldsymbol{V}_{2i}=\begin{Bmatrix} l_{2i} \\ m_{2i} \\ n_{2i} \end{Bmatrix}=\boldsymbol{V}_{3i}\times\boldsymbol{V}_{1i} \tag{6-81}$$

in which, the displacement components u_i , v_i and w_i are the nodal displacements at point nodes 1-12. The components u_i^0, v_i^0 and w_i^0 are the displacements of the line "a", "b" and "c" at the middle surface of the composite structure, ψ_{xi} and ψ_{yi} are two rotations of the nodal vector $\mathbf{V}_{3i}$ about orthogonal directions normal to it, and ψ_{zi} is a transverse normal deformation in the thickness direction.

6.2.5 Partial Strain Field and Partial Derivatives of the Displacement Field

The globally continuous strains are derived directly from the displacement field. They are

$$\{\boldsymbol{\varepsilon}_g\}=\begin{Bmatrix} \dfrac{\partial u}{\partial x} \\ \dfrac{\partial v}{\partial y} \\ \dfrac{\partial u}{\partial y}+\dfrac{\partial v}{\partial x} \end{Bmatrix}=[B_g]\boldsymbol{\delta}=[B_{g1}B_{g2}.\ .\ .\ .\ .B_{g15}]\begin{Bmatrix} \delta_1 \\ \delta_2 \\ . \\ . \\ \delta_{15} \end{Bmatrix} \tag{6-82}$$

where $\delta_{13}=\delta_a$, $\delta_{14}=\delta_b$ and $\delta_{15}=\delta_c$. The partial derivatives of the displacement are

$$\boldsymbol{D}_L\boldsymbol{u}=\begin{Bmatrix} \dfrac{\partial w}{\partial z} \\ \dfrac{\partial v}{\partial z}+\dfrac{\partial w}{\partial y} \\ \dfrac{\partial w}{\partial x}+\dfrac{\partial u}{\partial z} \end{Bmatrix}=[B_L]\boldsymbol{\delta}=\{B_{L1}B_{L2}.\ .\ .\ .\ .B_{L15}]\begin{Bmatrix} \delta_1 \\ \delta_2 \\ . \\ . \\ \delta_{15} \end{Bmatrix} \tag{6-83}$$

For nodes i = 1 - 12, the geometric matrices are

$$[B_{gi}]=\begin{bmatrix} N_{i,x} & 0 & 0 \\ 0 & N_{i,y} & 0 \\ N_{i,y} & N_{i,x} & 0 \end{bmatrix} \tag{6-84}$$

and

$$[B_{Li}]=\begin{bmatrix} 0 & 0 & N_{i,z} \\ 0 & N_{i,z} & N_{i,y} \\ N_{i,z} & 0 & N_{i,x} \end{bmatrix} \tag{6-85}$$

and the nodal displacements are

$$\boldsymbol{\delta}_i=\begin{Bmatrix} u_i \\ v_i \\ w_i \end{Bmatrix} \tag{6-86}$$

For nodes i = a , b and c, the geometric matrices are

$$[B_{gi}]=\begin{bmatrix} N_{i,x} & 0 & 0 & b_{11i}a_{ix} & b_{12i}a_{ix} & b_{13i}a_{ix} \\ 0 & N_{i,y} & 0 & b_{21i}a_{iy} & b_{22i}a_{iy} & b_{23i}a_{iy} \\ N_{i,y} & N_{i,x} & 0 & b_{11i}a_{iy}+b_{21i}a_{ix} & b_{12i}a_{iy}+b_{22i}a_{ix} & b_{13i}a_{iy}+b_{23i}a_{ix} \end{bmatrix} \tag{6-87}$$

and

$$[B_{Li}]=\begin{bmatrix} 0 & 0 & N_{i,z} & b_{31i}a_{iz} & b_{32i}a_{iz} & b_{33i}a_{iz} \\ 0 & N_{i,z} & N_{i,y} & b_{21i}a_{iz}+b_{31i}a_{iy} & b_{22i}a_{iz}+b_{32i}a_{iy} & b_{23i}a_{iz}+b_{33i}a_{iy} \\ N_{i,z} & 0 & N_{i,x} & b_{31i}a_{ix}+b_{11i}a_{iz} & b_{32i}a_{ix}+b_{12i}a_{iz} & b_{33i}a_{ix}+b_{13i}a_{iz} \end{bmatrix} \tag{6-88}$$

and the nodal displacements are

$$\boldsymbol{\delta}_i=[u_i^0\ v_i^0\ w_i^0\ \psi_{xi}\ \psi_{yi}\ \psi_{zi}]^T \tag{6-89}$$

and

$$\begin{aligned} a_{ix}&=N_{i,x}\zeta^I+N_i\zeta^I{}_{,x}\\ a_{iy}&=N_{i,y}\zeta^I+N_i\zeta^I{}_{,y}\\ a_{iz}&=N_{i,z}\zeta^I+N_i\zeta^I{}_{,z} \end{aligned} \tag{6-90}$$

In order to calculate $N_{i,x}$, $N_{i,y}$, $N_{i,z}$ and $\zeta'_{,x}$, $\zeta'_{,y}$, $\zeta'_{,z}$, the equation (6-36)-(6-40) for the 6-node transition element are also used.

6.2.6 Partial Stress Field

In the element, the partial stress field is independently assumed in the form,

$$\boldsymbol{\sigma}_g=\begin{Bmatrix}\sigma_z\\ \tau_{yz}\\ \tau_{zx}\end{Bmatrix}=[P_g]\,\boldsymbol{\beta} \tag{6-91}$$

where the stress matrix $[P_g]$ is derived directly from the assumed displacement field using the iso-function method. The iso-function partial stress matrix of the element is

$$
[P_g]=\left|\begin{array}{cccccccccccccccccccccccccccccccccccc}
1 & 0 & 0 & \xi & 0 & 0 & \eta & 0 & 0 & \zeta & 0 & 0 & \xi\eta & 0 & 0 & \xi\zeta & 0 & 0 \\
0 & 1 & 0 & 0 & \xi & 0 & 0 & \eta & 0 & 0 & \zeta & 0 & 0 & \xi\eta & 0 & 0 & \xi\zeta & 0 \\
0 & 0 & 1 & 0 & 0 & \xi & 0 & 0 & \eta & 0 & 0 & \zeta & 0 & 0 & \xi\eta & 0 & 0 & \xi\zeta
\end{array}\right.
$$

$$
\left.\begin{array}{cccccccccccccccccccccccccccccccccccc}
\eta\zeta & 0 & 0 & \xi\eta\zeta & 0 & 0 & \xi^2 & 0 & 0 & \eta^2 & 0 & 0 & \zeta^2 & 0 & 0 & \xi^2\eta \\
0 & \eta\zeta & 0 & 0 & \xi\eta\zeta & 0 & 0 & \xi^2 & 0 & 0 & \eta^2 & 0 & 0 & \zeta^2 & 0 & 0 \\
0 & 0 & \eta\zeta & 0 & 0 & \xi\eta\zeta & 0 & 0 & \xi^2 & 0 & 0 & \eta^2 & 0 & 0 & \zeta^2 & 0
\end{array}\right. \qquad (6\text{-}92)
$$

$$
\left.\begin{array}{cccccccccccccccccccccccccccccccccccc}
0 & 0 & \xi^2\zeta & 0 & \xi\eta^2 & 0 & 0 & \eta^2\zeta & 0 & \xi\zeta^2 & 0 & \eta\zeta^2 & 0 \\
\xi^2\eta & 0 & 0 & \xi^2\zeta & 0 & \xi\eta^2 & 0 & 0 & 0 & 0 & \xi\zeta^2 & 0 & 0 \\
0 & \xi^2\eta & 0 & 0 & 0 & 0 & \xi\eta^2 & 0 & \eta^2\zeta & 0 & 0 & 0 & \eta\zeta^2
\end{array}\right|
$$

There are 47 stress modes in the stress matrix.

In the element, there are twelve point nodes and three lines of nodes. The total degrees of freedom equals (n=) 54. The degrees of the rigid displacement are equal to (r=) 6. Thus, the element has 48 natural deformation modes. Because the rank of the partial stiffness matrix $[K_d]$ equals (n_d=) 30, the minimum number of necessary stress modes is 18. Based on the iso-function partial stress matrix (6-92), the classification method gives an optimal stress matrix as follows,

$$
[P_g]=\begin{bmatrix}
1 & 0 & 0 & \xi & 0 & 0 & \eta & 0 & 0 & \zeta & \xi\eta & 0 & 0 & 0 & \eta\zeta & 0 & 0 & 0 \\
0 & 1 & 0 & 0 & \xi & 0 & 0 & \eta & 0 & 0 & 0 & \xi\eta & 0 & 0 & 0 & \eta\zeta & \xi\eta\zeta & 0 \\
0 & 0 & 1 & 0 & 0 & \xi & 0 & 0 & \eta & 0 & 0 & 0 & \xi\eta & \xi\zeta & 0 & 0 & 0 & \xi\eta\zeta
\end{bmatrix} \qquad (6\text{-}93)
$$

6.2.7 Examination of Partial Hybrid Transition Element

The element is examined by using the eigenvalue test. Three groups of materials are examined. The first is for isotropic material (see Table 6-2); the second is for anisotropic material (see Table 6-3); The third is for the composite structure with fibre orientation [90, 0, 90] (see Table 6-4). In the tables,

$$\lambda_i = \frac{\lambda_{hi}}{\lambda_{ui}} \tag{6-94}$$

where λ_{hi} is the eigenvalue of the hybrid element; λ_{ui} is the eigenvalue of its displacement counterpart. The results of the element test show that the element does not have any kinematic deformation modes, and it has a desired capability for rigid-body displacement. In addition, the non-zero eigenvalues in the table are real and positive

Table 6-2 Eigenvalue of the transition element with 18 stress modes and isotropic materials: E=1100 GPa, ν=0.1

No.	λ_i	No.	λ_i	No.	λ_i
1	0.2071	17	0.8250	33	0.8731
2	0.4803	18	0.7449	34	0.8561
3	0.5921	19	0.8366	35	0.9672
4	0.6132	20	0.8215	36	0.9512
5	0.4749	21	0.8065	37	0.9352
6	0.5130	22	0.7871	38	0.9484
7	0.7002	23	0.8718	39	0.8896
8	0.6885	24	0.9215	40	0.9528
9	0.6687	25	0.7803	41	0.9070
10	0.6114	26	0.7887	42	0.9457
11	0.6351	27	0.8238	43	0.9157
12	0.7420	28	0.8160	44	0.9341
13	0.6695	29	0.8189	45	0.9163
14	0.6840	30	0.8569	46	0.9117
15	0.7370	31	0.7724	47	0.9821
16	0.9066	32	0.7999	48	0.9937

Table 6-3 Eigenvalue of the transition element with 18 stress modes and anisotropic materials: E_L=174.6 GPa, E_T=7.0 GPa, G_{LT}=3.5 GPa, G_{TT}=1.4 GPa, $\nu_{12}=\nu_{13}=\nu_{23}$=0.25

No.	λ_i	No.	λ_i	No.	λ_i
1	0.5415	17	0.8292	33	0.9141
2	0.5238	18	0.9127	34	0.9506
3	0.5200	19	0.8954	35	0.9509
4	0.6377	20	0.7824	36	0.8810
5	0.6938	21	0.8598	37	0.8568
6	0.6149	22	0.8410	38	0.8714
7	0.7558	23	0.9131	39	0.9966
8	0.7858	24	0.8118	40	0.9768
9	0.6984	25	0.9484	41	0.9976
10	0.5825	26	0.8229	42	0.9977
11	0.6447	27	0.8601	43	0.9921
12	0.7881	28	0.8674	44	0.9961
13	0.8234	29	1.0000	45	0.9907
14	0.8774	30	0.9756	46	0.9993
15	0.9520	31	0.9746	47	0.9959
16	0.8757	32	0.9410	48	0.9993

Table 6-4 Eigenvalue of the transition element with fibre orientation [90^0, 0^0,90^0], 18 stress modes and materials: E_L=174.6 GPa, E_T=7.0 GPa, G_{LT}=3.5 GPa, G_{TT}=1.4 GPa, $\nu_{12}=\nu_{13}=\nu_{23}$=0.25

No.	λ_i	No	λ_i	No.	λ_i
1	0.1828	17	0.7402	33	0.9464
2	0.4224	18	0.8149	34	0.8900
3	0.3981	19	0.7365	35	0.8766
4	0.4885	20	0.8655	36	0.9078
5	0.3759	21	0.7400	37	0.9665
6	0.5307	22	0.7757	38	0.9945
7	0.5726	23	0.7921	39	0.9928
8	0.8220	24	0.8156	40	0.9990
9	0.5805	25	0.7856	41	0.9913
10	0.6928	26	0.8156	42	0.9991
11	0.6623	27	0.8038	43	0.9951
12	0.7036	28	0.9790	44	0.9989
13	0.6086	29	0.9930	45	0.9961
14	0.5536	30	0.9130	46	0.9987
15	0.8042	31	0.9350	47	0.9937
16	0.8358	32	0.8143	48	0.9996

Chapter 7

PARTIAL HYBRID MULTILAYER ELEMENTS

In general, a multilayer element consists of a stack of sub-elements. According to the distribution of the material layers, a laminated composite structure is divided into many sub-layers along the thickness and each sub-layer is modeled by a sub-element. After formulating the matrices of sub-elements, they are assembled through the thickness using continuity conditions at the interfaces between different sub-elements, and then the multilayer element matrices are obtained. Therefore, there are two steps to obtain a multilayer element matrix: the first is to formulate the sub-element matrices and the second is to assemble them to form a multilayer element matrix. The general formulation of the multilayer element has been presented in Chapter 2. In this section, two multilayer elements [48,82] are presented.

7.1 Multilayer Solid Element

Partial hybrid multilayer elements consist of a stack of partial hybrid sub-elements. So the elements formulated by the composite variational principle can be used as sub-elements. For examples, 3-D, 8-node partial hybrid solid element and 3-D, 20-node partial hybrid solid element can be used to construct partial hybrid multilayer solid elements. For simplicity, a multilayer element based on 3-D, 8-node solid elements is presented [82].

7.1.1 Sub-Element Matrices

The multilayer solid element consists of a stack of 3-D, 8-node solid elements (see figure 7-1). For the i-th sub-element, the assumed displacement field is the same as that for 3-D, 8-node solid element in section 4.1 of Chapter 4. It is in the form,

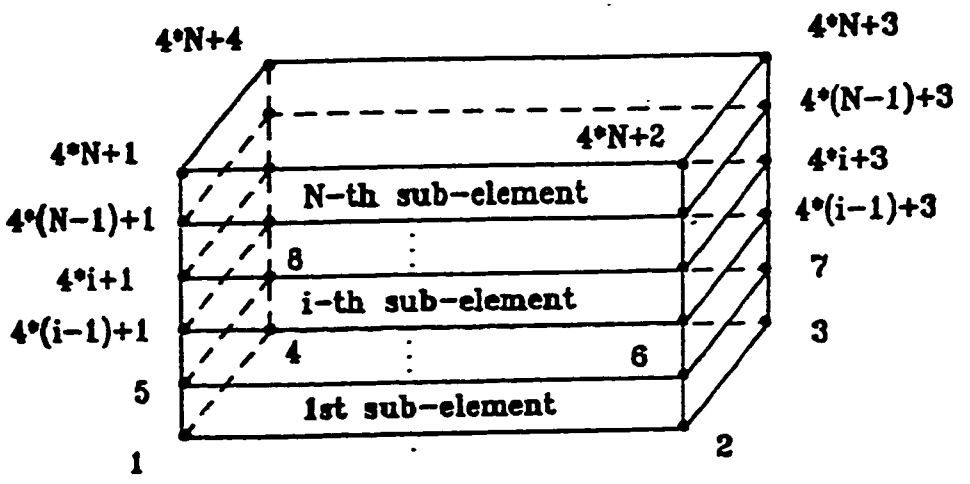

Figure 7-1 Multilayer solid element

$$\boldsymbol{u}^i = [N]\,\boldsymbol{\delta}^i = [N_1\boldsymbol{I}\ N_2\boldsymbol{I}\ \ldots\ N_8\boldsymbol{I}]\begin{Bmatrix}\boldsymbol{\delta}_1^i\\ \boldsymbol{\delta}_2^i\\ \ldots\\ \boldsymbol{\delta}_8^i\end{Bmatrix} \tag{7-1}$$

in which, [I] is a 3×3 unit matrix, N_i is the shape functions, and the nodal displacement vector is

$$\boldsymbol{\delta}_j^i = \begin{Bmatrix}u_j^i\\ v_j^i\\ w_j^i\end{Bmatrix} \qquad j=1,2,\ldots,8 \tag{7-2}$$

The nodal displacement vector of the i-th sub-element can be written in another form,

$$\begin{aligned}\boldsymbol{\delta}^i &= [\boldsymbol{d}^i\ \boldsymbol{d}^{i+1}]\\ &= [\boldsymbol{d}_1^i\ \boldsymbol{d}_2^i\ \boldsymbol{d}_3^i\ \boldsymbol{d}_4^i\ \boldsymbol{d}_1^{i+1}\ \boldsymbol{d}_2^{i+1}\ \boldsymbol{d}_3^{i+1}\ \boldsymbol{d}_4^{i+1}]\end{aligned} \tag{7-3)}$$

where $\mathbf{d}^i$ is the nodal displacement vectors related to the lower surface of the sub-element, and $\mathbf{d}^{i+1}$ is the nodal displacement vectors related to the upper surface of the sub-element. Within the sub-element, the partial stress field is assumed in the form

$$\sigma_g^i = \begin{Bmatrix}\sigma_z^i\\ \sigma_{yz}^i\\ \sigma_{zx}^i\end{Bmatrix} = [P_g]\,\boldsymbol{\Phi}^i = [P]\,\frac{1}{2}\left\{(1+\zeta)\,\alpha_T^i + (1-\zeta)\,\alpha_B^i\right\} \tag{7-4}$$

where α_T^i and α_B^i are the surface stress parameters corresponding to upper and lower surfaces of the i-th sub-element, respectively. When the matrix [P] is a function consisted

of even order terms of the coordinate ζ, the continuity condition at interfaces will be automatically satisfied (see Chapter 2). Using the equations (2-51) or (2-66) in Chapter 2, the sub-element matrices can be obtained as follows,

$$
\begin{aligned}
[H^i] &= -\int_{V_i} [P_g]^T [R_3^i]\ [P_g]\, dV \\
[G^i] &= \int_{V_i} [P_g]^T ([B_L] + [R_2^i]^T [B_g])\, dV \\
[K_d^i] &= \int_{V_i} [B_g]^T [R_1^i]\ [B_g]\, dV \\
\boldsymbol{f}^i &= \int_{V_i} [N]^T \boldsymbol{F} dV + \int_{S_{ti}} [N]^T \boldsymbol{T} dS
\end{aligned}
\tag{7-5}
$$

7.1.2 Multilayer Matrices

In order to assemble the sub-elements, the assembling rules (2-57) and (5-58) are used,

$$
\boldsymbol{\delta} = \sum_{i=1}^{N} \boldsymbol{\delta}^i = [\boldsymbol{d}^1\ \boldsymbol{d}^2\ \ldots\ \boldsymbol{d}^{N+1}]^T \tag{7-6}
$$

and

$$
\boldsymbol{\varphi} = \sum_{i=1}^{N} \boldsymbol{\alpha}^i = [\boldsymbol{\alpha}^1\ \boldsymbol{\alpha}^2\ \ldots\ \boldsymbol{\alpha}^{N+1}]^T \tag{7-7}
$$

the sub-element matrices from the 1st layer to N-th layer are added to form the multilayer matrices,

$$[K]_d=\sum_{i=1}^{N}[K_d^i] \qquad [H]=\sum_{i=1}^{N}[H^i]$$
$$[G]=\sum_{i=1}^{N}[G^i] \qquad \mathbf{f}=\sum_{i=1}^{N}\mathbf{f}^i \tag{7-8}$$

Then, the stiffness matrix of the multilayer element can be calculated using equation (2-61) or (2-66),

$$[K] = [K_d] + [K_h]$$
$$[K_h] = [G]^T[H]^{-1}[G] \tag{7-9}$$

7.1.3 Examination of the Element

For a single-layer element, a necessary and sufficient condition for guaranteeing the absence of kinematic deformation modes at the element level is,

$$n_h=n-r-n_d \tag{7-10}$$

However, for a multilayer element, the minimum number of necessary stress modes in an assumed stress matrix varies with the number of sub-elements in the multilayer elements. Using eigenvalue examination of matrices, the rank n_d of the displacement-formulated stiffness matrix $[K_d]$ can be calculated for different multilayer elements with different number of sub-elements. The minimum number n_h of stress modes in an assumed partial

stress matrix is given in table 7-1. In the table, N is the total number of sub-elements in the multilayer element; n is the total degrees of freedom of the multilayer element; r is the number of rigid body motions.

Table 7-1 Minimum number of necessary stress modes in the matrix $[P_g]$

N	n	r	n_d	n_h
1	24	6	10	8
2	36	6	15	15
3	48	6	20	22
.	.	.	.	.
10	132	6	55	71
.	.	.	.	.

From table 7-1, it is observed that the rank of semi-stiffness matrix $[K_d]$ increases by 5 when the multilayer element increases a surface. For example, there are two surfaces (top and bottom surfaces) in a fundamental multilayer element consisting of one sub-element, and the rank of semi-stiffness matrix equals 10. There is one increased surface in the multilayer element consisting of two sub-elements, and the rank of matrix $[K_d]$ equals 15. Furthermore, there are eleven surfaces in the multilayer element consisting of ten sub-elements, and the rank of matrix $[K_d]$ is equal to 55. Thus, each increased surface in a multilayer element corresponds to 5 deformation modes related to semi-stiffness matrix

$[K_d]$. Meanwhile, each added surface will increase four point nodes which correspond 12 degrees of freedom in the multilayer element. Thus, if a multilayer element contains N layers, it will have N+1 surfaces and one has

$$n = 12 * (N+1) \quad n_d = 5 * (N+1) \qquad r = 6 \qquad (7\text{-}11)$$

Define that m' is the number of stress modes in matrix [P] related to a surface. Thus, the total number of stress modes for the multilayer element is

$$m = (N+1)\, m' \qquad (7\text{-}12)$$

The necessary and sufficient condition (7-10) for avoiding kinematic deformation modes is

$$(N+1)\, m' = 12*(N+1) - 5*(N+1) - 6 \qquad (7\text{-}13)$$

Therefore, one obtains minimum number of necessary stress modes in the matrix [P] related to each surface for the multilayer element as follows,

$$m' = 7 - \frac{6}{N+1} \qquad (7\text{-}14)$$

Using this formulation, one can calculate the number of stress modes related to each surface for multilayer element consisted of different number of sub-elements.

N = 1	m' = 4
N = 2	m' = 5
N = 3	m' = 6
N = 4	m' = 6

N = 5	m' = 6
N = 6	m' = 7
.....	.....
N = 100	m' = 7

Therefore, the number of stress modes needed in the stress matrix [P] is different for a multilayer element in order to avoid kinematic deformation modes.

Sub-Element Stiffness Matrix and Kinematic Deformation Modes

When N=1, the multilayer element becomes a sub-element. The sub-element has (n=) 24 degrees of freedom and (r=) 6 degrees of the rigid displacement. Thus, the sub-element has 18 natural deformation modes. The eigenvalue examination indicates that the rank of the partial stiffness matrix $[K_d]$ for the sub-element is (n_d=) 10. Therefore, the minimum number of necessary stress modes in the assumed stress field $[P_g]$ is equal to 8. Due to a stress mode σ_j in the stress matrix [P] representing two stress modes $0.5*(1+\zeta)*\sigma_j$ and $0.5*(1-\zeta)*\sigma_j$ in the stress matrix $[P_g]$, the minimum number of stress modes in stress matrix [P] is equal to ($n_h/2$=) 4. Using iso-function method, the initial stress matrix [P] is derived directly from the assumed displacement field. It is

$$[P]=\begin{bmatrix} 1 & 0 & 0 & \xi & 0 & 0 & \eta & 0 & 0 & \zeta & 0 & 0 & \xi\eta & 0 & 0 & \eta\zeta & 0 & \xi\zeta & 0 \\ 0 & 1 & 0 & 0 & \xi & 0 & 0 & \eta & 0 & 0 & \zeta & 0 & 0 & \xi\eta & 0 & 0 & 0 & 0 & \xi\zeta \\ 0 & 0 & 1 & 0 & 0 & \xi & 0 & 0 & \eta & 0 & 0 & \zeta & 0 & 0 & \xi\eta & 0 & \eta\zeta & 0 & 0 \end{bmatrix} \qquad (7\text{-}15)$$

Then, by means of the classification method of stress modes, one obtains

$$[P] = \begin{bmatrix} 1 & 0 & 0 & 0 & 0 \\ 0 & 1 & 0 & \xi & 0 \\ 0 & 0 & 1 & 0 & \eta \end{bmatrix} \tag{7-16}$$

In the stress matrix [P], there are 5 stress modes. The results of the eigenvalue test of the element are presented in the table 7-2. In the table, all non-zero eigenvalues are real and positive. The number of zero eigenvalues is the same as that to be expected.

Table 7-2 Eigenvalue of Stiffness Matrix for the 3-D, 8-node Hybrid Element with 10 stress modes and isotropic materials: E=1100 GPa, v=0.3

No.	λ_i (*10^3)	No.	λ_i (*10^3)	No.	λ_i(*10^3)
1	0.09402	7	0.1813	13	0.8462
2	0.1410	8	0.2821	14	0.8462
3	0.1410	9	0.5440	15	0.8462
4	0.1410	10	0.5440	16	0.8462
5	0.1410	11	0.5641	17	0.8462
6	0.1813	12	0.7051	18	2.7500

Multilayer Element Stiffness Matrix

When N>2, the stress matrix [P] (7-16) can not be used to formulate the multilayer

element because it does not contain enough stress modes. According to equation (7-14), a stress matrix [P] should contain 7 stress modes at least for a general multilayer element. In this case, the iso-function partial stress matrix (7-15) does not contain enough necessary stress modes. Therefore, more polynomial terms have to be added into the stress matrix for examining. For instance, the quadratic terms should be included. Using the classification method, the following stress matrix [P] is obtained

$$[P]=\begin{bmatrix} 1 & 0 & 0 & 0 & 0 & \xi\eta & 0 & 0 \\ 0 & 1 & 0 & \xi & 0 & 0 & \zeta^2 & 0 \\ 0 & 0 & 1 & 0 & \eta & 0 & 0 & \zeta^2 \end{bmatrix} \qquad (7\text{-}17)$$

Using this stress matrix, the examination of the element indicates that the multilayer element, which consists of different sub-elements from N=1 to N=50, does not have any kinematic deformation modes.

7.2 Multilayer Transition Element

The 6-node partial hybrid transition elements also can be used to formulate a multilayer transition element which may connect a multilayer solid element with a degenerated plate element.

7.2.1 Sub-Element Matrices

The multilayer transition element consists of a stack of 6-node transition element (see

figure 7-2). For the i-th sub-element, the assumed displacement field is the same as that for 6-node transition element in section 6.1 of Chapter 6. It is in the form,

$$\begin{Bmatrix} u^i \\ v^i \\ w^i \end{Bmatrix} = \sum_1^4 N_j \begin{Bmatrix} u_j^i \\ v_j^i \\ w_j^i \end{Bmatrix} + \sum_a^b N_j \left[\begin{Bmatrix} u_j^0 \\ v_j^0 \\ w_j^0 \end{Bmatrix} + \zeta' [b_j] \begin{Bmatrix} \psi_{xj} \\ \psi_{yj} \\ \psi_{zj} \end{Bmatrix} \right] \qquad (7\text{-}18)$$

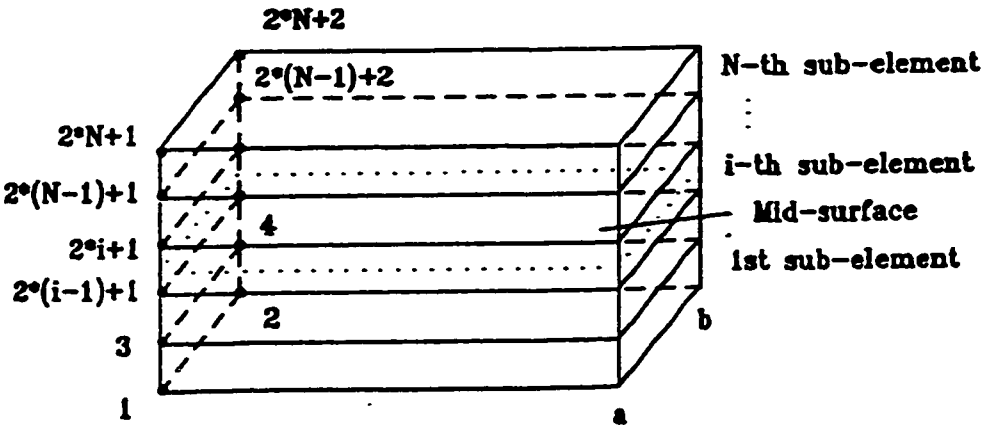

Figure 7-2 Multilayer transition element

The nodal displacement vector of the i-th sub-element can be written in the form,

$$\begin{aligned} \delta^i &= [d^i \; d^{i+1} \; d^0] \\ &= [d_1^i \; d_2^i \; d_1^{i+1} \; d_2^{i+1} \; d_1^0 \; d_2^0] \end{aligned} \qquad (7\text{-}19)$$

where $\mathbf{d}^i$ and $\mathbf{d}^{i+1}$ are the nodal displacement vectors related to the lower and upper

surfaces of the sub-element, and $\mathbf{d}^0$ is the nodal displacement vector related to the line of node. Within the sub-element, the partial stress field is assumed in the form,

$$\sigma_g^i=\begin{Bmatrix}\sigma_x^i\\ \sigma_{yz}^i\\ \sigma_{zx}^i\end{Bmatrix}=[P_g]\,\boldsymbol{\phi}^i=[P]\,\frac{1}{2}\left\{(1+\zeta)\,\alpha_T^i+(1-\zeta)\,\alpha_B^i\right\} \tag{7-20}$$

where the stress matrix [P] is a function consisted of even order terms of the coordinate ζ. Using the equations (2-66), the sub-element matrices can be obtained as follows,

$$\begin{aligned}
[H^i] &= -\int_{V_i}[P_g]^T[R_3^i]\,[P_g]\,dV\\
[G^i] &= \int_{V_i}[P_g]^T([B_L]+[R_2^i]^T[B_g])\,dV\\
[K_d^i] &= \int_{V_i}[B_g]^T[R_1^i]\,[B_g]\,dV\\
\boldsymbol{f}^i &= \int_{V_i}[N]^T\boldsymbol{F}dV+\int_{S_{ti}}[N]^T\boldsymbol{T}dS
\end{aligned} \tag{7-21}$$

7.2.2 Multilayer Matrices

The assembling rules (2-57) and (2-58) are used to assemble the element matrices,

$$\boldsymbol{\delta}=\sum_{i=1}^{N}\boldsymbol{\delta}^i=[\boldsymbol{d}^1\ \boldsymbol{d}^2\ \ldots\ \boldsymbol{d}^{N+1}]^T \tag{7-22}$$

and

$$\boldsymbol{\varphi}=\sum_{i=1}^{N}\boldsymbol{\alpha}^i=[\boldsymbol{\alpha}^1\ \boldsymbol{\alpha}^2\ \ldots\ \boldsymbol{\alpha}^{N+1}]^T \tag{7-23}$$

the sub-element matrices from the 1st layer to N-th layer are added into the multilayer matrices,

$$[K]_d=\sum_{i=1}^{N}[K_d^i] \qquad [H]=\sum_{i=1}^{N}[H^i]$$
$$[G]=\sum_{i=1}^{N}[G^i] \qquad \boldsymbol{f}=\sum_{i=1}^{N}\boldsymbol{f}^i \tag{7-24}$$

Then, the stiffness matrix of the multilayer element can be calculated using equation (2-61),

$$[K] = [K_d] + [K_h]$$
$$[K_h] = [G]^T[H]^{-1}[G] \tag{7-25}$$

7.2.3 Examination of the Element

Similar to the multilayer solid element, the minimum number of stress modes in an assumed stress matrix for a multilayer transition element varies with the number of sub-elements in the multilayer elements. Using eigenvalue examination method, the rank of the displacement-formulated stiffness matrix $[K_d]$ is obtained for different multilayer elements with different number of sub-elements. The minimum number of stress modes in an assumed partial stress matrix is given in table 7-3.

Table 7-3 Minimum number of stress modes in the matrix $[P_g]$

N	n	r	n_d	n_h
1	24	6	10	8
2	30	6	14	10
3	36	6	18	12
.	.	.	.	.
10	78	6	46	26
.	.	.	.	.

The results of eigenvalue examination shows that the rank of semi-stiffness matrix $[K_d]$ increases by 4 when the multilayer element increases a surface. For example, there are two surfaces in a fundamental multilayer element consisted of a sub-element, and the rank of semi-stiffness matrix equals 10. There is one increased surface in the multilayer element consisted of two sub-elements, and the rank of matrix $[K_d]$ equals 14. Furthermore, there are eleven surfaces in the multilayer element consisting of ten sub-elements, and the rank of matrix $[K_d]$ is equal to 46. Thus, each increased surface in a multilayer element corresponds 4 deformation modes related to semi-stiffness matrix $[K_d]$. Meanwhile, each added surface will increase two point nodes which correspond 6 degrees of freedom in the multilayer element. Thus, if a multilayer element contains N layers, it will have N+1 surfaces and one has

$$n = 12+6 * (N+1) \qquad n_d = 2+4 * (N+1) \qquad r = 6 \qquad (7\text{-}26)$$

Define that m' is the number of stress modes in matrix [P] related to a surface. Thus, the total number of stress modes is

$$m = (N+1)\ m' \qquad (7\text{-}27)$$

The necessary and sufficient condition (7-10) for avoiding kinematic deformation modes is

$$(N+1)\ m' = 12+6*(N+1) -2 -4*(N+1) - 6 \qquad (7\text{-}28)$$

Thus, one obtains minimum number of stress modes in the matrix [P] related to each surface for the multilayer element as follows,

$$m' = 2+\frac{4}{N+1} \qquad (7\text{-}29)$$

Using this formulation, one can calculate the number of stress modes in the stress matrix [P] related to each surface for multilayer element consisting of different number of sub-elements.

N = 1	m' = 4
N = 2	m' = 4
N = 3	m' = 3
N = 4	m' = 3
N = 5	m' = 3
N = 6	m' = 3

....

N = 100 m' = 3

Therefore, the number of stress modes needed in a sub-element is different in order to avoid kinematic deformation modes.

Sub-Element Stiffness Matrix and Kinematic Deformation Modes

When N=1, the multilayer element becomes a sub-element. The sub-element is a 6-node partial hybrid transition element. The examination of the element has been given in section 6.1.7 of Chapter 6. For completeness, the analysis is given here again. The sub-element has (n=) 24 degrees of freedom and (r=) 6 degrees of rigid motion. Thus, the sub-element has 18 natural deformation modes. The eigenvalue examination indicates that the rank of the partial stiffness matrix $[K_d]$ is 10. Therefore, the minimum number of the stress modes in the assumed stress field $[P_g]$ is equal to 8. Due to the fact that a stress mode σ_j in the stress matrix [P] represents two stress modes in the stress matrix $[P_g]$, the minimum number of stress modes in stress matrix [P] is equal to (n_h/2=) 4. Using iso-function method, the initial stress matrix [P] is derived directly from the assumed displacement field. It is

$$[P]=\begin{bmatrix} 1 & 0 & 0 & \xi & 0 & 0 & \eta & 0 & 0 & \zeta & 0 & 0 & \xi\eta & 0 & 0 & \eta\zeta & 0 & \xi\zeta & 0 \\ 0 & 1 & 0 & 0 & \xi & 0 & 0 & \eta & 0 & 0 & \zeta & 0 & 0 & \xi\eta & 0 & 0 & 0 & 0 & \xi\zeta \\ 0 & 0 & 1 & 0 & 0 & \xi & 0 & 0 & \eta & 0 & 0 & \zeta & 0 & 0 & \xi\eta & 0 & \eta\zeta & 0 & 0 \end{bmatrix} \quad (7\text{-}30)$$

Then, by means of the classification method of stress modes, one obtains an optimal stress matrix,

$$[P]=\begin{bmatrix} 1 & 0 & 0 & 0 & 0 \\ 0 & 1 & 0 & \xi & 0 \\ 0 & 0 & 1 & 0 & \eta \end{bmatrix} \quad (7\text{-}31)$$

In the stress matrix [P], there are 5 stress modes. The result of eigenvalue examination show that there are not any kinematic deformation modes.

Multilayer Element Stiffness Matrix and Locking Phenomenon

When N=2, the stress matrix [P] (7-31) can be used to formulate the multilayer element. But when N≥3, the stress matrices [P] can not be used to formulate a multilayer transition element due to the fact that the locking phenomenon appears.

The locking means that the solution becomes zero when the plate element becomes thin. This phenomenon appears in C^0 finite element because the Kirchhoff constraint can not be satisfied when plate element becomes thin. In the multilayer transition element, the sub-element will become thin when their number within a fixed thickness multilayer

element increases. For the multilayer transition element, equal order interpolation is used for lines of nodes which are used to meet with plate elements. Therefore, when sub-element becomes thinner and thinner, two spurious constraints produce the locking action on Ψ_{xi} and Ψ_{yi} . The locking phenomenon stands out. In order to remove it, several methods can be used such as unequal order interpolation, reduced integration, assumed strain approach, additional incompatible modes, field-redistribution, and so on [4]. In this work, the advantage of hybrid stress finite element is used to overcome locking phenomenon in the element.

By calculating m' (7-29), it has been shown that the minimum number of stress modes in the stress matrix [P] decreases to 3. Therefore, there are unnecessary stress modes in the matrix [P] (7-31) for multilayer transition elements ($N \geq 3$) and the extra stress modes in the stress matrix [P] results in over-stiffness and lead to locking phenomenon. The classification method gives following stress matrix that can be used to avoid locking phenomenon

$$[P] = \begin{bmatrix} 1 & 0 & 0 \\ 0 & 1 & 0 \\ 0 & 0 & 1 \end{bmatrix} \qquad (7\text{-}32)$$

The results of the eigenvalue examination for the multilayer element with 3 sub-elements are given in the table 7-4.

Other multilayer elements with different number of sub-elements are also examined. The

examination of the multilayer elements shows that there is no spurious constraints in the multilayer element when the stress matrix [P] (7-32) is used. In addition, the non-zero eigenvalues are real and positive.

Table 7-4 Eigenvalue of stiffness matrix for hybrid multilayer element with 3 sub-elements and isotropic materials: E=1100 GPa, ν=0.3

No.	λ_i (*10^3)	No.	λ_i (*10^3)	No.	λ_i(*10^3)
1	0.00060	11	0.1602	21	0.9849
2	0.00141	12	0.2971	22	1.0190
3	0.00186	13	0.3059	23	1.1640
4	0.00239	14	0.4109	24	1.2140
5	0.00967	15	0.5011	25	1.3130
6	0.03671	16	0.5534	26	1.5580
7	0.04086	17	0.6002	27	1.6150
8	0.08544	18	0.6734	28	2.0050
9	0.1077	19	0.7466	29	2.9820
10	0.1393	20	0.8111	30	4.2070

Chapter 8

APPLICATIONS OF PARTIAL HYBRID FINITE ELEMENTS AND GLOBAL/LOCAL ANALYSIS

8.1 Introduction

The finite element method has been widely used for stress analysis of laminated composite structures [115]. A variety of element types are available today. The analyst or designer can mix element types to solve one problem. It should be noted that the choice of element types and element mesh is problem-dependent. The number of nodes and the type of elements to be used in a finite element model is a matter of engineering judgment. As a general rule, the larger is the number of nodes and elements, the more accurate is the finite element solution, but also the more expensive the solution is. More memory space is needed to store the finite element model, and more computer time is needed to obtain the solution. Recently, a lot of global/local approaches [90-104,116-122] are proposed to improve the efficiency of the finite element method.

In practice, most laminated composite structures contain local regions where thick conditions prevail throughout. In order to obtain the stress fields in these localities, a detail 3-D finite element analysis is required. However, a detailed full 3-D analysis of these structures to obtain accurate stresses may require a huge number of nodes and elements. They may exhaust the computer resources.

In order to keep the number of nodes and elements down, one way is to classify the domain of the structure to be analyzed into different regions. Each region uses an appropriate type of element for modelling the structure. This model is called as the simultaneous global/local model. It does not require reanalysis and saves computer time.

In this chapter, the simultaneous global/local finite element models will be established to analyze laminated composite structures using partial hybrid elements that are presented in Chapter 4-7. Firstly, the partial hybrid elements will be individually used to perform the finite element analysis for verifying the accuracy of these elements.

8.2 Application of the 3-D 20-node Hybrid Solid Element

In order to verify the accuracy of the 3-D, 20-node solid element, a long laminated strip subjected to bending loads is investigated [46] since closed-form elasticity solution available for this structure.

A long laminated strip with three layers of equal thickness and fibre orientation [0,90,0] is supposed to be infinitely long in the y direction and simply supported along the two edges x=0 and L (see figure 8-1). On the top surface, it is subjected to sinusoidal transverse load of intensity q_0. The loading function is given in equation (8-1).

$$q(x) = q_0 \sin\left(\frac{\pi x}{L}\right) \tag{8-1}$$

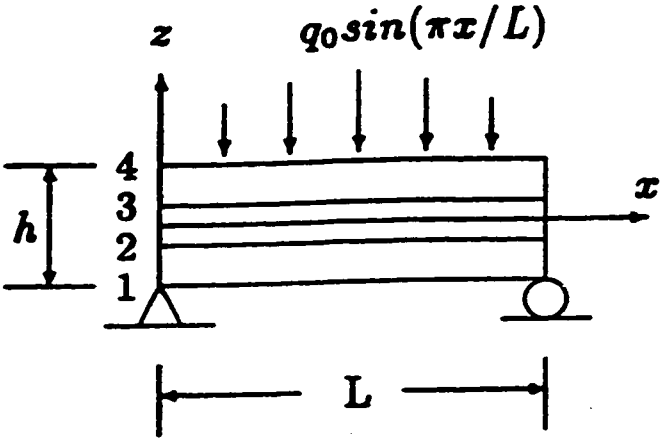

Figure 8-1 The cross section of infinitely long laminated strip [0,90,0]

The lamina material properties in the principal material direction are

$$E_L = 174.6 \text{ GPa} \qquad E_T = 7 \text{ GPa} \qquad \upsilon_{LT} = \upsilon_{TT} = 0.25$$

$$G_{LT} = 3.5 \text{ GPa} \qquad G_{TT} = 1.4 \text{ GPa} \tag{8 - 2}$$

Because the laminate is quite long in y direction, the displacement gradients can be neglected with respect to the y coordinate. Hence, a slice was taken out from the laminated strip for establishing the finite element model. Because of symmetry, finite

element analysis is carried out over half of the slice and there are four uniform elements in the half along the x-direction, one element in the y direction, and one element in each layer. This problem has been solved by using 432 3-D, 20-node displacement elements [123]. It also has the elasticity solution [124] and the CLT (Classical Lamination Theory) solution. The numerical results are presented in terms of normalized values which are defined as

$$\overline{\sigma_x}=\frac{\sigma_x(1/2,z)}{q_0} \qquad S=\frac{L}{h}$$

$$\overline{w}=\frac{100E_T h^3 w(L/2,z)}{q_0 l^4} \tag{8-3}$$

The results are presented in Table 8-1 and Figure 8-2. The excellent agreement between the partial hybrid finite element solution and the exact solution is shown.

Table 8-1 Maximum central deflection (S=10)

Surface No.	Exact Solution	Hybrid FE	Disp. FE	CLT
1 Bottom	0.929	0.929	0.927	0.5096
2	0.931	0.931	0.931	0.5096
3	0.933	0.933	0.932	0.5096
4 Top	0.934	0.934	0.933	0.5096
Element No.		12 elements	432 elements	

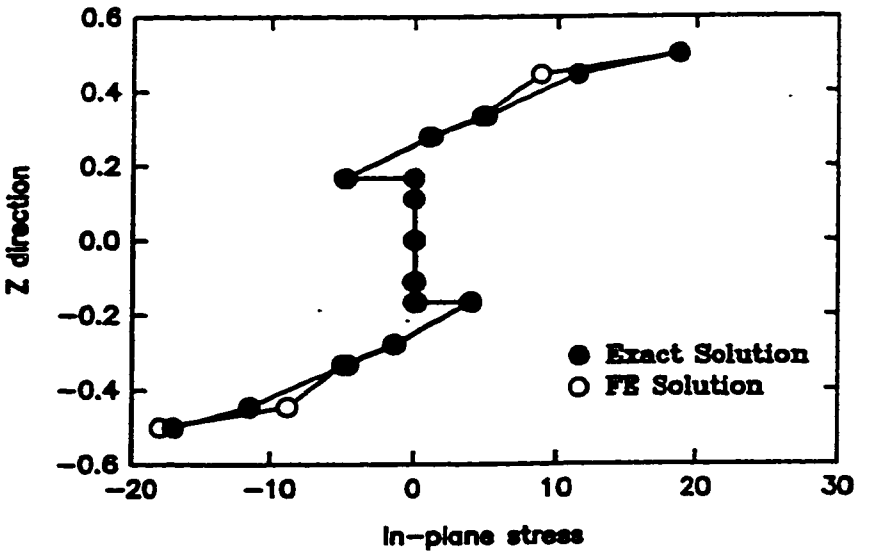

Figure 8-2 Normalized in-plane stress σ_x obtained from partial hybrid element model

8.3 Application of the Degenerated Plate Element

The accuracy of the finite element model using partial hybrid degenerated plate elements is demonstrated by studying the behaviour of a square laminated plate and a long laminated strip [44-45]. The two laminates are used to verify the degenerated element since closed-form elasticity solutions are available.

8.3.1 Deflection of a Square Laminate Subjected to Uniform Loading

A three-ply square laminate with identical top and bottom plies is analyzed by using the

8-node degenerated element. Each layer in the laminate is idealized as a homogeneous orthotropic material. The relative values of the moduli in the principal material coordinate system are the same in all the plies as follows,

$$
\begin{aligned}
&E_2 / E_1 = 0.525000 \qquad && E_3 / E_1 = 0.569399 \\
&G_{12} / E_1 = 0.292813 \qquad && G_{23} / E_1 = 0.297133 \qquad (8-4) \\
&G_{13} / E_1 = 0.178088 \qquad && \upsilon_{12} = 0.440462 \\
&\upsilon_{23} = 0.180666 \qquad && \upsilon_{13} = -0.061321
\end{aligned}
$$

An uniform loading q_0 acts on the top of the simply supported laminate. The dimensions of the plate are a, b (=a) and thickness H (= 0.1a). The thickness of the top and bottom plies h_1 is equal to 0.1H, and the thickness of the middle ply h_2 is equal to 0.8H. By means of the symmetry of the problem, only one quadrant of the plate is modeled ($0<x<a/2$, $0<y<b/2$, $0<z<H$). The computational domain is modeled using 2×2 uniform meshes (see figure 8-3). For this particular problem, a 3-D elasticity solution was presented by Srinivas and Rao [125]. The results of the deflection w at the centre of the laminate are given in the Table 9-2. In the Table, E_{1t} is the modulus of the top and bottom plies and E_{1m} is the modulus of the middle ply. E_{x2} is a parameter which can be calculated from the material constants of the middle ply. In the calculation, E_1 is equal to 0.8979495×10^6, and then E_{x2} is equal to 10^6. The present solutions of the centre deflection are close to the 3-D elasticity solutions.

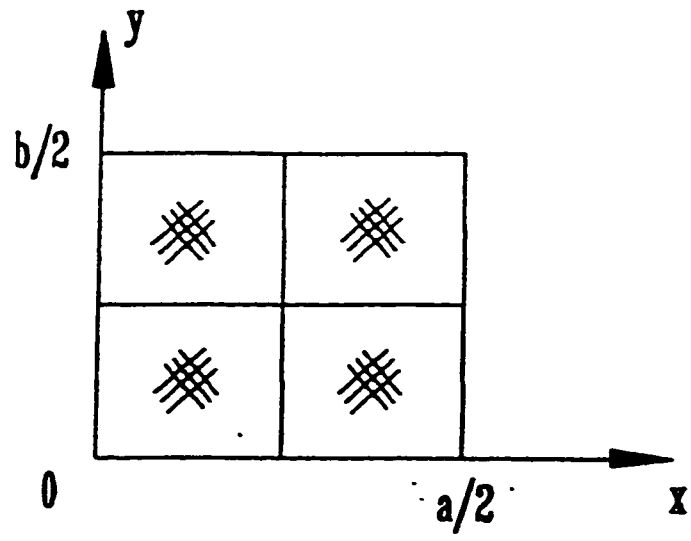

Figure 8-3 2×2 uniform mesh of a quadrant of the laminate

Table 8-2 Deflection of the simply supported laminate subjected to uniform loading

E_{1t} / E_{1m}		1	5	10	15	20
$\frac{wE_{x2}}{Hq_0}$	Elasticity Solution	688.58	258.97	159.38	121.72	---
	Present Solution	693.91	261.36	162.27	123.78	102.98

8.3.2 Bending of a Square Laminate

The 8-node degenerated element is also used to solve a square, simply supported, laminated plate with the [0,90,0] layers of equal thickness. Each layer of the laminated plate is also idealized as a homogeneous orthotropic material with the following material coefficients in the principal material coordinate system:

$$E_L=172.4\ \text{GPa} \qquad E_T=6.90\ \text{GPa} \qquad \upsilon_{LT}=\upsilon_{TT}=0.25$$
$$G_{LT}=3.45\ \text{GPa} \qquad G_{TT}=1.38\ \text{GPa} \qquad (8-5)$$

The upward transverse load is distributed on the top surface,

$$q(x,y)=q_0\sin\left(\frac{\pi x}{a}\right)\sin\left(\frac{\pi y}{b}\right) \qquad (8\text{-}6)$$

The dimensions of the plate are a, b and thickness H. The ratio S is defined as a/H. Due to the symmetry of the problem, only one quadrant of the plate is modeled (0<x<a/2, 0<y<b/2, 0<z<H). The computational domain is modeled using 2×2 uniform meshes. For this particular problem, the solution exists using 3-D elasticity theory[126] and classical laminate theory (denoted CLT). The CLT solution for τ_{xz} was found by the equations of equilibrium as discussed in [124]. The solutions for thick plate S=4 are given in figures 8-4 and 8-5. Each function is plotted along the vertical line on which it assumes its maximum value. The following normalized quantities are defined,

$$\overline{\tau_{xy}}=\frac{1}{q_0S^2}\tau_{xy} \qquad \overline{\tau_{xz}}=\frac{1}{q_0S}\tau_{xz} \qquad \overline{W}=\frac{100E_TW}{q_0HS^4} \qquad (8\text{-}7)$$

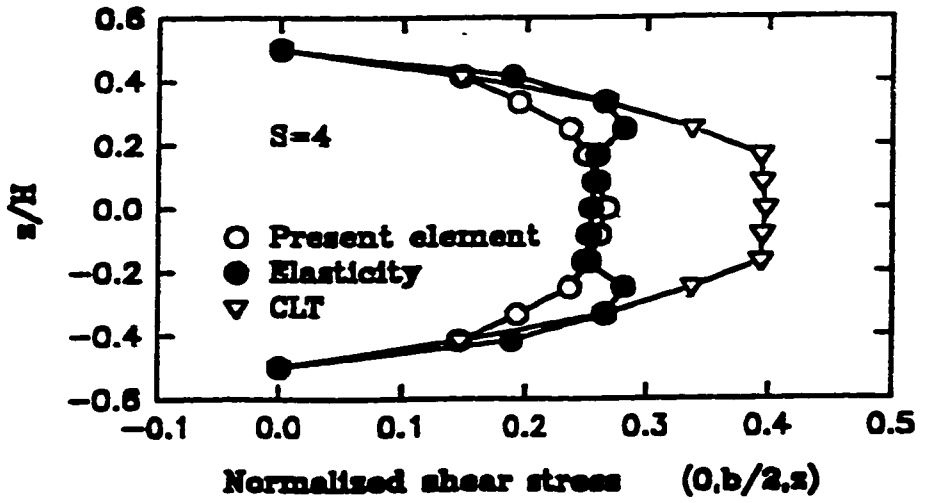

Figure 8-4 Normalized transverse shear stress τ_{xz} distribution (a=b)

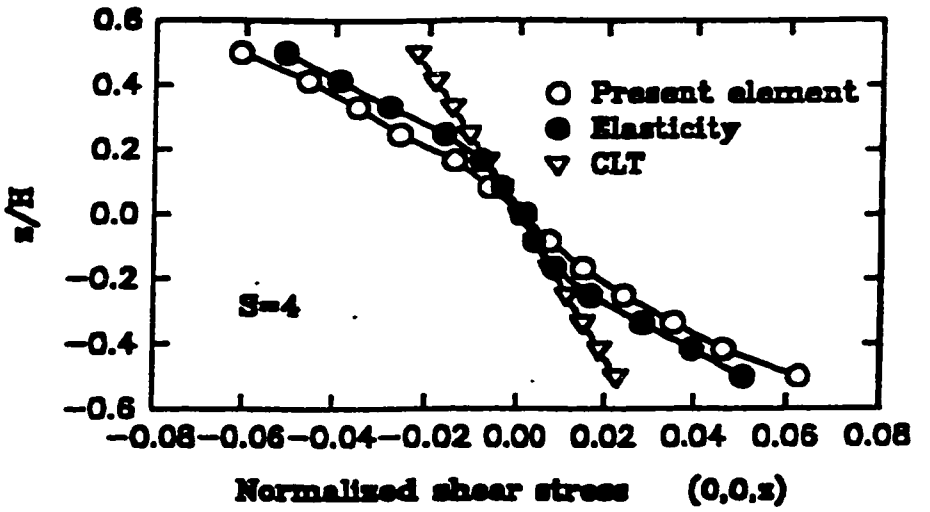

Figure 8-5 Normalized in-plane shear stress τ_{xy} distribution (a=b)

The performance of finite element analysis only takes 2.03 seconds CPU time on VAX 6510 computer by using the degenerated element. The degenerated finite element solutions are close to the exact three-dimensional elasticity solutions shown in figures 8-4 and 8-5 for the shear stresses.

8.3.3 Cylindrical Bending of A Laminated Strip

Two infinitely long laminated strips with layers of equal thickness are analyzed. The laminated strips are simply supported along the two edges and are subjected to sinusoidal transverse load of intensity q_0

$$q(x) = q_0 \sin\left(\frac{\pi x}{l}\right) \tag{8-8}$$

The lamina material properties are given by equation (8-5) in section 8.3.2. Because the laminate is quite long in y direction, the displacement gradients can be neglected with respect to the y coordinate. Hence, a slice which is taken out from the structure was modeled. Because of symmetry, numerical analysis is carried out over one half of the slice and it is subdivided into 2 equal elements. This problem has an elasticity solution[124] and a CLT solution. Pian and Li[36] also calculated stresses for this problem using a 14 DOF, 2-D partial hybrid element. For 3-layer laminate [0,90,0], the maximum central deflection as a function of span-to-depth ratio is plotted in figure 8-6. The result is in agreement with the elasticity solution. It takes 1.55 seconds CPU time to solve the problem on the VAX 6510 computer. For the 20-layer laminate $[90,0]_{10T}$, the result of the transverse shear stress which is normalized by the applied load q_0 is also in agreement with the elasticity solution as shown in figure 8-7.

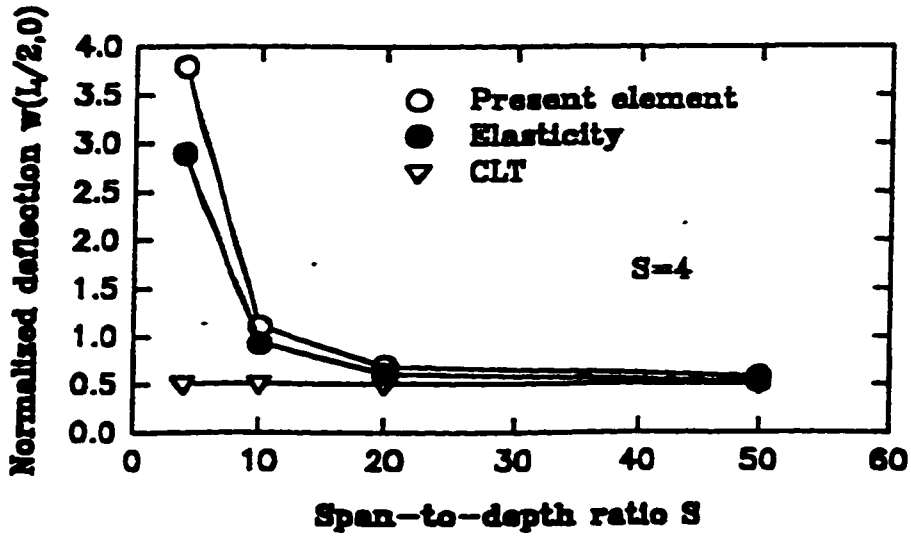

Figure 8-6 Maximum central deflection as function of span-to-depth ratio

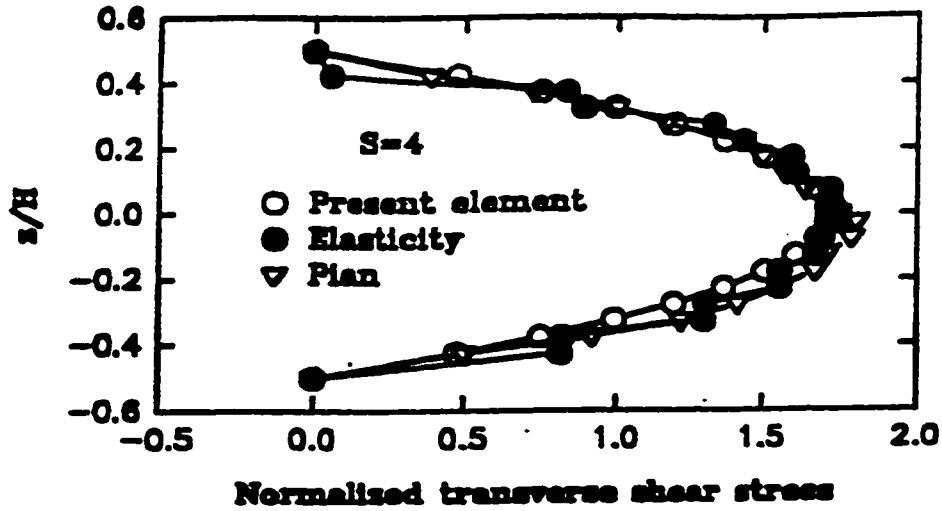

Figure 8-7 Shear stress distribution at edge of 20-layer $[90,0]_{10T}$ laminate

In the examples, it has been shown that finite models using the degenerated element is computationally most efficient for the stress analysis of composite laminates. It can provide accurate solutions for the deflection of laminates. It also can predict stresses accurately in the laminates with large number of layers. However it can not be used to evaluate stress concentration because of the limitations of assumed displacement field over the whole thickness.

8.4 Application of the Multilayer Solid Element

In order to verify the efficiency and accuracy of the multilayer element, the interlaminar stresses in the laminated strip (shown in Figure 8-8) with three layers [0/90/0] is investigated again [82]. The laminated strip is infinitely long in the y-direction and simply supported at the ends x = 0 and x = l. The ratio of length l to thickness h is of l/h = 4. The material properties on material axis are

$$\begin{aligned} &E_L = 171 \text{ GPa} \qquad E_T = 3.42 \text{ GPa} \\ &G_{LT} = 3.42 \text{ GPa} \qquad G_{TT} = 1.37 \text{ GPa} \\ &\nu_{LT} = \nu_{TT} = 0.25 \end{aligned} \tag{8-9}$$

By means of symmetry, only half the length of the laminated strip is modelled. The finite element model contains ten uniform multilayer elements in half the length and one element in the width. Each multilayer element is composed of 24 sub-elements along the thickness of the laminated strip. On the top surface, there is a sinusoidally distributed transverse loading,

$$q(x) = q_0 \sin\left(\frac{\pi x}{l}\right) \tag{8-10}$$

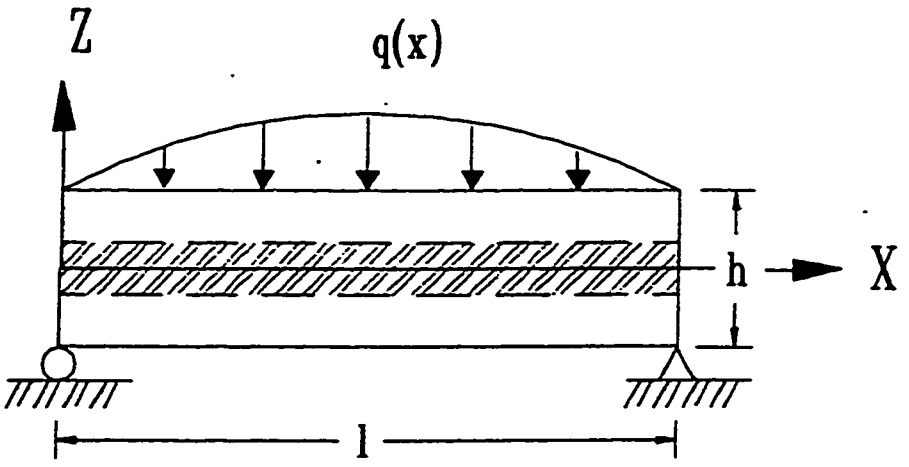

Figure 8-8 The laminated strip with three layers [0,90,0]

The problem also was solved by using 3-D displacement element [123], which modelled the laminated strip with 432 3-D, 20-node displacement elements. Furthermore, there is an elasticity solution for this problem [124]. The finite element results of shear stress τ_{xz} are given in figure 8-9, compared with the result of Pagano's elasticity solution [124]. In the figure, the results is presented in the terms of normalized values which are defined as

$$\bar{\tau}_{xz} = \tau_{xz} / q_0$$
$$\bar{z} = z / h \qquad (8\text{-}11)$$

In Figure 8-9, it is shown that the multilayer element solution is in better agreement with the Pagano's elasticity solution, although it using less elements and take less computer CPU time.

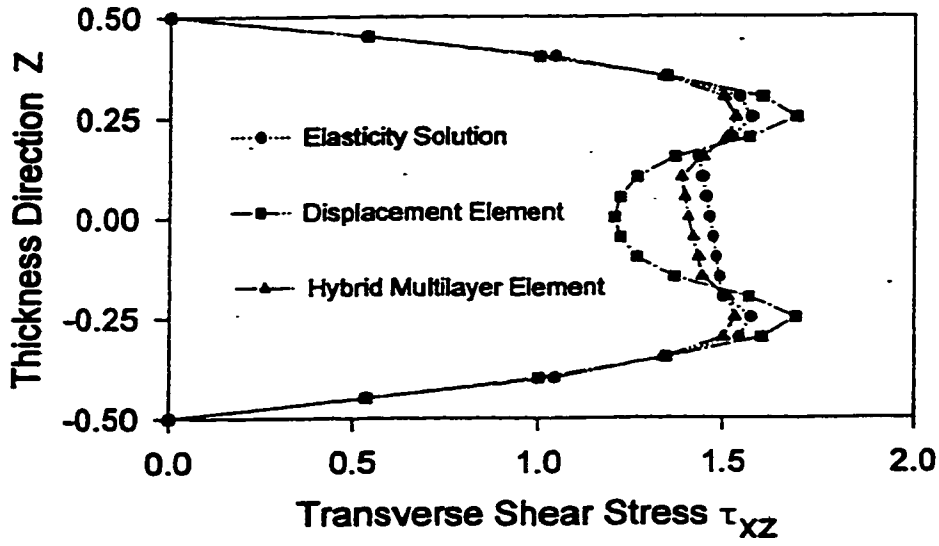

Figure 8-9 Transverse shear stress τ_{xz} at the edge x=0 along the thickness of the strip

8.5 Global/local Analysis of Laminated Composites

As mentioned above, the analysis of a laminated composite structure may require a detail 3-D finite element analysis. However, a detailed full 3-D finite element analysis of these structures may require huge computer resources. One way to solve these problems is to set up a global/local finite element model using different element types in different regions. It will take advantage of the properties of different elements and keep the computer storage requirement down.

In this section, the effectiveness of the global/local finite element model using different element types is demonstrated by obtaining the interlaminar stresses for a laminated strip with free edges and a laminated plate with a hole. All numerical studies were performed on a VAX 6510 computer. The computational effort of each analysis is quantified by the number of degree of freedom used in the finite element model and the computational time required to perform a stress analysis. The computational time is measured in central

processing unit (CPU) time.

8.5.1 Global/local Analysis of A Laminated Strip with Free Edges

Free edge effect is an important problem in the analysis of laminated composite structures. The interlaminar stresses generated around the free edges and interlaminar surfaces are recognized to be the primary sources of delamination of laminated composite structures initiated at the free edges. Many approaches have been proposed to solve this problem. It is an ideal example to verify the efficiency and accuracy of various approaches due to the existence of high stress gradient near free edges. In this section, the global/local finite element models built by three types of elements are presented to solve this problem [101-104].

Model 1 - Using 20-node Solid Elements and 15-node Transition Elements and 8-node Degenerated Elements

The laminated strip with free edges to be analyzed is an angle-ply laminated strip with the [45/-45/-45/45] sequence subjected to uniaxial extension (X-direction). The strip (shown in figure 8-10) has length of 2L (X-direction), width 2b (Y-direction), and thickness $4h_0$ ($W=8h_0$). Each layer in the laminate is also idealized as a homogeneous orthotropic material. The material properties are

$$E_L = 137.93 \text{ GPa} \qquad E_T = 14.48 \text{ GPa}$$
$$G_{LT} = G_{TT} = 5.86 \text{ GPa} \qquad v_{LT} = v_{TT} = 0.25 \qquad (8\text{-}12)$$

Because the strip is infinitely long in x direction, the displacement gradient with respect to x coordinate can be neglected and stress and strain states are independent of x coordinate. Therefore, the length of the sample to be analyzed in x direction does not affect the results of stress analysis. Thus, a slice can be taken out from the strip to establish a finite element model. Furthermore, it can be assumed that stress distributions

are symmetric about the mid-plane because the geometry, material properties, and loading are symmetric. Thus, a quarter of the slice only is needed to be analyzed.

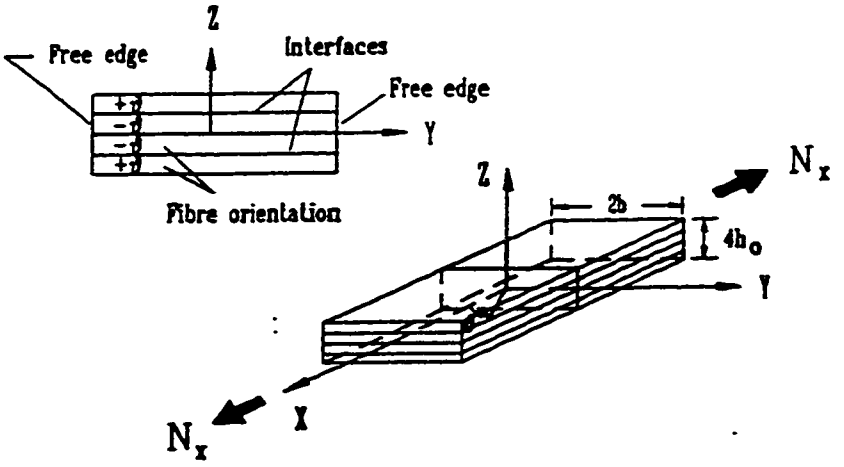

Figure 8-10 The laminated strip subjected to axial loading

The domain of the strip to be analyzed is divided into three areas: local region, global region, and transition region. The finite element mesh used for analysis is shown in figure 8-11. In the local model, the high stress gradient is expected. Forty eight 3-D, 20-node solid elements are used: 8 elements in thickness direction, 6 elements in y direction, and 1 element in x direction. In the central region of the laminate, five 8-node degenerated elements are used: 1 element in the thickness direction, 5 elements in y direction, and 1 element in x direction. At the transition region, eight transition elements are used to connect eight solid elements with one degenerated element. The width of the elements decreases as the free edge is approached. The problem is also analyzed by the layerwise model [24] and conventional 3-D displacement model. The mesh on the X-Y plane for the two finite element models is same as that for the global/local model.

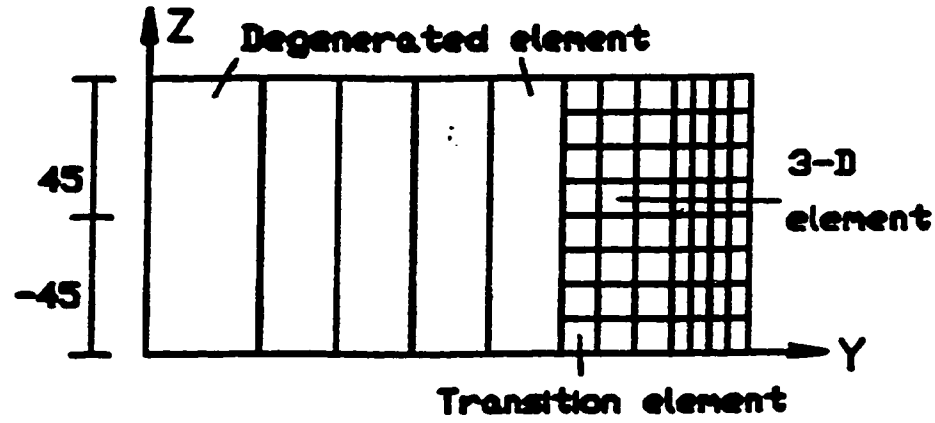

Figure 8-11 Global/local finite element mesh for study of free edge

The results of interlaminar stresses σ_z and τ_{xz} are shown in figures 8-12 and 8-13. The stresses in the figures has been non-dimensionalized by multiplying it by the factor $\sigma/(\varepsilon_0 * 10^6)$, where ε_0 is the nominal applied axial strain of $u_0/(2L)$. The global/local model only takes 62.09 seconds CPU time on VAX 6510 Computer to solve the problem. The layerwise finite element model takes 204.40 seconds CPU time and the 3-D conventional displacement element model takes 287.06 seconds CPU time on the same computer. For the analysis, the present global/local model uses 1154 active degrees of freedom totally, the layerwise model uses 2441 active degrees of freedom, and 3-D model uses 2849 active degrees of freedom. It shows that the present global/local model takes less time and uses less active degrees of freedom than other models to solve the same problem and to get the same degree of accuracy.

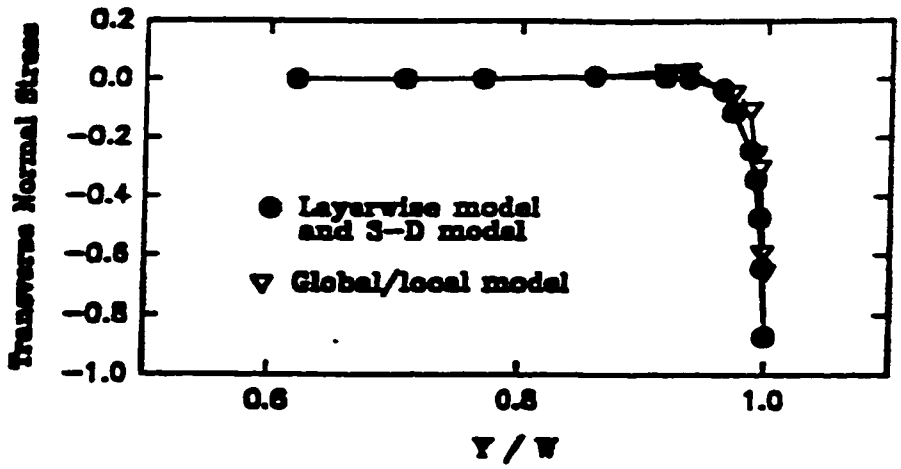

Figure 8-12 Interlaminar stress σ_z along interlaminar surface

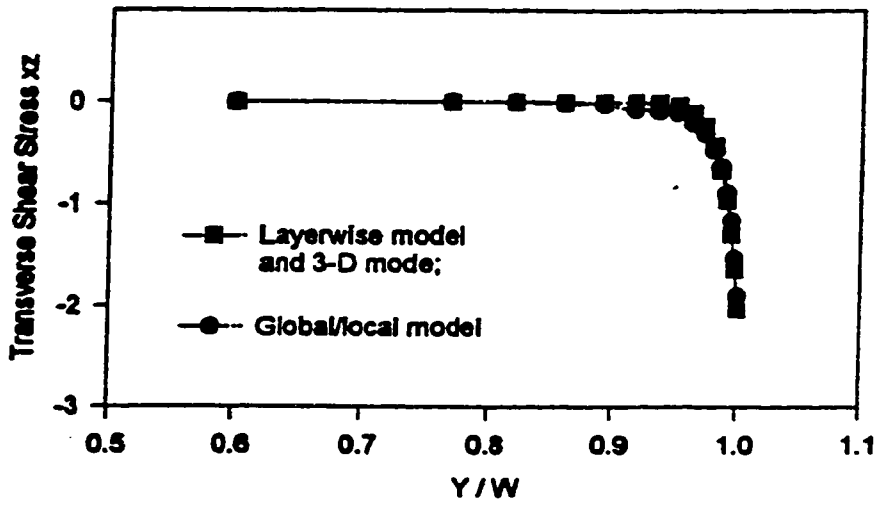

Figure 8-13 Interlaminar stress τ_{xz} along interlaminar surface

Model 2 - Using Multilayer Elements and Multilayer Transition Elements and 4-node Degenerated Elements

A global/local model built by 3-D solid element, transition element, and degenerated element can predict interlaminar stresses accurately. However, it is a labour intensive task to make 3-D element mesh in the local region. In the new global/local model, 3-D solid element and 3-D transition element are replaced by multilayer elements. The model built by multilayer element, multilayer transition element, and 4-node degenerated element is used to analyze the free edge problem again.

The problem to be solved is same as that above in this section. The domain of the strip along the Y-direction is also divided into three regions: local, global, and transition regions. The element mesh used for analysis is shown in figure 8-14. In the vicinity of free edge (local region), twelve multilayer elements are used along the Y-direction and each multilayer element contains 16 8-node sub-elements in the thickness of the strip. In the central part (global region), ten 4-node degenerated elements are used in y direction. In the transition region, one multilayer transition element is used to connect the multilayer element with the degenerated element. Along the X-direction, the strip is modelled by using two elements and all elements have the same length (=L). The results of interlaminar stresses σ_z and τ_{xz} are shown in figures 8-15 and 8-16. The stresses in the figures have been non-dimensionalized by multiplying it by the factor $\sigma/(\varepsilon_0*10^6)$, where ε_0 is the nominal applied axial strain of $u_0/(2L)$.

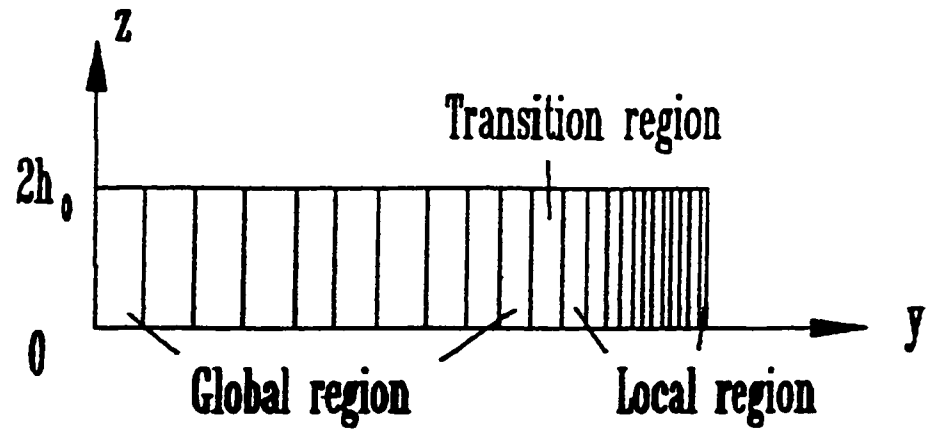

Figure 8-14 Model -2: Element mesh for free edge problem

The problem is also analyzed by a full 3-D finite element model using 3-D, 20-node solid displacement element and a previous global/local finite element model using 20-node solid elements, 8-node degenerated elements, and transition solid elements. The results of interlaminar stresses σ_z and τ_{xz} calculated by the two models are also shown in figure 8-15 and 8-16. In the figures, the "previous global/local model" indicates the model 1 above, and the "current global/local model" indicates the model 2. The difference of the results obtained from three finite element models is not significant. However, the computer CPU time required by three models for performance is quite different.

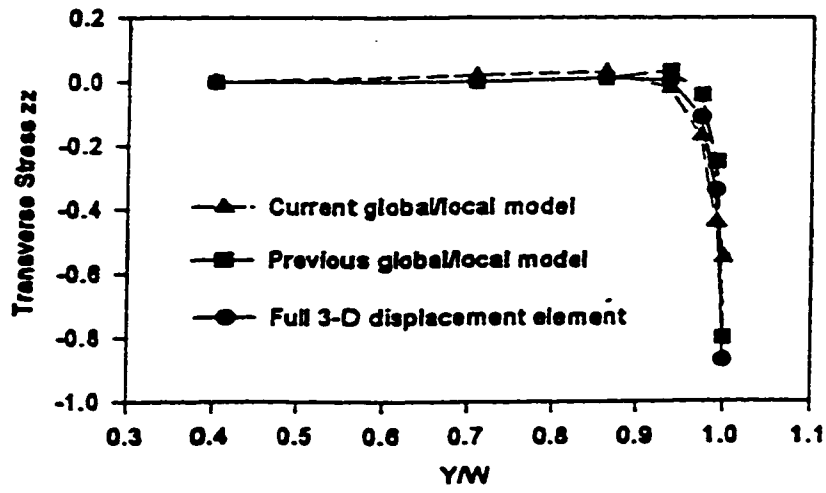

Figure 8-15 Stress σ_z at interlaminar surface along y direction

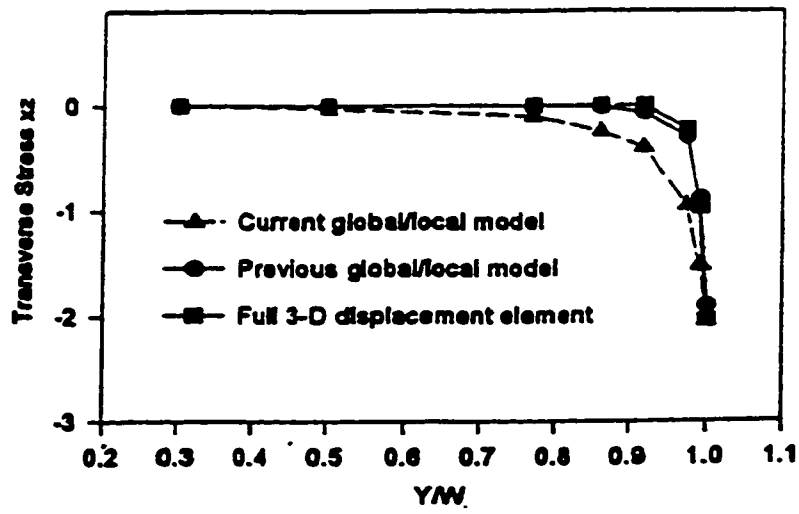

Figure 8-16 Stress τ_{xz} at interlaminar surface along y direction

For the performance of the finite element analysis, the current global/local model takes 100.45 seconds CPU time, the previous global/local finite element model takes 62.09 seconds CPU time, and the full 3-D finite element model takes 287.06 seconds CPU time on VAX 6510 Computer. Therefore, the current global/local model takes about one-third computer CPU time used by the full 3-D finite element model, and the previous global/local finite element model takes about one-fifth computer CPU time used by the full 3-D finite element model. The current global/local model takes more CPU time than the previous global/local model for calculation due to the fact that during the calculation of element stiffness matrix, the current global/local model using multilayer elements must inverse the matrix [H] whose size is larger than that of solid element used in the previous global/local model. In spite of that, the current global/local model is still more efficient than the full 3-D finite element model. Furthermore, the current global/local model has 2-D data structure in the finite element mesh. This is extremely beneficial to set up a global/local finite element model.

8.5.2 Global/local Analysis of A Square Laminate with an Open Hole

A square laminate $[45,-45]_s$ with an open hole is also an ideal structure to verify the efficiency of the global/local model. The stress analysis of the laminate is performed under uniaxial loading (Y-direction). The radius of the hole is R. The laminate (shown in figure 8-17) has length of 2L (=8R) and thickness 2h (=R). The material constants in the principal material coordinate system are given in equation (8-12).

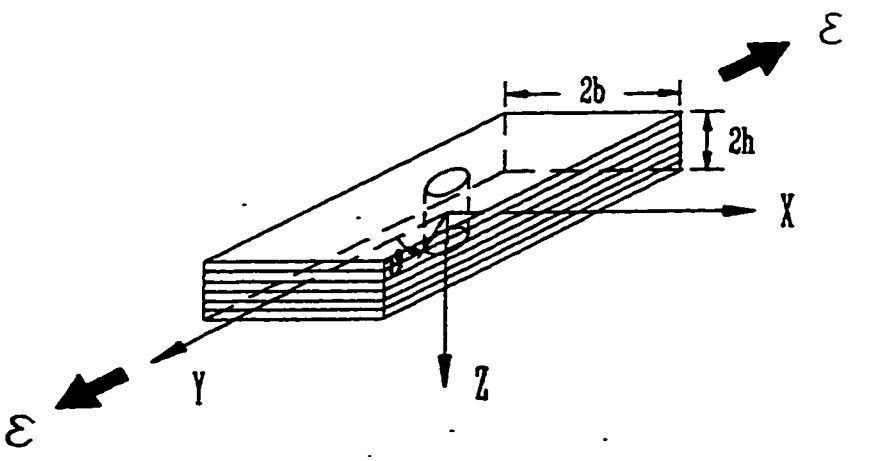

Figure 8-17 An angle-ply laminate with an open hole

Due to symmetry of geometry and loading in this problem, the domain to be analyzed may be reduced to one eighth portion of the laminate. In the global/local model, the domain is divided into three areas: local region, global region, and transition region (shown in Figure 8-18). In the local region, forty 3-D, 20-node elements are used as there is high stress gradient near the hole edge. Each layer is modeled by two 3-D, 20-node elements along the thickness. In the global region, a few degenerated elements are used. One element is used along the thickness. Between them, twenty transition elements are used to connect them. Along the thickness of the laminate, four transition elements are used to connect four 3-D solid elements with one degenerated element. The problem is also calculated by the layerwise model based on layerwise theory [24] and conventional 3-D displacement element model. The mesh on the X-Y plane in the two models is same as that in the global/local model.

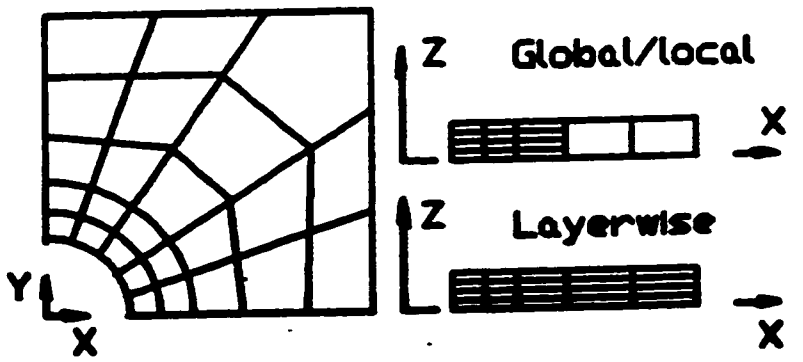

Figure 8-18 Finite Element Mesh for Analysis

The results of interlaminar stresses σ_z , τ_{yz} and τ_{xz} are shown in figures 8-19, 8-20, and 8-21. The stress in the figures has been non-dimensionalized by multiplying it by the factor σ/σ_0, where σ_0 is the applied axial stress. The global/local model only takes 61.29 seconds CPU time on VAX 6510 Computer to solve the problem. The layerwise model takes 198.31 seconds CPU time and the 3-D model takes 291.17 seconds CPU time on the same computer. For the analysis, the global/local model uses 1051 active degrees of freedom totally, the layerwise model uses 2298 active degrees of freedom, and 3-D model uses 2948 active degrees of freedom. It shows that the global/local model takes less time and uses less active degrees of freedom than other models to solve the same problem and to get the same degree of accuracy.

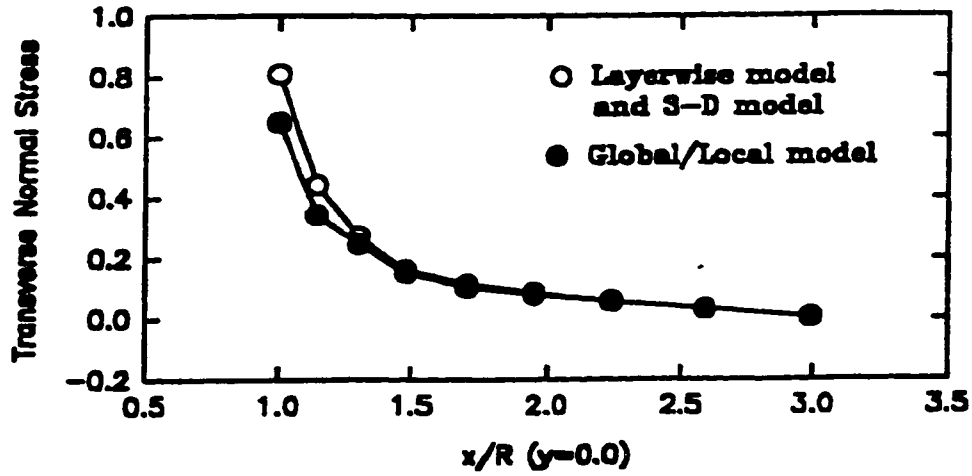

Figure 8-19 Interlaminar stress σ_z along interlaminar surface

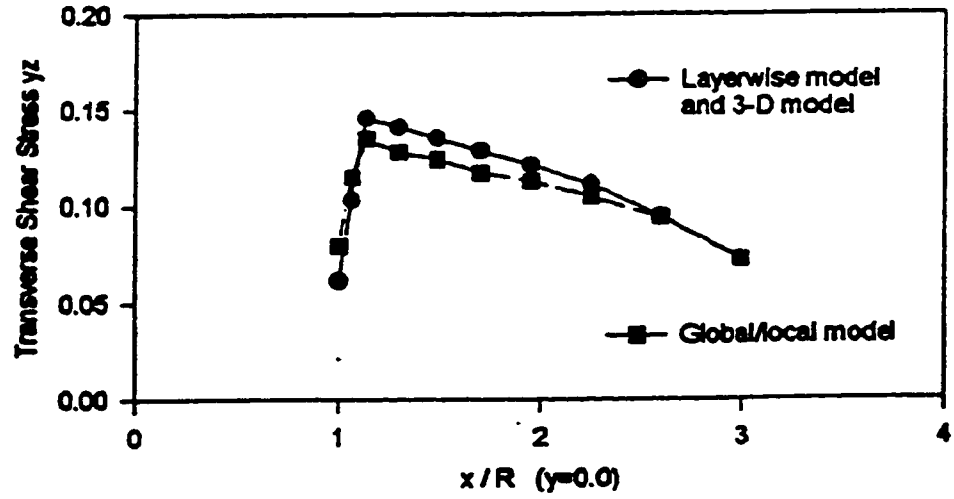

Figure 8-20 Interlaminar stress τ_{yz} along interlaminar surface

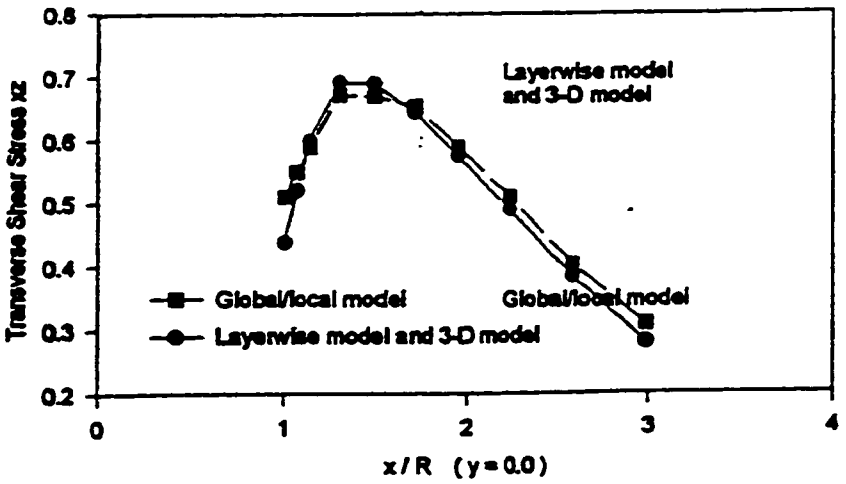

Figure 8-21 Interlaminar stress τ_{xz} along interlaminar surface

8.6 Conclusion

In this chapter, the accuracy and efficiency of the finite element models built by partial hybrid elements have been verified. The global/local model built by 3-D, 20-node solid elements, 15-node transition elements, and 8-node degenerated plate elements is also used by Zhao [127] to analyze the stress field of the composite laminates with delamination crack under out-of-plane loading. The results of the examples studied show that partial hybrid elements can predict more accurate stresses than displacement elements for composite laminates. The global/local finite element approach using partial hybrid elements is more efficient than other finite element models. Once the accuracy of the finite element models built by partial hybrid elements is established, they can be applied to more general problems.

Chapter 9

CONTRIBUTION OF THE THESIS AND SUGGESTION FOR FUTURE RESEARCH

9.1 Contribution of Current Work

The contributions of this thesis are:

1. The general formulations of the partial hybrid single-layer finite element and multilayer finite element have been presented using the composite variational principle. They can be used to develop various new partial hybrid finite elements.

2. In order to determine optimal stress polynomials for hybrid stress elements, a classification method of stress modes has been presented. The method can be used to classify stress modes, select optimal stress modes, and set up an assumed stress matrix for a hybrid element. In addition, the optimal condition of assumed stress field is presented. Using the classification method, the stress polynomials are constrained by the number of degrees of freedom associated with a hybrid stress element. The method is also

extended to determine the partial hybrid stress field for partial hybrid elements.

3. Two degenerated plate elements based on the composite variational principle and the equivalent single-layer model have been presented using the general formulation of single-layer elements. The continuities of interlaminar stresses are satisfied at the interlaminar surface and the number of degrees of freedom per node is independent from the number of layers. The traction free conditions are also satisfied on the upper and lower surfaces of a laminated composite structure by assuming the transverse stress components independently. The transverse normal strain is taken into account in order to consider the full 3-D effect in a laminated composite structure. The results of the element eigenvalue test show that the elements have the capability of rigid-body motion to be expected and are without any zero-energy deformation modes.

4. Two 3-D solid elements have been developed by means of the general formulation of the single-layer element. The classification method has been used to determine the optimal stress matrix which contains minimum number of necessary stress modes. The elements are examined by the eigenvalue test. The results of examination show that the elements have the capability of rigid-body motion to be expected and are without any zero-energy deformation modes.

5. Two transition elements have been proposed by means of the concept of moving node. The two elements can be used to smoothly connect the 3-D solid elements with the

degenerated plate elements. In order to enforce the compatibility at the interfaces between different elements, new shape functions are derived for the shape functions of 3-D solid elements. The new shape functions can fit any functions of degenerated plate elements along the thickness. By means of the transition elements, one can establish global/local finite element models using three different types of elements.

6. The multilayer solid element and multilayer transition element are formulated using the general formulation of multilayer elements. They consist of a stack of 3-D, 8-node partial hybrid solid element and 6-node partial hybrid transition element, respectively. The surface stress parameters are directly used to assume partial stress fields and the transfer between layer stress parameters and laminate stress parameters is avoided.

7. The Global/Local finite element models have been established using the new partial hybrid finite elements for the analysis of laminated composite structures. A square laminate with a hole and a laminated strip with free edge are investigated by using the global/local finite element models. It has been shown that the present global/local models using partial hybrid element is efficient and accurate for stress analysis of laminated composites. They take advantage of the capacity of both 3-D solid elements and 2-D degenerated plate elements. The global/local model can be used to predict local stress distribution such as the interlaminar stresses near the discontinuities of composite structures, with low requirement on computer storage size.

8. A computer program COMSA has been developed using the partial hybrid finite elements. The introduction of the program COMSA will be given in the appendix.

9.2 Suggestion for Future Research

1. Combining with the failure criteria of laminates composite structures, the finite element models could be used to simulate the failure process of composite structures.

2. The partial hybrid finite elements could be extended to dynamic problems of laminated composite structures.

3. The partial hybrid finite elements could also be extended to non-linear problems of laminated composite structures.

REFERENCES

[1] Zienkiewicz, O.C. and Cheng, Y.K., The Finite Element Method in Structural and Continuum Mechanics, McGraw-Hill, London, 1967.

[2] Irons, B. and Ahmad S., Techniques of Finite Elements, Ellis Horwood Limited, England, 1980.

[3] Hughes, T.J.R., The Finite Element Method, Prentice-Hall, Inc., Englewood Cliffs, New Jersey, 1987.

[4] Prathap, G., The Finite Element Method in Structural Mechanics, Kluwer Academic Publishers, The Netherlands, 1993.

[5] Noor, A.K., 'Bibliorgraphy of books and monographs on finite element technology', Apply Mechanics Review, Vol. 44, no. 6, (1991).

[6] Cook, R.D., Malkus, D.S. and Plesha, M.E., Concepts and Applications of Finite Element Analysis, Third edition, John Wiley and Sons, New York, 1995.

[7] Bathe, K.J., Finite Element Procedures in Engineering Analysis, Prentice-Hall, Inc., Englewood Cliffs, New Jersey, 1981.

[8] Hoa, S.V. and Feng, W., 'Finite elements for analysis of composite Structures', in Hoa, S.V. (ed.) : Computer-Aided Desing of Polymer-Matrix Composite Structures, Marcel Dekker, Inc., New York, 1995.

[9] Hoa, S.V. and Feng, W., Hybrid Finite Element Method for Stress Analysis of

Laminated Composites, Kluwer Academic Publishers, USA. (1998)

[10] Ochoa, O.O. and Reddy, J.N., Finite Element Analysis of Composite Laminates, Kluwer Academic Publishers, USA, 1992.

[11] Kardestuncer, H. & Norrie, D.H., Finite Element Handbook, McGraw-Hill Book Company, 1987.

[12] Pilkey, W. & Perrone, N. (eds.), Structural Mechanics Software Series, University Press of Virginia, Charlottesville, vols. I - V, 1984.

[13] Fong, H.-H., 'An evaluation of eight U.S. general purpose finite element computer programs', Proceedings of the 23d AIAA/ASME/ASCE/AHS Structures, Structural Dynamics and Materials Conference, part 1, 145-160, New Orleans (1982).

[14] Taig, J.C., 'Finite element analysis of composite materials', NAFEMS Rep. No. R0003, NAFEMS, Scotland, 1991.

[15] Dhatt, G. and Touzot, G., The Finite Element Method Displayed, John Wiley & Sons, New York, 1984.

[16] Tsai, S.W., Composite Design, Think Composites, Ohio, USA, 1988.

[17] Noor, A.K. and Burton, W.S., 'Assessment of shear deformation theories for multilayered composite plates', Appl. Mech. Rev., vol. 42, no. 1, 1-9(1989).

[18] Reissner, E. and Stavsky, Y., 'Bending and stretching of certain types of heterogeneous aeroisotropic elastic plates', J. Appl. Mech. ASME, 28, 402-408(1961).

[19] Lo, K.H., Christensen, R.M., and Wu, E.M., 'A higher-order theory of plate deformation: Part 1, Homogeneous plates; Part 2, Laminated plates', J. Appl. Mech. ASME, 44, 663-676(1977).

[20] Reddy, J.N., 'A simple higher-order theory for laminated composite plates', J. Appl. Mech. ASME, 51,745-752(1984).

[21] Reddy, J.N., 'A refined nonlinear theory of plates with transverse shear deformation', Int. J. Solids Struct., 20, 881-896(1984).

[22] Whitney, J.M. and Sun, C.T., 'A higher order theory for extensional motion of laminated composites', J. Sound Vib., vol. 30, 85-97(1973).

[23] Chao, W.C. and Reddy, J.N., 'Analysis of laminated composite shell using a degenerated 3-D element', Int. J. for Numer. Methods in Eng., vol. 20, 1991-2007(1984).

[24] Robbins, JR. D.H. and Reddy, J.N., 'Modelling of thick composites using a layerwise laminate theory', Int. J. Numer. Methods in Eng., vol. 36, 655-677(1993).

[25] Reddy, J.N. and Robbins, JR. D.H., 'Theories and computational models for composite laminates', Apply Mechanics Review, vol. 47, no. 6, part 1, (1994).

[26] Robbins, JR. D.H. and Reddy, J.N., 'Variable kinematic modelling of laminated composite plates', Int. J. Numer. Methods in Eng., vol. 39, 2283-2317(1996).

[27] Chang, T.Y. and Sawamiphakdi, K., 'Large deformation analysis of laminated shell by finite element method', Comput. & Struct., vol. 13, 331-340(1981).

[28] Hoa, S.V., Yu, C.W., and Sankar, T.S., 'Analysis of filament wound vessel using finite elements', Composite Structures, vol. 3, 1-18(1985).

[29] Natarajan, R., Hoa, S.V., and Sankar, T.S., 'Stress analysis of filament wound tanks using 3-D finite elements', Int. J. Numer. Methods Engrg, vol. 23, 623-633(1986).

[30] Hoa, S.V., Journeaux, B.H., and Di Lalla, L., 'Computer aided design for composite structures', Proc. 7th Int. Conf. on Composite Materials, (eds. Wu, Y-S. et al.), 383-

390(1989).

[31] Pian, T.H.H., 'State-of-the-art development of hybrid/mixed finite element method', Finite Elements in Analysis and Design, vol. 21, 5-20(1995).

[32] Mau, S.T., Tong, P. and Pian, T.H.H., 'Finite element solutions for laminated thick plates', J. Composite Materials, vol.6, 304-311(1972).

[33] Spilker, R.L. 'Hybrid-stress eight-node elements for thin and thick multilayer laminated plates', Int. J. Numer. Methods Engrg, vol.18, 801-828(1982).

[34] Cheung, Y.K. & Chen, W. 'Generalized hybrid degenerated elements for plates and shells', Computers & Structures, vol. 36, no. 2, 279-290(1990).

[35] Spilker, R.L., Chou, S.C., and Orringer, O., 'Alternate hybrid-stress elements for analysis of multilayer composite plates', J. Composite Materials, vol.11, 51-70(1977).

[36] Pian, T.H.H. and Li, M.-S., 'Stress analysis of laminated composites by hybrid finite elements', in Discretization Methods in Structural Mechanics (Ed. Kuhn, G. and Mang, H.), 1989.

[37] Liao, M.-L., Jing, H.-S., and Hwang, M., 'Improvements on the higher order plate element with partial hybrid stress model', Computers & Structures, vol. 42, no. 1, 45-51(1992).

[38] Wang, C.-Y. and Ching, H.-K., 'A modified partial hybrid stress finite element method for the aminated composite plate analysis', Composites Modelling and Processing Science, ICCM/9, vol. III, ed., Antonio Miravete, University of Zaragoza, Woodhead Publishing Limited, 1993.

[39] Han, J. and Hoa, S.V., 'Three dimensional composite elements for finite element

analysis of anisotropic laminated structures', in Computer Aided Design in Composite Material Technology, III, (Ed. Advani, S.G. et al.), pp. 255-268, Computational Mechanics Publications, 1992.

[40] Huang, Q., Hoa, S.V., and Sankar, T.S., 'Three dimensional finite element formulation for stress analysis of anisotropic laminated structures', in Composite Material Design and Analysis, (Ed. W.P.de Wilde and W.R. Blain), 1990.

[41] Huang, Q., 'Three dimensional composite finite element for stress analysis of anisotropic laminate structures', Ph. D. Dissertation, Concordia University, Montreal, Canada (1989).

[42] Han, J. and Hoa, S.V., 'A three-dimensional multilayer composite finite element for stress analysis of composite laminates', Int. J. Numer. Methods Engrg., vol.36, 3903-3914(1993).

[43] J. Han, 'Three dimensional multilayer composite finite element for stress analysis of composite laminates', Ph.D. Dissertation, Concordia University, Montreal, Canada, (1994).

[44] Feng, W. and Hoa, S.V., 'A degenerated plate/shell element with assumed partial stress field for the analysis of laminated composites', 4th International Conf. on Computer Aided Design in Composite Material Technology, Southampton, UK (1994).

[45] Feng, W. and Hoa, S.V., 'A partial hybrid degenerated plate/shell element for the analysis of laminated composites', Int. J. Numer. Methods Eng., vol. 39, 3625-3639(1996).

[46] Feng, W. and Hoa, S.V., 'A 3-D partial hybrid laminated element for analysis of thick laminates', Third Int. Conf. on Composites Engineering, New Orleans, USA (1996).

[47] Feng, W. and Hoa, S.V., '3-D transition element formulation for the global-local analysis of laminated structures', Int. Conf. on Design and Manufacturing Using Composites, Montreal, Canada (1994).

[48] Feng, W. and Hoa, S.V., 'Partial hybrid finite elements for composite laminates', Finite Elements in Analysis and Design, (in press).

[49] Hoa, S.V. and Feng, W., 'Finite element method for composites', Composites '96 and Oriented Polymers Symposium, Montreal, Canada (1996).

[50] Hoa, S.V. and Feng, W., 'Development of hybrid finite elements for stress analysis of composite structures', the 3rd International Conf. on Fracture and Strength of Solids, Hong Kong, China (1997).

[51] Bogdanovich, A., Kumar, V., Pastore, C., and German, M., '3-D stress analysis in laminated plates using a combination of ANSYS and sub-element/deficient approximation function analysis', Proc. of the American Society for Composites, Ninth Technical Conference, Delaware, 1994.

[52] Pian, T.H.H., 'Derivation of element stiffness matrices by assumed stress distributions', AIAA J. vol. 2, 1333-1336(1964).

[53] Atluri, S.N., Gallagher, R.H., and Zienkiewicz, O.C. eds., Hybrid and Mixed Finite Element Models, John Wiley, 1983.

[54] Pian, T.H.H. and Tong, P., 'Basis of finite element methods for solid continua', Int. J. Numer. Methods Engrg., vol. 1, 3-28(1969).

[55] Poceski, A., Mixed Finite Element Method, Springer-Verlag Berlin Heidelberg, 1992.

[56] Brezzi, F. and Fortin, M., Mixed and Hybrid Finite Element Methods, Springer-Verlag New York Inc. 1991.

[57] Pian, T.H.H., 'A historical note about hybrid elements', Int. J. Numer. Methods Engrg., vol. 12, 891-892(1978).

[58] Pian, T.H.H., 'Recent advances in hybrid/mixed finite elements', in: He, G.Q. and Cheung, Y.K. (eds.), Proc. Conf. on Finite Element Methods, Shanghai, China, 82-89(1982).

[59] Pian, T.H.H., 'Thirty-year history of hybrid stress finite element methods', in: Lee, P.K.K. and Tham, L.G. (eds.), Y.K. Cheung Symposium, 15 December 1994, University of Hong Kong, 23-31(1994).

[60] Liou, W.-J. & Sun, C.T. 'A three dimensional hybrid stress isoparametric element for the analysis of laminated composited plates', Computers & Structures, vol. 25, no. 2, 241-249(1987).

[61] Noor, A.K., 'Multifield (mixed and hybrid) finite element models', in: Noor, A.K. and Pilkey, W.D. (eds), State-of-the-art Survey on Finite Element Technology, ASME, 1983.

[62] Henshell, R.D., 'On hybrid finite elements', Proceeding of the Brunel University Conference of the Institute of Math and Its Application, April, 1972.

[63] Fraeijs de Veubake, B.M., Proceeding of the Conference on Matrix Methods in Structure Machanics, AFFDL-TR-66-80, (1966).

[64] Brezzi, F., 'On the existence, uniqueness and approximation of saddle point problems arising from Lagrange multiplers', RAIRO 8(R2), 129-151(1974).

[65] Babuska, I, Oden, J.T. and Lee, J.K., 'Mixed-hybrid finite element approximations of second-order elliptic boundary-value problems, Part I ', Computer Methods in Applied Mechanics and Engineering, vol. 11, 175-206(1977).

[66] Fraeijs de Veubake, B., 'Displacement and equilibrium models in the finite element methods', in: Zienkiewicz, O.C. and Holister, G.S. (eds.), Stress Analysis, John Wiley, London, 1965.

[67] Stolarski, H. and Belytschko, T., 'Limitation principles for mixed finite elements based on the Hu-Washizu variational formulation', Comput. Meth. Appl. Mech. Engng. vol. 60, 195-216(1987).

[68] Punch, E.F. and Atluri, S.N., 'Development and testing of stable, invariant, isoparametric curvilinear 2- and 3-D hybrid-stress elements', Computer Methods in Applied Mechanics and Engineering, vol. 47, 331-356(1984).

[69] Rubinstein, R., Punch, E.F. and Atluri, S.N., 'An analysis of, and remedies for, kinematic modes in hybrid-stress finite elements: selection of stable, invariant stress fields', Computer Methods in Applied Mechanics and Engineering, vol. 38, 63-92(1983).

[70] Pian, T.H.H. and Chen, D.P., 'On the suppression of zero energy deformation modes', International Journal for Numerical Methods in Engineering, vol. 19, 1741-1752(1983).

[71] Pian, T.H.H. and Tong, P., 'Relations between incompatible displacement model and hybrid stress model', International Journal for Numerical Methods in Engineering, vol. 22, 173-181(1986).

[72] Pian, T.H.H. and Wu, C.C., 'A rational approach for choosing stress terms for hybrid

finite element formulations', International Journal for Numerical Methods in Engineering, vol. 26, 2331-2343(1988).

[73] Wu, C.C. and Cheung, Y.K., 'On optimization approaches of hybrid stress elements', Finite Elements in Analysis and Design, vol. 21, 111-128(1995).

[74] Sze, K.Y., Chow, C.L., and Chen, W. J., 'A rational formulation of iso-parametric hybrid stress element for three dimensional stress analysis', Finite Elements in Analysis and Design, vol. 7, 61-72(1990).

[75] Chen, W. J. and Cheung, Y.K., 'Three-dimensional 8-node and 20-node refined hybrid isoparametric elements', International Journal for Numerical Methods in Engineering, vol. 35, 1871-1889(1992).

[76] Sze, K.Y., 'Control of spurious mechanisms for 20-node and transition sub-integrated hexahedral elements', International Journal for Numerical Methods in Engineering, vol. 37, 2235-2250(1994).

[77] Sze, K.Y., 'A novel approach for devising higher-order hybrid elements', International Journal for Numerical Method in Engineering, vol. 36, 3303-3316(1993).

[78] Sze, K.Y. and Chow, C.L., 'Efficient hybrid/mixed elements using admissible matrix formulation', Conputer Methods in Applied Mechanics and Engineering, vol. 99, 1-26(1992).

[79] Reissner, E. 'On a certain mixed variational theorem and a proposed application', Int. J. Numer. Methods. in Eng., vol. 20, pp.1366-1368(1984).

[80] Reissner, E. 'On a mixed variational theorem and on shear deformable plate theory', Int. J. Numer. Methods. in Eng., vol. 23, pp.193-198(1986).

[81] Moriya, K. 'Laminated Plate and Shell Elements for Finite Element Analysis of Advanced Fibre Reinforced Composite Structures', (in Japanese), Trans. Japan Soc. Mech. Eng. (series A), 52, No. 478, pp.1600-1607(1986).

[82] Feng, W. and Hoa, S.V., 'A multilayer element with partial assumed stress field for analysis of laminated structures', The 16th Canadian Congress of Appplied Mechanics CANCAM 97, Quebec, Canada, (1997).

[83] Noor, A.K., 'Mechanics of anisotropic plates and shells-a new look at an old subject', Computers & Structures, vol. 44, no.3, 499-514(1992).

[84] Epstein, M. and Huttelmaier, H.P., 'A finite element formulation for multilayered and thick plates', Comp. Struct., 16, 645-650(1983).

[85] Hinrichsen, R.L. and Palazotto, A.N., 'Nonlinear finite element analysis of thick composite plates using a cubic spline function', AIAA J., 24, 1836-1842(1986).

[86] Muc, A., 'Computational models and variational formulations for laminated composite structures', Composites Modelling and Processing Science, ICCM/9, vol. III, Antonio Miravete (ed.), University of Zaragoza, Woodhead Publishing Limited (1993).

[87] Rybicki, E.F., 'Approximate three-dimensional solution for symmetric laminates under in-plane loading', J. Compo. Mater., vol. 5, p354(1971).

[88] Lessard, L.B., Shokrieh, M.M., and Schmidt, A.S., '3-D stress analysis of composite plates with or without stress concentrations', Composites Modelling and Processing Science, III, ICCM/9, Antonio Miravete (ed.), Woodhead Publishing Limited, (1993).

[89] Barker, R.M., Lin, F.T., and Dana, J.R., '3-D finite element analysis of laminated composites', Computers & Structures, vol.2, 1013-1029(1972).

[90] Mote, Jr. C.D., 'Global-local finite element', Int. J. Numer. Methods Eng., vol. 3, 565- 574(1971).

[91] Noor, A.K., 'Global-local methodologies and their application to nonlinear analysis', Finite Elements in Analysis and Design, vol.2, 333-346(1986).

[92] Jara-Almonte, C.C. and Knight, C.E., 'The specified boundary stiffness/force SBSF method for finite element subregion analysis', Int. J. Numer. Methods Eng., vol.26, 1567-1578(1988).

[93] Ransom, J.B. and Knight, Jr. N.F., 'Global/local stress analysis of composite panels', Computers & Structures, vol. 37, no. 4, 375-395(1990).

[94] Wiggenraad, J.F.M. and Bauld, Jr. N.R., 'Global/local interlaminar stress analysis of a grid-stiffened composite panel', Sixth Technical Conf., America Society for Composites, 1991.

[95] Griffin, Jr. O.H. and Vidussoni, M.A., 'Global/local finite element analysis of composite materials', Computer Aided Design in Composite Material Technology, Eds., C.A.Brebbia, W.P.de Wilde and W.R.Blain, Springer-Verlag, (1988).

[96] Larrode, E., Alba, J.J., Bravo, P. and Antequera, P., 'Analysis of composite structures using the substructure technique', Composite Modelling and Processing Science', ICCM/9, vol. III, ed., Antonio Miravete, University of Zaragoza, Woodhead Publishing Limited(1993).

[97] Robbins, Jr. D.H. and Reddy, J.N., 'Analysis of laminated composite structures using multiple assumed displacement fields', Proc. 2nd Int. Symp. on Composite Materials and Structures, Beijing(1992).

[98] Pagano, N.J. and Soni, S.R., 'Global-local laminate variational model', Int. J. Solids Struct., vol. 19, 207-228(1983).

[99] Fish, J. and Markolefas, S., 'The s-version of the finite element method for multilayer laminates', Int. J. Numer. Methods Eng., vol. 33, 1081-1105(1992).

[100] Lucking, W.M., Hoa, S.V. and Sankar, T.S., 'The effect of geometry on interlaminar stresses of [0/90]s composite laminates with circular holes', J. Composite Materials, vol.17, 188-198(1984).

[101] Hoa, S.V. and Feng, W., 'A global/local model for analysis of composites', 10th International Conf. on Composite Materials, Whistler, Canada (1995).

[102] Hoa, S.V. and Feng, W., 'Global/local approach using hybrid elements for composites', 5th International Conf. on Computer Aided Design in Composite Material Technology, Udine, Italy (1996).

[103] Hoa, S.V. and Feng, W., 'A global/local model using partial hybrid elements', XIXth International Conf. of Theoretical and Applied Mechanics, Kyoto, Japan (1996).

[104] Hoa, S.V. and Feng, W., 'Application of a global/local finite element model to composite laminates', Science and Engineering of Composite Materials, vol. 5, 151-168(1996).

[105] Spilker, R.L. 'A hybrid stress finite element formulation for thick multilayer laminates', Computers & Structures, vol.11, 507-514(1980).

[106] Feng, W., Hoa, S.V. and Huang, Q., 'Classification of stress modes in assumed stress fields of hybrid finite elements', Int. J. Numer. Methods in Eng., vol. 40, 4313-4339(1997).

[107] Ahmad, S., Irons, B.M. and Zienkiewicz, O.C., 'Analysis of thick and thin shell structures by curved finite elements', Int. J. Numer. Methods Eng., vol. 2, 419-451(1970).

[108] Blocki, J., 'A high-order linear theory for isotropic plate -I. theoretical considerations', Int. J. Solid Structures, vol. 29, no. 7, 825-836(1992).

[109] Surana, K.S., 'Geometrically nonlinear formulation for the three dimensional solid-shell transition finite elements', Comp. Struct., vol. 15, 549-566(1982).

[110] Liao, C.L., Reddy, J.N. and Engelstad, S.P., 'A solid-shell transition element for geometrically non-linear analysis of laminated composite structures', Int. J. Numer. Methods Eng., vol. 26, 1843-1854(1988).

[111] Han, K.J. and Gould, P.L., 'Line node and transitional shell element for rotational shells', Int. J. Numer. Methods Eng., vol. 18, 879-895(1982).

[112] Zienkiewicz, O.C., The Finite ELement Method, 3rd eds, McGraw-Hill, New York, 1977.

[113] Akin, J.E., Application and Implementation of Finite Element Methods, Academic Press, London, 1982.

[114] Guo, F.Y., Feng, G.K., Shi, Z.Y., and Zhu, Y.Z., (eds.), FORTRAN Algorithm, Defense Industry Press, Beijing, 1982.

[115] Mackerle, J., 'Finite element and boundary element library for composites - A bibliography (1991-1993)', Finite Elements in Analysis and Design, vol. 17, 155-165(1994).

[116] Murty, A.V.K., Harikumar, H.K., and Shah, C.G., 'Towards damage tolerant design of laminated composites', in Reddy, J.N. and Murty, A.V.K., (eds.), Composite Structures

-Testing, Analysis and Design, Springer-Verlag, Berlin, 1993.

[117] Luo, J. and Sun, C.T., 'Global-local methods for thermoelastic stress analysis of thick fibre-wound cylinders', J. Composite Materials, vol. 25, (1991).

[118] Mao, K.M. and Sun, C.T., 'A refined global-local finite element analysis method', Int. J. Numer. Methods Eng., vol.32, 29-43(1991).

[119] Kong, J. and Cheung, Y.K., 'Three-dimensional finite element analysis of thick laminated plates', Computers & Structures, vol. 57, no. 6, 1051-1062(1995).

[120] Voleti, S.R., Chandra, N. and Miller, J.R., 'Global-local analysis of large-scale composite structures using finite element methods', Computers & Structures, vol. 58, no. 3, 453-464(1996).

[121] Woo, K. and Whitcomb, John, 'Global/local finite element analysis for textile composites', J. Composite Materials, vol. 28, no. 14, 1305-1321(1994).

[122] Saito, K., Araki, S., Kawakami, T. and Moriwaki, I., 'Global-local finite element analysos of stress intensity factor for a crack along the interface of two phase material', 10th International Conf. on Composite Materials, Whistler, Canada (1995).

[123] Hoa, S.V., Journeaux, B.H., and Di Lalla, L., 'Computer aided design for composite structures', Composite Structures, vol. 13, 67-79(1989).

[124] Pagano, N.J., 'Exact solutions for composite laminates in cylindrical bending', J. Composite Materials, vol. 3, 398-411(1969).

[125] Srinivas, S. and Rao, A.K., 'Bending, vibration and buckling of simply supported thick orthotropic rectangular plates and laminates', Int. J. Solid Struct., vol. 6, 1463-1481(1970).

[126] Pagano, N.J., 'Exact solutions for rectangular bidirectional composites and sandwich plates', J. Composite Materials, vol. 4, 20-34(1970).

[127] Zhao, J.Z., Hoa, S.V., Xiao, X., and Hanna, I., 'Partial hybrid finite element analysis of stress field in composite laminates with delamination crack under out-of-plane loading', 6th Int. Conf. on Computer Methods in Composite Materials, Montreal, Canada, 1998.

Appendix

IMPLEMENTATION OF PARTIAL HYBRID FINITE ELEMENTS ------- COMPUTER PROGRAM *COMSA*

A.1 Introduction

In the previous chapters, a series of finite elements have been established. They can be used to analyze laminated composite structures. However, the actual application of finite element procedure requires extensive programming effort. Usually, a finite element computer code includes the following functional blocks [15]:

1. Input, generation and verification of all the information required to define the problem to be solved and to dimension the working space to be used;

2. Construction of element matrices and element vectors by using numerical integration, followed by an assembly process to set up the overall system equations and load vectors;

3. Application of displacement boundary conditions and solution of the system equations;

4. Computations of strains and stresses depending on the solution of the system equations and post-processing of results.

In this Chapter, the finite element computer code COMSA will be briefly introduced according to the functional blocks.

A.2 General Procedure of Finite Element Analysis using *COMSA*

To perform a finite element analysis using COMSA, first of all is to divide a continuum, problem domain, into a finite number of quasi-disjoint non-overlapping subregions, called finite elements, using imaginary lines or surfaces. These elements are connected by using a set of key points, called nodes. Thus, approximations of element geometry, displacement field, and partial stress field can be introduced by means of the equations in the previous chapters.

In order to solve an established finite element model using the computer program COMSA, the nodes have to be assigned identifying integer numbers (node numbers) beginning with unity and ranging to some maximum value, say NODT. A number of degrees of freedom, say NNFM, will be associated with each and every node. In the partial hybrid stress element, the nodal displacements are chosen as unknown nodal parameters. Thus, the total number (NNFMT) of degrees of freedom (DOF) in the system is the product of the number of nodes (NODT) and the number (NNFM) of nodal

displacements per node, NNFMT=NODT×NNFM. If there are different nodes (point nodes in 3-D solid element and lines of nodes in transition element), the total number (NNFMT) of DOF in the system is equal to the sum of the number of DOF per node. For instance, if there are NPO point nodes (NNFM=3) and NPL lines of nodes (NNFM=6), the total number (NNFMT) of DOF in the system equals 3×NPO+6×NPL. Similarly, the elements must be assigned identifying integer numbers (element numbers). They also begin with unity and extend to a maximum value, say NELT. If there are a number (NEG) of different elements in a finite element model, the total number (NELT) of elements is equal to the sum of the numbers (NEN) of different elements. For example, in a global/local finite element model consisting of three types elements: NEN(1) 8-node plate element, NEN(2) 20-node solid element, and NEN(3) 15-nod transition element, the total number (NELT) of elements equals the sum of NEN(1), NEN(2), and NEN(3). These numbers will be used to define the dimension of the storage space. In the COMSA, a number of control parameters is determined firstly to define three common vectors of a size large enough to contain a number of matrices needed in a typical problem. A set of pointers is defined to locate the position, in the storage vector, of the first coefficient of each matrix of interest [113, 114]. The three common arrays and the pointers will be described in detail in the next section.

It is necessary to supply data XYZ which define the coordinates of nodes and determine the geometry of the finite element model to be analyzed. Also, data JKG which list the global node numbers attached to an element has to be supplied. These data JKG must be

input to formulate element matrices and assemble elements. In addition, an array of data BC must be given to indicate which, if any, of the nodal displacements have boundary constraints specified by means of the node number. Moreover, a number of material data E&, V&, and G& must be assigned to every element. The data to be input in COMSA will be shown in detail later.

After discretizing a structure into a number of nodes and elements, the interpolation functions for element geometry, displacement field, and partial stress field have to be assumed in terms of the values of the nodal displacements and stress parameters that are connected to that particular element. In the COMSA, isoparametric elements are used. Therefore, the displacement interpolation functions are the same as the geometric shape interpolation functions. Stress interpolation functions are determined by classification method. After the element behaviour has been assumed, the element stiffness matrices and load vector can be established. The element formulation has been presented in Chapter 2-8. Due to using isoparametric element, it is impossible to integrate the expression of the element matrices in closed form. The numerical integration must be utilized to perform the evaluation of element matrices. Therefore, the Gauss quadrature formula is used in the integration of the element matrices.

Once the element equations have been established, the contribution of each element is added to form the system equations:

$$[A]\{X\}=\{LR\} \tag{A-1}$$

From consideration of the technique used to approximate the element behaviour, the maximum half-bandwidth, say NBAND, is calculated. The quantity NBAND is one of the important quantities which govern the storage requirements and solution time of the system equations. Because the maximum half-bandwidth NBAND is directly proportional to the value of the maximum difference in node numbers of the nodes within an element, in practice, it should be tried to minimize the maximum difference in node numbers associated with an element, although the assignment of node numbers is arbitrary in the mathematical point of view.

After the system equations have been established, it is necessary to apply the boundary constraints before solving for the unknown nodal displacements. In the computer program COMSA, the penalty modifications are used to treat the prescribed boundary displacements. Let 'i' denote the degree of freedom to be assigned a given value D. The procedure to apply the constraint is to modify two terms of the system matrix and column vector, i.e. A_{ii} and LR_i. These terms are redefined to be

$$A_{ii}=\alpha A_{ii} \qquad\qquad LR_i=\alpha DA_{ii} \tag{A-2}$$

where α is a very large number. This yields the i-th system equation

$$A_{i1}X_1+\ldots+\alpha A_{ii}X_i+\ldots+A_{in}X_n=\alpha DA_{ii} \tag{A-3}$$

which is a good approximation of the boundary condition $X_i = D$ if α is sufficiently large. Then, the unknown nodal displacements can be solved. In the COMSA, the solution

algorithm is the Gauss elimination. From the standpoint of calculation efficiency, it has been proven that no algorithm for equation solving can involve fewer calculations than Gauss elimination. After nodal displacements are obtained, the displacement field and partial stress field can be determined. The quantities of interest can be output in a practical form.

The flowchart of main program of finite element code COMSA is presented in Figure A-1. It illustrates the major steps that fall under the control of the main program, COMSA. The first half of the steps, down to point 1, deal with initializing the system, determining the input options, reading and printing the input data, and assigning storage location that will hold the information to be generated in later phases.

The steps from points 1 to 2, in Figure A-1, deal with the generation of element matrices, assembling the system matrices, and applying the essential boundary conditions. The steps between point 2 and 3 are to solve system equations, obtain the values of known nodal displacements, calculate the stresses within the elements.

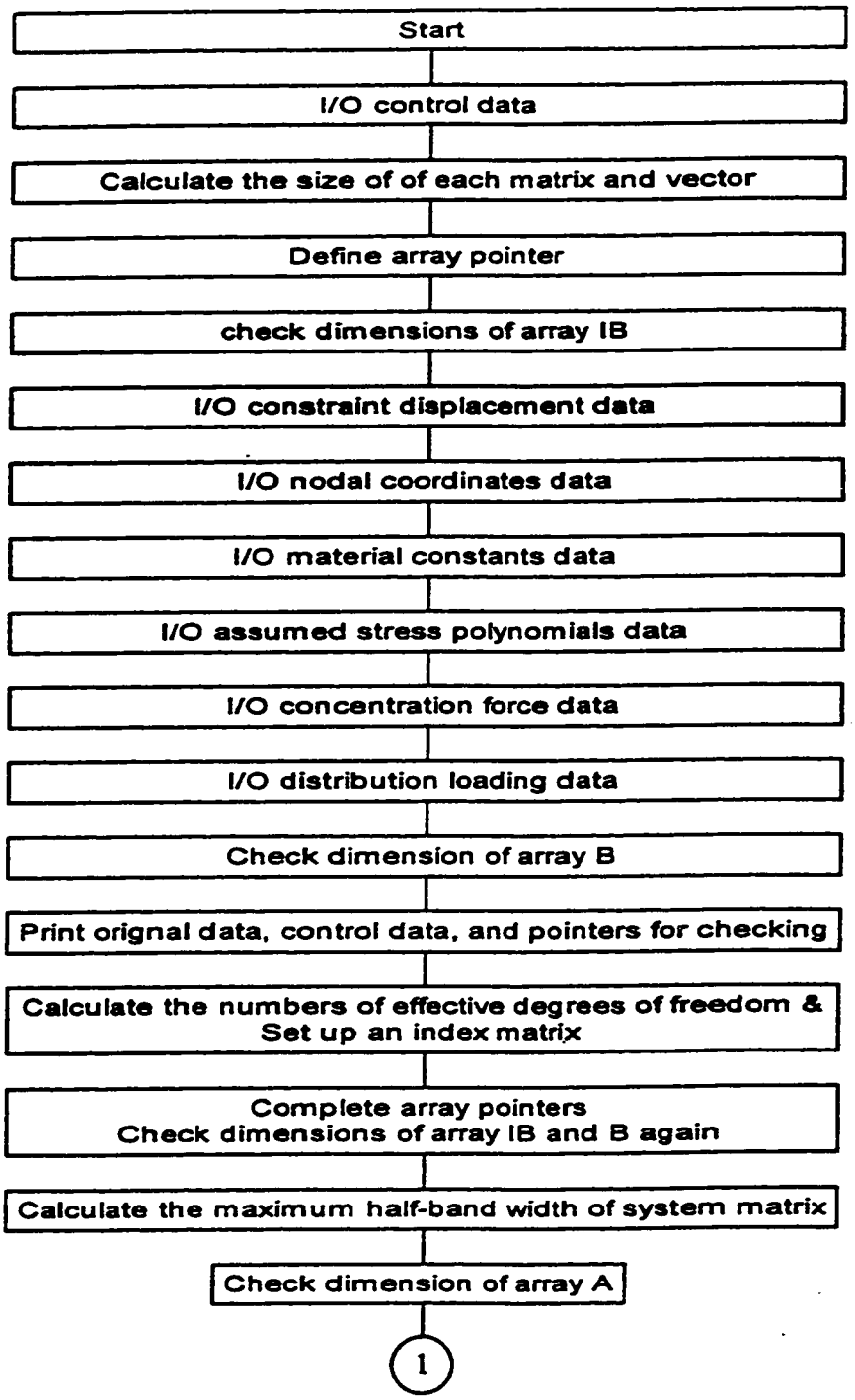

Figure A-1 The flowchart of main program COMSA (to be continued)

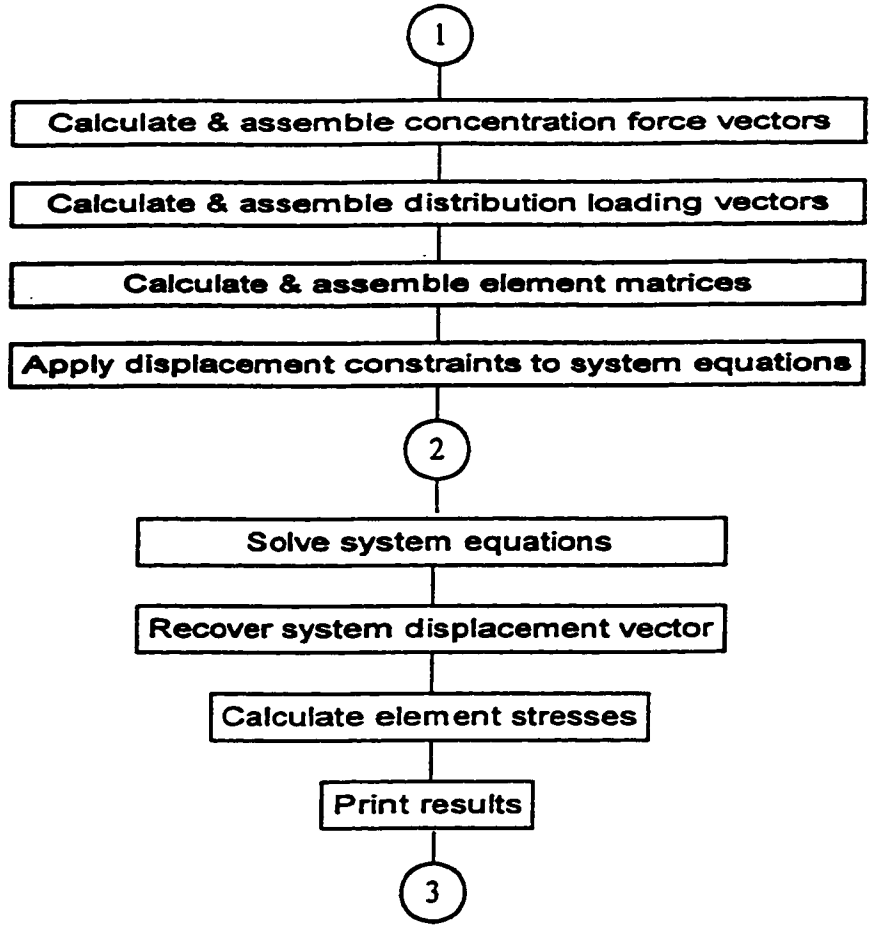

Figure A-1 The flowchart of main program COMSA (continued)

A.3 Common Arrays and Pointers in Program COMSA

In the COMSA, three large arrays A, B, and IB are dimensioned to store various matrices. A set of pointers is defined to locate the position of the initial address of each matrix of interest in the storage arrays. The three common arrays are dimensioned as follows,

```
COMMON /AARRAY/  A(1000000)
COMMON /BARRAY/  B(10000)
COMMON /IBARRAY/ IB(10000)
```

in which, the sizes of array A is 1,000,000, B is 10,000, and IB is 10,000. These sizes can be extended to the size to be expected. The COMMON statements are used to allow various subroutines to use them. The three arrays are divided by a set of pointers to store various element matrices and vectors. The pointers are defined as follows,

For array A(1000000):

LAK: the pointer of the global stiffness matrix in array A.

For array IB(10000):

LLD: the initial address of the pointer array LD(NEQ) of the diagonal elements of total stiffness matrix

LID: the initial address of the array ID(NNFM,NODT) storing the effective degree number of freedom for each degree of freedom in the model.

LADJK: the initial address of the pointer array ADJK(NEG) of node number arrays of

different elements.

LADGP: the initial address of the pointer array ADGP(NEG) of material constant arrays of different elements.

LADPM: the initial address of the pointer array ADPM(NEG,NLC) of the information array of different distribution loading.

LJKG: the initial address of the node number array JKG(NEG) of elements.

LOAD: the initial address of the array OAD(NLC) storing the number of nodes subjected to concentration force.

LMOAD: the initial address of the array MOAD(NEG,NLC) storing the number of elements subjected to distribution loading.

LSTRES1: initial address of the array STRESS1 (NLC) storing the information of stress calculation.

LSTRES2: initial address of the array STRES2(NEG,NLC) storing the number of elements in which the stresses are output.

LSTRES3: initial address of the array storing the element number for stress calculation.

LLM: initial address of the working array for degree index of freedom of elements.

For array B(10000):

LBC: the initial address of the constraint information array BC(2,NBC).

LXYZ: the initial address of the nodal coordinate array XYZ(NCOR,NODT).

LGPH: the initial address of the material constant array GPH(NGPHC,NGPH).

LRFG: the initial address of the concentration force array RFG(2,).

LRFM: the initial address of the distribution loading array RFMI(I,J).

LR: the initial address of the working array storing loading vector or nodal displacement vector

LEK: the initial address of the working array storing the element stiffness matrix.

This storage procedure allows for the semi-dynamic allocation of storage for the various matrices. It saves computer space and is easy to change the storage size available to different problems.

A.4 The Basic Variables and the Input Data Files

In the computer program COMSA, there are four input files: Finput.dat, Input3.dat, Input4.dat, and Input 5.dat for supplying original data to set up a finite element model. The details are given in the following pages.

A.4.1 File 1 --- Finput.dat

System Parameters:

Card 1

NPROBL, NCHE, NPUT

NPROBL	---	Number of Problems	
NCHE	---	0	Calculation
		1	Check input data
NPUT	---	0	Not print input data
		1	Print input data

Card 2

NCTYPE, NODT, NLC, NEG, NNFM, NCOR, NBC, NPO, IUNI

NCTYPE	---	1	Deformation analysis
		2	Stress analysis
NODT	---	Total number of nodes in structures (<= 600)	
NLC	---	Total number of loading cases (<= 2)	
NEG	---	Number of element types in structures (<= 3)	
NNFM	---	Maximum number of D.O.F. per node in structures	
		6	Degenerated element and Transition element
		3	Solid element only in structures
NCOR		---	Maximum number of nodal coordinates
		6	Line nodes
		3	Point nodes
NBC	---	Total number of constrain conditions	
NPO	---	Number of point nodes	
		xxx	Transition elements used and point nodes firstly
		0	No transition element
IUNI	---	Type of loading	
		1	q_0 uniform loading
		2	$q_0 \sin(\pi x/a)\sin(\pi y/b)$
		3	$q_0 \sin(\pi x/a)$

Card 3

NETYP, NEN, NOD, NNF, NGPHC, NGPH (NEG LINES)

NETYP	---	Type of elements	
		3	Degenerated element
		4	Solid element
		5	Transition element
NEN	---	Number of this element	
NOD	---	Number of nodes in this element	
		8	Degenerated element
		20	Solid element
		15	Transition element
NNF	---	Number of nodal D.O.F.	
		6	Degenerated element
		3	Solid element
		4	Transition element
NGPHC	---	0	
NGPH	---	0	

Card 4

APL, BPL

APL	---	a
BPL	---	b

Used in loading $q_0 \sin(\pi x/a)\sin(\pi y/b)$

Node Number Array:

Card 5 (Solid element)

Element 1

Node 1, Node 2, ... , Node 10

Node 11, Node 12, ... , Node 20, MATG

.

.

.

Element NEN

Node 1, Node 2, ... , Node 10

Node 11, Node 12, ... , Node 20, MATG

Node 1	---	Node Number of the first node
Node 2	---	Node Number of the second node

.

.

.

Node 20	---	Node Number of the twentieth node
MATG	---	Group number of the materials (lay-up)

Card 5 (Transition element)

Element 1

Node 1, Node 2, ... , ..., Node 10

Node 11, Node 12, .. , Node 15, MATG

.

.

.

Element NEN

Node 1, Node 2, ... , ..., Node 10

Node 11, Node 12, .. , Node 15, MATG

Node 1	---	Node Number of the first node
Node 2	---	Node Number of the second node

.

.

Node 15	---	Node Number of the fifteenth node
MATG	---	Group number of the materials (lay-up)

Card 5 (Degenerated element)

Element 1

Node 1, Node 2, ... , Node 8, MATG

.

.

.

Element NEN

Node 1, Node 2, ... , Node 8, MATG

Node 1	---	Node Number of the first node
Node 2	---	Node Number of the second node
.		
.		
.		
Node 8	---	Node Number of the eighth node
MATG	---	Group number of the materials constants

Information array for concentration forces:

Card 6

OAD(1)

OAD(2)

.

.

.

OAD(NLC)

OAD(I)	---	Number of points subjected to loading
		I = 1, 2, ... , NLC
		NLC is the number of loading cases.

Information array for distribution loadings:

Card 7

MOAD(1,1), MOAD(1,2), ..., MOAD(1,NEG),

MOAD(2,1), MOAD(2,2), ..., MOAD(2,NEG),

.

.

.

MOAD(NLC,1), MOAD(NLC,2), ..., MOAD(NLC,NEG),

MOAD(I,J) --- Number of element in the j-th element type under the i-th loading case

I = 1, 2, ... , NLC

J = 1, 2, ... , NEG

Information array for stress calculation:

Card 8

IST(1,1), IST(1,2), ..., IST(1,NEG),

IST(2,1), IST(2,2), ..., IST(2,NEG),

.

.

.

IST(NLC,1), IST(NLC,2), ..., IST(NLC,NEG),

IST(I,J) --- Number of element in the j-th element type under the i-th loading case for stress calculation

I = 1, 2, ... , NLC

J = 1, 2, ... , NEG

Element number for stress calculation:

Card 9

ISN(1)

ISN(2)

.

.

.

ISN(N)

ISN(I) --- Element number for stress calculation

$$I = 1, 2, \ldots, N$$

$$N = \sum_{I=1}^{NLC} \sum_{J=1}^{NEG} IST(I,J)$$

Constraint condition:

Card 10

BOUN.DIR(1), DISN (1)

BOUN.DIR(2), DISN (2)

.

.

BOUN.DIR(NBC), DISN(NBC)

BOUN --- Node number of the node subjected to prescribed displacement

DIR --- Direction of the prescribed displacement

1 X

2 Y

3 Z

4 Ψ_x

5 Ψ_y

6 Ψ_z

DISN --- The value of the prescribed displacements

Nodal coordinates:

Card 11

XB(1), YB(1), ZB(1), XT(1), YT(1), ZT(1)

XB(2), YB(2), ZB(2), XT(2), YT(2), ZT(2)

.

.

.

XB(NODT), YB(NODT), ZB(NODT), XT(NODT), YT(NODT), ZT(NODT)

For point nodes:

XB(I) = X(I) --- the value of coordinate X of node I

YB(I) = Y(I) --- the value of coordinate Y of node I

ZB(I) = Z(I) --- the value of coordinate Z of node I

XT(I) = 0.0

YT(I) = 0.0

ZT(I) = 0.0

For line nodes:

XB(I) --- the value of coordinate X of node I on the bottom of laminates

YB(I) --- the value of coordinate Y of node I on the bottom of laminates

ZB(I) --- the value of coordinate Z of node I on the bottom of laminates

XT(I) --- the value of coordinate X of node I on the top of laminates

YT(I) --- the value of coordinate Y of node I on the top of laminates

ZT(I) --- the value of coordinate Z of node I on the top of laminates

Concentration forces:

Card 12

RFG(1,1), RFG(1,2)

RFG(2,1), RFG(2,2)

.

.

.

RFG(N,1), RFG(N,2)

RFG(I,1) --- FORCE.DIR

FORCE --- Node number of the node subjected to loading

DIR --- Direction of the loading

RFG(I,2) --- value of the loadings

$$N = \sum_{I=1}^{NLC} OAD(I)$$

Distribution forces:

Card 13

RFM(1,1), RFM(1,2)

RFM(2,1), RFM(2,2)

.

.

.

RFM(N,1), RFM(N,2)

RFM(I,1) --- Element number of the element subjected to distribution loading

RFM(I,2) --- value of the loadings q_0

$$N = \sum_{I=1}^{NLC} \sum_{J=1}^{NEG} MOAD(I,J)$$

A.4.2 File 2 --- Input3.dat (degenerated element)

Information about stress field

Card 1

MODMAX

MODMAX --- The number of stress modes

Information about material

Card 2

NMAT

NMAT --- The number of material constant groups

Material constants

Card 3

E1(1), V12(1), G12(1)

E2(1), V23(1), G23(1)

E3(1), V13(1), G31(1)

E1(2), V12(2), G12(2)

E2(2), V23(2), G23(2)

E3(2), V13(2), G31(2)

.

.

.

E1(NMAT), V12(NMAT), G12(NMAT)

E2(NMAT), V23(NMAT), G23(NMAT)

E3(NMAT), V13(NMAT), G31(NMAT)

E1(I) --- E_1

V12(I) --- v_{12}

G12(I) --- G_{12}

E2(I) --- E_2

V23(I) --- v_{23}

G23(I) --- G_{23}

E3(I) --- E_3

V13(I) --- v_{13}

G31(I) --- G_{31}

I = 1,2, ..., NMAT

Information about lay-up

Card 4

NLAT

NLAT --- The number of layers in laminates

Card 5

MLAY(1), CTA(1)

MLAY(2), CTA(2)

.

.

.

MLAY(NLAT), CTA(NLAT)

MLAY(I) --- Group number of material constants for the I-th layer

CTA(I) --- The orientation of the fibre in the I-th layer

Stress modes

Card 6

For σ_z

N

C_1, l_1, m_1, k_1

C_2, l_2, m_2, k_2

.

C_n, l_n, m_n, k_n

0

0

For τ_{yz}

0

N

C_1, l_1, m_1, k_1

C_2, l_2, m_2, k_2

.

C_n, l_n, m_n, k_n

0

For τ_{zx}

0

0

N

C_1, l_1, m_1, k_1

C_2, l_2, m_2, k_2

.

C_n, l_n, m_n, k_n

$$\begin{Bmatrix} \sigma_z \\ \tau_{yz} \\ \tau_{zx} \end{Bmatrix} = \begin{Bmatrix} \sum_{i=1}^{n} f_i(\xi,\eta,\zeta) \\ \sum_{i=1}^{n} g_i(\xi,\eta,\zeta) \\ \sum_{i=1}^{n} h_i(\xi,\eta,\zeta) \end{Bmatrix}$$

$$f_i, g_i, h_i \quad \text{-----} \quad C_i\ \xi^{l_i}\ \eta^{m_i}\ \zeta^{k_i}$$

A.4.3 File 3 -- Input4.dat (solid element)

Information about stress field

Card 1

MODMAX

MODMAX --- The number of stress modes

Information about material

Card 2

NMAT

NMAT --- The number of material constant groups

Material constants

Card 3

E1(1), V12(1), G12(1)

E2(1), V23(1), G23(1)

E3(1), V13(1), G31(1)

E1(2), V12(2), G12(2)

E2(2), V23(2), G23(2)

E3(2), V13(2), G31(2)

.

.

.

E1(NMAT), V12(NMAT), G12(NMAT)

E2(NMAT), V23(NMAT), G23(NMAT)

E3(NMAT), V13(NMAT), G31(NMAT)

E1(I) --- E_1

V12(I) --- v_{12}

G12(I) --- G_{12}

E2(I) --- E_2

V23(I) --- v_{23}

G23(I) --- G_{23}

E3(I) --- E_3

V13(I) --- v_{13}

G31(I) --- G_{31}

I = 1,2, ..., NMAT

Information about lay-up

Card 4

NLAT

NLAT	---	The number of different lay-up in laminates

Card 5

MLAY(1), CTA(1)

MLAY(2), CTA(2)

•

•

MLAY(NLAT), CTA(NLAT)

MLAY(I)	---	Group number of material constants for the I-th layer
CTA(I)	---	The orientation of the fibre in the I-th layer

Card 6

NLAY

NLAY --- The number of different type of element

Card 7

NLAYN(1)

NLCT(1,1), NLCT(1,2), ..., NLCT(1,NLAYN(1))

NLAYN(2)

NLCT(2,1), NLCT(2,2), ..., NLCT(2,NLAYN(2))

.

.

NLAYN(NLAY)

NLCT(NLAY,1), NLCT(NLAY,2), ..., NLCT(NLAY,NLAYN(NLAY))

NLAYN(I) --- Number of layers in the I-th type element

NLCT(I,J) --- Group number of the lay-up within the j-th layer in I-th type element

Stress modes

Card 8

For σ_z

N

C_1, l_1, m_1, k_1

C_2, l_2, m_2, k_2

.

C_n, l_n, m_n, k_n

0

0

For τ_{yz}

0

N

C_1, l_1, m_1, k_1

C_2, l_2, m_2, k_2

.

C_n, l_n, m_n, k_n

0

For τ_{zx}

0

0

N

C_1, l_1, m_1, k_1

C_2, l_2, m_2, k_2

.

C_n, l_n, m_n, k_n

$$\begin{Bmatrix} \sigma_z \\ \tau_{yz} \\ \tau_{zx} \end{Bmatrix} = \begin{Bmatrix} \sum_{i=1}^{n} f_i(\xi, \eta, \zeta) \\ \sum_{i=1}^{n} g_i(\xi, \eta, \zeta) \\ \sum_{i=1}^{n} h_i(\xi, \eta, \zeta) \end{Bmatrix}$$

$$f_i, g_i, h_i \quad \text{-----} \quad C_i \, \xi^{l_i} \, \eta^{m_i} \, \zeta^{k_i}$$

A.4.4 File 4 -- Input5.dat (transition element)

The data format is the same as that in input4.dat (solid element)

A.4.5 Node number in different elements

Degenerated Element

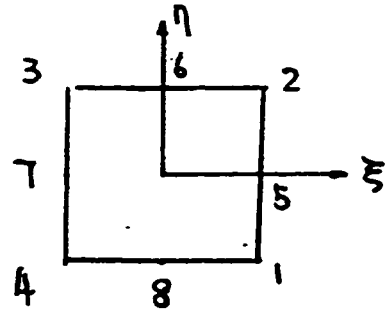

Solid Element

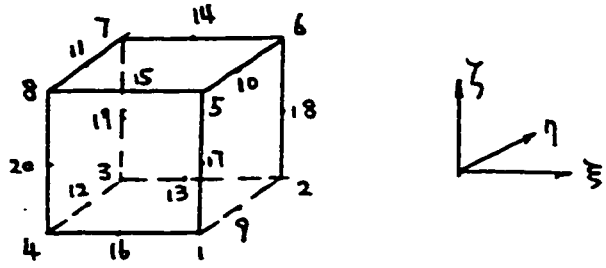

Transition Element

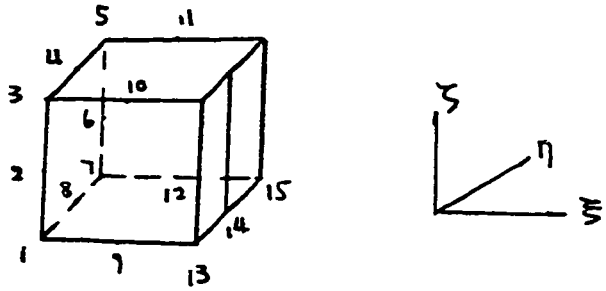

A.5 Discussion

For simplicity, the 4-node degenerated plate element and multilayer elements are installed into another program COMSA-1 which has the same control structure and main program as the COMSA.

For generation of the mesh, ANSYS program is used to generate the coordinates of nodes, the node numbers of elements. Then, the data format in the ANSYS file is converted to that in the Finput file.

For presentation of results, Matlab program is used to show the displacement field and the stress field in the structures.